UCSF

UC San Francisco Electronic Theses and Dissertations

Title

Complex Tissue Model Generation via DNA Programmed Assembly

Permalink

https://escholarship.org/uc/item/0q52q4x3

Author

Jee, Noel

Publication Date

2015

Peer reviewed|Thesis/dissertation

eScholarship.org Powered by the California Digital Library
University of California

Complex Tissue Model Generation via DNA Programmed Assembly

by

Noel Youngho Jee

DISSERTATION

Submitted in partial satisfaction of the requirements for the degree of

DOCTOR OF PHILOSOPHY

in

Chemistry and Chemical Biology

in the

GRADUATE DIVISION

of the

UNIVERSITY OF CALIFORNIA, SAN FRANCISCO

[redacted]

Copyright (2015)

By

Noel Y. Jee

Acknowledgements

My wife, Cindy, is the first person that I must thank. She has been with me through it all, and I never would have successfully completed my doctoral degree without her.

To my thesis, the entire STDPAC protocol was co-developed with Michael Todhunter, without whom this thesis would not have been possible.

Specific to my thesis work, I'd also like to thank Dr. Alex Hughes for following up with the Ras experiments, Maxwell Coyle for following up with the HUVEC experiments, Michael Todhunter for following up with the 10% AT tube experiment, Alec Cerchiari for the imaging and tissue culture of the Twinkies and long-term MCF-10A tissues, and Robert Weber for help in the design of DNA strands for the theoretical STDPAC tissue printer.

Samantha Liang was instrumental in making life in lab enjoyable, even during the slump years. And Dr. Kyle Broaders and Dr. Jennifer Liu never ceased to contribute intellectually, wisely, and sassily to the work and life I had in graduate school. And of course, the members of the entire Gartner lab have supported me morally and intellectually throughout the course of my graduate work.

To my advisor and mentor, Professor Zev Gartner, I give many thanks for providing me with financial, intellectual, and moral support to be as creative as I wished to be in the laboratory. Zev spared no expense so that I could work on the cutting edge of scientific technology.

I've had a long and productive graduate career, however untraditional from the path followed by typical Ph.D. students. Specifically, I've been able to focus on my true passion – startups and business within the life sciences – while conducting cutting-edge and fascinating biological research. While I've had to pursue my interests and passions on my own, the UCSF graduate program was especially amenable to life outside of the laboratory. The humble truth about life in UCSF graduate school is that students are happy. They are happy because they can enjoy life outside of their research, and are not forced to spend every waking hour at the bench because the university culture does not lend itself towards a workaholic science-and-science-only mindset. I owe a great deal to the people of UCSF and the UCSF graduate program for fostering such an awesome culture. Specifically, the Chemistry and Chemical Biology program was instrumental in creating an environment that led to, not only this work, but also my successful development as a supercritical and creative thinker.

My thesis committee members, Professors Jim Wells and Tejal Desai, were great mentors for advice.

Several graduate students and friends outside of the Gartner lab impacted my development as a scholar – they are Kliment Verba, Justin Rettenmaier, and Aaron Mendez.

I would like to thank my family for the support that they have given me. My parents and brother have never doubted my abilities for a moment. My Cornerstone family has also supported me with moral and spiritual support. And finally, I'd like to thank the taxpayers of the United States of America, who were able to fund this research. Only in this blessed country can the son of immigrants rise to the highest level of academic achievement at such a great academic institution.

Parts of this dissertation are a reproduction of materials previously published or submitted for publication and contains contributions from collaborators listed therein. The Abstract, Chapter 1 and Supplemental Text 3 are reproduced in part with permission from Todhunter ME*, Jee NY* (Co-First Authorship), Cerchiari AE, Garbe J, Farlow JT, Gartner ZJ. 2015. Rapid 3D tissue prototyping by DNA-programmed assembly. *In Review*. The artwork in Figure 2-2 is reproduced in part with permission from Selden NS, Todhunter ME, Jee NY, Liu JS, Broaders KE, Gartner ZJ. (2012). Chemically Programmed Cell Adhesion with Membrane-Anchored Oligonucleotides. J Am Chem Soc. *134*, 765-8.

This thesis work was a joint project between myself - Noel Jee - and Michael Todhunter. The entire work was directed by Professor Zev Gartner. **All work presented in this dissertation were completed by Noel Jee with the following exceptions:**

The procedural details relating to flow cells and surface passivation described in Figures 2-1, 2-3, and 2-5 are attributed to Michael Todhunter.

Alec Cerchiari fixed and stained the tissues and collected the images in Figure 2-7C-D. Noel Jee conducted the experiment.

Samantha Liang conceived of the artwork and Michael Todhunter completed the STDPAC experiment in Figure 3-2.

Michael Todhunter conceived of the patterns used in Figure 3-5 and Figure 3-6. Noel Jee conducted all experiments.

Michael Todhunter created the digital pattern in Figure 3-6A-E. Justin Farlow performed the analyses in Figure 3-6G-H. Noel Jee conducted all experiments.

James Garbe passaged and prepared the cells used in Figure 3-14C-D. Alec Cerchiari fixed, stained, and imaged the tissues in Figure 3-14C-D.

Michael Todhunter conducted the data analysis and created all graphs in Figure 4-2.

Michael Todhunter conducted the data analysis and created all graphs in Figure 4-4C.

Michael Todhunter conducted the experiments, data analyses, and graphical depictions in Figure 4-8C-D.

Michael Todhunter conducted the data analyses and created all graphs in Figure 4-15C.

Alex Hughes conducted the experiments, data analyses, and graphical depictions in Figure 5-9C-D.

Michael Todhunter created the digital pattern used in Supplemental Figure S3-3.

Kyle Broaders created the mathematical models in Supplemental Figure S4-3A-B. Michael Todhunter conducted the experiments, data analyses, and images for

Supplemental Figure S4-3C.

Alex Hughes conducted the experiments, data analyses, and graphical depictions Supplemental Figure S4-6.

Michael Todhunter and Robert Weber intellectually contributed to the theoretical STDPAC printer project depicted in Supplemental Figure S6.

Michael Todhunter contributed the entirety of Supplemental Text 1.

Many of the basic images that form the figure artwork panels were collaborations with Michael Todhunter and Zev Gartner.

Abstract

Tissue-level biology is an important, but experimentally challenging field within the biological sciences. Generation of correct tissue models *in vitro* is limited by the lack of scientific techniques available to fully control the correct physical arrangement of cells, extracellular matrix (ECM), and diffusible factors that are vital for homeostasis and proper function. This dissertation presents a method that combines a top-down patterning technique with the bottom-up assembly of cells to generate tissue models, called Surface Templated DNA Programmed Assembly of Cells (STDPAC). At its core, the method uses cell-surfaced grafted oligonucleotides as “zip codes” to direct cell-surface and cell-cell interactions through Watson-Crick base pairing. Herein we demonstrate the method, a showcase of technological applications, and complex tissue models generated to probe the biological function of tissues within the mammary gland.

Table of Contents

Chapter 1: Introduction **1**

Why build tissues? *2*

3D In Vitro Models and Methods *3*

References *7*

Chapter 2: The Unabridged STDPAC Protocol **10**

Introduction *11*

Protocol 1: Preparation of PDMS Flow Cells *13*

Creating the Flow Cell Masters 17

Preparation of PDMS Flow Cells 18

Protocol 2: Surface Patterning, Slide Preparation, and Flow Cell Application *21*

Protocol 3: DNA Cell Labeling *34*

Labeling Cells with DAG DNA for STDPAC 34

Protocol 4: Surface Templated DNA Programmed Assembly of Cells *37*

Supporting Information: Culturing Cells, Data Collection, and Image Analysis *49*

Supporting Information: Basic Operation of the BioForce Nano eNabler *51*

Materials *53*

Protocol 1: Preparation of PDMS Flow Cells 53

Protocol 2: Surface Patterning, Slide Preparation, and Flow Cell Application 53

Protocol 3: Cell Labeling 53

Protocol 4: STDPAC 54

Commentary *54*

References **55**

Chapter 3: Technical Applications of STDPAC **58**

Introduction *59*

Generating Complex Models with STDPAC *60*

Surface Patterning 60

Matrix Embedding, Gel Transfer, and 3D Culture 68

Control of Tissue Composition 75

Orthogonal DNA and Logical Order of Assembly 85

Commentary *90*

References *92*

Chapter 4: Modeling Mammary Gland Components with STDPAC **95**

Introduction *96*

Simple Models of the Mammary Epithelium *99*

Simple models of the Mammary Stroma: Fibroblasts *116*

Commentary *132*

References *134*

Chapter 5: Considerations in Method Development and Experimental Design **135**

Practical Considerations in Experimental Design with STDPAC 136

Matrix Considerations 152

Media Considerations 158

Commentary 165

References 167

Chapter 6: Conclusion and Perspective **169**

Appendix 1: Supplemental Figures and Tables **171**

Supplemental Figures 171

Supplemental Table 200

Appendix 2: Supplemental Text **202**

Supplemental Text 1: Alternative Surface Passivation 202

PREPARATION 202

TREATMENT OF PATTERNED SLIDE AND FLOW CELL ASSEMBLY 202

Supplemental Text 2: An Outline of Paper Figures Detailing a Theoretical STDPAC Tissue Printer 206

Figure 1: Proof of Concept with DNA 207

Figure 2: Proof of Concept with Cells 207

Figure 3: Demonstration with Useful Cells and Fidelity of Pattern Regeneration 207

Figure 4: Demonstration of Method to Create Compositionally Controlled MCF-10A Tissues (over time) 208

Supplemental Text 3: General Materials and Methods 209

General Materials and Reagents 209

Cell Culture 209

DNA sequences 210

Antibodies 211

Preparation of PDMS Flow Cells 211

Preparation of DNA-patterned Surfaces 211

Preparation of DNA-labeled Cells 212

Programmed Assembly and Tissue Embedding of Cell Patterns 213

Immunofluorescence 214

Image Acquisition 214

Cell Growth Measurements 214

HUVEC Extension Measurements 215

Tissue Clearing 215

References 216

Supplemental Text 4: Glossary of Terms, Acronyms, and Phrases *217*

Appendix 3: List of Publications and Patents **219**

Appendix 4: Contributor Validations for Thesis Work Attributions **221**

Table of Figures and Tables

FIGURE 2-1 PDMS flow cell preparation. 14

FIGURE 2-2 Cell surface modification and lipid DNA synthesis scheme. 16

FIGURE 2-3 Glass surface preparation for STDPAC. 23

FIGURE 2-4 Schematic and Timeline of DNA-Programmed Assembly. 28

FIGURE 2-5 PDMS flow cell application. 33

FIGURE 2-6 STDPAC proof of concept with three cell types. 47

FIGURE 2-7 3D culture of MCF-10A tissues following STDPAC. 48

FIGURE 3-1 Large-scale multi-component triangle monomer spiral fractal. 62

FIGURE 3-2 Micron scale artwork. 64

FIGURE 3-3 Reconstituted pattern of a human fingerprint. 65

FIGURE 3-4 Pattern resolution with STDPAC. 67

FIGURE 3-5 3D culture of MCF-10A triangles to compositionally control tissues. 70

FIGURE 3-6 Transfer fidelity of patterns from glass into 3D culture. 73

FIGURE 3-7 Pattern fidelity over time of tissues in 3D culture. 75

FIGURE 3-8 Size and composition-controlled microtissues assembled with STDPAC. 77

FIGURE 3-9 A second example of size and composition-controlled microtissues assembled with STDPAC. 79

FIGURE 3-10 Large tissues synthesized via STDPAC. 81

FIGURE 3-11 Synthetic control of the size and scale of tissues by STDPAC. 83

FIGURE 3-12 Large-scale tissue synthesis via STDPAC. 84

FIGURE 3-13 Spatial and compositional control within large tissues via STDPAC. 86

FIGURE 3-14 Layer-by-layer intra-tissue patterning with STDPAC - the Twinkie. 88

FIGURE 3-15 Multi-scale multi-component tissue synthesis via STDPAC. 90

FIGURE 4-1 Components of the human mammary gland**.** 98

FIGURE 4-2 Investigating normal epithelial tissue growth via STDPACC. 102

FIGURE 4-3 Investigating the effects of Ras epithelial tissue growth on normal epithelial tissues. 105

FIGURE 4-4 Intra-tissue effects of communication of normal and Ras on individual cell proliferation. 108

FIGURE 4-5 Representative images of intra-tissue communication and proliferation given homogeneous or heterogeneous conditions. 109

FIGURE 4-6 Normal tissues growing next to Ras tissues with tissue-specific single-cell proliferation resolution. 111

FIGURE 4-7 The effect of normal tissues growing next to Ras tissues on single-cell proliferation. 113

FIGURE 4-8 Investigating the effects of Ras and normal cell signaling within large tissues on collective cell behavior. 115

FIGURE 4-9 Patterns to investigate the mechanical signaling of fibroblasts on epithelium. 119

FIGURE 4-10 Epithelial tissue boundary disruption by fibroblast mechanical signaling. 121

FIGURE 4-11 Representative images of fibroblast-epithelium interactions over time. 123

FIGURE 4-12 Spatial controls for fibroblast-mediated epithelial tissue boundary disruption. 125

FIGURE 4-13 Representative images of fibroblast-epithelium “capacitor” patterns. 126

FIGURE 4-14 Minimal fibroblast-induced mechanical signaling on Ras epithelial tissues. 128

FIGURE 4-15 Fibroblast-induced mechanical signaling on HUVEC tubes. 130

FIGURE 4-16 Representative images of fibroblast-HUVEC interaction patterns. 131

FIGURE 5-1 Spatial considerations for patterns assembled via STDPAC. 139

FIGURE 5-2 Time considerations for DNA patterning with the Nano eNabler. 141

FIGURE 5-3 Time considerations for STDPAC. 143

FIGURE 5-4 DNA cross reactivity and implications for STDPAC. 146

FIGURE 5-5 SMDPA and order of addition logic. 148

FIGURE 5-6 Building from the bottom up. 149

FIGURE 5-7 The bottom-up nature of surface-mediated assembly. 151

FIGURE 5-8 Different matrix formulations for 3D culture. 153

FIGURE 5-9 Creation of an interface during SMDPA. 155

FIGURE 5-10 Large MCF-10A tube-like tissues growing under different matrix formulations. 157

FIGURE 5-11 MCF-10A tissues growing under different media conditions. 160

FIGURE 5-12 Multi-component pattern growing in LSGS HUVEC media. 162

FIGURE 5-13 Multi-component pattern growing in M87a media. 164

SUPPLEMENTAL FIGURE S3-1 Nearly patterned multi-component MCF-10A tubes. 171

SUPPLEMENTAL FIGURE S3-2 Repositioned pattern of multi-component MCF-10A tubes. 172

SUPPLEMENTAL FIGURE S3-3 Large pattern transfer fidelity in Matrigel. 173

SUPPLEMENTAL FIGURE S3-4 Highly synthetic multi-component patterns of HUVECs and MCF-10A cells. 174

SUPPLEMENTAL FIGURE S3-5 First pass vascular bed multi-component patterns of HUVECs and MCF-10A cells. 175

SUPPLEMENTAL FIGURE S4-1 Scoring fibroblast line experiments. 176

SUPPLEMENTAL FIGURE S4-2 Examples of fibroblast line experiments. 178

SUPPLEMENTAL FIGURE S4-3 Modeled fibroblast mechanical pull. 179

SUPPLEMENTAL FIGURE S4-4 Pattern perturbation by changing Ras cell locations. 180

SUPPLEMENTAL FIGURE S4-5 MFC-10A tubes in Matrigel/collagen. 181

SUPPLEMENTAL FIGURE S4-6. Measuring the impact of composition on single and collective cell behaviors in 3D epithelial microtissues. 182

SUPPLEMENTAL FIGURE S5-1 MCF-10A tubes in Matrigel/collagen. 183

Supplementary Figure S5-2. HUVEC tubes in Matrigel/collagen. 184

Supplementary Figure S5-3. MCF-10A grids growing in Assay Media. 185

Supplementary Figure S5-4. MCF-10A grids growing in LVES HUVEC media. 187

Supplementary Figure S5-5. MCF-10A grids growing in LSES HUVEC media. 189

Supplementary Figure S5-6. Multi-scale multi-component patterns growing in different media. 190

Supplementary Figure S5-7. MCF-10A lines of various spacing growing Matrigel with a 0.5 mg/ml collagen supplement. 192

Supplementary Figure S5-8. MCF-10A lines of various spacing growing at an interface of Matrigel and Matrigel with a 0.5 mg/ml collagen supplement. 194

Supplementary Figure S5-9. MCF-10A lines of various spacing growing at in Matrigel. 196

SUPPLEMENTAL FIGURE S6 Theoretical STDPAC Printer. 198

SUPPLEMENTAL TABLE 1 List of modified DNA sequences.

Chapter 1: Introduction

Why build tissues?

The idea of *de novo* tissue synthesis as a way to cure many diseases has been a popular notion for decades. A liver ravaged by cancer is of no concern if one can simply grow a new liver in a laboratory for transplantation. Indeed, there are entire labs dedicated to building *de novo* kidneys, livers, and hearts via tissue engineering for the purpose of regenerative medicine (Lancaster & Knoblich. 2014). Consistent advances in tissue engineering technology hold much promise to one day making this dream a reality. For this is reason, the field of tissue engineering immediately conjures up thoughts of translational science and human ears grown on the backs of mice (Cervantes et al. 2013). Despite the apparent advances in tissue engineering, tissue biology is still a largely unexplored area in basic science. To build tissues to cure disease, one must first understand the basics tissue biology.

There are two major approaches in the study of tissue biology, *in vivo* by animal models or *in vitro* with three-dimensional organotypic culture (3D culture). When looking at tissue biology through the lens of *in vitro* models, the field is - largely - an extension of the field of cell biology. Decades of focused research have yet to completely unravel the complexities of a single cell, much less an entire tissue. Still, an extension of the study of cell behavior necessarily requires the context of a tissue environment, which is the natural home of most cells in biology. To this end, *in vitro* 3D culture models fill the gap between traditional 2D cultures and complex animal models (Yamada & Cukierman, 2007).

A variety of 3D culture models are used as surrogates for *in vivo* tissue behavior, from the kidney (O'Brien et al. 2002) to the breast (Peterson et al. 2003). These culture systems usually treat the tissue as a single unit, and are useful for observing the collective behavior of all cells within a single microtissue. However, tissues are almost always more complex than the simple microtissues used for experiments in vitro. Tissues are composed of multiple cell type and matrices, with specific architectures that give rise to function (Sasai et al. 2013; Bissel et al. 2003). Organized communication – transferred through chemical, electrical, and mechanical information – allow cells to collectively organize their behaviors and decisions (Nelson & Bissel, 2006). Microtissues, conversely, are homogenous structures grown from either single cells or clusters of cells from a single lineage. In a disease context, such as cancer, tissue biology becomes even more complex. Several advancements have been made over the past few years to give rise to more complex tissue models for the study of normal or disease biology.

3D In Vitro Models and Methods

3D culture of microtissues still dominates most experiments done at the tissue level, but recent advancements allow for the compositional control of the microtissues. The MCF-10A acinus is an *in vitro* breast epithelial 3D culture model that forms a single-layer, polarized, and lumenized microtissue when cultured in a 2.5D or 3D embedded culture system with laminin rich matrix (lrMatrix, Matrigel) (Debnath & Brugge, 2005). Recent advances to the MCF-10A acinus system enable the ability to change the genotype of a single cell within a fully developed acinus (Leung & Brugge, 2012). Low titers of lentivirus containing single oncogenes can be delivered to the 2.5D culture system such that a virus can infect a single cell of an acinus. However, because of the stochastic nature of the viral delivery, only one in 10,000 tissues are likely to be infected by the virus. If one were to arbitrarily assume that 100 tissues are necessary to obtain statistical significance, 1 million tissues are required to successfully draw a conclusion. Conversely, our lab recently demonstrated the ability to use the DNA-programmed assembly of cells to create compositionally controlled clusters of MCF-10As (Liu et al. 2012) that can be cultured in 2.5D culture. However, this strategy only provides compositional control of an MCF-10A cluster before it begins to grow into an acinus, and the control decreases as the acinus matures. Still, with new advancements including recent advances in optogenetics that allow for controlled gene expression in mammalian cells, it is possible to imagine how microtissue composition may be manipulated in a fully embedded in 3D culture (Motta-Menna et al. 2014).

The challenges inherent to controlling tissue structure *in vivo* have motivated efforts to reconstitute, control, and interrogate (design, build, and test) tissue structure *in vitro* to study its impact on single and collective cell behavior. Common to all efforts is 3D cell culture, a requirement for proper structure formation and cell behavior. For example, 3D culture in mechanically and chemically defined ECM gels directs the morphogenesis of stem cells and cancer cells into microtissues that model normal development and tumorigenesis, respectively (van de Wetering et al. 2015; Shamir & Ewald. 2014). However, these rudimentary 3D culture methods rely on intrinsic developmental programs and lack key microenvironmental cues from surrounding tissue components that specify tissue architecture over larger distances. Dielectrophoretic patterning and micromolding can control tissue size and shape to observe their effect on cell anabolic activity, differentiation, autocrine signaling, mechanics, and tissue outgrowth (Albrecht et al. 2006; Nelson et al. 2006). However, dielectrophoresis is limited to ECM and media with low ionic strength, and micromolding techniques struggle when working with multiple cell types in precise arrangements, and with ECM formulations with physiological elasticities (<10 kPa). A variety of techniques have demonstrated that tissue composition, or heterogeneity, contributes to a spectrum of collective cell behaviors absent from more homogeneous tissues (Murphy & Atala. 2014; Stevens et al. 2014).

While a variety of methods have contributed to our understanding to tissue structure and its effect on cell behavior, it remains challenging to control tissue size, shape, composition, and embedding ECM systematically using a single experimental system. Moreover spatial heterogeneity has proven considerably more difficult to reconstitute *in vitro*, particularly for cell-dense tissues and at high spatial resolution. To provide a rapid, modular means of reconstituting multiple aspects of tissue structure in 3D culture, we envisioned a bottom-up strategy that uses DNA patterned substrates as tissue templates and temporary DNA-based cellular adhesions as synthetic linkages between the cellular building blocks. This process, which combines the previously described bottom-up DNA programmed assembly of cells (DPAC) and a top down surfacetemplating strategy, is accordingly called Surface Templated DNA Programmed Assembly of Cells (STDPAC).

References

Cervantes, T. M., et al. (2013). Design of composite scaffolds and three-dimensional shape analysis for tissue-engineered ear. Interface *10*.

Yamada, K.M. & Cukierman, E. (2007). Cell *130*, 601–610.

Sasai, Y. (2013). Cytosystems dynamics in self-organization of tissue architecture. Nature *493*, 318–326.

Nelson, C. & Bissell, M. (2006). Of extracellular matrix, scaffolds, and signaling: tissue architecture regulates development, homeostasis, and cancer. Annu Rev Cell Dev Biol *22*, 287–309.

Lancaster, M. A. & Knoblich, J. A. (2014). Organogenesis in a dish: modeling development and disease using organoid technologies. Science *345*, 1247125–1247125.

Peterson, O.W., et al. (2003). Epithelial progenitor cell liens as models of normal breast morphogenesis and neoplasia. Cell Prolif *36*, 33-44.

O'Brien LE, Zegers MMP, Mostov KE. (2002). Building epithelial architecture: insights from three-dimensional culture models. Nat Rev Mol Cell Biol *3,* 531–7.

Bissell, M. J., Rizki, A. & Mian, I. S. (2003). Tissue architecture: the ultimate regulator of breast epithelial function. Current opinion in cell biology *15*, 753–762.

Debnath J, Brugge JS. (2005). Modelling glandular epithelial cancers in three-dimensional cultures. Nat Rev Cancer *5*, 675–88.

Leung, C. T. & Brugge, J. S. Outgrowth of single oncogene-expressing cells from suppressive epithelial environments. (2012). Nature *482*, 410–413.

Liu, J. S., Farlow, J. T., Paulson, A. K., LaBarge, M. A. & Gartner, Z. J. Programmed cell-to-cell variability in Ras activity triggers emergent behaviors during mammary epithelial morphogenesis. (2012). Cell Reports *2*, 1461–1470.

Motta-Mena, L.B., Reade, A., et al. (2014). An optogenetic gene expression system with rapid activation and deactivation kinetics. Nature Chem Biol *10*, 196–202.

Van de Wetering, et al. (2015). Prospective Derivation of a Living Organoid Biobank of Colorectal Cancer Patients. Cell *161*, 933–945.

Shamir, E. R. & Ewald, A. J. Three-dimensional organotypic culture: experimental models of mammalian biology and disease. (2014). Nature Reviews Molecular Cell Biology *15*, 647–664.

Albrecht, D., Underhill, G., Wassermann, T., Sah, R. & Bhatia, S. Probing the role of multicellular organization in three-dimensional microenvironments. (2006). Nat Methods *3*, 369–375.

Nelson, C., Vanduijn, M., Inman, J., Fletcher, D. & Bissell, M. Tissue geometry determines sites of mammary branching morphogenesis in organotypic cultures. (2006). Science *314*, 298–300.

Murphy, S. V. & Atala, A. 3D bioprinting of tissues and organs. (2014). Nat Biotechnol *32*, 773–785.

Stevens, K. R. *et al.* InVERT molding for scalable control of tissue microarchitecture. (2013). Nat Commun *4*, 1847.

Chapter 2: The Unabridged STDPAC Protocol

Introduction

New scientific innovations are published almost daily. A truly useful scientific innovation, however, needs be broadly applicable within its field of use. If one specific technology were developed to answer one scientific question, it would become obsolete after that singular question was answered. Thus, a method worthy of being labeled an innovation needs to be modular – that is, able to be molded to answer a wide range of questions. Additionally, as with all experimental methods, the method must try to be orthogonal to the biological system it is perturbing. If a method necessarily affects the biological system that is being examined, all results would be skewed and not applicable to its natural biological counterpart. Similarly, the method should be reproducible, not only in the results produced experiment-to-experiment, but reproducible also in the hands of other scientists. Our approach to method design focused on these three aspects: modularity, orthogonality, and reproducibility.

In nature, DNA is mostly used as an encoder of information. The properties that enable DNA to encode information in biological settings also enable its use as a smart adhesion molecule, useful for applications from cellular barcoding to DNA origami (Rothemund. 2006; Pinheiro et al. 2011; Mali et al. 2013). As a programmable adhesion tool, synthetic single-stranded DNA (ssDNA) has also been demonstrated for use in attaching cells to other biological or non-biological surfaces (Gartner & Bertozzi. 2009; Hsiao et al. 2010). If the DNA self-assembly can be utilized to create macromolecular structures in the nano-scale and create assemblies of cells in the micro-scale, its utilization on the meso-scale should also be possible.

Surface Templated DNA-Programmed Assembly of Cells (STDPAC) is a powerful method that enables rapid design and synthesis of compositionally controlled, meso-scale patterns of tissues. The complexity of the method requires that the utmost care is given to every step of the method. Details that seem like minutia are likely to introduce imperfections into the final tissue patterns, and certain steps of the method require dexterity to the level of a Tibetan monk creating a Kalachakra Mandala. For these fragile steps, even an overdose of caffeine can be fatal to the successful completion of an experiment. However, with practice, any trained scientist can use STDPAC to create a pattern of micro-scale tissues from conception to 3D culture within a single day.

New scientific methods and innovations are mostly built upon the shoulders of existing techniques. As such, the foundations of STDPAC are built upon a combination of several different methods. Specifically, a breakdown of STDPAC yields five component methods: patterning of DNA, self-assembly of cells via DNA hybridization, embedding in matrix, and 3D embedded culture. Micro-scale patterning of DNA is possible through many methods, including lithographic (Onoe et al. 2012) and soft-lithographic methods (Bernard et al. 2000). We employ a molecular printing system developed by BioForce Nanosciences to rapidly create DNA patterns. Expensive instrumentation, as noted, is not required. The component method of self-assembly of cells includes concepts from DNA-programmed assembly (Gartner & Bertozzi. 2009) and cellular microfabrication (Onoe et al. 2012). Matrix embedding methods are also general, but the method of combining microfluidics and gel embedding is recognizant of boundary microfluidics (Sung et al. 2011). Finally, 3D embedded culture is and has been widely used for decades (Shamir & Ewald. 2014).

STDPAC is modular specifically because its component methods are open to multiple technologies. And because the DNA-mediated adhesions are temporary and orthogonal to biological sequences, the method is orthogonal to the biological systems it creates. Reproducibility also becomes abundantly clear during data analysis of multiple technical and biological replicates, detailed in the later chapters.

The following sets of protocols were written for detail and practicality in application so that any trained scientist can learn how to generate tissues models with the STDPAC method.

Protocol 1: Preparation of PDMS Flow Cells

It is possible to create flow cells using photolithography, but not every lab has access to a clean room, nor can they afford to have custom chips made. As such, the protocol highlights a method in which simple lab tools create makeshift flow cells of sufficient height and various dimensions (Figure 2-1A).

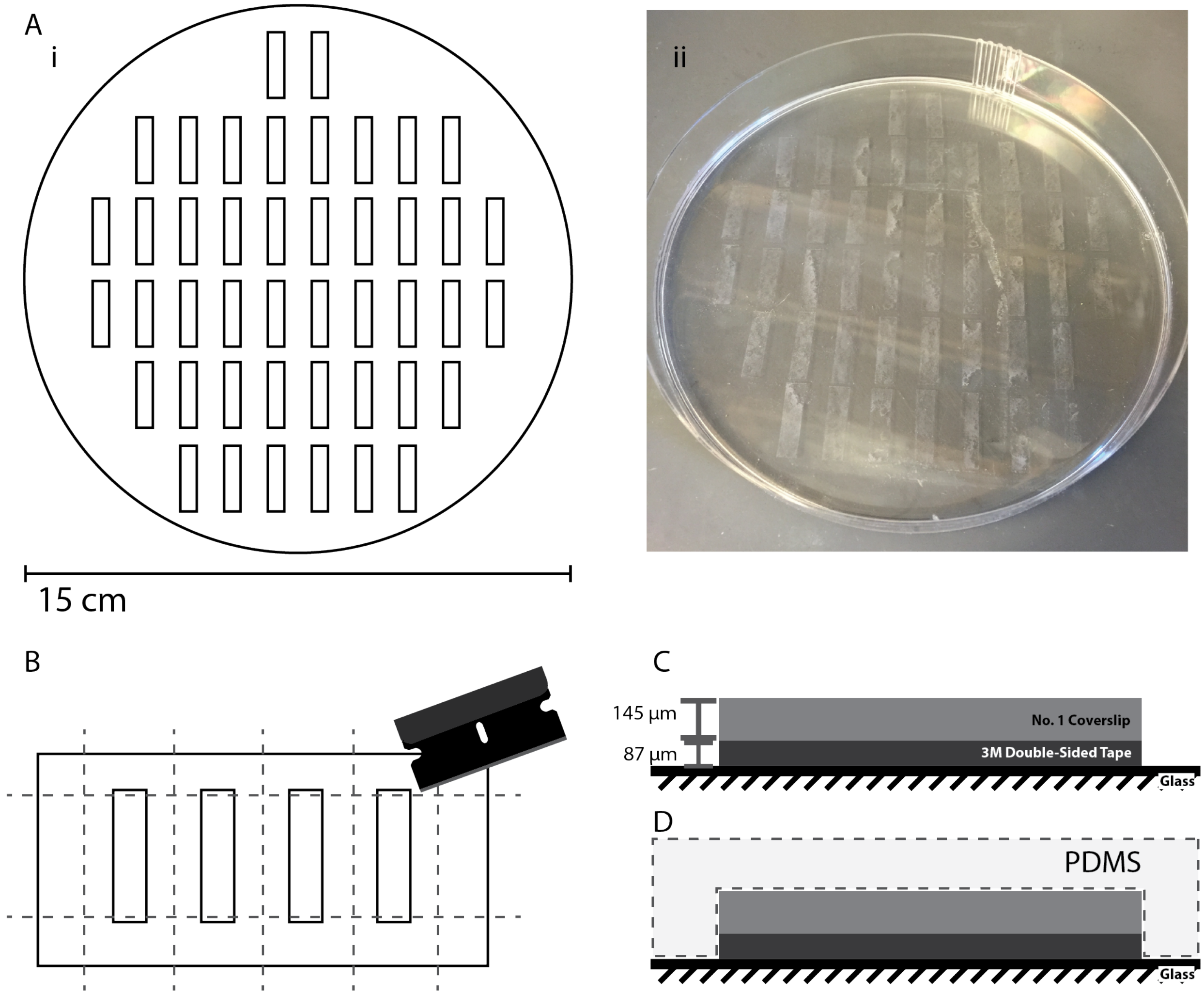

Figure 2-1. PDMS flow cell preparation. (A) A PDMS flow cell master is created as a pattern of flow cells (i) within a 15-cm petri dish (ii). (B) Individual flow cells are prepared by cutting the flow cells such that inlets and outlets are open to flow and PDMS side walls are sufficiently wide to support the flow cell roof. (C) Individual flow cell masters are created by stacking 3M double-sided tape and a number 1 thickness coverslip to create a structure approximately 232 µm in height. (D) PDMS is cured over the flow cell master to create PDMS flow cells.

To create flow cells, it is important to first choose the dimensions desired. Determining the proper dimensions of a flow cell is important. The dimensions of the flow cell can limit the size of a given pattern, but are more likely to limit the number of events that fit into a single experiment. This is due to the scale in which the technology is most proficient. Generally, the flow cells used are sized on the scale of single centimeters.

However, the technique is developed for studying cell-cell and cell-tissue interactions on the scale of tens to hundreds of microns. While one can build centimeter long tissues, as demonstrated in Chapter 3, the utility of the technique is with patterns/events across a few hundred microns. Assuming that events must be spaced a large fixed distance apart, depending on diffusion and mechanical force translation across a single matrix, much of the patterns within the flow cell must be occupied by empty space.

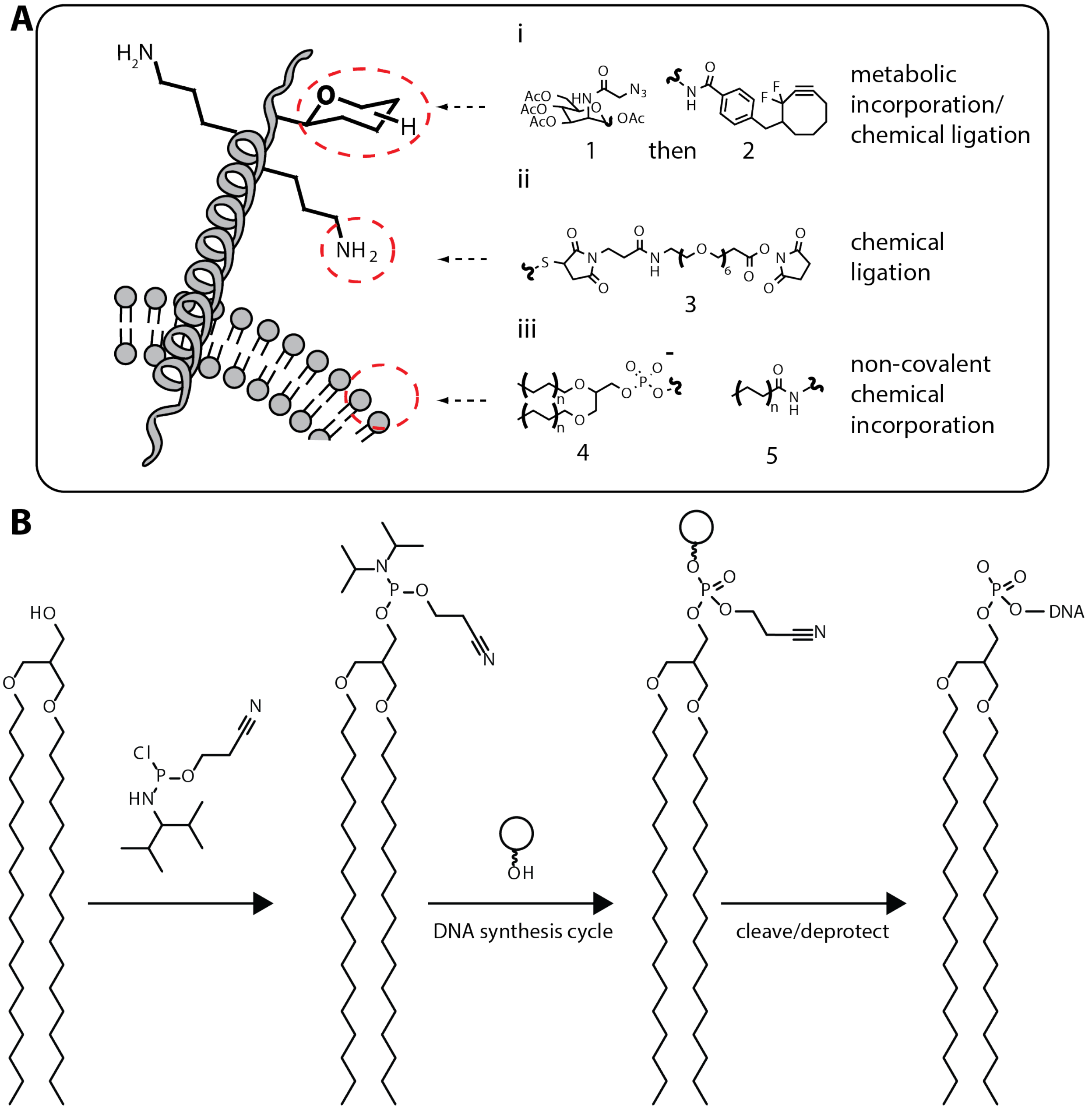
A
i
metabolic incorporation/ chemical ligation
1
then
2
ii
chemical ligation
3
iii
non-covalent chemical incorporation
4
5
B
DNA synthesis cycle
cleave/deprotect
DNA

Figure 2-2. Cell surface modification and lipid DNA synthesis scheme. (A) Cell surfaces can be modified with DNA by targeting unnatural cell-surface glycans via metabolic incorporation (i), via chemical ligation to free lysines (ii), or via non-covalent chemical incorporation in the lipid membrane (iii). (B) DAG DNA is prepared by the chemical ligation of a lipid tail onto the 5-prime end of an oligonucleotide sequence during traditional oligonucleotide synthesis with phosophoramidites.

Creating the Flow Cell Masters

1. Obtain No. 1 size coverslips and cut them into the x and y dimensions desired using a diamond scribe. Using No. 1 size coverslips is critical - thicker coverslips will cause the height of the flow cell, and thus the matrix in later steps, to become greater than the typical diffusion limit for nutrients in biology.

2. Use 3M double-sided tape and attach it flush against one side of the cut coverslips. The principle of tape application is the same as applying a screen protector on a phone. If at all possible, ensure that there are no air bubbles in between the tape and the glass coverslip. The total thickness of the coverslip and the double-sided tape should be no greater than 250 microns, including the manufacturing margins of error in take and coverslip thickness (Figure 2-1C).

3. Apply the taped coverslip onto the petri dish and gently press to permanently attach it to the surface (Figure 2-1C). While any petri dish is sufficient, using a large petri dish (> 10cm) is helpful in creating a large “master” of flow cells that can provide flow cells for many experiments. The rest of the protocol assumes that a 15 cm petri dish was used.

4. Repeat step 3 as necessary to create a grid of coverslip “plateaus.” Ensure that there is at least 5 mm of distance between each of the coverslips (Figure 2-1B).

Preparation of PDMS Flow Cells

1. Add 20 grams of Sylgard 184 (PDMS) and 2 grams of the curing agent into a 50 mL falcon tube - a 10 to 1 ratio. It is easiest to place the falcon tube in a rack and on a tared scale while slowly pouring the Sylgard into the falcon tube through a funnel.

2. Mix the polymer and curing agent well to ensure that the curing agent is evenly dispersed throughout the entire PDMS mixture. It is useful to use a plastic stir rod or a plastic 10 mL pipette tube to stir the thick polymer. If mixed correctly, there will be many bubbles that are introduced into the tube to the point that the Sylgard seems white.

3. Take the entire tube of prepared PDMS and de-gas the entire mixture by placing it in a vacuum chamber (connected to the house vacuum) and waiting 1 to 3 hours for the bubbles to dissipate. It is easiest to place the falcon tube, uncapped, into a rack and placing the rack inside of the vacuum chamber. A 50 mL falcon tube is used because the bubbling Sylgard foam created by the de-gassing process does not overflow past the opening of the falcon tube. If the Sylgard still contains air bubbles after 3 hours, move it to a more powerful vacuum source. If a more powerful vacuum is not available, proceed to the next step, and include the second de-gassing step.

4. Carefully pour the entire solution onto the master flow cell pattern after the de-gassing is complete and take care not to introduce any air bubbles. If air bubbles

are introduced, the entire master with PDMS can be moved into the vacuum chamber for a second de-gassing step. The fluid PDMS polymer should completely cover the individual flow cell masters (Figure 2-1D).

5. Cover the petri dish and leave the flow cell master on a level surface overnight, using a bubble level if necessary. Ensuring that the flow cell master is level is very important - a slight tilt could cause the PDMS to pool to one side of the petri dish, creating uneven, flimsy, and useless flow cells. The flow cell master may even become ruined if it becomes impossible to remove residual thin PDMS. Forgetting to cover the petri dish may cause dust particles to become trapped in the PDMS and affect the optical clarity of the flow cells.

6. Place the flow cell master in a 70 ºC oven for 4 hours to finish curing the PDMS after the PDMS mostly solidifies overnight. The PDMS can finish curing over a longer period of time in a cooler oven temperature or a shorter period of time in a warmer oven temperature. It is important to consider the melting point of the petri dish plastic. Even if the plastic does not melt, the plastic may warp, which would ruin the flow cells, and worse, the flow cell master.

7. Remove the flow cells from the oven and cool to room temperature. It is important not to over-cure the PDMS flow cells by leaving them for a prolonged period of time in the oven - the PDMS will become to brittle for use in STDPAC.

8. Remove the slab of flow cells from the flow cell master petri dish by inserting, with some force, a flat spatula between the PDMS and the petri dish wall. Once

the spatula is inserted between the PDMS and the petri dish wall, the edge of the PDMS pattern can be pried out of the petri dish, enabling a small area to grip and peel the PDMS out of the petri dish.

9. Cut out as many flow cells as required for the experiment. A typical experiment utilizes four flow cells (Figure 2-1B). If possible, cut out a strip of 4 flow cells, taking care not to cut out individual flow cells, or cutting openings into the outlet or the inlet. Do not yet cut along the dotted lines in Figure 2-1B.

10. Clean the PDMS flow cells by sticking and removing scotch tape across the entire surface of the flow cells multiple times. This will ensure that dust and debris are removed from the PDMS, but will not render the flow cells sterile. The subsequent plasma treatment can sterilize the flow cells. It is important not to soak the PDMS flow cells in ethanol because the flow cells will absorb the ethanol and swell, becoming brittle or slowly releasing ethanol into the cell pattern during STDPAC.

11. Place the strip of PDMS flow cells flat into the inside surface of a brand new 10 cm petri dish. New petri dishes are required to minimize particulates that may dirty the flow cells. Ensure that the flow cells are placed upside down - the tops of the flow cells are completely adhered to the plastic of the petri dish, exposing the indentations to the atmosphere (Figure 2-5B). If possible, adhere the PDMS flow cells to the petri dish such that there are no air bubbles between the flow cells and the petri dish plastic. The placement of the flow cells is important for the next step.

12. Treat the flow cells with pure or atmospheric oxygen plasma using a plasma cleaner (Figure 2-5B). This step serves two purposes - to render the flow cell insides hydrophilic, and to sterilize the surface of the flow cell that will be exposed to cells. Depending on the machine, this amount of plasma applied will vary. The power and level of plasma varies from machine to machine, thus the specific settings for the machine must be empirically derived to ensure proper plasma treatment.

13. Cut out individual flow cells after the plasma treatment is complete - demonstrated by the dotted lines in Figure 2-1B. Turning over the flow cells immediately after plasma treatment is recommended to minimize dust collection onto, what will become, the fluidics chamber. Flow cells must be cut and applied to glass within 5 minutes of plasma treatment - otherwise the effects of surface oxidation diminish, complicating the gel-lifting step. This process is facilitated with the use of a cutting mat that is cleaned with tape prior to use.

Protocol 2: Surface Patterning, Slide Preparation, and Flow Cell Application

Care for the slides by keeping them under vacuum in dry conditions - a vacuum desiccator - and making sure that they are kept in a covered container to keep them dust free. Slides are expensive and delicate, but most importantly, it’s very hard to judge the quality of a slide without a significant time investment in patterning and attaching cells. That means holding it properly, never letting the patterning side touch any surface, using powder-free gloves, etc. All references to the aldehyde-silanized glass slides will be shortened to slide.

Handle the slide with care by holding the slide only along the edges and making sure that you are wearing powder free gloves. Holding the slide only by the sides is important to keep the printable surface of the glass slide free of dust or particulates, which can easily block the printing of the DNA spots and necessitate the preparation and printing of an entirely new slide.

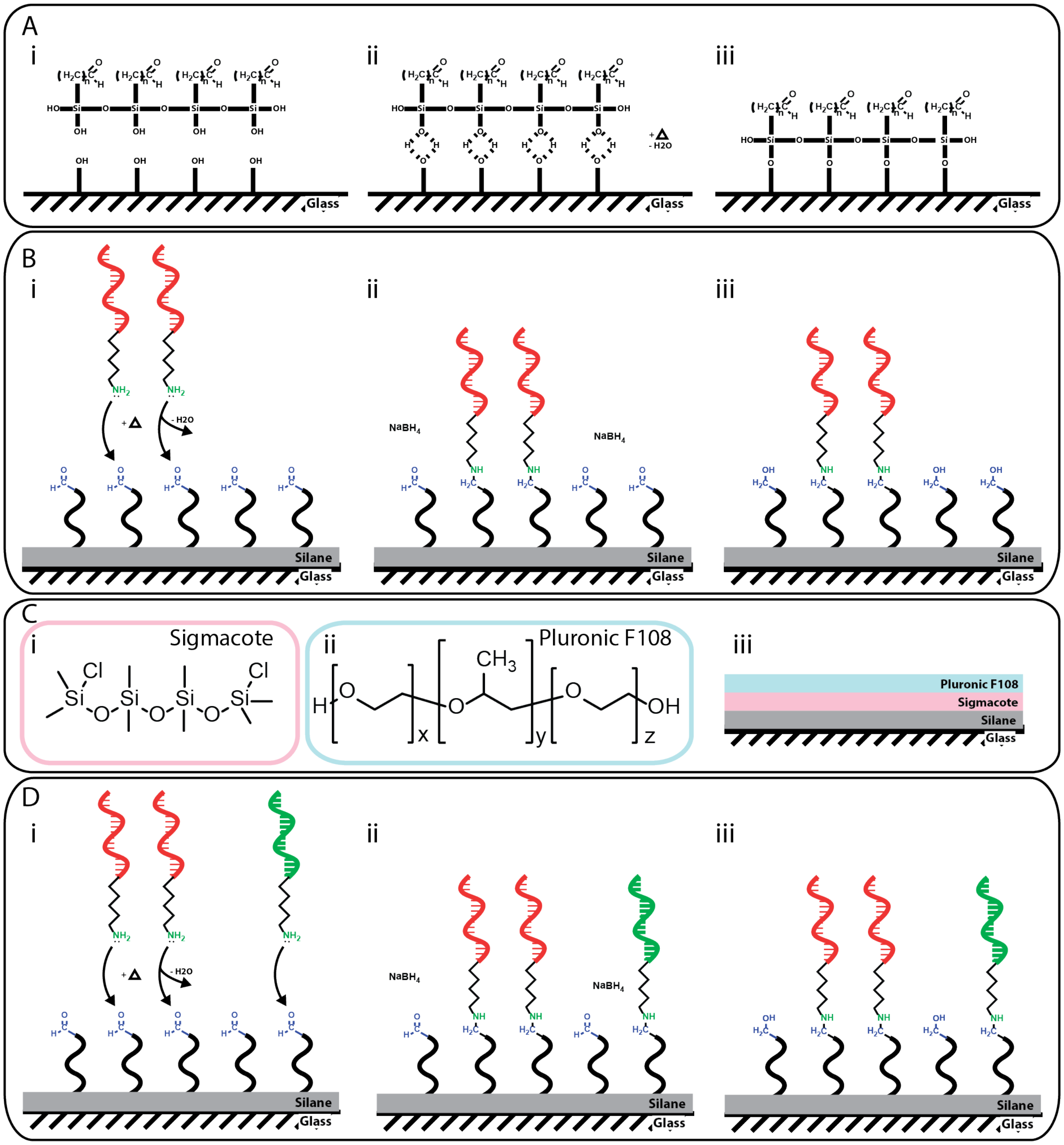
A
i
ii
iii
Glass
HO
OH
Si
O
H2O
B
Silane
Glass
NH2
NaBH4
NH
OH
C
Sigmacote
Pluronic F108
Cl
Si
O
CH3
H
x
y
z
Pluronic F108
Sigmacote
Silane
Glass
D

Figure 2-3. Glass surface preparation for STDPAC. (A) A glass surface is modified with aldehydes via stepwise aldehyde silanization (i - iii). (B) DNA is covalently patterned onto the glass slide via reductive amination (i) and the free aldehydes fully reduced to alcohols with the addition of sodium borohydride (ii - iii). (C) Sigmacote (i) and pluronic F108 (ii) are added stepwise to the DNA-patterned glass substrate to passivate the surface against non-specific attachment. (D) Multiple sequences of DNA are patterned onto the glass substrate depending on the pattern (i - iii).

Slides can be purchased or created (Figure 2-3A).

1. Remove the slide from the desiccator and place it into a new 10 cm petri dish and apply the cover. When handling the slide, never touch the flat surfaces of the slides and only grip it along the edge.

2. Retrieve the diamond scribe in the writing hand and hold the slide in the other hand. Make sure that the slide is retrieved such that the flat surface that touched the bottom of the petri dish is facing upwards and ready for inscription. Do not inscribe a slide on its untouched surface - that surface will only be used to print DNA.

3. Create etch marks on only one side of the glass to give the slide an identity, differentiate between the etched side and the DNA-patterned side, and to denote where the DNA pattern will be printed (Figure 2-5A). A diamond scribe should be used to make the etch marks to ensure that the marks stay in place throughout the wash steps. A tungsten carbide scribe is not recommended, as the etch marks are not easily visible by eye. There needs to be an asymmetric mark to denote which side of the slide is contains the etchings and which side contains the DNA patterns. For example, PA, PB, etc. are commonly used to mark the slides as an asymmetric identifier (Figure 2-5A).

4. Place the slide, etch marks down, into the 10 cm petri dish and keep it covered to minimize dust settling onto the glass slide.

5. Bring it to the Nano eNabler and pattern DNA onto the slide (Support Protocol 2). A DNA-patterned slide is referred to as a substrate.

6. Place the completed substrates in a drying oven at 120 ºC for a minimum of 15 minutes and a maximum of 3 hours. Drying the spots of DNA with heat catalyzes the reductive amination between the amine-modified past the Schiff's base to completion - the heat catalyzes the dehydration of the immine formed between the amine-DNA and the aldheyde glass to form a covalent bond (Figure 2-3B). Place the substrates only into the drying oven and do not place any plastic into the oven unless the melting temperature far exceeds the oven temperature.

7. Remove the substrate and place it etch-marks-down onto a cooling rack to allow the slide to cool to room temperature. Proper cooling will eliminate the risk of the substrate melting the plastic petri dish.

8. Place the cooled substrate into the 10 cm petri dish and store it in a vacuum desiccator until it is ready for use. Maximal storage length without pattern degradation for printed substrates is qualitatively found to be 2 weeks.

9. Take the substrate out of storage and place it into a petri dish, DNA pattern-side up. Substrates are sometimes stored under vacuum in slide racks rather than petri dishes to optimize space saving.

10. Wash the patterned slide with the wash solution (aqueous 0.1% SDS w/v) by adding enough wash solution to the petri dish such that the solution sufficiently

covers the entire slide. Gently swish the wash solution in the dish to ensure that the entire slide surface is being washed for a minimum of 5 seconds.

11. Decant the wash solution and the repeat step 10 one additional time.

12. Wash the slide, as described in step 10, with DI water.

13. Decant the DI water and repeat two more times. After the completion of all the wash steps, there should be a wet slide in a petri dish with most of the water removed.

14. Take out Sigmacote from the refrigerator and slowly warm up to room temperature. It is important that the Sigmacote is at room temperature because condensation can occur on the inside of the glass bottle. The silanes in Sigmacote are reactive with water and are susceptible to polymerization if water is introduced into the organic solvent in which the silanes are dissolved (Figure 2-3C). This renders the entire stock of Sigmacote useless because it creates an uneven layer on the surface of the patterned glass. It is simplest to take the Sigmacote out of the refrigerator before any other steps are taken.

15. Prepare the reducing solution (0.25% w/v $NaBH_4$, 25% pure ethanol, and 75% PBS). For every substrate, combine 50 mg of sodium borohydride, 5 mL pure ethanol, and 15 mL PBS - 20 mL of solution is sufficient to reduce a slide. All of the chemicals and solvents can be combined in a 50 mL falcon tube. The solution should produce visible bubbling of hydrogen gas.

16. Add the reducing solution to the petri dish with the substrate. Bubbles should begin to form along the surface of the substrate as the NaBH4 reacts with the free aldhehydes on the glass surface. Allow the reduction of the aldehyde slide to continue for a minimum of 15 minutes. Excess time in the reducing solution is not harmful to the patterned slide. It is strongly suggested that the petri dish with the substrate and reducing solution is placed on a orbital shaker for the duration of the slide reduction. This allows even distribution of the reducing solution across the substrate.

17. Decant the reducing solution into a clean container and neutralize the waste with weak acid. The liquid waste can be poured down the drain once properly neutralized.

18. Wash the substrate with as described in steps 10 - 13.

19. Blow the substrate dry by using a high-pressure air source, such as the house air. It is easiest to use a strong airflow to push water droplets off of the glass slide as in an automated car wash.

20. Bake the substrate in the drying oven at 130 ºC for an additional 5 minutes only. Make sure that the slide is out of the petri dish (which will melt) and that the DNA side is facing up (never touching another surface). The substrate is baked to remove any residual water that may have adsorbed onto the glass surface.

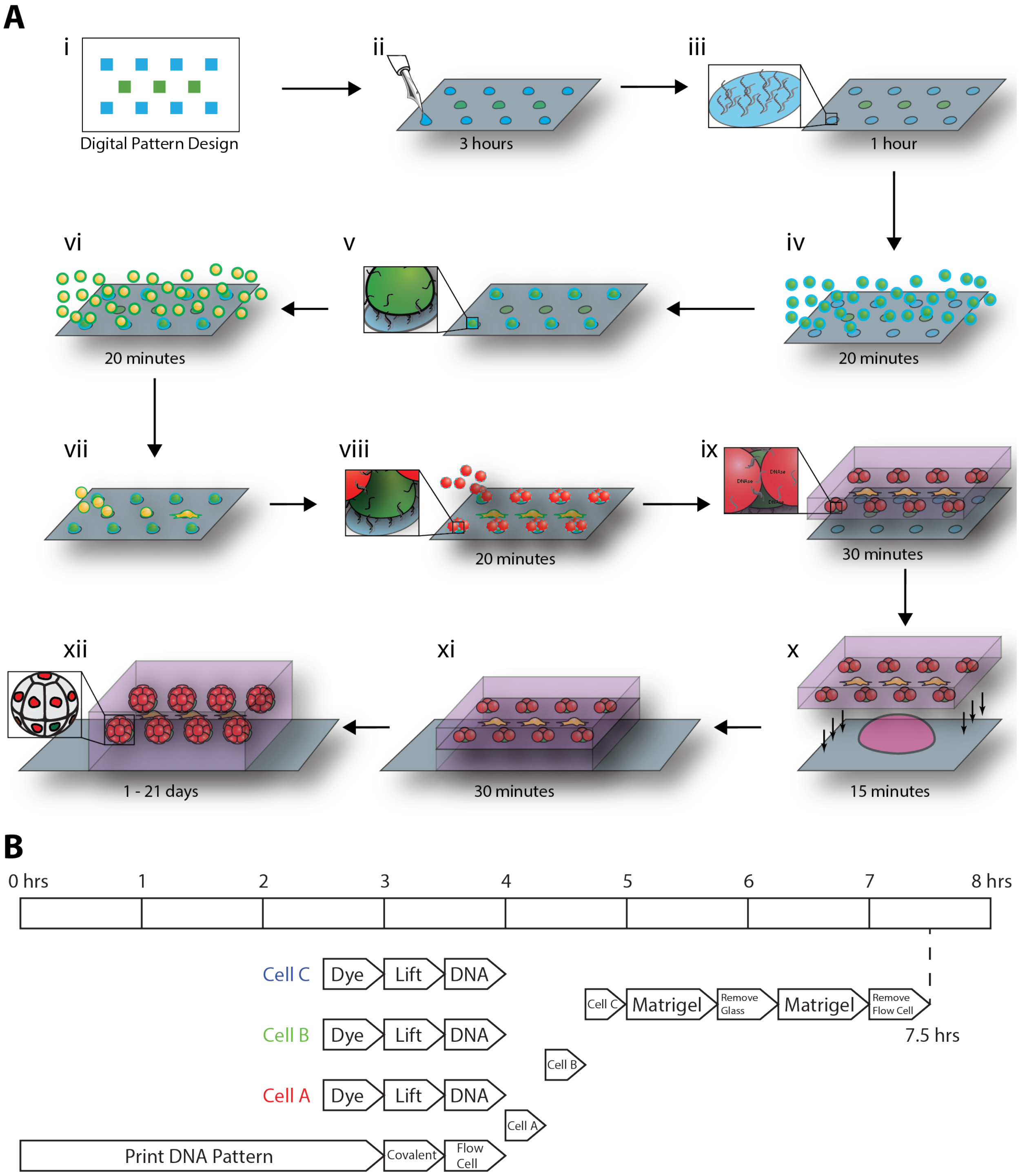
A
i
Digital Pattern Design
ii
3 hours
iii
1 hour
iv
20 minutes
v
vi
20 minutes
vii
viii
20 minutes
ix
30 minutes
x
15 minutes
xi
30 minutes
xii
1 - 21 days
B
0 hrs
1
2
3
4
5
6
7
8 hrs
Cell C
Dye
Lift
DNA
Cell B
Dye
Lift
DNA
Cell A
Dye
Lift
DNA
Print DNA Pattern
Covalent
Flow Cell
Cell A
Cell B
Cell C
Matrigel
Remove Glass
Matrigel
Remove Flow Cell
7.5 hrs

Figure 2-4. Schematic and Timeline of DNA-Programmed Assembly. (A) A digital pattern is conceived (i), patterned into DNA (ii), and covalently bound to the surface (iii). Cells bearing complementary strands are incubated (iv), attached (v), and repeated for each cell type (vi - vii). Cells can be assembled onto specific, attached cells (viii). The entire pattern is embedded into matrix (ix), lifted off of the glass within cured matrix (x), and placed on additional matrix (xi) to crate a fully embedded pattern (xi) for 3D

organotypic culture over multiple days (xii). (B) A generalized timeline of the entire STDPAC process is outlined.

21. Remove the slide from the oven and allow it to cool to room temperature by placing it on a cooling rack. Do not place the slide on a surface that has a melting temperature lower than the drying oven.

22. Place the cool slide in a new petri dish with the etch marks facing down.

23. Add 60 µL of room temperature Sigmacote directly on the DNA-patterned surface of the patterned slide and immediately place a large coverslip (24 mm x 60 mm) on top of the Sigmacote solution to spread the Sigmacote across the entire surface of the slide. Make sure that the entire surface of the slide has touched the Sigmacote by sliding the coverslip on top of the substrate and spreading the Sigmacote to all areas of the slide. The Sigmacote can be delivered with a P200 pipette.

24. Immediately remove the coverslip and fully immerse the substrate in pure ethanol as soon as the entire surface has come into contact with the Sigmacote. A 50mL falcon tube full of ethanol is a sufficient vehicle to fully immerse a substrate into liquid. Cap the falcon tube and invert the tube of ethanol with the substrate 10 times.

25. Carefully remove the substrate from the tube of ethanol, minimizing the amount of ethanol left on the surface of the substrate, and place it in a second tube of

ethanol until it is fully immersed. Paddle tweezers may be used to handle the substrates. Invert the tube of ethanol and the substrate 10 times.

26. Carefully remove the substrate from the tube of ethanol and minimize the amount of ethanol left on the surface of the substrate and place the substrate in a container of DI water until fully submerged. Invert the tube of DI water and substrate 10 times.

27. Carefully remove the substrate from the tube of DI water and blow dry with a high-pressure air source, as in step 19. The contact angle of water droplets on the side of the substrate with Sigamacote applied should be vastly smaller than the side without Sigmacote applied. The substrate is now ready for the addition of flow cells. An alternative passivation technique can be found in the supplemental text.

28. To administer the final cuts to the flow cells, place them chamber-face-down on a clean surface (a new petri dish) and cut them into individual flow cells by cutting an inlet and outlet approximately 500 um from each end of the flow cell (Figure 2-1B). Afterwards, cut a sliver of PDMS from each of the flow walls to ensure that there are no hydrophilic surfaces available except for the flow cell chamber and the bottoms of the flow cell walls.

29. Place individual flow cells such that the DNA pattern is in the middle of the flow cell, and the inlets and outlets are minimally 2 mm from the edge of either side of the patterned glass slide (Figure 2-5A). After the DNA patterns are printed, etch

marks can be administered on either side of the pattern to permanently mark the location of the pattern and to facilitate flow cell placement (Figure 2-5C). After placement, flow cell walls should be gently pressed to remove any air bubbles between the flow cell wall and the glass slide. Occasionally, a dust particle or fiber may be trapped between the flow cell wall and the glass slide. Unless the particulate is partially inside the flow cell or large enough to traverse the entire flow cell wall to connect the inside of the flow cell to the outside of the flow cell, the experiment can proceed without re-administering the flow cell. If any of these previous conditions are true, the flow cell must be taken off the slide, the particulate cleaned off with fine tweezers, and the flow cell reapplied. All of this should be completed as quickly as possible, as the oxidized surface of the PDMS quickly reduces over a matter of minutes.

30. Prime the flow cells once they are applied onto the substrate with 50 µL of priming buffer (1% w/v pluronic F108, 10% v/v FBS, RPMI 1640 media). Flow cells must be wetted to allow continuous flow from the inlet to the outlet. No air bubbles should be introduced into the flow cell, as they can obstruct the deposition of cells onto the DNA pattern as well as produce failures during the lifting stage of STDPAC. To prime the flow cells, the patterned slide with flow cells applied should be turned vertical and 50 µL of priming buffer should be administered to the inlet of each flow cell, which is facing the ground. Because the flow cell chamber is hydrophilic, the priming buffer will instantly travel through the entire flow cell and completely fill the flow cell, even if the priming buffer is traveling opposed to gravity. Care should be taken not to pipette any air bubbles

into the inlet of the flow cell, as small bubbles may be sucked into the flow cell with the liquid. Small bubbles within flow cells have a tendency to remain trapped within the flow cell chamber and occlude cells and gel from their DNA spots. The proteins contained within the priming buffer predispose the solution to bubble formation, thus the solution must be carefully pipetted.

31. Block the substrate surface to render the surface completely to unreactive to cells. The pluronic f108 contained within the priming buffer acts as a blocking agent for the passivation of a glass slide (Figure 2-3C). The priming buffer should be left in the flow cells at 4oC. Substrates can be kept cold at 4 ºC by keeping them in a petri dish and placing the dish on ice in an ice bucket. The priming buffer should be left incubating the insides of the flow cells, and thus on the DNA surface of the substrate, for a minimum of 5 minutes and no longer than 10 minutes.

32. Wash out the flow cells with the same buffer in which cells are kept for STDPAC. The default buffer is PBS CMF (calcium magnesium free PBS). To wash out flow cells, 4 flow cell volumes of wash buffer should be passed through the length of the flow cell. In most scenarios, the wash buffer will be the same as the buffer in which cells are kept. Due to laminar flow, 4 flow cell volumes are required for complete displacement of the contents of the flow cell. The majority of flow cells used for the experiments subsequently described are of the dimension 4.5 mm x 16 mm x 250 um. These flow cell volumes are calculated to be 18 µL. To be safe, these flow cells are washed with 100 µL of wash buffer. Specifically, flow cells

are washed by flowing through 50 µL of PBS CMF, discarding the effluent, flowing through another 50 µL of PBS CMF, and discarding the effluent again.

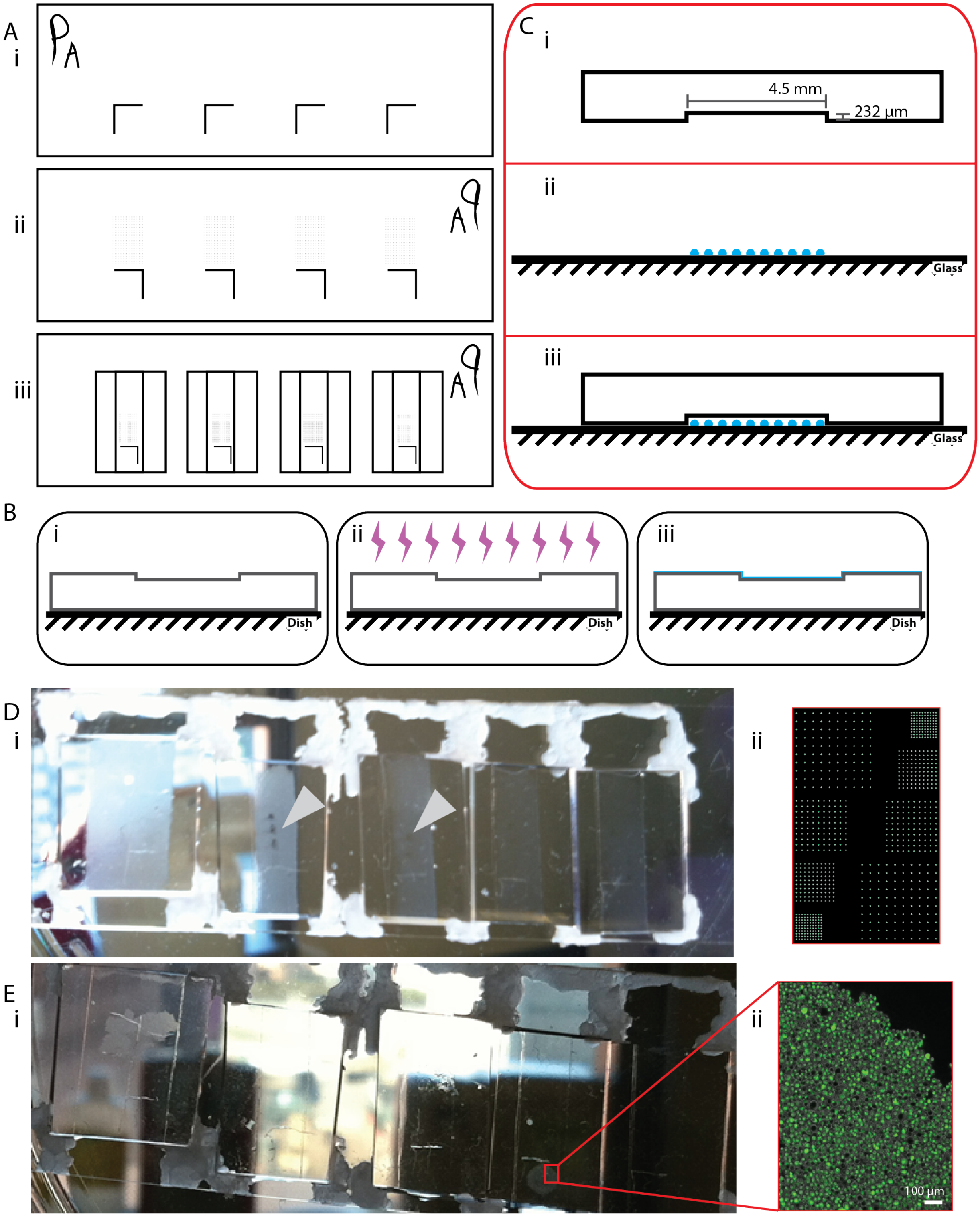
A
i
ii
iii
C
i
4.5 mm
232 µm
ii
Glass
iii
Glass
B
i
Dish
ii
Dish
iii
Dish
D
i
ii
E
i
ii
100 µm

Figure 2-5. PDMS flow cell application. (A) A glass slide is etched (i) patterned (ii)

and fitted with flow cells (iii). (B) Flow cells are placed channel-side up in a petri dish (i) plasma treated (ii) and rendered hydrophilic only on one side (iii). (C) Individual flow cells are created to fit specific dimensions (i) and placed specifically over DNA patterns on the substrate (ii - iii). (D) STDPAC is performed to create single-cell resolution patterns seen in large scale (i) and as a digitized pattern (ii). (E) Circular patterns of cells can be created with low resolution (i-ii).

Protocol 3: DNA Cell Labeling

Several methods of cell labeling with DNA have been applied to STDPAC (Figure 2-2A). For the vast majority of experiments, dialkyl-glycerol (DAG) DNA was synthesized as previously described and used to label cells with ssDNA (Figure 2-2B) (Selden et al. 2012). However, there are nuances in the DNA-labeling process that are specific to STDPAC. Certain cell types, including primary epithelial cells and primary and immortalized fibroblast cells were challenging to label with DAG DNA previously described. For these challenging cell-types, we adopted an improved non-covalent DNA labeling method developed by a colleague (Weber et al. 2014).

Labeling Cells with DAG DNA for STDPAC

1. Prepare 5 μM solutions of DAG DNA in PBS CMF. The absence of calcium and magnesium in the PBS is critical - it removes the possibility for proper adherens junction formation, and thus decreases non-DNA mediated aggregation of cells. Typically, DAG DNA is stored measured and dry in Eppendorf tubes. Before an experiment, the DAG DNA is rehydrated in PBS CMF to create a 5 μM solution.

To rehydrate the DAG DNA, it is best to vortex the tube for 30 seconds after triterating the PBS CMF 30 times with a P200 pipette.

2. Remove cells from passaging and re-suspend the cells such that there are 1 million cells in 100 µL of cell buffer (PBS CMF or PBS equivalent), with each million cells separated into individual 1.5 mL Eppendorf tubes. Cells must be assayed for viability with a hemocytometer or hemocytometer equivalent. Traditionally, under-confluent and over-confluent cells in culture exhibit diminished viability. For MCF-10A cells, maximal viability is seen at 90% confluency. The preparation of cells also require that they be washed thoroughly before labeling with DNA, at least 3 times in PBS CMF, to prevent the failure of DNA cell labeling. Excess proteins remaining from cell culture may inhibit the labeling of cells with DAG DNA. Alternatively, the following buffers have also been used to minimize natural cell-cell adhesion: PBS CMF + 0.04% w/v EDTA and PBS + 1% w/v BSA.

3. Pellet the cells and remove the supernatant. Pellets of 1 million cells are small, and extra care must be taken in supernatant removal. Typically, a P200 pipette is used to carefully suck up the supernatant after tilting the Eppendorf tube 30 degrees to pool the supernatant away from the top of the pellet.

4. Immediately add 50 µL of the 5 µM DAG DNA solution to each pellet and carefully re-suspend the cells into the DAG DNA solution by slowly triterating with a P200 pipette 5 times. Take care not to introduce any air bubbles into the pellet, as they can cause sheer and cell death during the triteration process. It is

important to carefully note which cell population is labeled with which sequence of DNA in order to ensure that no mistakes are made later in the STDPAC process.

5. Place each Eppendorf tube of DNA labeling cells onto a shaker and shake on a low setting for 5 minutes at room temperature. Depending on the shaker, the settings can vary. It may be prudent to do a viability test of the cells before and after shaking to find an optimal shaker setting. Increasing the DNA labeling time past 10 minutes will begin to decrease the viability of the cells.

6. Remove excess DAG DNA from the cells by washing the pellets three times with PBS CMF. It is simplest to add 1 mL of PBS CMF into the Eppendorf tube immediately after DNA labeling, triterate, and then pelleting the cells. Cell pellets can be washed by removing supernatant and triterating the pellet with an additional 1 mL of PBS. This process should be repeated at least 3 times. Carefully removing 1 mL of supernatant is simplest by first removing most of the supernatant with a P1000 pipette, and then performing a second removal of supernatant with a P200 pipette. Keeping cells in 1.5mL Eppendorf tubes is optimal because it is the most convenient for pellet shaking during the DNA labeling and allows for the washing of cells with 1 mL of buffer, which is qualitatively found to be much better than 0.5 mL Eppendorf tubes.

7. Re-suspend the DNA-labeled cells into 100 µL of PBS CMF and store them at 4 ºC. Merely placing the Eppendorf tubes of cells in ice is sufficient - working in a cold room is not necessary.

Protocol 4: Surface Templated DNA Programmed Assembly of Cells

A complete overview of Surface Templated DNA Programmed Assembly of Cells is sub-divided into 12 basic steps (Figure 2-4A). The protocol for is a relatively simple, with only a few key steps that are technically challenging. If protocols 1, 2, and 3 have been completed, only half of the time-to-completion of an experiment remains (Figure 2-4B). The generality of STDPAC necessarily makes it impossible to generate a protocol that can be applicable to all possible experimental scenarios. Therefore a protocol is described which follows the sample experiment demonstrated schematically in Figure 2-4. This protocol, while specific to a particular pattern, demonstrates multi-component 2D patterning of cells and selective programmed assemblies of cell clusters - the combination of which can be applied to most possible experiments with STDPAC.

In general STDPAC is broken down into 5 steps: seed-cell attachment, programmed assembly, gel embedding, gel lifting, and culture. Assuming that the steps in protocol 1, 2, and 3 have been completed, the protocol for STDPAC as shown in Figure 2-4 is as follows.

1. Flow in the first population of cells into the first flow cell by pipetting the cell suspension onto the inlet of the flow cell with the substrate tilted at an angle. Gravity will pull the cell suspension through the flow cell and displace the liquid in the flow cell so that it flows out of the outlet. DNA-labeled cells were previously re-suspended to a concentration of 10^7 cells/mL. Flowing 20 μL of the cell

suspension is sufficient to fill a flow cell. At this concentration, the filling of the flow cell with the cell suspension is visible by eye. A cloudy, colloidal mixture should be displacing the PBS CMF previously within the flow cell (Figure 2-5D).

2. Collect the flow cell effluent including any excess cells that flow out of the outlet. It is easiest to use a P200 pipette to collect the effluent and collect the solution in a 1.5 mL Eppendorf tube. Cells that don't attach to the surface may be discarded. However, these same cells should be collected for possible reuse later in the protocol. For example, if only 2 million cells are available, and each million cells are labeled with complementary DNA, greater than 2 programmed assembly steps are possible through the recycled use of cells that did not attach to the DNA spots. This is an advantage of using cell numbers in great excess compared to DNA spots.

3. Spin the substrate with cell-filled flow cells in a swinging bucket centrifuge at 300 RPM for 3 minutes with the slowest possible acceleration and deceleration of the centrifuge. If possible, set the centrifuge temperature to 4 ºC in order to keep the temperature consistent throughout STDPAC. A makeshift slide adapter may need to be used so that the substrate fits snugly and well balanced within a centrifuge. The centrifugation is not necessary, but will dramatically increase the attachment efficiency (percentage filling of the total spots of DNA by DNA-labeled cells) within a short period of time. If centrifugation is not possible, the cells may be allowed to settle by gravity onto the surface of the substrate. Depending on the cell type, the time it takes for cells to completely settle across a DNA pattern may be greater than 5 minutes. In any case, cells must sample the substrate

surface so that DNA hybridization can occur. Cells that have attached to their DNA “zip-codes” are called seed cells.

4. Add 10 µL of PBS CMF to each of the flow cell inlets. Then hold the entire substrate by the edges, and gently rock it back and forth such that the 10 µL of PBS CMF moves back and forth through the flow cell, gently moving the cells with the fluid. This allows the cells to roll across the DNA pattern on the glass surface, maximizing their ability to sample the DNA patterned surface.

5. Wash the flow cells once the cells have sampled the surface. Cells should now be attached to one set of DNA spots (Figure 2-4A v). Washing the flow cells are similar to Protocol 2 Step 31. However, the effluent should be collected instead of discarded. The effluent, and the unattached cells contained therein, can be recollected in the same Eppendorf tube from step 2. This tube should now contain 1 million cells minus the number of cells that attached to the DNA patterns within the flow cells. The cells can be pelleted and re-suspended to a concentration of 10^7 cells/mL for later use.

6. Repeat steps 1 through 5 exactly with the second population of cells. These cells should be labeled with orthogonal DNA sequences to the first population of cells, and thus attach only to their complementary DNA spots (Figure 2-4A vii).

7. Repeat steps 1 through 5 with the third population of cells. However, instead of centrifuging the substrate, rest the substrate on ice for 5 minutes and allow the cells to settle towards the patterned seed-cells. Because seed cell surfaces are 3 dimensional, there is a greater surface area for the third population of cells to

bind. Also, the seed cells are lifted off of the glass surface, which allows assembly cells to more easily reach them. When other cells are attached via DNA to seed cells, they form assemblies (Figure 2-4A viii). This step, contrary to the previous attachment step in which cells were attached to 2D spots of DNA on glass, is known as an assembly step. It is important to note that, with increased assembly steps, assemblies become much larger and more prone to experiencing increased force due to flow. Accordingly, subsequent wash steps should become increasingly gentler in order to minimize forced displacement of assemblies.

8. Prepare the pattern for gel embedding by mixing the molten matrix formulation. For example, pure Matrigel is often used as the matrix of choice for 3D culture. However, even if pure Matrigel is used, it must be supplemented with 2% Turbo DNase so that all surface DNA can be cleaved. Any matrix formulation used must be supplemented with 2% v/v Turbo DNase before addition to the flow cells. It is easiest to add the Turbo DNase after the matrix formulation is prepared, and mixing the components by gentle pipetting and stirring. Preparing a gel formulation is not trivial. Like other steps during this process, no air bubbles can be introduced into the molten gel. Once introduced, it is very difficult to remove these air bubbles, and the air bubbles will most likely cause the gel lifting step to fail. Because the entire procedure relies on microfluidics, it is also important to ensure that the matrix formulation is completely liquid. Partially set gels are exponentially more viscous than molten gels, and will not flow through the flow cell. For example, Matrigel that has been sitting at room temperature for 15

minutes becomes too viscous to flow through the flow cell. Accordingly, Matrigel must be kept on ice throughout the entire procedure. It is also important to note that certain matrices, like collagen I, are known to organize over time once they are neutralized. This indicates that a collagen gel that was prepared right away is different from a collagen gel that was prepared 4 hours prior. In order to keep details consistent across experiments, matrix formulations should be prepared immediately before use.

9. Flow through the molten gel once the formulation is complete. As before, 4 flow cell volumes of the molten gel are required to completely displace the fluid previously occupying the flow cell. In general, 50 μL of molten gel are flowed through the flow cell, the effluent discarded, and an additional 50 μL of molten gel flowed through. The viscosity of the gel will most certainly be higher than the PBS CMF, thus the duration of the gel flowing step is longer than a typical cell attachment step. However, patience is important - forcing a viscous gel through a flow cell at a high velocity may cause enough sheer to kill the cells. As a side note, it is possible to flow through media in the flow cells immediately before the addition of the gel in order to replenish the cells with a food source. This possible positive impact of this replenishment has not been verified.

10. Place the entire substrate into a sterile petri dish and move it into a tissue culture incubator to set the gel. Many biomimetic gels (e.g. Matrigel, collagen) will set under warm conditions, in contrary to other gels (e.g. gelatin, agarose) that set under cold conditions. Depending on the matrix formulation, there is a range of time required for the gels to set. For example, Matrigel requires a minimum of 15

minutes at 37 ºC whereas collagen I requires a minimum of 30 minutes at 37 ºC. To ensure that the integrity of the gel is sufficient for the gel lifting step of the protocol, Matrigel is set for a minimum of 30 minutes and any gels with collagen I are set for a minimum of 45 minutes.

11. Apply the underlay while the gel is setting. This step is optional, but highly recommended. The tissue patterns must be placed into a dish or chamber for 3D culture. In order to prevent the gels from detaching (or lifting) from the culture chamber, a thin layer of matrix proteins can be added to the bottom of the chamber before the pattern is added. For example, in many experiments, a dilute underlay of 50% Matrigel in PBS is used to coat the floor of the chamber. The underlay acts as an additional adhesive onto which the matrix during long-term 3D culture. In order to apply an underlay, a minimal volume of 50% Matrigel/PBS solution should be spread across the floor of the petri dish or chamber that will be used for 3D culture of the tissue pattern.

12. Remove the substrate/petri dish from the tissue culture incubator but do not return it to the ice bucket.

13. Pipette 20 µL of the 3D culture media onto the side of the flow cell while the pattern is still warm.

14. With a razor blade, gently spread the media around the flow cell to create a moat of media surrounding the flow cell.

15. Insert, with great care, the tip of the razor in between the flow cell wall and the glass slide. It is easiest to begin with the corner of the flow cell. The razor tip should not penetrate past the width of the flow cell wall - it should only be inserted about 1 mm. When the tip of the razor is inserted, the moat of media should follow the razor and wet the underside of the PDMS flow cell wall.

16. Move the inserted razor gently along the entire length of the flow cell. The process is necessary to loosen the flow cell from the glass. The media acts as a liquid buffer between the flow cell/gel and the glass slide, which allows for easy gel lifting. The underside of the PDMS is hydrophilic because it was previously plasma treated (Figure 2-5B, Protocol 1 Step 12). Therefore, the razor movement creates an opening for the media to preferentially spread across the underside of the flow cell walls, as well as to the gel, which is also hydrophilic. The entire flow cell/attached gel will float on top of the media as soon as the media from the moat covers a sufficient surface area of the bottom of the flow cell.

17. Very carefully, lift the floating flow cell with its attached gel off of the glass substrate. This is accomplished by gently nudging the floating flow cell to the edge of the slide, carefully grabbing the flow cell by the sides, and peeling it off of the substrate. This is the weak point of the protocol, where failure is most common. Grasping the flow cell too hard will destroy the pattern, and grasping it too softly will increase the probability of dropping the flow cell. Because sterile gloves also diminish the tactile sensitivity of fingers, it is very difficult to know exactly how the flow cell is gripped. These delicacies can be overcome with much practice, but there are other strategies that may help with lifting. For

example, the razor can be used to nudge the flow cell to the edge of the slide and the flow cell can be flipped onto the razor itself. The main challenge with all of these gel lifting strategies is that the gel is not permanently attached to the flow cell, and so the gel may detach from the flow cell without the utmost precision.

18. Place a 20 µL droplet of molten gel in the center of the petri dish or chamber that was previously prepared with an underlay. This step should be completed at 4 ºC so that the gel does not begin to set.

19. Place the flow cell gel-side-down onto the droplet of molten gel within the petri dish or chamber. The molten gel will spread across the entire area of the flow cell to create a matrix sandwich in which the pattern is at the center (Figure 2-4A xi).

20. Place the newly sandwiched flow cell into a tissue culture incubator to set the bottom layer of gel. If the same matrix formulation is used, the time to set the gel should be the same as before, in step 10.

21. Remove the petri dish from the incubator. The petri dish should now have, from the bottom up, an underlay of Matrigel, a matrix sandwich with the tissue pattern in the middle plane, and a flow cell on top.

22. Add warm (37 ºC) assay media to the petri dish until the entire flow cell is completely submerged.

23. Use ultra-fine forceps to carefully lift the corner of the flow cell by 1 mm. Leave the flow cell alone for 30 seconds. Lifting the corner of the flow cell encourages

“media creep” at the interface between the matrix and the PDMS. Specifically, the PDMS flow cell surface is hydrophilic, which means that it will be at its lowest state of energy when in contact with an aqueous solution. The matrix is a hydrogel, and thus preferentially stuck with the PDMS throughout the lifting process. However, the hydrogel does not contain the same water content as media. Also, the top layer of matrix is now stuck to bottom layer of matrix, which is stuck to the underlay, which is stuck to the petri dish. Because the matrix now prefers to stick to other matrix, and the PDMS prefers to be covered with water, allowing a small amount of media to creep between the gel-PDMS interface will allow the media to subsequently spread across the entire surface of the PDMS, creating another buffer zone, except that this time the buffer zone is between the PDMS and the matrix. Careful prodding of the PDMS flow cell after 30 seconds of media creep and along the major axis of the flow cell causes the PDMS flow cell to float off the matrix, leaving a single, intact matrix with a tissue pattern in its middle plane.

24. Remove the floating PDMS flow cell with the ultra-fine forceps taking care not to touch anything else. Inverted forceps may provide easier access to the flow cells.

25. The petri dish with the tissue pattern may now be placed in a tissue culture incubator for long-term 3D culture. A secondary containment source (e.g. a larger petri dish) may be beneficial for handling the pattern when performing live-cell imaging.

The entire process, until the gel setting step, should be completed at 4 ºC. If possible, the entire process should also take place in a tissue culture hood to minimize the chance of contamination from components external to the protocol. The protocol should also be repeated for each flow cell on the substrate. Performing the each step serially for each flow cell is recommended.

Completion of all four protocols should result in a 3D culture tissue model, simple or complex, that is ready for rigorous analysis.

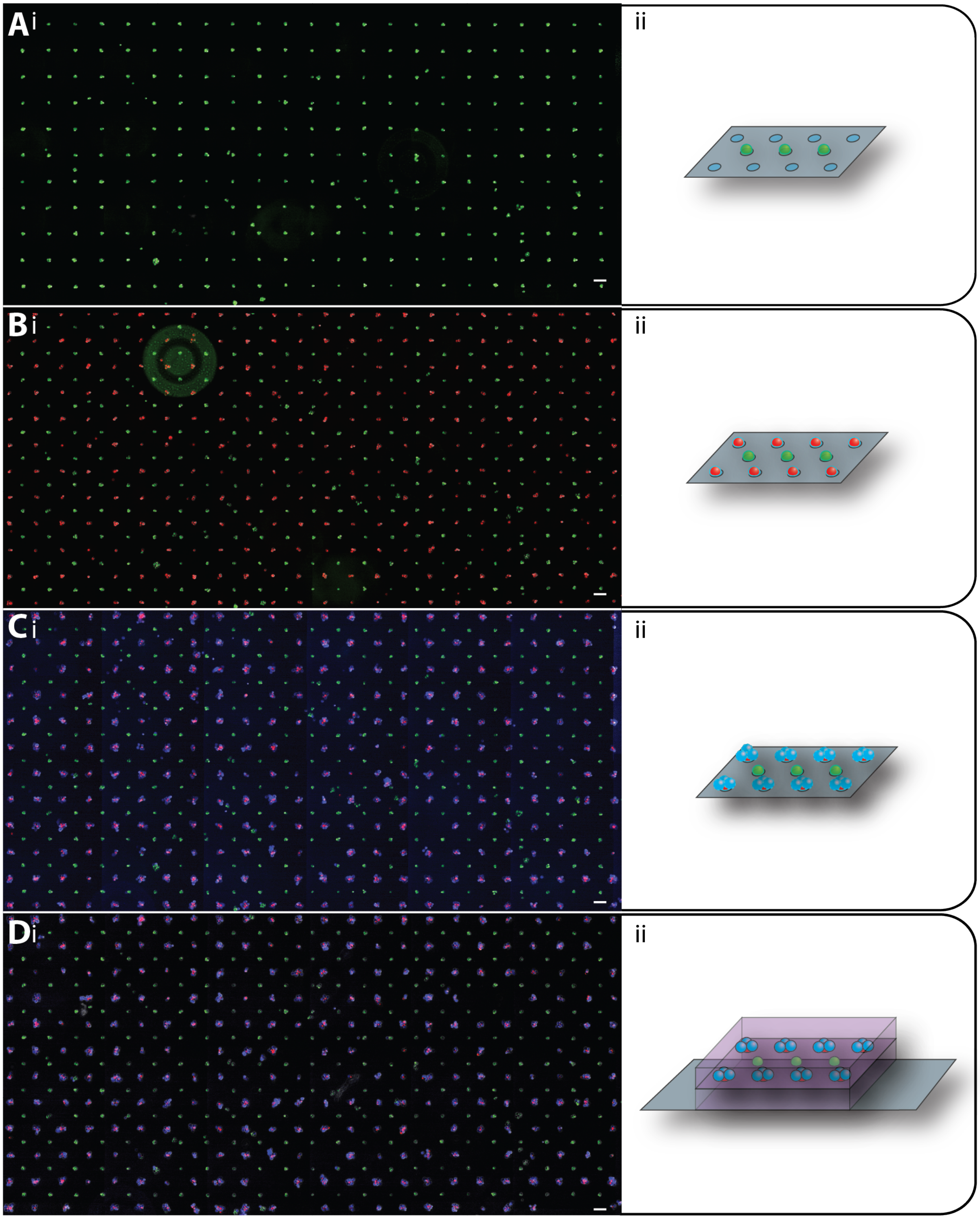

Figure 2-6. STDPAC proof of concept with three cell types. (A) Green Jurkat cells are initially attached to glass (i - ii), red MCF-10AT cells are attached interspersed with the green Jurkat cells (i - ii), (C) blue MCF-10A cells are assembled only onto the red MCF-10AT cells (i - ii), and (D) the entire pattern is embedded into Matrigel (i - ii). All scale bars are 100 μm.

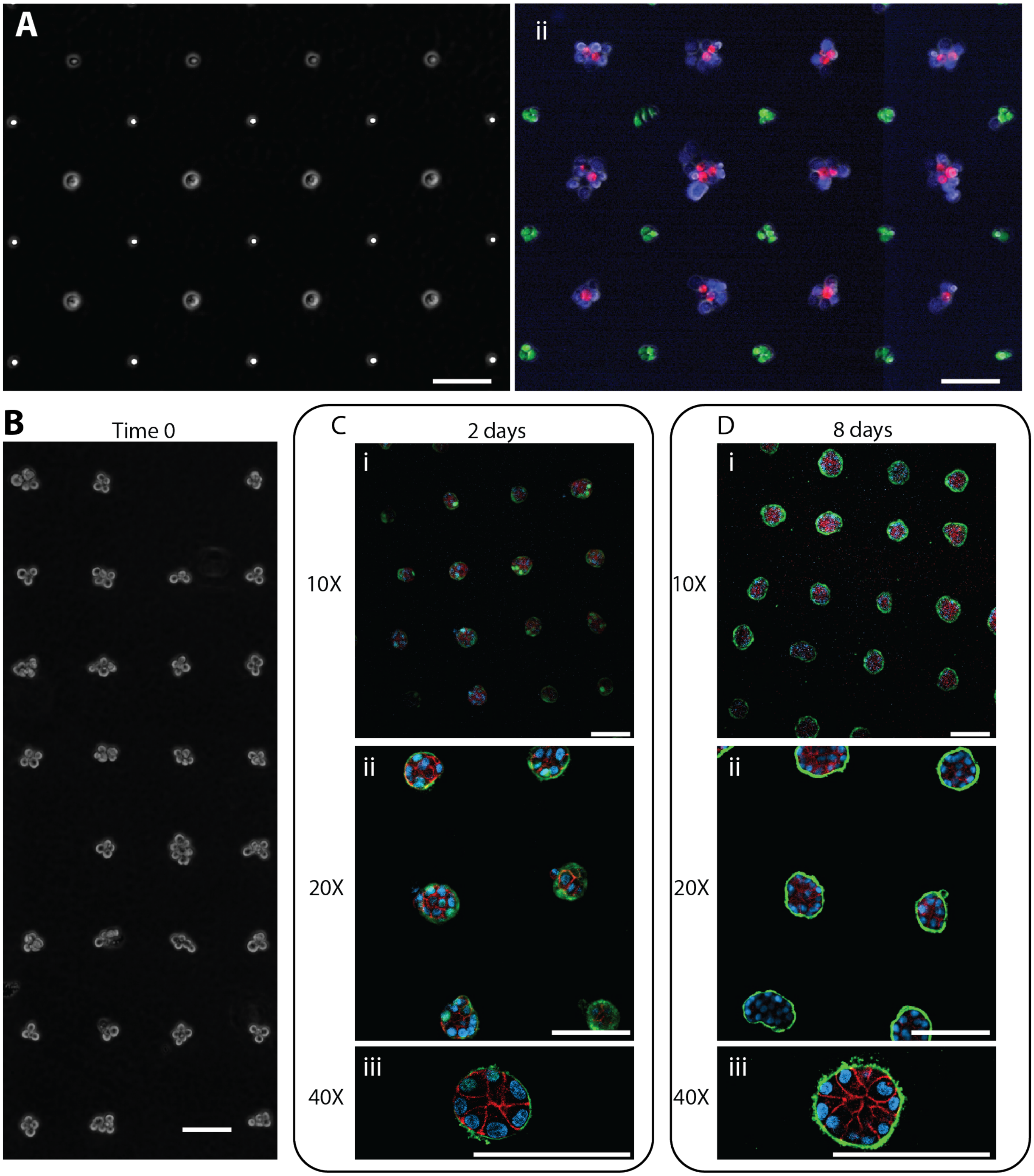
A
ii
B
Time 0
C
2 days
D
8 days
i
ii
iii
10X
20X
40X

Figure 2-7. 3D culture of MCF-10A tissues following STDPAC. (A) DNA spots are patterned onto glass (i) and cells are sequence specifically attached (ii) (B) MCF-10A assemblies are patterned as a grid via STDPAC. (C) MCF-10A tissues cultured in 3D are shown growing for 2 days or (D) 8 days at 10X, 20X, and 40X magnifications (i - iii). All scale bars are 100 μm.

Supporting Information: Culturing Cells, Data Collection, and Image Analysis

When an experiment is complete and a tissue pattern is growing in 3D cell culture, several factors must be considered. First, the frequency of culture media change is important. Growth factors and glucose molecules are normally depleted by 96 hours. However, then dynamic change in media composition over the 96 hours may affect tissue behavior in culture. Therefore, it is recommended that media be replaced every 24 or 48 hours. Second, live-cell imaging requires great care in handling the petri dishes or chambered slides containing the patterns. The gels are attached to the surface of the petri dish or chambered slide by non-covalent forces. Too much jostling will detach the gels and render the entire pattern unimageable, therefore negating the possibility of collecting later time points for an experiment. Similarly, changing the media requires care. Too much forceful pipetting will also dislodge or damage the gel, which is normally of a delicate matrix formulation and sets based on entropic forces rather than cross-linking.

It is also important to properly choose a culture chamber during the 3D culture process. While chambered slides with glass coverslip bottoms are far more expensive than 35 mm plastic tissue culture petri dishes, they allow for live-cell confocal microscopy. This confers the ability to obtain high-resolution data at multiple time points without fixing the tissue samples. Thirty-five mm plastic tissue culture petri dishes, however, only enable live-cell epifluorescence microscopy because of the nature of the chamber medium. High-resolution microscopy data can only be obtained by fixing the tissue samples.

Finally, during long-term 3D culture, non-growth arresting tissues and will continue to grow larger than the thickness of the gel. This is especially true of oncogenic tissues. If a tissue grows past the surface of a gel, or conversely, reaches the bottom of a gel to touch the culture dish, the tissue will disseminate upon contact with the surface (Figure S4-4). Tissues that grow past a gel cannot be trusted for structural integrity, and therefore must not be included in the data analysis. It is important to plan for these various aspects of an experiment in order to adequately plan for proper 3D culture conditions.

When planning a series of experiments, it is important to plan to use one microscope such that the camera, sensor, laser power, and general settings are all the same. To make direct comparisons between experiments, especially when they are linked, it’s important to be able to directly compare the images that are taken. It is possible to directly compare images taken on different microscopes, with different objectives, and different cameras. However, it takes much time to fine-tune the image settings to make two images from different sources directly comparable. Similarly, a complete series of experiments, instead of single experiments, should be planned in order to prepare proper methods for data collection. For example, if it becomes necessary to employ confocal microscopy for latter experiments, consistency can be reached if all experiments were imaged with a confocal microscope, even though epifluorescence might be sufficient.

For immunofluorescence staining of tissues, the following procedure was generally followed. All samples were fixed with 4% formaldehyde for 20 minutes and then incubated in blocking buffer (10% heat-inactivated goat serum in PBS+0.5% Triton X-100) at 4C for at least one day. Primary antibodies were then diluted in blocking buffer and added to the sample. After at least one day incubating at 4C with the primary antibody, samples were washed several times with PBS+Triton X-100 for at least one day and incubated with Alexa-conjugated secondary antibodies diluted at a concentration of 1:200 in blocking buffer for approximately one day. All sample were washed with PBS+1ug/mL DAPI for at least one hour before imaging.

Supporting Information: Basic Operation of the BioForce Nano eNabler

Instructions for operating the BioForce Nano eNabler are available through BioForce Nanosciences. However, there are some modifications that are necessary to facilitate the printing of amine-modified DNA onto aldehyde glass slides to ensure proper reaction of the DNA onto the glass surface, as well as dramatically increasing the speed of patterning the DNA onto the glass slide. A brief protocol is described below.

With the side of the glass slide with etch marks facing towards the slide holder and the clean surface facing up, press down the slide in the center of the sticky pad on the slide holder while ensuring that you are not actually touching the printing surface of the slide. Place the SPT onto the SPT holder. Load the SPT reservoir with 0.4uL of 1.5mM DNA in the spotting buffer of 225mM NaCL, 22.5 mM sodium citrate, 5% w/v trehalose, 0.1 mg/mL N-octylglucoside, pH 9.5. Gently load the SPT holder with the loaded SPT onto the machine. DNA spots can be printed at a maximum of 1 hertz by turning the laser off, setting the contact time to 0, and setting contact speed to 0.35 um/second. Changing the humidity of the chamber can control spot size. Used SPT chips with DNA can be stored dry and the DNA printing solution re-humidified by placing the chip in a saturating humid environment for 1 hour.

It is important to know that the machine is not perfectly accurate, and that there is an approximate error of +/- 1 um in accuracy of the printed spot pitch. However, the machine is precise. Thus the spot distances can be calibrated by printing spots of solution (Figure 3-4) and then measuring the center-to-center distance for these spots to normalize the nominal pitch versus the actual pitch.

When printing multiple strands of DNA, the accuracy error can be accentuated because a human element is introduced into the alignment of the various strands of DNA. Each pattern that requires multiple DNA strands must be split into individual patterns containing a single sequence of DNA, and then each of these patterns must be patterned sequentially until the multi-DNA pattern is made. This strategy relies on the alignment of each of these sub-patterns by eye such that the final pattern contains each of the various strands of DNA in the correct spot in relation to each other. A single origin point to which all patterns are aligned is crucial in order to avoid a compounding effect of errors that arise from misalignment.

Materials

Protocol 1: Preparation of PDMS Flow Cells

- Sylgard 184 and curing agent
- Vacuum chamber
- Petri dish
- No. 1 thickness coverslips
- 3M Double-sided tape

Protocol 2: Surface Patterning, Slide Preparation, and Flow Cell Application

- Aldhehyde silanized glass slide
- Sigmacote: Cas 2474-02-4
- Ethanol
- Sodium Borohydride
- Reducing Solution
- Wash Solution
- Cover slips sized 60mm x 24mm

Protocol 3: Cell Labeling

- DAG DNA
- Cells
- PBS CMF
- Ependdorf tubes
- Pipettes

- Trypsin (0.05%)
- SBTI
- Media

Protocol 4: STDPAC

- DNA-labeled cells
- Glass slide with flow cells assembled, primed, and filled with PBS CMF
- Sorvall Legend RT+ Centrifuge
- Pipette
- Razor blade
- Ultra-fine forceps
- Matrigel, Collagen, or other matrix
- Turbo DNAse
- Media
- Chambered slide or 35 mm dish
- PBS CMF or cell buffer
- Ice bucket with ice

Commentary

There are a few things to note about the STDPAC protocol. First, the entire process - until the gel-setting step - should be completed at 4 ºC. If possible, the entire process should also take place in a tissue culture hood to minimize the chance of contamination from components external to the protocol. It is important to note that several steps of the STDPAC protocol can be performed simultaneously in order to speed up the entire process. Caution is advised, however, for the slightest mistakes can cause the entire experiment to fail. Steps should not be combined until the entire STDPAC protocol becomes second nature to the experimenter.

Accordingly, it is crucial to plan ahead when designing an experiment with STDPAC. While many other scientific techniques require a lengthy method, there are usually periods of lull in which one must wait for a particular step to finish. STDPAC is different – it requires a great amount of physical stamina, as there are no breaks in the protocol for hours. However, the constant activity required to complete a STDPAC experiment is precisely why an entire experiment can be planned and completed within a typical workday. It the protocol becomes second nature, and experiments are adequately planned ahead of time, most experimental goals can be reached with high throughput.

Successful completion of the protocol also allows for easy creation of complex patterns composed of multiple cell types (Figure 2-6). Successful completion of the protocol also renders STDPAC orthogonal to the biological systems that are under experimentation. As a proof of concept, and to examine whether the STDPAC method itself affects tissue behavior in 3D culture, MCF-10A tissues were assembled, cultured in Matrigel, and assayed for proper tissue polarization (Figure 2-7). Based on these, and other, results, we are comfortable in stating that STDPAC can be applied most 3D culture systems without affecting the innate biological machinery of the cells that are used.

References

Rothemund, P.W.K. (2006). Folding DNA to create nanoscale shapes and patterns. Nature *440*, 297–302.

Pinheiro, A.V., Han, D., Shih, W.M., Yan, H. (2011). Nature Nanotech *6*, 763–772.

Mali, P., Aach, J., Lee, J., Levne, D., Nip, L., & Church, G.M. (2013). Barcoding cells using cell-surface programmable DNA-binding domains. Nature Methods *10*, 403–406.

Gartner, Z. J. & Bertozzi, C. R. Programmed assembly of 3-dimensional microtissues with defined cellular connectivity. (2009). Proc Natl Acad Sci USA *106*, 4606–4610.

Hsiao, S. *et al.* Direct cell surface modification with DNA for the capture of primary cells and the investigation of myotube formation on defined patterns. (2009). Langmuir *25*, 6985–6991.

Onoe, H., et al. (2012). Cellular Microfabrication: Observing Intercellular Interactions Using Lithographically-Defined DNA Capture Sequences. Langmuir *28*, 8120–8126.

Bernard, A., et al. (2000). Microcontact printing of proteins. Adv Mater *12*, 1067–1070.

Sung, K.E., et al. (2011). Transition to invasion in breast cancer: a microfluidic in vitro model enables examination of spatial and temporal effects. Integr Biol *3*, 439–450.

Shamir, E. R. & Ewald, A. J. Three-dimensional organotypic culture: experimental models of mammalian biology and disease. (2014). Nature Reviews Molecular Cell Biology *15*, 647–664.

Selden, N. S. *et al.* Chemically programmed cell adhesion with membrane-anchored oligonucleotides. (2012). J Am Chem Soc *134*, 765–768.

Weber, R. J., Liang, S. I., Selden, N. S., Desai, T. A. & Gartner, Z. J. Efficient Targeting of Fatty-Acid Modified Oligonucleotides to Live Cell Membranes through Stepwise Assembly. (2014). Biomacromolecules *15*, 4621–4626.

Chapter 3: Technical Applications of STDPAC

Introduction

Two main philosophies motivate the development of a new method in the biological sciences. The first philosophy, and hopefully the main motivation, is to develop a method that solves a problem such that previously untestable hypotheses now become testable, expanding the empirical boundaries of science. The second philosophy, seemingly less noble, is to create a technical achievement that was not previously attainable. When DNA origami entered into the field, it was well received because it was, for the lack of a better word, cool (Rothemund. 2006). Some criticized its usefulness. But the demonstration of boundary pushing by DNA origami has presented applications in fields such as nanotechnology (Douglas et al. 2012).

The development of STDPAC was motivated by a need to model multi-cellular tissues in vitro, with more control than given by DNA-programmed assembly of cells (DPAC). However, throughout the course of its long-lived development, there have been many seized opportunities to push the boundaries of the technology itself - seemingly, for no real applications. Yet, expanding the horizons of the technology have allowed for the creation of complex tissue assemblies like the “twinkie”, which led to insights in cellular self-organization (Cerchiari et al. 2014). Large multi-component tissue synthesis proof-of-concept experiments also led to interesting observations in collective cell behavior (Figure 4-8).

This chapter demonstrates the technical application of STDPAC. As such, much of the chapter focuses on pushing boundaries of the STDPAC and creating demonstrative tissue models rather than true complex tissue models for experimentation. However, it is important to recognize that the pursuit of a better and more capable scientific technique leads to, and has led to, interesting and previously unsurfaced questions about tissue biology.

Generating Complex Models with STDPAC

Surface Patterning

The versatile nature of surface templated DPAC allows for its application to multiple uses outside of creating complex tissue models. At its core, STDPAC exploits a method of precisely sticking cells onto surfaces. The addition of complex patterning methods, microfabrication techniques, and cell culture techniques expand the capabilities of STDPAC to broader applications. A simple use of STDPAC is to create complex 2D patterns of cells.

Other scientists have pursued the ability to create complex patterns of cells on a flat surface, motivated by engineering achievement and scientific discovery. Some examples include printing of cell patterns by using inkjet printing (Xu et al. 2005), microfluidics (Sung et al. 2011), micro-contact printing (Braunschweig, Huo, & Mirkin. 2009), micromolding (Stevens et al. 2013), and DNA (Hsiao et al. 2009). In general, these techniques have been limited to observing broad, collective behaviors of many tissues, due to the limited resolution of the patterning techniques.

The Nano eNabler by BioForce enables the deposition of picoliters of fluid as micron-scale droplets onto surfaces with micron-level precision. The working area of the machine is in the multi-centimeter range, and thus the machine is able to produce centimeter-scale droplet patterns with micron-level precision. With manual tweaking, the machine can also be modified to align multiple types of droplets into a single multi-component pattern.

The combination of DPAC and the Nano eNabler enables the creation of large, multi-component 2D cell patterns with single-cell precision. For example, two interwoven spirals composed of MCF-10A cells dyed with CellTracker red or green create a 2D pattern on glass that is 1.5cm in diameter (Figure 3-1A). Due to the scale of the pattern, multiple epifluorescence microscopy images taken with a 10x objective are stitched together to create a single image of the larger pattern. However, increasing the magnification on part of the red spiral reveals that the spatial resolution of the large pattern often surpasses the stitching algorithm resolutions of scientific imaging software (Figure 3-1B). It is possible that the cause is a combination of single cell resolution repeating over distances that are orders of magnitude larger. For example, the spirals are composed of monomers, themselves composed of three cells in a pattern of equilateral triangles (Figure 3-1C). The resolution of the 3-cell monomers themselves is less than the size of a single cell.

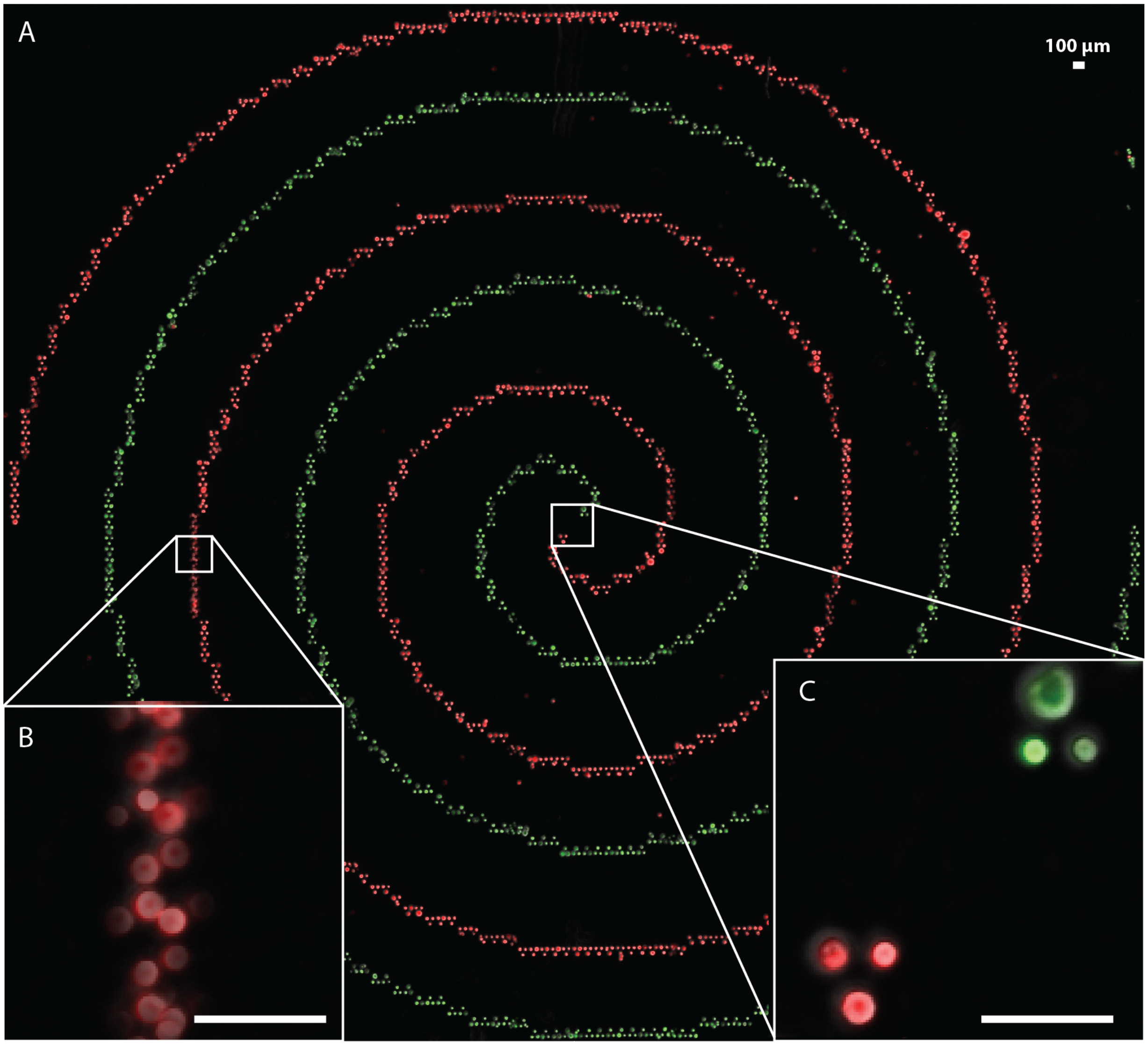

Figure 3-1. Large-scale multi-component triangle monomer spiral fractal. (A) A large grid of 10x images are stitched together to create an image of a ~1.5 cm diameter spiral of differentially labeled and colored cells are patterned onto glass via orthogonal pairs of DNA sequences. (B) The spatial resolution of the individual cells surpass the stitching algorithms of most scientific imagine software. The stitching algorithm of the imaging software mistakenly offsets cell triangles because the cells are at the edge of a 10x field of view. (C) Spatial resolution via STDPAC is maintained on length-scales spanning orders of magnitude (microns - centimeters). All scale bars are 100 µm.

The ability to create centimeter-scale patterns with micron-level precision allows for the application of STDPAC into realms of engineering and art. Any conceived artwork that can be digitized and rasterized can be recreated with patterns of cells. To celebrate the passing of a qualification exam, a congratulatory artwork by Samantha Liang is digitized, rasterized, and recreated with STDPAC and Jurkat cells by Michael Todhunter (Figure 3-2). While scientifically uninteresting, this pattern creates implications for advanced applications in engineering. For example, a fingerprint of the late Beatles singer, John Lenon, is digitized (Figure 3-3A) and recreated with green fluorescent MCF-10A cells (Figure 3-3B). While the scale of the fingerprint is much smaller than that of a real fingerprint, the pattern implies that one can reconstitute the pattern of a real finger with dermal cells, and create it to scale. This enables the recreation of a natural fingerprint, potentially with the cells of the person to whom the fingerprint belongs.

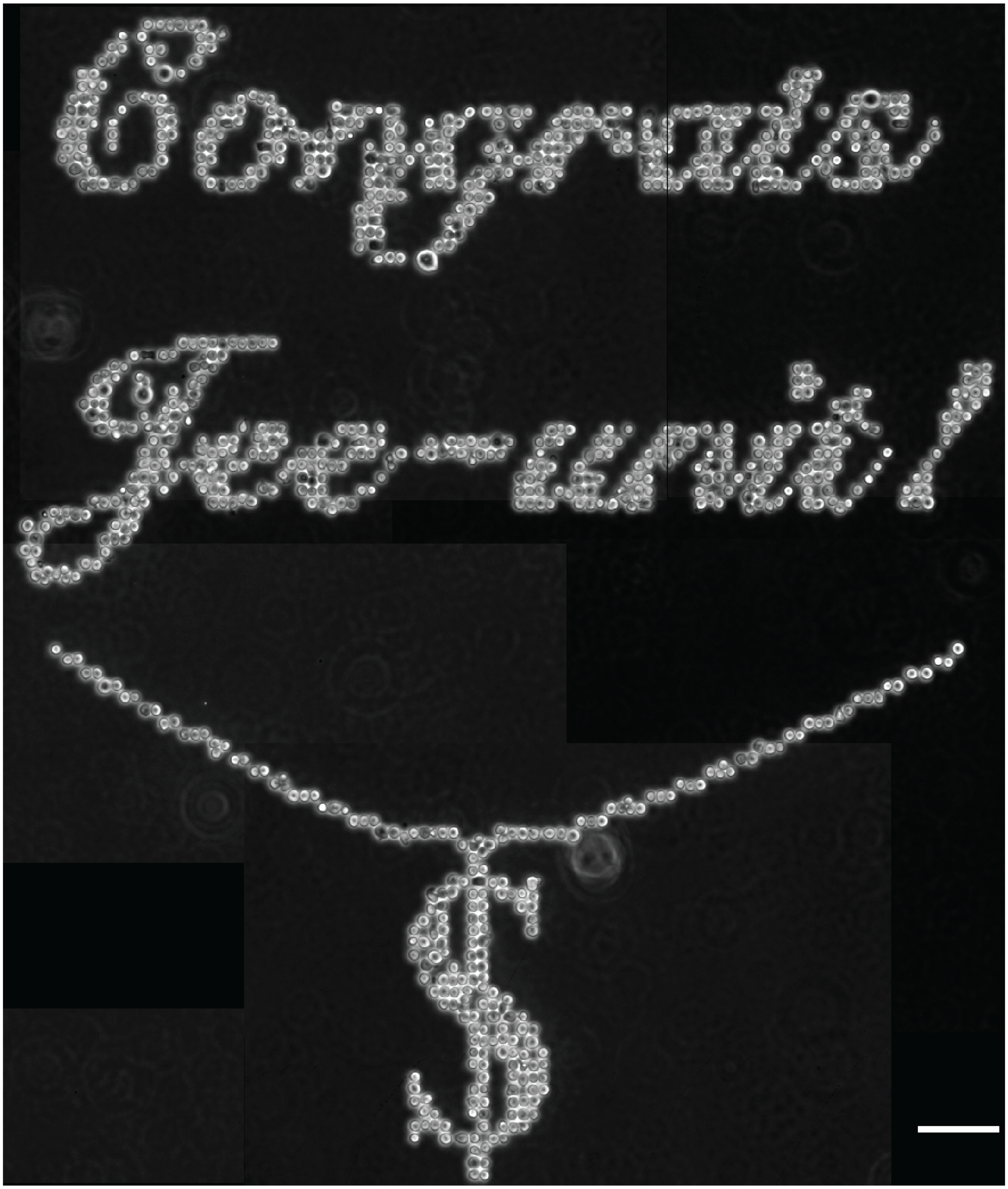

Figure 3-2. Micron scale artwork. Any conceivable artwork can be rasterized and patterned via cell “pixels” to create micron-scale cell-based art. Scale bar is 100 µm.

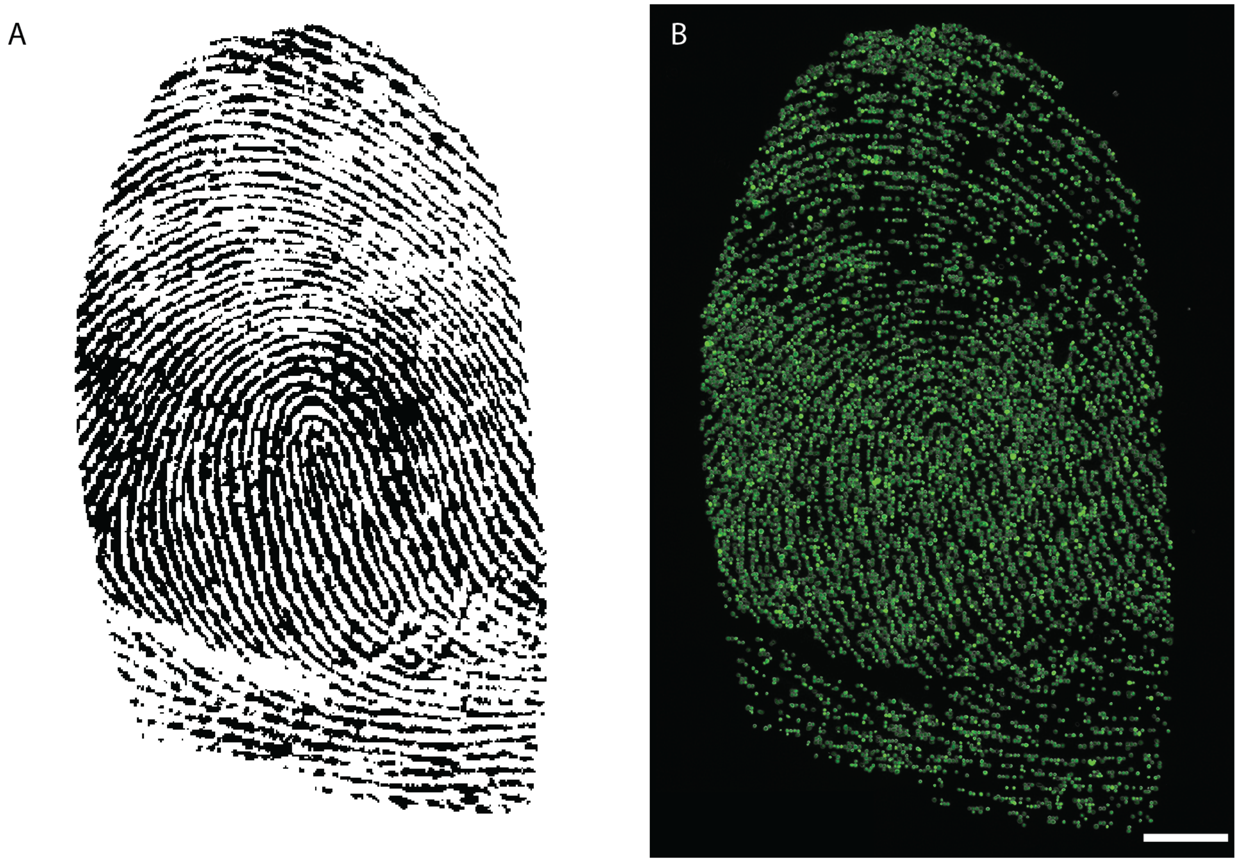

Figure 3-3. Reconstituted pattern of a human fingerprint. (A) A picture of a finger was converted to a rasterized bitmap file and printed with DNA spots onto glass. (B) Green fluorescent MCF-10A cells were used to reconstitute the fingerprint pattern on glass. Scale bar is 100 µm.

While two-component patterns have been created with high precision via methods including micro-contact printing and employing microfluidic devices, patterns including three or more cell types have been challenging to create by these methods. There are theoretically an infinite number of possible DNA sequences, allowing STDPAC to overcome the challenge of creating multi-component patterns of many cell-types. Three-component patterns can be created by labeling cells with three orthogonal DNA sequences (Figure 3-4A). Employing STDPAC, the three complementary DNA sequences can be patterned onto glass and covalently bound, then the DNA-labeled cells can be attached onto the DNA spots into specific patterns, such as an array of equilateral triangles (Figure 3-4B). Such a pattern of three-component equilateral triangles is shown as an array of triangles, half of which the pitch is 36 microns, and half of which the pitch is 18 microns (Figure 3-4C). MCF-10A cells were separated into three populations and dyed with CellTracker Red, CellTracker Green, or CellTracker Violet. Each population was labeled with DAG-DNA of sequence A, B, or D, and attached to a complementary pattern of DNA spots via STDPAC (Supplementary Table 1). Because CellTracker Violet was found to be toxic to the MCF-10A cells, the process was repeated without dyeing the third population of cells. The equilateral cell triangle is shown at high magnification with pitches of 18 um and 36 um (Figure 3-4D i-ii). The same triangle as spots of DNA solution is shown with a nominal pitch of 36 um (Figure 3-4D iii). When printing DNA patterns, a nominal pitch is entered into the BioForce Nano eNabler software. However, because the machine has a precision of about 4 microns, the nominal pitch and the measured pitch may be different. The center-to-center distances of 30 cell pairs were measured for nominal pitches of 18 um and 36 um and compared to the center-to-center measurements of DNA spots of 36 um pitch immediately following printing by the Nano eNabler (Figure 3-4E). For the cell pairs with 18 um pitch, the average measured cell-cell distance was found to be 20 um. For the cell pairs with 36 um pitch, the average measured cell-cell distance was found to be 40 um. Interestingly, the measured DNA spot-spot distance for the nominal 36 um pitch was found to actually be an average of 38 um, implying that there is an internal machine bias of adding 2 um to the nominal pitch entered into the machine. Despite the error between the nominal pitch and measured pitch of a pattern, the precision of cell patterning via STDPAC is found to be of a resolution lower than a single cell diameter.

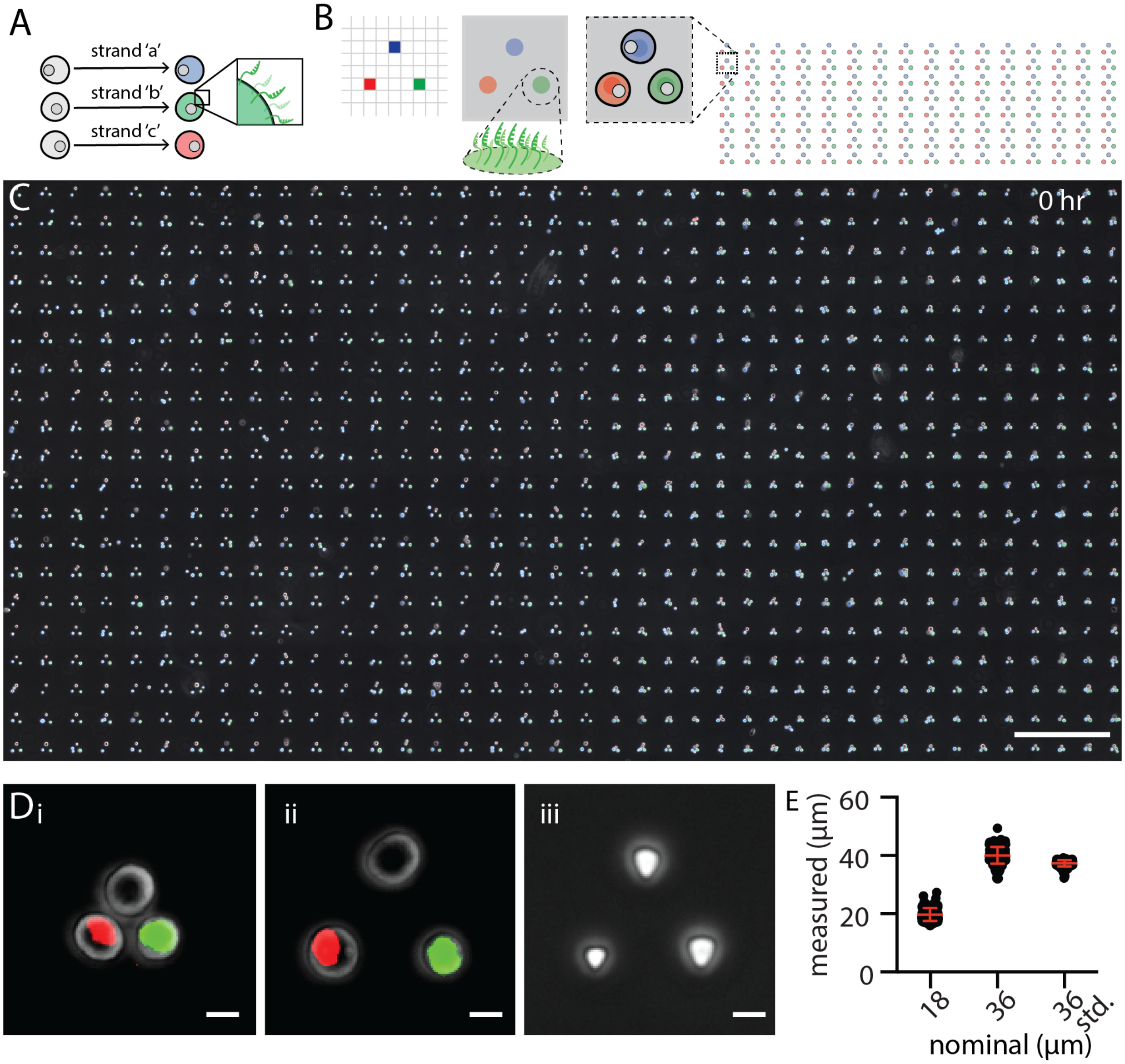
A
strand 'a'
strand 'b'
strand 'c'
B
C
0 hr
Di
ii
iii
E
measured (µm)
60
40
20
0
18
36
36 std.
nominal (µm)

Figure 3-4. Pattern resolution with STDPAC. (A) Cells identities are encoded with sequence specific DAG-DNA modification and (B) Attached to patterned DNA spots on glass. (C) A large array of triangles composed of 3 distinct populations of MCF-10A cells are shown with cell-cell distances of close spacing (18 µm) and far spacing (36 µm). Scale bar is 100 µm (D) A zoom in of cell triangles of 18 µm spacing (i), 36 µm spacing (ii), and a triangle of DNA solution printed by the Nano Enabler with 36 µm spacing (iii). Scale bars are 10 µm. (E) A comparison of the cell-cell distance distributions between the nominal distances when DNA spots are printed, and the measured distances after cells are attached.

Matrix Embedding, Gel Transfer, and 3D Culture

Creating 2D patterns of cells on surfaces have applications in observing cell-cell interactions. However, to better reconstitute a biological environment, cells must be completely surrounded by an environment mimetic of their in vivo counterpart. In vitro, this is best reconstituted by embedding cells into 3D culture, within a biomimetic matrix (Debnath et al. 2003). Many cell types that are grown in 3D culture form microtissues or tissues mimetic of their biological counterparts (Shamir & Ewald. 2014). Previous work done by Michael Todhunter has shown that MCF-10A cells patterned at a distance of 18 um or closer fuse into single tissues, whereas cells patterned at distances greater than 18 um tend to grow into individual tissues (Todhunter. 2015). By using the patterning precision offered by the Nano eNabler, and the self-assembly afforded by STDPAC, MCF-10A cells were patterned as previously described in Figure 3-4. These cell patterns were then transferred into laminin-rich matrix (Matrigel) via the STDPAC protocol described in Chapter 2. The patterns retained their overall structure after lifting into gel - the 36 um triangles remained 36 um triangles both as patterns on 2D glass and after transfer into 3D matrix - a process denoted as transfer fidelity. MCF-10A cells patterned as equilateral triangles with a nominal pitch of 36 um (Figure 3-5A i - ii) or 18 um (Figure 3-5B i - ii). Cell triangles with a 36 um pitch grew into three separate tissues over 24 hours (Figure 3-5A iii), and cell triangles with an 18 um pitch grew into a single tissue of 3 cell components over 24 hours (Figure 3-5B iii). In order to maximize cell viability, CellTracker dyes were not used, and cells were replaced with MCF-10A cells transduced to stably express H2B-GFP or H2B-mCherry. One cell of the cell triangle was left unstained as before in order to preserve a differentiation of identity (Figure 3-4D). However, tissues were fixed and stained for DAPI after 24 hours such that individual nuclei could be imaged, and that the 3 cell identities could be distinguished. While all cells would have their nuclei stained blue, two separate cell-types have nuclei doubly positive for GFP or mCherry. Entire arrays of cell triangles were transferred into Matrigel for 3D culture and imaged at 24 hours (Figure 3-5C). Surprisingly, the entire array of cell triangles retained its micron-level precision across the entire length of the large array.

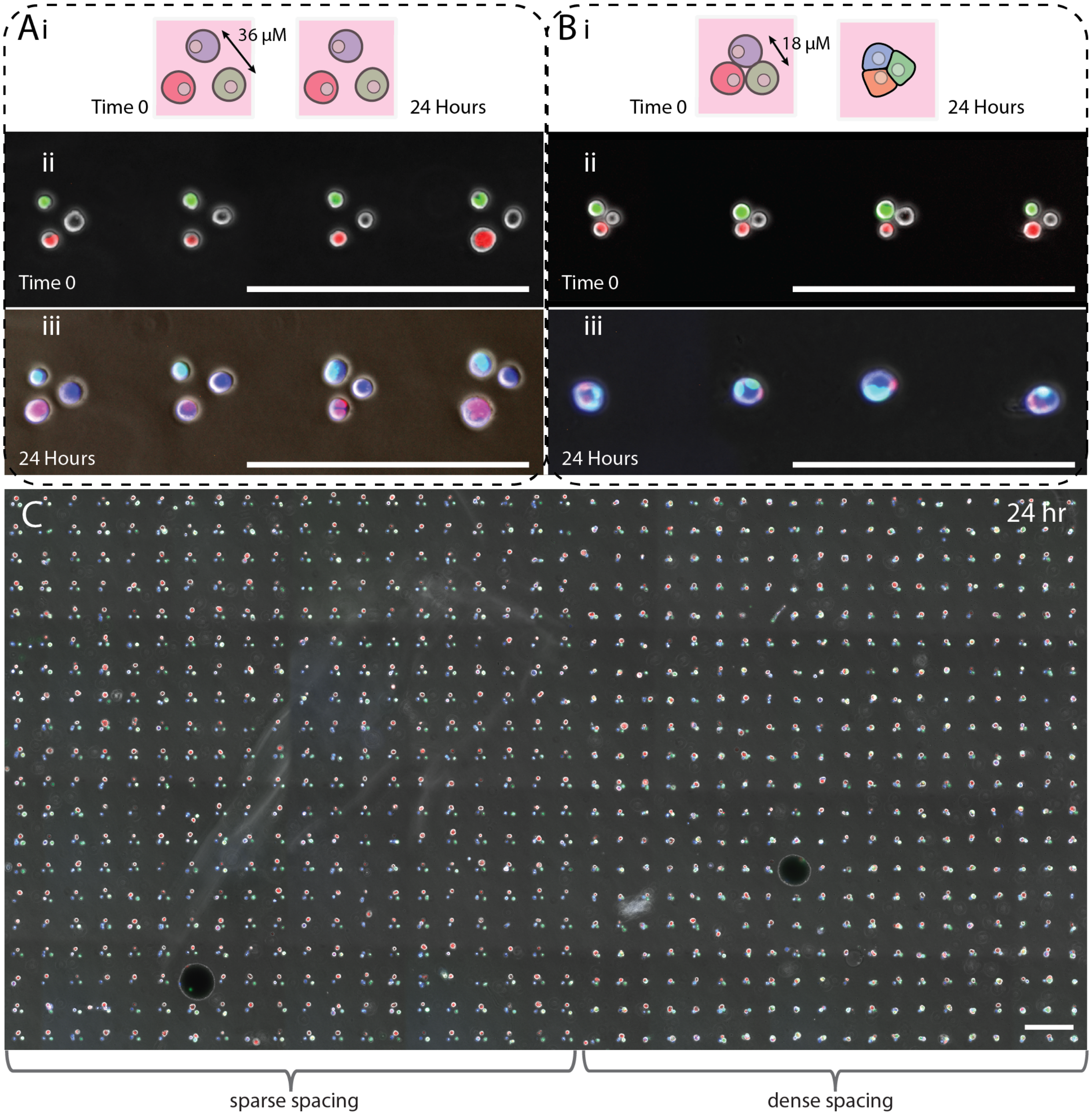
Ai
36 µM
Time 0
24 Hours
ii
Time 0
iii
24 Hours
B i
18 µM
Time 0
24 Hours
ii
Time 0
iii
24 Hours
C
24 hr
sparse spacing
dense spacing

Figure 3-5. 3D culture of MCF-10A triangles to compositionally control tissues. (A) An equilateral triangle of three different MCF-10A cells grown 36 µm apart grow into three separate tissues over 24 hours (i - iii) (B) An equilateral triangle of three different MCF-10A cells grown 18 µm apart grow into a single tissue composed of three different cells over 24 hours (i - iii). (C) A large array of triangles composed of 3 distinct populations of MCF-10A cells are shown with cell-cell distances of close spacing (18 µm) and far spacing (36 µm) shown after 24 hours. All scale bars are 100 µm.

In order to qualify and quantify the transfer fidelity of a large pattern of cells from a surface into gel, a large (>1 cm), asymmetric pattern of cells was imaged before and after transfer into matrix. Specifically, a histology image of a mouse mammary fat pad (reproduced with permission of Dr. William Muller) was digitized, printed as DNA, assembled with cells via STDPAC, and embedded in Matrigel for 3D culture (Figure 3-6A). The transferred pattern was able to retain the overall architecture of the mammary gland image across the 1.6 cm length of the pattern and the resulting 3D culture is shown to scale as an inverted image to enhance contrast for clear visibility (Figure 3-6B). When comparing images of the pattern on a 2D glass surface and after transfer into Matrigel, the transfer fidelity was found to be excellent, with almost complete overlap between a portion of the pattern on a 2D glass surface and the same portion of the pattern in a 3D ECM gel (Figure 3-6C, Figure S3). The histology image of the mouse mammary fat pad is enlarged for direct comparison to the MCF-10A pattern on a 2D glass surface (Figure 3-6D). Strikingly, a view of the MCF-10A pattern reflects near-perfect retention of the overall structure of the mouse mammary fat pad histology section (Figure 3-6E).

Two-dimensional patterns with single-cell resolution have been reported by other groups (Zhang et al. 2014). However, STDPAC is unique in its ability to retain the high-resolution in 3D culture. To quantify the transfer fidelity qualitatively observed in figure 3-6C, we derived a method by which the pattern before and after gel transfer was aligned to a mathematically derived pattern centroid (alignment point) for each state of the pattern - that is, before gel transfer and after gel transfer. The distance of a cell from the alignment point was denoted Ds before transfer, and the distance of the same cell from the alignment point after transfer was denoted Dg (Figure 3-6F). The absolute positions of individual cells within the 1.6 cm pattern remained mostly unchanged compared to the alignment point (Figure 3-6G). Subsequent analysis of the average pairwise distances - before and after gel transfer - between each cell and every other cell within the pattern (n > 36 million) showed that cells retained their relative positions to other cells after gel transfer, even at distances approaching 2 cm, with an average error in displacement of 20 um (Figure 3-6H). While transfer fidelity analysis can be applied to any given pattern, even those as complex as the reconstituted mouse mammary fat pad, such analysis can be more easily applied to large asymmetric patterns. An example of such a pattern would be lines of cells zig-zagging across centimeter long distances (Figure 3-6I).

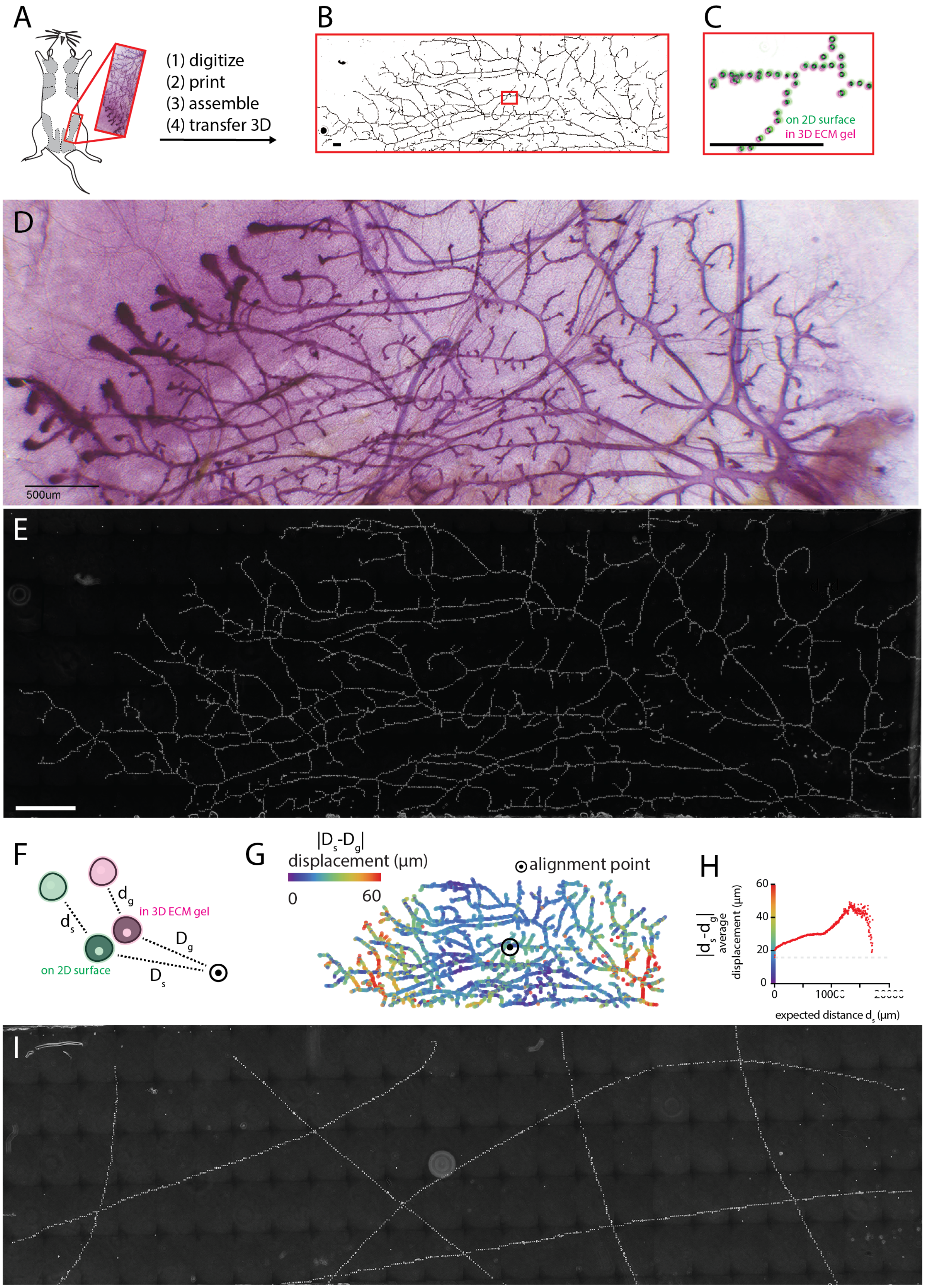
A
(1) digitize
(2) print
(3) assemble
(4) transfer 3D
B
C
on 2D surface
in 3D ECM gel
D
500um
E
F
d_g
d_s
in 3D ECM gel
D_g
on 2D surface
D_s
G
$|D_s-D_g|$
displacement (μm)
0
60
alignment point
H
60
40
20
0
$|d_s-d_g|$
average displacement (μm)
0
10000
20000
expected distance d_s (μm)
I

Figure 3-6. Transfer fidelity of patterns from glass into 3D culture. (A) An image of a mouse mammary fat pad was (B) reconstituted as a pattern of MCF-10A cells on glass (image inverted for clarity). (C) The pattern transferred into 3D culture precisely transposes to the original pattern on glass (scale bar 300 µm). (D) The image of the mouse mammary fat pad is expanded for clarity and comparison. Scale bar is 500 µm. (E) Larger view of the patterned cells to show single-cell resolution of the 1.5 cm wide pattern (scale bar 1 mm). (F) Displacement vectors of cells from a single alignment point are denoted as Ds (pattern on surface) or Dg (pattern transferred to gel). (G) A heat map of the mammary fat pad pattern denoting the average displacement of cells when transferred from a surface to a gel. (H) The average displacement of cells given as a function of the distance the cell is from other cells. (I) An asymmetric pattern of lines that is easily stitched to measure the transfer fidelity of a pattern from glass to gel (scale bar is 1 mm).

Transfer fidelity is maintained to a high degree of precision during STDPAC. The overall structure of the pattern - pattern fidelity - throughout 3D culture is also retained, somewhat surprisingly. Cells and microtissues are dynamic and express behaviors such as collective growth and motility. However, a pattern of MCF-10A grids embedded in Matrigel and 3D cultured with assay media were seen to qualitatively retain the overall pattern architecture over 96 hours in culture (Figure 3-7). Tissues mostly remained within the space in which they were patterned, which is contrary to some behaviors seen when MCF-10A assemblies are grown in 2.5D culture on top of Matrigel (Liu et al. 2012). Pattern fidelity throughout 3D culture enables the creation of arrays of tissues that are easily imaged via microscopy, due to the fact that tissue locations are simple to array within the same plane.

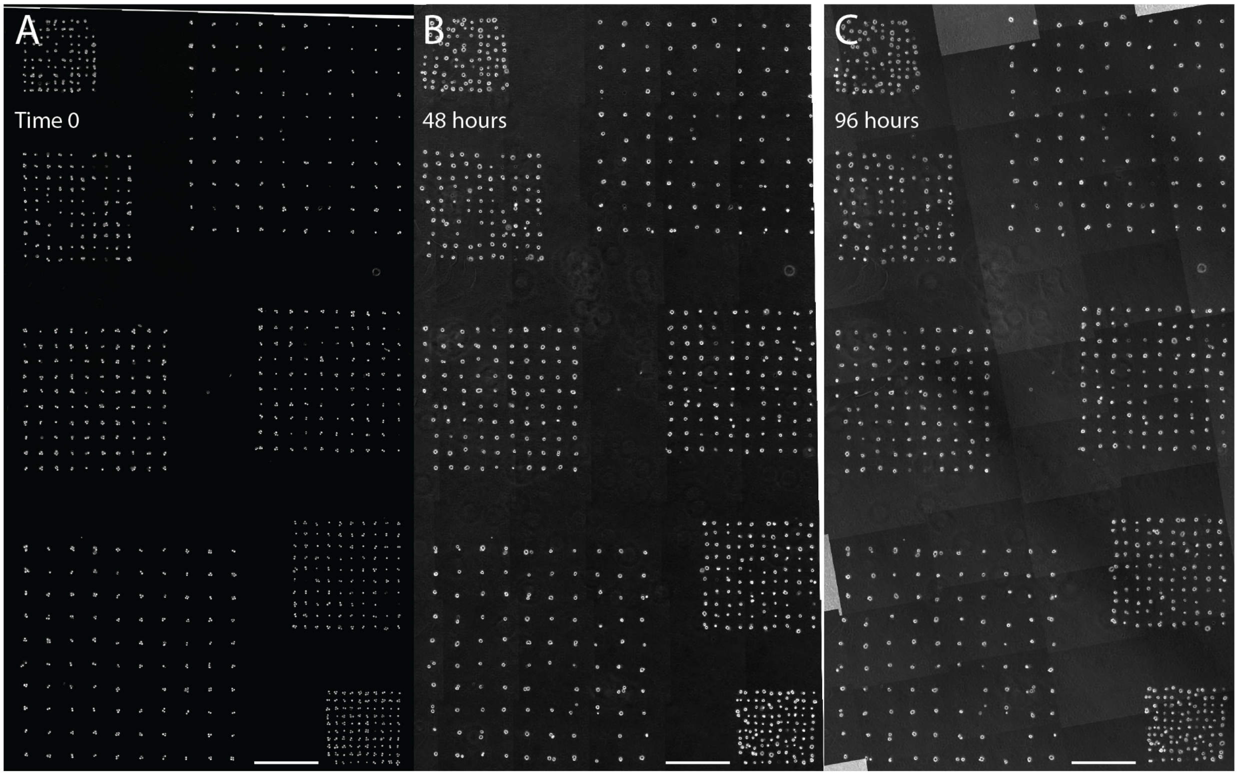

Figure 3-7. Pattern fidelity over time of tissues in 3D culture. (A) A pattern of multiple grids of MCF-10A tissues are cultured in Matrigel and imaged at time zero, (B) Imaged after 2 days, (C) and imaged after 4 days. Pattern fidelity is mostly retained over 4 days. All scale bars are 500 μm.

Control of Tissue Composition

Making use of pattern fidelity, many applications of SMDPAC were demonstrated by creating arrays of tissues. For example, to demonstrate control of size and composition of tissues assembled by STDPAC, we created arrays of 800 tissues in which assemblies of MCF-10A cells were controlled to contain only one green cell. To create these assemblies, a pattern of an equilateral triangle was spotted onto glass via the Nano eNabler. Two of these spots contained A DNA, and one of the spots contained B DNA. Then, a green cell labeled with both A-prime and B-prime lipid DNA was attached to the B DNA spot. Non-fluorescent cells were labeled with A-prime lipid DNA and subsequently attached to the A DNA spots. STDPAC was employed to assemble non-fluorescent MCF-10A cells labeled with A-sequence DNA onto the equilateral triangle of seed cells. After transfer to Matrigel, assemblies self-organized into tissues containing only a single green cell (Figure 3-8A). The entire array of 800 tissues is shown assembled as a 20 x 40 grid at 0 hours, and then growing as tissues with single green cells at 24 hours (Figure 3-8B). When looking closely, it is possible to see that both assembly size and subsequent tissue size are tightly controlled across the array (Figure 3-8C). Cells are, however, dynamic. Some assemblies that have one green cell at time 0, as allowed by the level of control of STDPAC, grow into tissues with 2 green cells at 24 hours. Cells divide, and although we can control the initial composition and size of tissues, they will exhibit behaviors inherent to their genetic code when growing in 3D culture (Cerchiari et al. 2014).

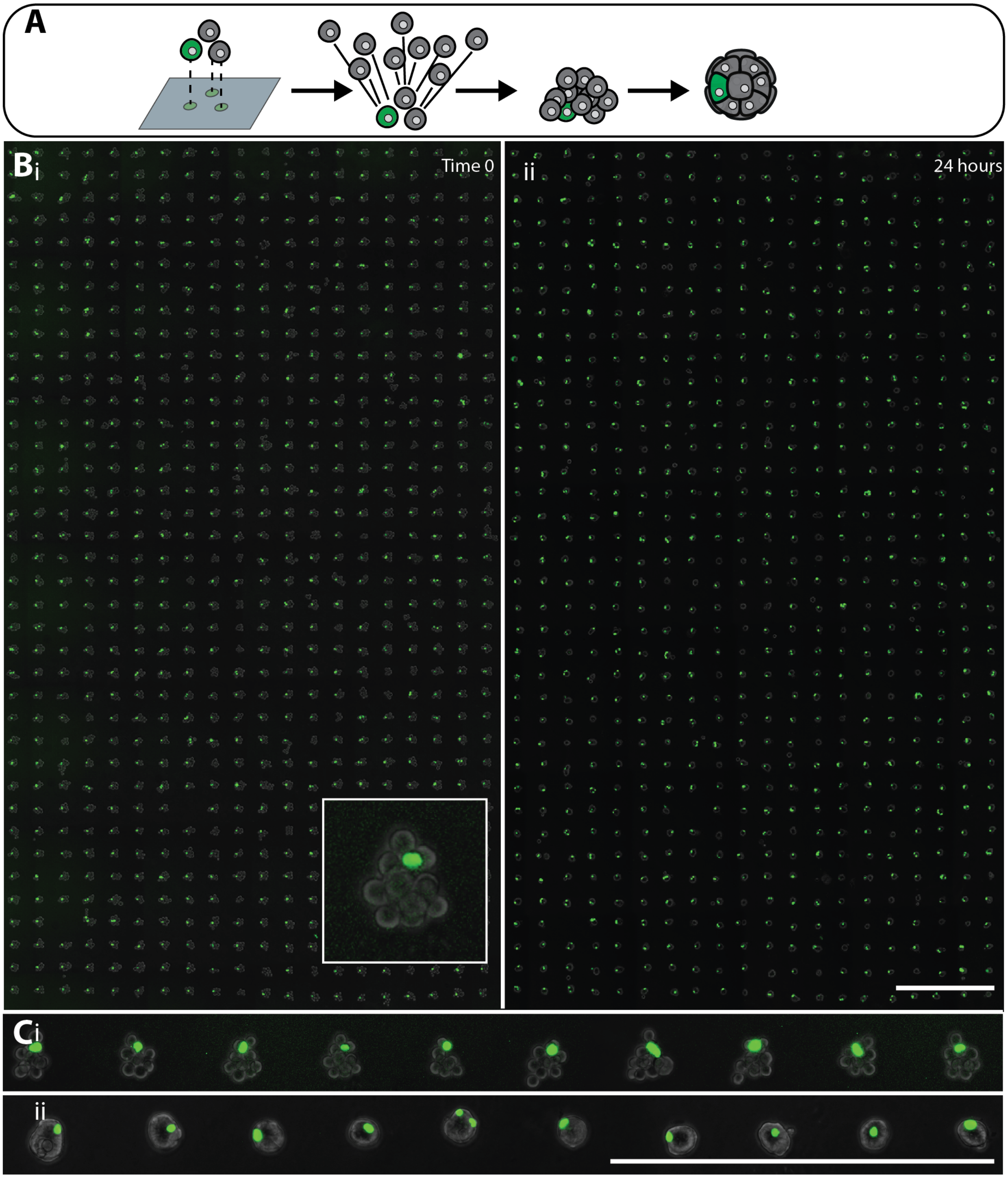

Figure 3-8. Size and composition-controlled microtissues assembled with STDPAC. (A) Microtissues are assembled as described earlier with the exception of using 3 seed-cells to initiate assembly. A single cell within the 3 seed-cells can be of different identity to create compositional control (B) An array of microtissues with a minority population of a single green cell is shown as assemblies at time 0 (i) and as condensed microtissues 24 hours later (ii). (C) A zoomed image of the array shows

detailed cell and tissue outlines of assemblies at time 0 (i) or 24 hours (ii). All scale bars are 500 μm.

To further demonstrate the power of STDPAC to create tissues of controlled size and composition, we created tissues of the same size as demonstrated in figure 3-8. Instead of a single green cell, however, we created tissues of the same size but with three green cells. To accomplish this, we patterned three green cells as equilateral triangles onto glass using A DNA to pattern glass and A-prime lipid DNA to label cells. A single round of assembly created assemblies of MCF-10A cells with three green cells, which grew into tissues of the same composition in 3D culture with Matrigel (Figure 3-9A). An entire array of 800 tissues is shown at 0 hours and 24 hours, mostly retaining the composition over time (Figure 3-8B). A magnification of a small portion of the array confirms that assembly sizes are the same as seen in figure 3-7, while differing in green cell composition.

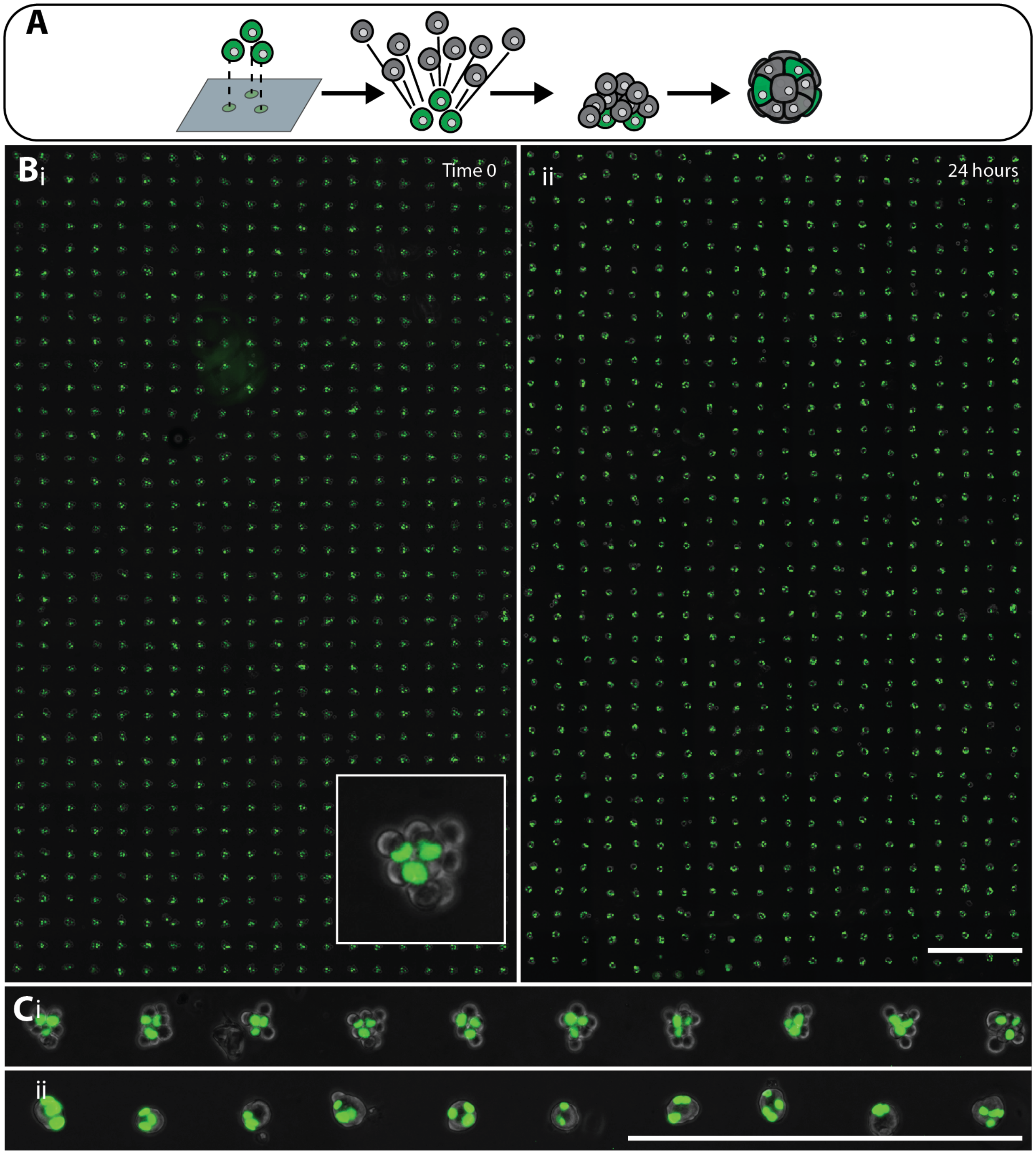

Figure 3-9. A second example of size and composition-controlled microtissues assembled with STDPAC. (A) Microtissues are assembled as described earlier with the exception of using 3 seed-cells to initiate assembly. All 3 seed-cells are of a single identity. (B) An array of microtissues with a minority population of 3 green cells is shown as assemblies at time 0 (i) and as condensed microtissues 24 hours later (ii). (C) A zoomed image of the array shows detailed cell and tissue outlines of assemblies at time 0 (i) or 24 hours (ii). All scale bars are 500 µm.

Assemblies of large sizes can also be easily created. With considerations of both matrix and media composition, large assemblies can grow into contiguous tissues in 3D culture. A large, rectangular assembly of cells was created via STDPAC by patterning rectangular patterns of DNA and performing four rounds of MCF-10A assemblies on top of them (Figure 3-10A). After transfer into Matrigel/collagen (6 mg/ml non-growth factor reduced Matrigel homogenously mixed with 2 mg/ml rat tail collagen 1), the assemblies grew into single, contiguous tissues of almost a millimeter in length (Figure 3-10B). A closer look of an assembly at 0 hours highlights the density of cells packed into a single assembly (Figure 3-10C). The density of cells in the assembly also ensures that a similarly sized tissue will be retained, even after 48 hours in culture (Figure 3-10D). Even large tissues can be built via STDPAC can be arrayed for simple microscopy and ease in performing assays.

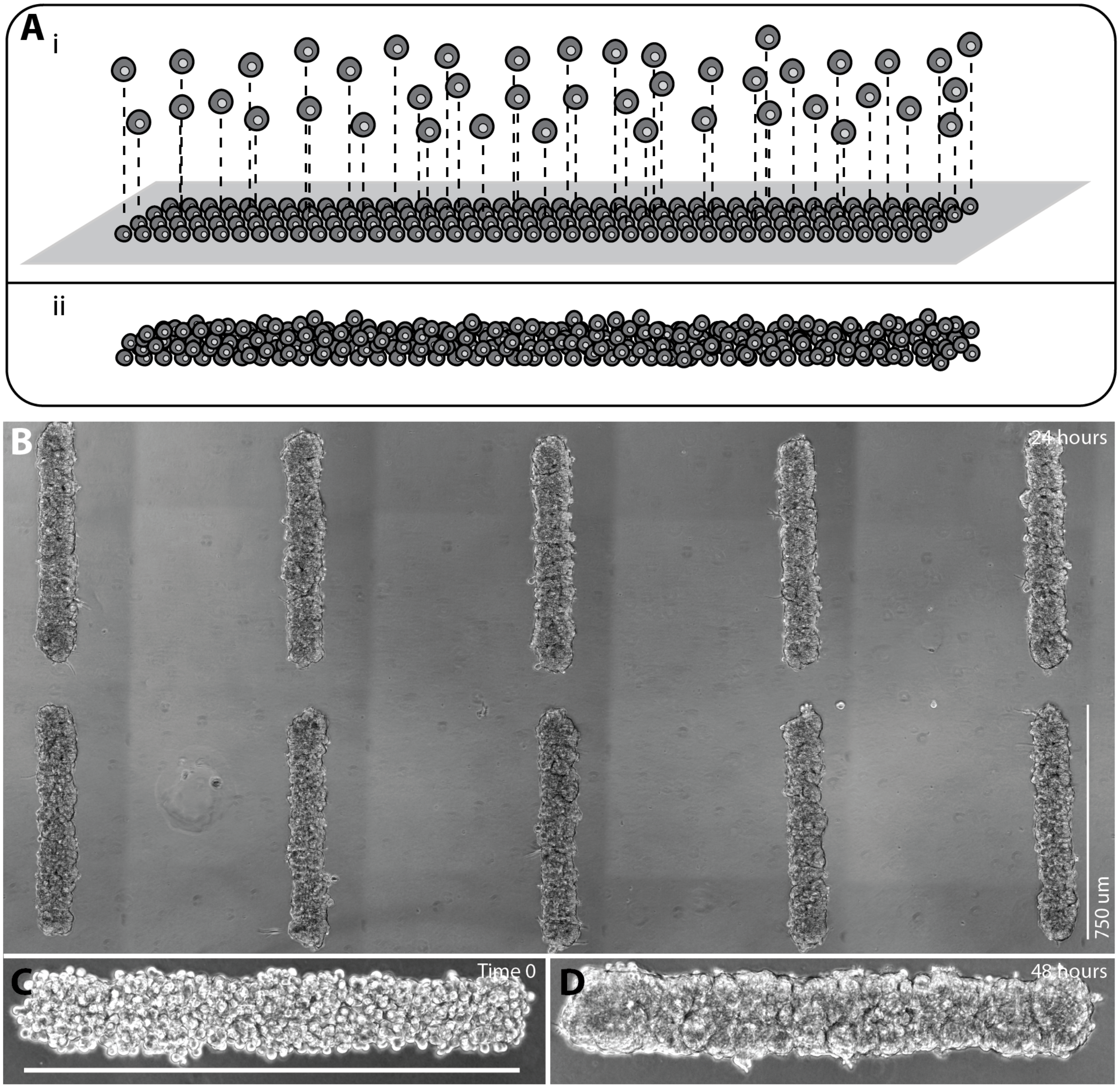

Figure 3-10. Large tissues synthesized via STDPAC. (A) Large patterns of cells on glass can be used entirely as seed cells (i) to create large tissues with the application of programmed assembly (ii). (B) An array of contiguous MCF-10A cords are synthesized via STDPAC. (C) A single MCF-10A assembly is shown immediately after transfer to 3D culture. (D) The same assembly condenses into a single tissue over 24 hours. All scale bars are 750 µm.

To ensure that tissue synthesis via STDPAC was compatible with other cell-types, we also demonstrated the synthesis of large, contiguous Madin Darby Canine Kidney (MDCK) epithelial tissues, some of which were over two millimeters long (Figure 3-11A).

The MDCK tissues also maintained their structure when imaged over 48 to 96 hours in 3D culture within Matrigel/collagen (Figure 3-11B-C). In fact, even tissues as large as a centimeter in length were able to maintain their structure over time (Figure 3-12). HUVECs (Human Umbilical Vascular Endothelial Cells) were patterned into the shape of an engineered vascular bed spanning more than one centimeter in length (Figure 3-12A). After three steps of assembly, the HUVEC pattern was transferred into Matrigel/collagen (Figure 3-12B) and cultured into a tissue over 24 hours (Figure 3-12C). When imaged next to a penny, the HUVEC tissue is seen to be about the length of Abraham Lincoln's head. All in all, tissues synthesized by STDPAC are remarkably uniform in cross sectional area, with tighter distribution correlated to larger tissue size (Figure 3-11D). This is due to the fact that cells are heterogeneous in size and thus cell-to-cell variability in size will more greatly affect small tissues. Also, the imprecision of the cell assembly steps onto existing seed-cells is highly masked when the tissue is large compared to a cell size. However, with small tissues, total size and composition can be tightly controlled compared to random loading (Figure 3-11E). Regardless of composition (one green cell or three green cells), assemblies from figures 3-8 and 3-9 have the same number of total cells, and most of the cells for each condition maintain their composition of one green cell or three green cells with utmost specificity.

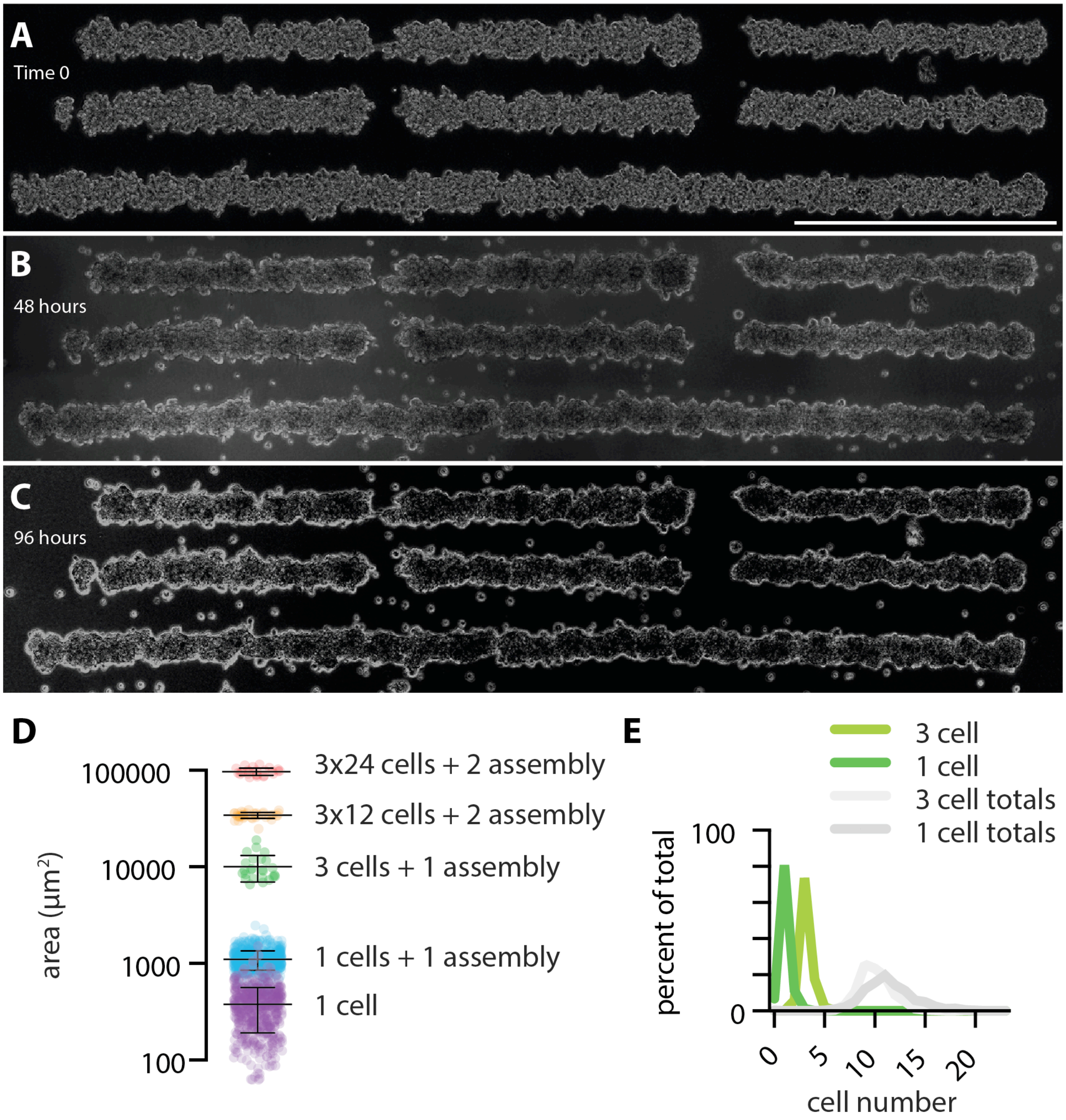

Figure 3-11. Synthetic control of the size and scale of tissues by STDPAC. (A) Multiple sizes of MDCK assemblies are created via STDPAC and shown at time 0, (B) 48 hours, and (C) 96 hours. Scale bar is 750 μm. (D) The cross sectional areas of 5 different assemblies show the capability of size control by STDPAC. The pitches between cells are 30 μm for large patterns. (E) Microtissue assemblies are controlled for total cell number while varying the number of minority cells between 1 and 3.

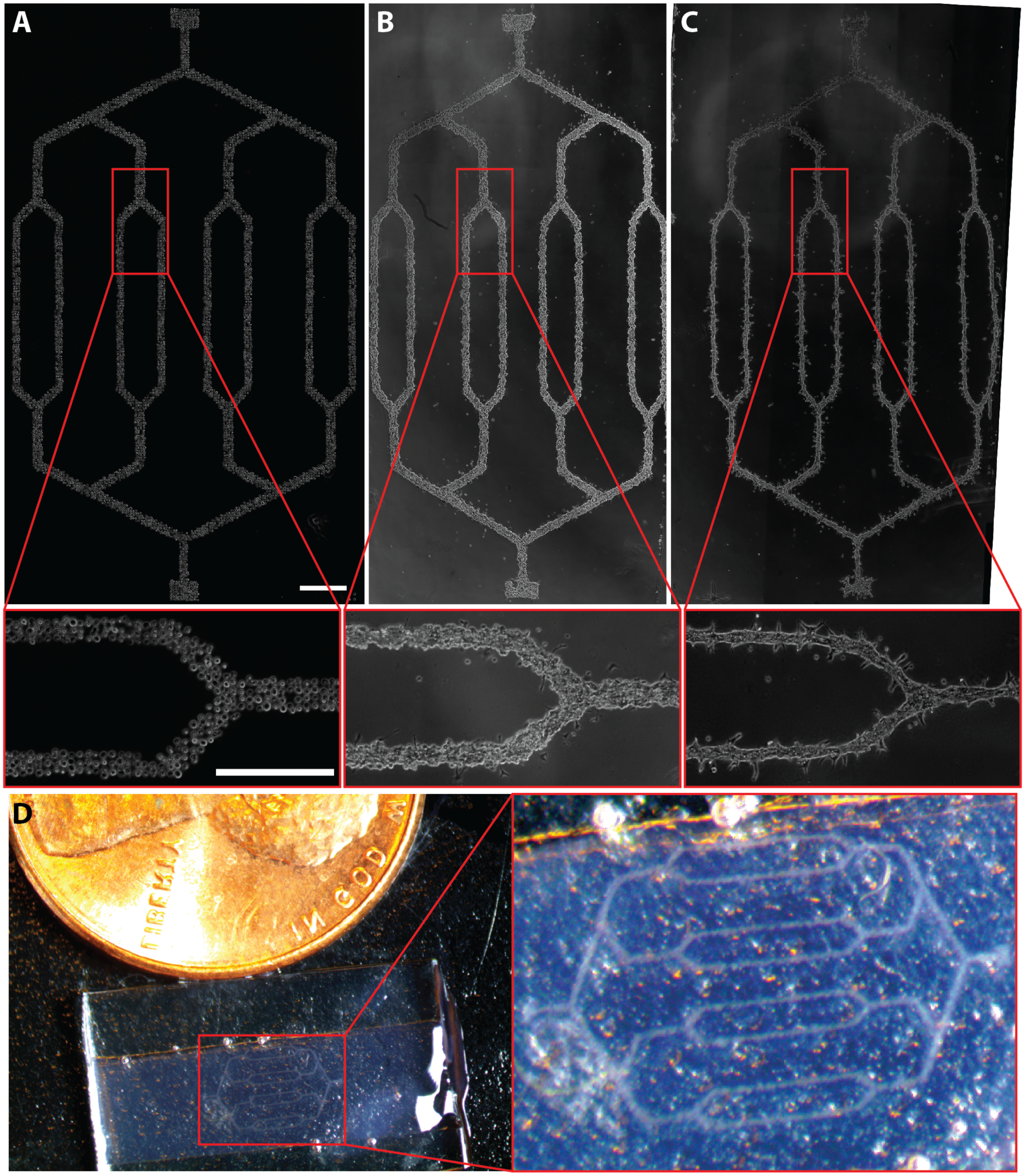

Figure 3-12. Large-scale tissue synthesis via STDPAC. (A) A 1.5 cm long pattern of HUVEC seed-cells in the form of a vascular bed with a zoomed area (B) The HUVEC pattern with 3 steps of assembly and shown immediately after transfer to 3D culture (C) The HUVEC tissue grown out over 24 hours. (D) The HUVEC tissue shown embedded in matrix and directly compared to the size of a penny. The zoomed image is enhanced in contrast to improve tissue visibility. All scale bars are 500 μm.

Orthogonal DNA and Logical Order of Assembly

Multiple experiments necessarily demonstrate control of composition, size, and location in space - sometimes all within a single experiment (Figure 3-5). However, we were also interested in demonstrating such control combined within a single, large tissue. Thus a thought experiment devised a theoretical tube-like tissue with a gradient of two different cell types that would start on either end of the tissue and fade into each other in the middle of the tissue. Instead of relying on natural mechanisms that are known to create gradients in biology (Nellen et al. 1996), we designed a gradient of pixels that demonstrated this concept as a digital design (Figure 3-13A). Using the Nano eNabler, we patterned the gradient design with two orthogonal strands of amine-DNA (Figure 3-13B). Using STDPAC, we attached cells to the pattern and only assembled cells of like identity on top of each other (Figure 3-13C - F). By using MCF-10A cells that were dyed with CellTracker Green or CellTracker Red, we were able to create a large, high-aspect ratio assembly that represented the digitized gradient (Figure 3-13G). The concept of creating an intra-tissue gradient, while intellectually stimulating, was not more challenging than creating other intra-tissue patterns. As a demonstration of our ability to control size, composition, and spatial positioning of cells within a tissue, this strategy was employed to create MCF-10A tubes of single composition, striations, and spatially segregated minority populations of cells - all within a single flow cell (Figure 3-13H). While there technical challenges in creating these multi-component tissues (described in chapter 4, Figure S3), the STDPAC techniques employed were merely a combination of the techniques previously described to create less complicated tissues.

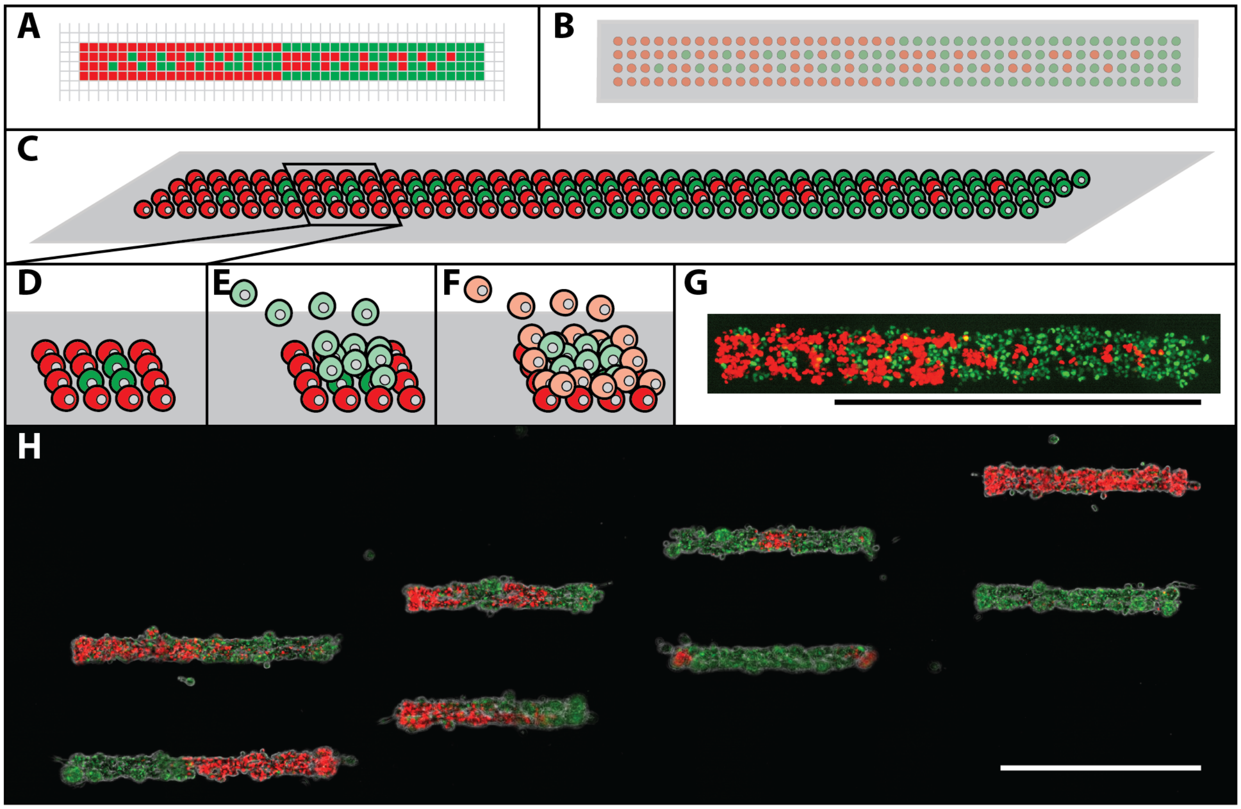

Figure 3-13. Spatial and compositional control within large tissues via STDPAC. (A) A simplified and rasterized two-component gradient is created as a digitized pattern. (B) The digital pattern is translated into a DNA pattern using direct microscale writing. (C) Seed-cells of 2 separate colors are attached to their complementary DNA spots. (D - F) Cells of a single color are only assembled onto seed-cells of the same color via selective DNA hybridization. (G) A maximum intensity projection of a MCF-10A gradient tissue after three rounds of assembly for both red and green cells (time 0). (H) A set of tissues demonstrating a variety of spatially-controlled, intra-tissue patterns after 24 hours in 3D culture. All scale bars are 1 mm.

Composition, size, and spatial resolution in x-y space were demonstrated in the creation of a gradient tube. One component of complex control that was missing, however, was specific control in the z direction of space. In order to build more complexity into our tissue models, we decided to harness clever design and logic with STDPAC to create a tissue dubbed “twinkie” - a tissue in which all outer cells are of one identity and all of the inner cells are of another identity. In the mammary gland, most epithelial tissue is composed of a bilayer of cells, in which the outer layer is composed of myoepithelial cells (MEPs) and the inner layer is composed of luminal epithelial cells (LEPs) (Ewald et al. 2008). An important principle of STDPAC is the ability to temporarily change the adhesive identity of cells without changing their genetic identity. This means that two sibling cells of the same genetic makeup can obtain and maintain different adhesive identities throughout the process of STDPAC. Given this reality, DNA patterns on surfaces can be designed to accommodate differential assembly while maintaining layers of cells of the same genetic identity. In the creation of the “twinkie” tissue, we first patterned two concentric circles of orthogonal DNA, onto which cells of the same genetic, but different adhesive, identity were attached (Figure 3-14A). Then, cells of a different genetic identity were assembled via STDPAC only onto the center circle of seed cells. A final round of assembly with cells of the same genetic makeup as the first layer of cells completed the “twinkie” tissue (Figure 3-14B i -ii). As with all STDPAC procedures, layer-by-layer assembly was required to create the final tissue (Figure 3-14B iii). While we initially demonstrated the synthesis of a “twinkie” tissue with differentially dyed cells, MEPs and LEPs were employed subsequently because of their biological significance (Figure 3-14C) (Ewald et al. 2008). As expected, a “twinkie” tissue of MEPs and LEPs, synthesized and imaged at 0 hours, maintained its organization after 24 hours in 3D culture with Matrigel and M87a media (Figure 3-14D). Interestingly, research conducted with another colleague suggests that even a biologically inverted “twinkie” tissue of MEPs and LEPs would self-organize into a proper biological structure over time (Cerchiari et al. 2014).

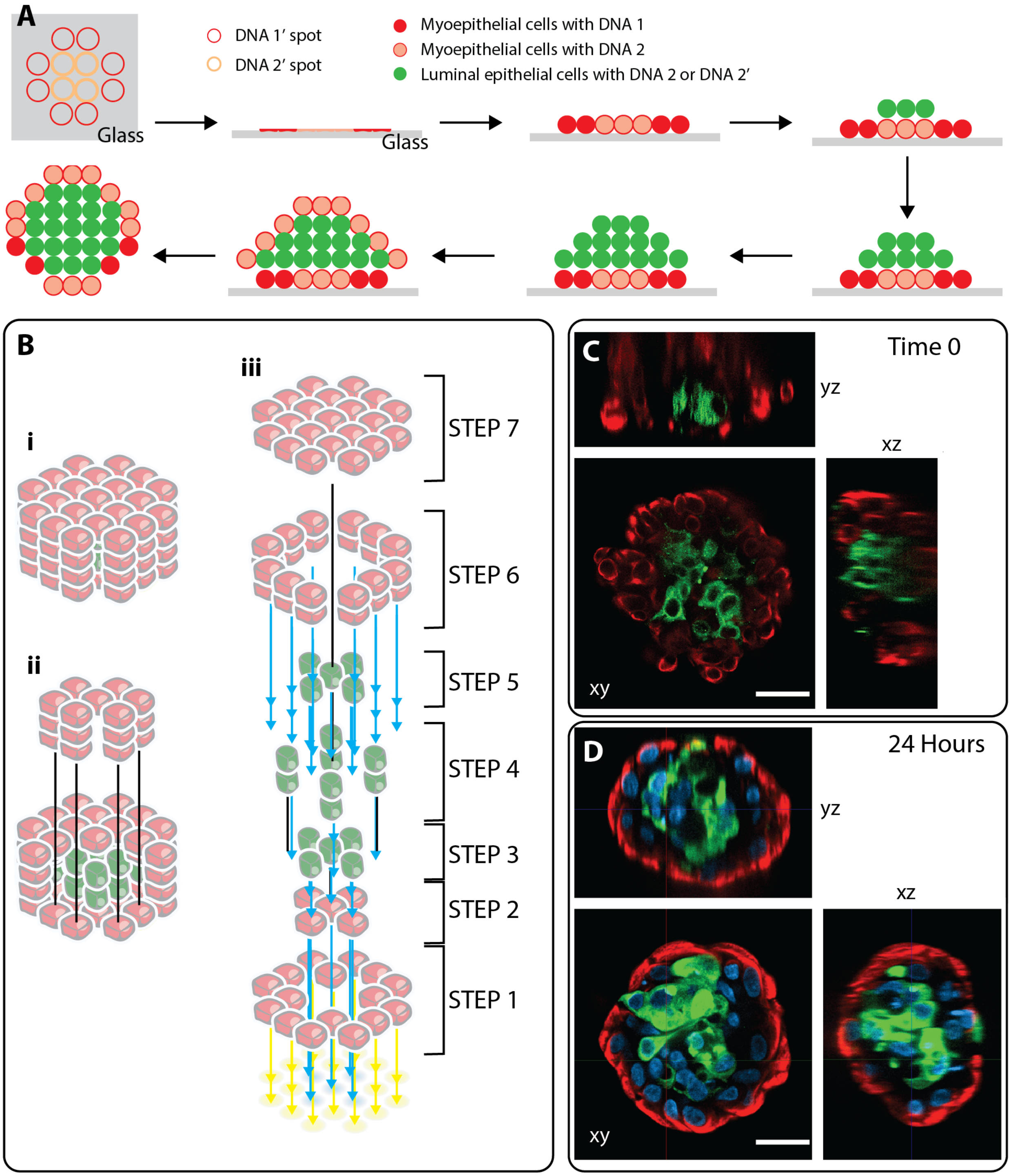
A
Glass
DNA 1′ spot
DNA 2′ spot
Myoepithelial cells with DNA 1
Myoepithelial cells with DNA 2
Luminal epithelial cells with DNA 2 or DNA 2′
Glass
B
i
ii
iii
STEP 7
STEP 6
STEP 5
STEP 4
STEP 3
STEP 2
STEP 1
C
Time 0
yz
xz
xy
D
24 Hours
yz
xz
xy

Figure 3-14. Layer-by-layer intra-tissue patterning with STDPAC - the Twinkie. (A) A STDPAC scheme depicting the synthetic tissue that is composed of red cells completely surrounding a core of green cells. (B) A fully assembled “twinkie” tissue (i) with part of the outer shell of red cells removed (ii). An exploded-view diagram of the “twinkie” tissue (iii). (C) A fully assembled HMEC “twinkie” at time 0 with an inner core of LEPs (green) surrounded by an outer layer of MEPs (red). (D) An HMEC “twinkie”

condensed into a bilayered, polarized tissue at 24 hours in 3D culture. All scale bars are 20 μm.

Control in tissue size, shape, composition, and spatial organization have all been demonstrated in the context of single tissues. However, all tissues in biological settings require interactions with other surrounding cell types in order to function properly (Wiseman & Werb. 2002). Also, an additional demonstration of complex model creation was necessary to truly set STDPAC completely apart from other tissue synthesis and reconstitution methods. To do so, we created a multi-component pattern of epithelial tissues, endothelial tissues, and fibroblasts in an organized pattern of tissues to create a complex model of a simplified mammary gland component previously impossible to model within an *in vitro* setting (Figure 3-15A). Using HUVECs, green MCF-10As, and Human Mammary Fibroblasts (HMFs), we reconstituted and 3D cultured in Matrigel/collagen a pattern mimicking epithelial tissues next to fibroblasts and surrounded by vasculature (Figure 3-15B). In fact, more than six different synthetic models were created, 3D cultured, and imaged over 24 hours (Figure 3-15C-D, Figure S3). While the tissues were not assayed for biological behavior, they were cultured until the 48 hour time point in multiple media conditions (Figure S3). The goal of complex model generation via STDPAC is, eventually, to create functional models of vascularized tissues (Figure S3). While we have not yet succeeded in this endeavor, creating patterns in which size, shape, composition, and spatial organization is controlled is a step in the right direction.

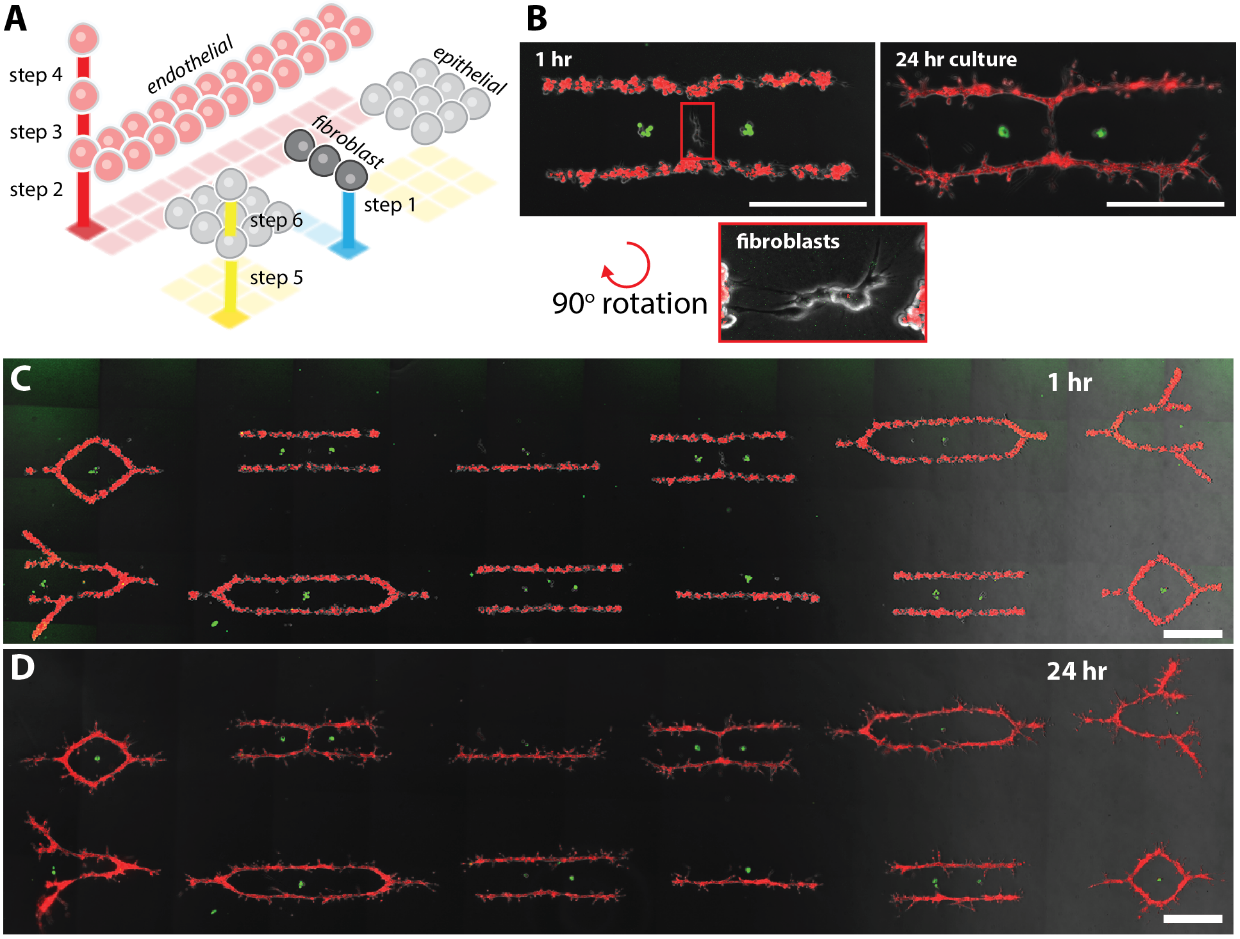
A
step 4
step 3
step 2
endothelial
epithelial
fibroblast
step 1
step 6
step 5
B
1 hr
24 hr culture
fibroblasts
90° rotation
C
1 hr
D
24 hr

Figure 3-15. Multi-scale multi-component tissue synthesis via STDPAC. (A) A scheme depicting the construction of a pattern of tissues with 3 separate cell-types and 2 sets of assemblies (B) The scheme assembled with HUVEC endothelial, MCF-10A epithelial, and 71C fibroblast cells. Images are shown immediately after transfer to gel and grown out for 24 hours in 3D culture. The zoom of the fibroblasts has been contrast enhanced for increased visibility. (C) Various patterns of 3-component tissues are shown immediately after transfer to 3D culture. (D) The same patterns after 24 hours in 3D culture. All scale bars are 500 μm.

Commentary

Science, due to its empirical nature, requires a controlled system. A fully controlled system would be perfect, but nothing is fully controlled. For example, even a single cell type is not fully controlled. Within a given cell line, grown up from a single clone, there are still heterogeneities that are present. Some are due to epigenetic factors, and some are due to different responses to the environmental cues. In general, cells are never in homogeneous environments because there is always information that is being communicated - chemically, electrically, or physically - by the neighbors. Thus, if there is a distribution of cell identities even within a clonal population of cells, there is a question of what really is under control. Clearly, it’s impossible to control cells – so the focus then lies on being able to control almost everything else. 3D culture is exceptionally hard to control because there are many different variables not present in 2D. Glass or plastic, on which cells are grown, are mostly uniform in composition.

Matrix is a different matter. Because the nature of biomimetic gels, there will always be a variable concentration of proteins in every section of the gel. This would still be a problem even if the gels were completely compositionally defined, which they are not. Matrigel - one of the most commonly used forms of matrix for 3D culture experiments - especially when the experiments are claimed to mimic an in vivo environment, is not completely defined. Vague percentages of protein are given, and they vary batch to batch. Not only do the matrix protein concentrations vary, and are not reported with detailed concentrations, other components like growth factors and cytokines are also not reported in detail. The fact that Matrigel is such a poorly defined matrix has led scientists to test separate lots of Matrigel in cell-based assays. Testing of the Matrigel consists of growing cells in the Matrigel, assaying for a desired phenotype, and then observing whether or not the specific lot of Matrigel yields the phenotype desired. In this way, bias is purposefully introduced into any experiment because the ingredients used were specifically chosen because they yielded what the experimenter wanted to see.

While complete control is impossible for any scientist, inputs into a system can be constantly optimized as we strive to create a perfect system. While sufficiency is enough in biology, it should never be enough for a technology. STDPAC, while unable to create a completely controlled system, still aims to bring as much control as possible to the systems in which complex tissues are modeled.

References

Rothemund, P.W.K. (2006). Folding DNA to create nanoscale shapes and patterns. Nature *440*, 297–302.

Douglas, S.M., et al. (2012). A logic-gated nanorobot for targeted transport of molecular payloads. Science *335*, 831–834.

Cerchiari, A.E., et al. (2014). A strategy for tissue self-organization that is robust to cellular heterogeneity and plasticity. P.N.A.S. *112*, 2287–2292.

Xu, T., Jin, J., Gregory, C., Hickman, J.J., Boland, T. (2005). Inkjet printing of viable mammalian cells. Biomaterials *26*, 93–99.

Sung, K.E., et al. (2011). Transition to invasion in breast cancer: a microfluidic in vitro model enables examination of spatial and temporal effects. Integr Biol *3*, 439–450.

Braunschweig, A.B., Huo, F., Mirkin, C.A. (2009). Molecular printing. Nat Chem *1*, 353–358.

Stevens, K. R. *et al.* InVERT molding for scalable control of tissue microarchitecture. (2013). Nat Commun *4*, 1847.

Hsiao, S. *et al.* Direct cell surface modification with DNA for the capture of primary cells and the investigation of myotube formation on defined patterns. (2009). Langmuir *25*, 6985–6991.

Debnath, J., Muthuswarmy, S.K., Brugge, J.S. (2003). Morphogenesis and oncogenesis of MCF-10A mammary epithelial acini grown in three-dimensional basement membrane cultures. Methods *30*, 256–268.

Todhunter, M. (2015). Rapid Synthesis of 3D Tissues by Chemically Programmed Assembly. Dissertation & Theses @ University of California.

Shamir, E. R. & Ewald, A. J. Three-dimensional organotypic culture: experimental models of mammalian biology and disease. (2014). Nature Reviews Molecular Cell Biology *15*, 647–664.

Zhang, K., Chou, C., Xia, X., Hung, M., Qin, L. (2014). Block-Cell-Printing for live single-cell printing. P.N.A.S. *111*, 2948–2953.

Liu, J. S., Farlow, J. T., Paulson, A. K., LaBarge, M. A. & Gartner, Z. J. Programmed cell-to-cell variability in Ras activity triggers emergent behaviors during mammary epithelial morphogenesis. (2012). Cell Reports *2*, 1461–1470.

Nellen, D., Burke, R., Struhl, G., Basler, K. (1996). Direct and long-range action of a DPP morphogen gradient. Cell *85*, 357–368.

Ewald AJ, Brenot A, Duong M, Chan BS, Werb Z (2008) Collective epithelial migration and cell rearrangements drive mammary branching morphogenesis. Dev Cell *14*, 570–581.

Wiseman, B.S., Werb, Z. (2002). Stromal Effects on Mammary Gland Development and Breast Cancer. Science *296*, 1046–1049.

Chapter 4: Modeling Mammary Gland Components with STDPAC

Introduction

Biological applications are required of any new scientific technique for good reason. Technique development without a proper application is an engineering accomplishment, not scientific progress. STDPAC, while a generalizable method to study the behaviors of any tissues or cells, was specifically developed to study the tissue components of the human mammary gland. The mammary gland is a fantastic experimental model system because many of its biological behaviors are generalizable to other organ systems (Bissel, Polyak, & Rosen. 2011).

Of all of the different organs in the mammalian body, the mammary gland is the only organ that undergoes the majority of its development after puberty instead of in utero (Marcias & Hinck. 2012). Thus, it is no coincidence that the mammary gland is a well-studied system of human biology – it is easier to study biological systems in developed organisms than in fetuses. There is also a wealth of information and human resources available because the breast is one of the few organs that yield non-diseased tissue samples from elective surgery. Finally, the unfortunate prevalence of breast cancer has yielded significant contributions to the rising body of scientific literature describing the mammary gland.

Modeling the human mammary gland is not complete without trying to recapture the organization of the main component of the mammary gland itself - the epithelium. The mammary gland epithelium is neither significantly more complex nor interesting compared to other epithelia. However, as already described, it is both relevant and practical as a model system. Similarly, the epithelium cannot be properly studied without consideration of the stromal components. Epithelial-stromal interaction is implicated in proper function of the mammary gland and is also a very important component of breast cancer and tumorigenesis (Wiseman & Werb. 2002).

The human mammary gland and stromal cell components engage in constant cross-talk to maintain proper structure and function (Figure 4-1A). In vivo, each component is also organized in a very specific manner that is important to the maintenance of tissue homeostasis (Figure 4-1B). This chapter details the exploration of communication between mammary gland components by the generation of several tissue model systems.

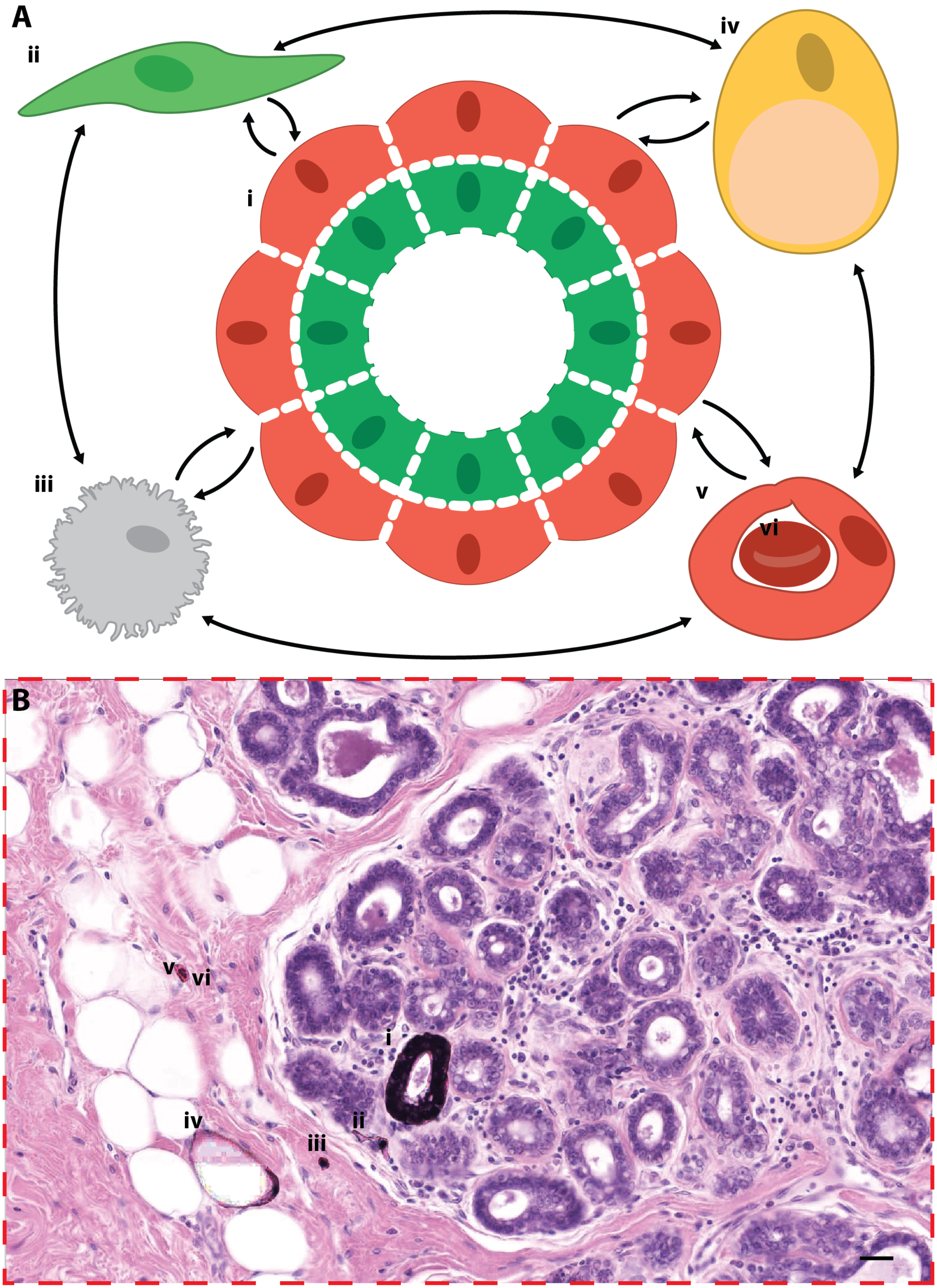
A
ii
iv
i
iii
v
vi
B
v
vi
i
iv
ii
iii

Figure 4-1. Components of the human mammary gland. (A) The human mammary gland is a communication network composed of epithelial tissue units (i) and their surrounding stromal cells including fibroblasts (ii), immune cells (iii), adipocytes (iv), vasculature (v) and red blood cells (vi). (B) A histology section of the human mammary gland has tissue components contrast-enhanced to make them visible. They include epithelial tissue (i), fibroblasts (ii), immune cells (iii), adipocytes (iv), vasculature (v) and red blood cells (vi). Scale bar is 100 µm.

Simple Models of the Mammary Epithelium

Throughout the development of STDPAC, proof of concept technical applications and biological inquiry were necessarily done in tandem. The major motivation for the development of STDPAC was to probe previously unobservable, tissue-level biological behaviors *in vitro*. The mammary gland as a model system provided the cellular toolkit necessary to build and test STDPAC in useful biological applications. Inquiry into the behaviors of the epithelium and surrounding stromal cells provided a means to apply the technical aspects of STDPAC - control over size, shape, composition, and location of cells and tissues - to model components of the mammary gland.

The initial experiments began with inquiry into simple mammary epithelial tissue behaviors in highly synthetic systems. For all of the experiments pertaining to mammary epithelial tissues thus described, the MCF-10A model system was employed (Debnath et al. 2003). Briefly, the MCF-10A model system comprises single cells or assemblies of MCF-10A cells (described as normal cells) fully embedded in growth-factor reduced Matrigel (GFR Matrigel) and 3D cultured with MCF-10A assay media. Single cells or assemblies grow into polarized acini over time. Experiments that required aberrant versions of epithelial cells used MCF-10AT cells (described as Ras cells), which are MCF-10A cells that are transduced to stably express an oncogenic version of H-Ras. Many of the experiments also required the labeling of specific cell populations with a fluorescent marker to distinguish each cell population over time. Descriptions of colored cells refer to cells transduced to express H2B-fluorescent protein (e.g. green cell means that the cell expresses H2B-eGFP). Case scenarios in which cells are dyed with fluorescent dyes will be explicitly stated in the text. Finally, most of the experiments on the mammary epithelium were completed in traditional 3D culture - that is, full embedding in GFR Matrigel and cultured with assay media.

One simple aspect of epithelial tissue growth that was hard to probe with previous technologies was the question of effects of surrounding epithelial tissues on growth. Traditional culture models could ask these questions by randomly seeding 3D cultures with a specific density of cells to create tissue cultures of varied densities, but we were able to specify the center-to-center distance between tissues with STDPAC. Specifically, a pattern was designed in which green MCF-10A cells were placed in grids with spacing distances of 60, 90, 120, and 180 um from other cells (Figure 4-2A). While the pattern did not reach perfect, single-cell occupancy of cells, cells attached with great efficiency to each of the grids (Figure 4-2B). After 96 hours in 3D culture, the cells grew into tissues that retained the general center-to-center distances as originally patterned (Figure 4-2C). An analysis of the cross-sectional area of each tissue after 96 hours showed that, while there is a slight increase in individual tissue size, the further they are spaced from other tissues, the change is not significant (Figure 4-2D). This result, all in all, was not surprising. Normal cells are expected to grow into normal tissues, and in their biological counterpart, mammary epithelial lobules grow in clusters at the terminal ductal lobular units (Macias & Hinck. 2014).

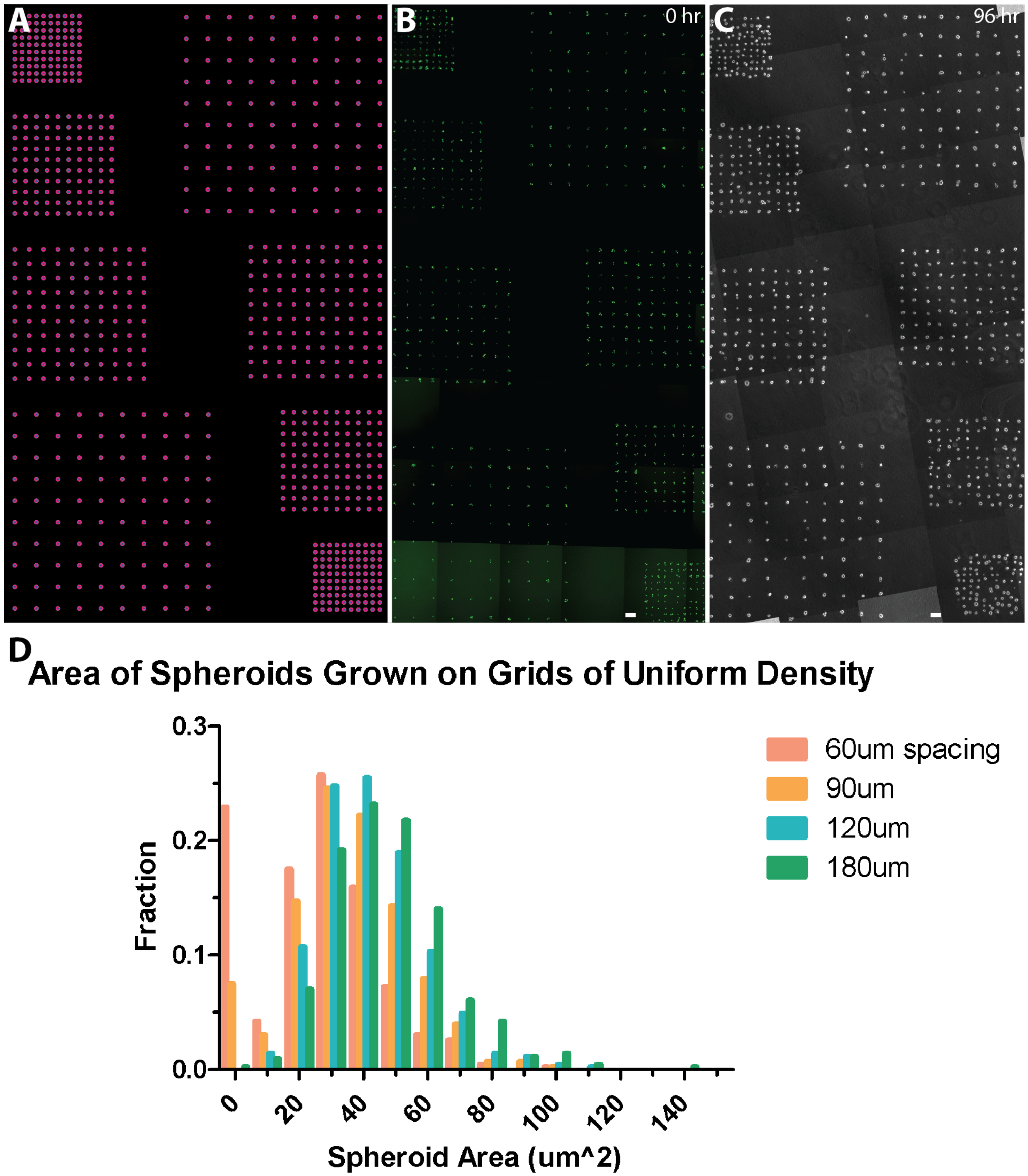

Figure 4-2. Investigating normal epithelial tissue growth via STDPAC. (A) A digital pattern of epithelial tissues at distances of 60, 90, 120, and 180 µm apart is designed with a reverse-mirrored tandem pattern. (B) Single cells are patterned to the designed via STDPAC. (C) The same pattern is shown after 96 hours in 3D culture. (D) Cross-sectional area analysis of MCF-10A acini after 96 hours in culture show that increased inter-tissue distance is correlated with larger tissue cross-sectional area. Scale bars are all 100 µm.

While the normal tissue growth under homogenous conditions was not surprising, it led us to ask if the result would be different if normal tissues were grown next to Ras tissues. To ask this question, the original pattern from the previous experiment was altered to create a similar pattern in which one set of grids of increasing pitch was changed. These changed grids became mosaic grids in which every other cell was a Ras cell, such that normal cells and Ras cells would be growing into tissues at varied distances from each other (Figure 4-3A). Normal green cells and Ras red cells were patterned via STDPAC and grown over eight days in traditional 3D culture (Figure 4-3B - C). The tissues were cultured over eight days rather than four because we wished to observe any emergent tissue behaviors that might arise from delayed signaling between the two tissue types. As expected, Ras cells grew into larger tissues over eight days in 3D culture (Figure 4-3D). They did, however, exhibit a great extent of heterogeneity as to how big the tissues grew. Surprisingly, the size of the Ras tissue did not correlate with the number of seed cells that grew into the single tissue (Figure 4-3D i vs ii). Normal cells, in contrast, were completely unsurprising in their growth behavior. Normal tissues remained remarkably homogeneous in size, even after eight days in 3D culture (Figure 4-3E). A magnified view of the pattern of Ras tissues next to normal tissues demonstrates the large extent to which Ras tissue size is heterogeneous, while a magnified view of the normal tissue only pattern clearly demonstrates that normal tissues are very homogeneous in size (Figure 4-3F - G). The most surprising observation was that normal tissues that were growing next to Ras tissues were of the same general size as normal tissues growing next to other normal tissues, despite the fact that the Ras tissues were so large (Figure 3-4H). This result strongly suggested that

Ras tissues may utilize growth-promoting intra-tissue signaling to promote growth, but do not or are unable to signal to normal tissues across the 3D cell culture medium.

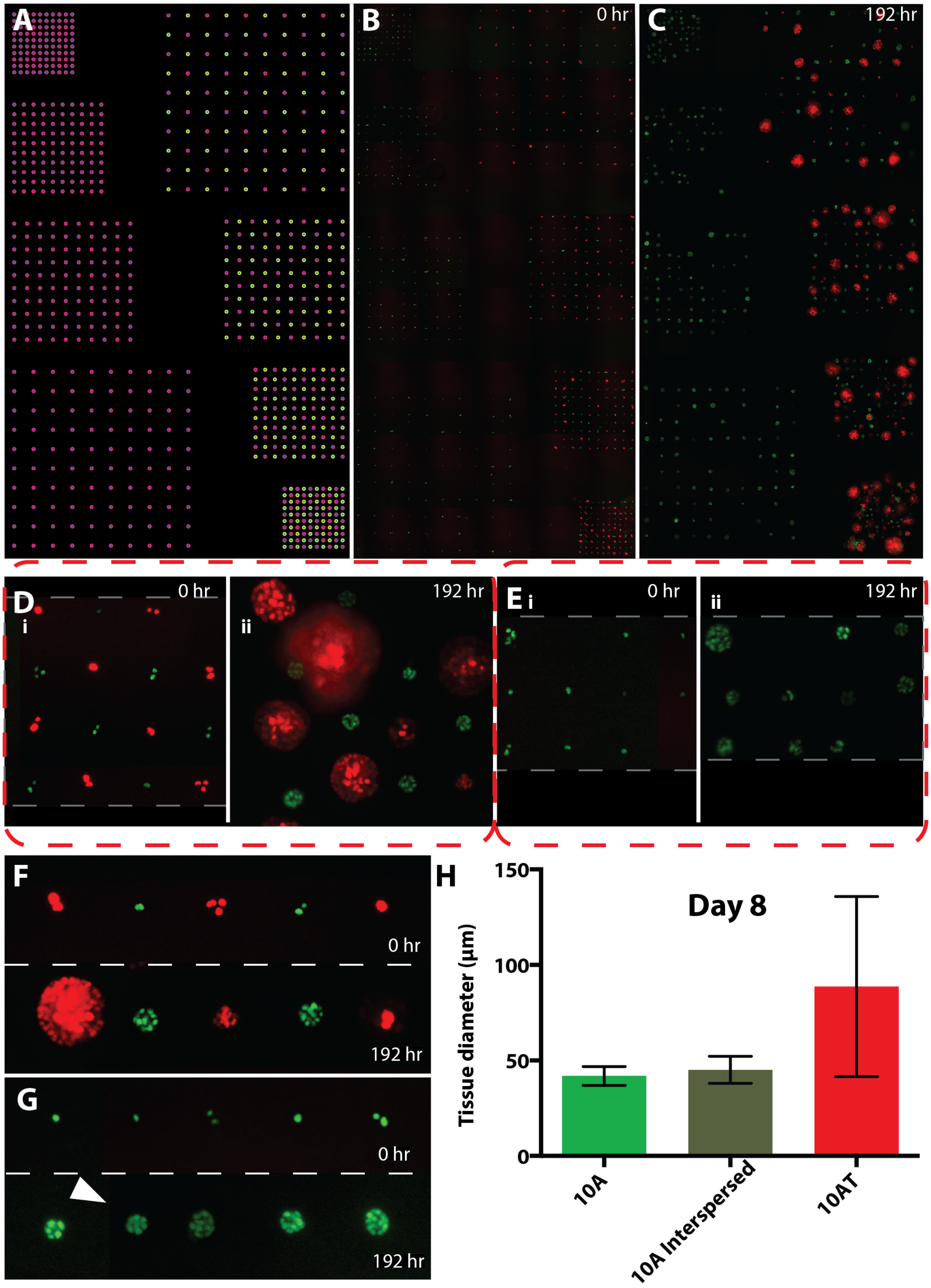
A
B
0 hr
C
192 hr
D
i
0 hr
ii
192 hr
E i
0 hr
ii
192 hr
F
0 hr
192 hr
G
0 hr
192 hr
H
Day 8
Tissue diameter (μm)
150
100
50
0
10A
10A Interspersed
10AT

Figure 4-3. Investigating the effects of Ras epithelial tissue growth on normal epithelial tissues. (A) A digital pattern of epithelial tissues at distances of 60, 90, 120, and 180 µm apart is designed with a reverse-mirrored tandem pattern. The second pattern contains a mosaic of Ras tissues evenly dispersed between normal tissues. (B) Single cells are patterned to the design via STDPAC. Normal cells have GFP-tagged nuclei and Ras cells have mCherry-tagged nuclei. (C) The same pattern of tissues is shown after 8 days in 3D culture. (D) A magnified view of the 120 µm pitch grid of tissues are shown to highlight differences between the Ras tissues and normal tissues. The microscopy image is outlined in grey dashed lines and placed on a black background (i). The image at 192 hrs is shown without a false background (ii). (E) A magnified view of the 120 µm pitch grid of tissues are shown to highlight the homogeneity of the normal tissues. The microscopy images at 0 hr (i) and 192 hr (ii) are outlined in grey dashed lines and placed on a black background. (F) A second pattern of interspersed Ras and normal tissues is shown at high magnification. (G) A second pattern of normal tissues is shown at high magnification. The boundary of two stitched microscopy images is denoted by the white arrow. (H) A graph of the tissue diameters of normal tissues, normal tissues growing with Ras tissues, and Ras tissues growing next to normal tissues are presented with standard deviation error bars. Scale bars are all 100 µm.

Rather than fixate on STDPAC optimizations to force observable behaviors that arise from inter-tissue signaling, we decided to focus on interesting observation that Ras cells may employ intra-tissue signaling to promote tissue growth. More generally, our goal was to observe the effect of a tissue on one of its component cells over time - regardless the method of signaling. To accomplish this goal, heterogeneous assemblies of cells were grown into tissues in which only a single cell within the tissue contained a fluorescent protein-tagged nucleus.

The four conditions tested were green normal cells growing within normal tissues and Ras tissues, and red Ras cells growing within normal tissues and Ras tissues (Figure 4-4A). These fluorescent cells were assayed for proliferation over time - a metric more easily measurable than growth by cross-sectional area as before (Figure 4-4B). As expected, normal cells growing within normal tissues did not exhibit much proliferation behavior. However, normal cells growing within Ras tissues exhibited a greater than two-fold increase in nuclei count over normal cells growing within normal tissues. Ras cells, in contrast, did not substantially change in proliferation regardless of the tissue composition. These data strongly suggested that Ras cells have internal and external mechanisms promoting the rapid growth of a tissue, regardless of the tissue's cellular composition. Each condition was an average of three biological replicates, all of which comprised over 3000 total events (Figure 4-4C). While each condition was imaged over 96 hours, only data up to 48 hours in 3D culture were analyzed because nuclei counts became un-interpretable with epifluorescence microscopy (Figure 4-5). Utilizing confocal microscopy, this work was continued by Dr. Alex Hughes in more detail and included the analysis of minority cell influences on the surrounding tissue cells (Supplemental Figure S4).

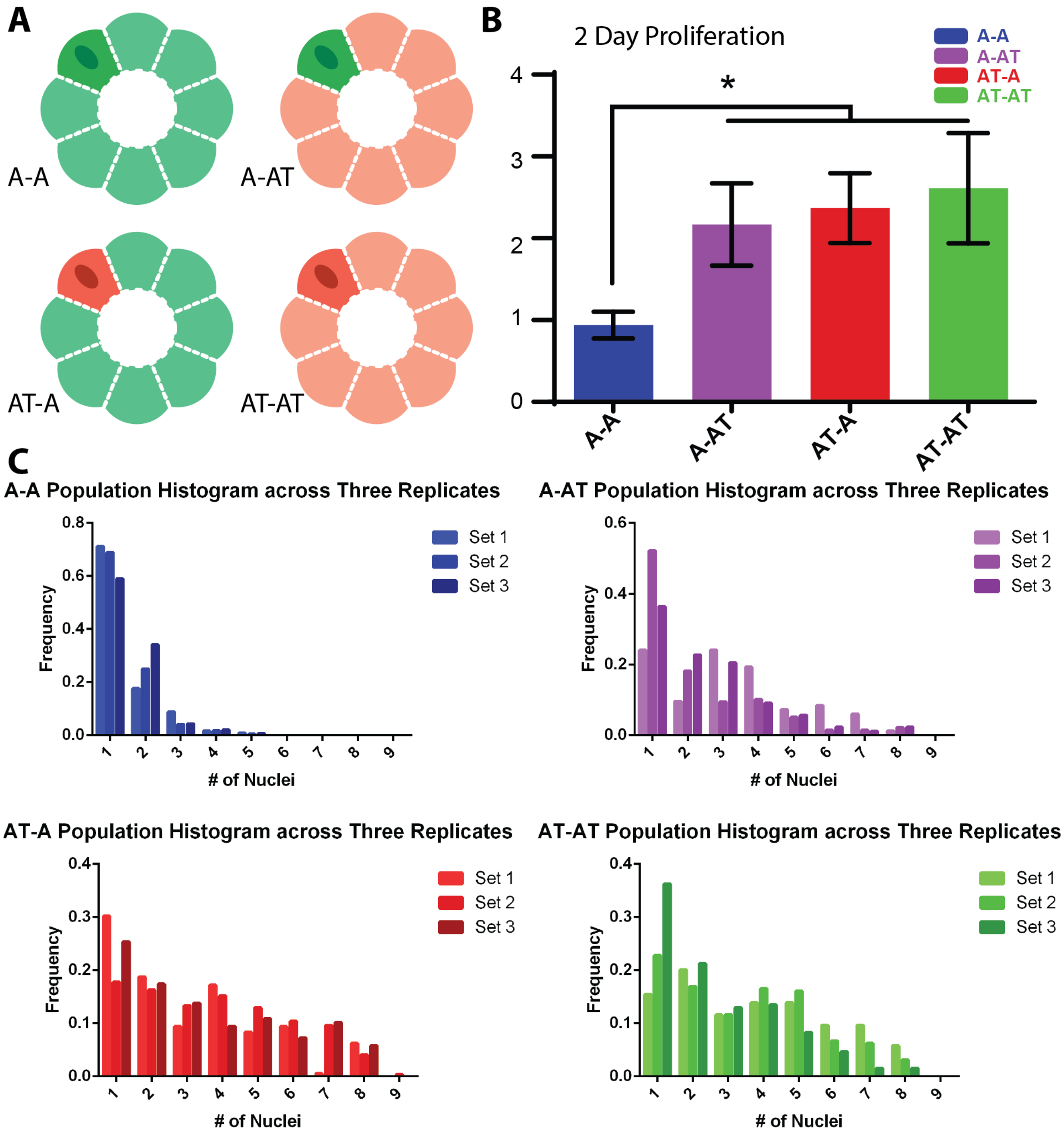

Figure 4-4. Intra-tissue effects of communication of normal and Ras on individual cell proliferation. (A) Multi-component tissues are built via STDPAC. Tissues entirely composed of normal cells in which one normal cell has a GFP-tagged nucleus is denoted as A-A. Tissues composed of Ras cells in which one normal cell is included and has a GFP-tagged nucleus is denoted as A-AT. Tissues composed of normal cells in which one Ras cell is included and has a mCherry-tagged nucleus is denoted as AT-A. Tissues composed entirely or Ras cells in which one Ras cell has a mCherry-tagged nucleus is denoted as AT-AT. (B) The two-day proliferation of single cells within patterned assemblies by STDPAC are shown as nuclei counts. 3000 events were considered in the creation of the graphs. (C) Each condition and associated data sets

are distributed by the number of nuclei counted after 48 hours and the frequency of counts.

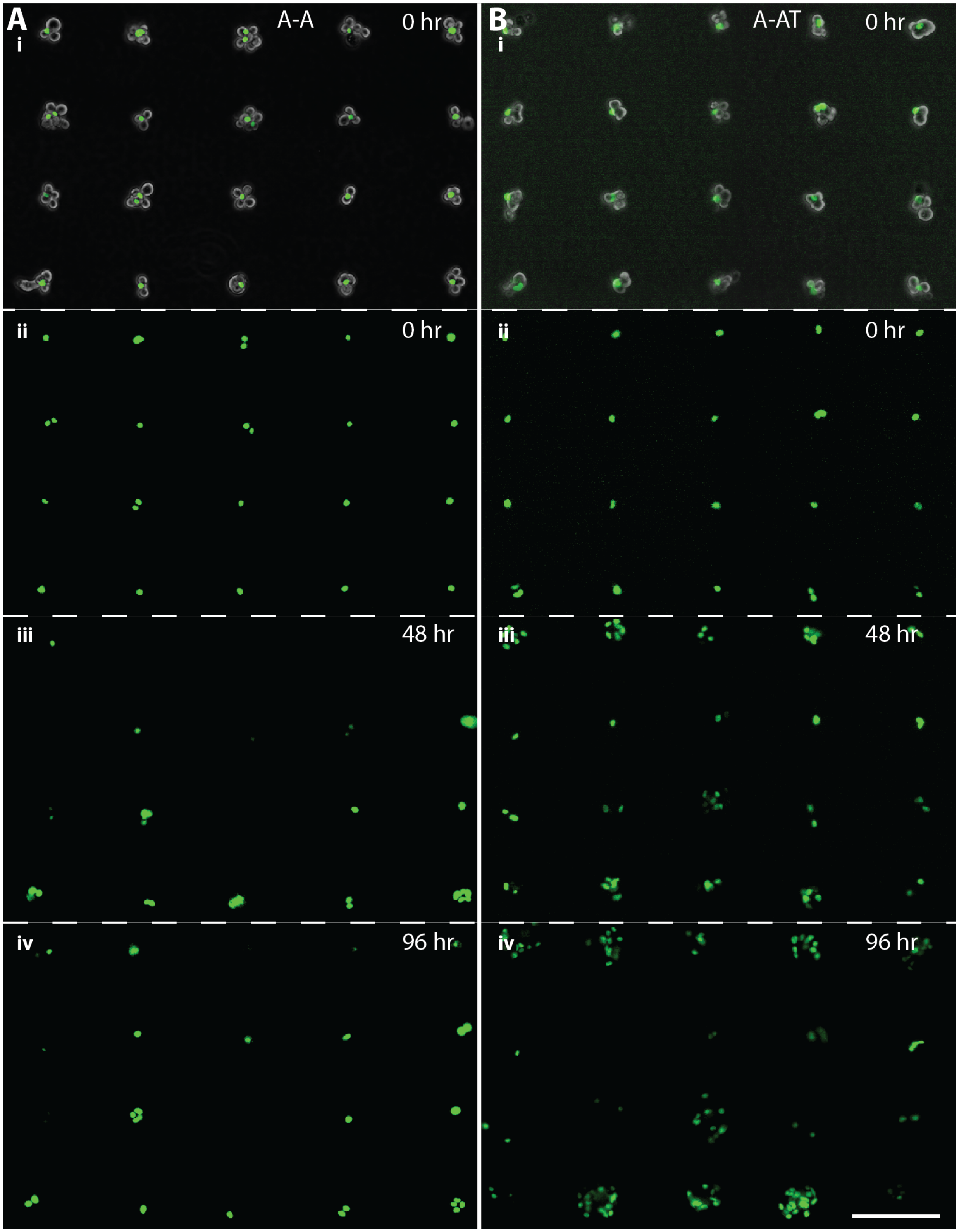
A
A-A
0 hr
i
B
A-AT
0 hr
i
ii
0 hr
ii
0 hr
iii
48 hr
iii
48 hr
iv
96 hr
iv
96 hr

Figure 4-5. Representative images of intra-tissue communication and proliferation given homogeneous or heterogeneous conditions. (A) The A-A condition is shown at 0 hours with the fluorescent nucleus of a minority normal cell surrounded by other normal cells in a combination of epifluorescence and phase microscopy (i). The same image is shown without phase contrast (ii), and imaged in 3D culture at 48 hours (iii), and 96 hours (iv). (B) The A-AT condition is shown at 0 hours with the fluorescent nucleus of a minority normal cell surrounded by Ras cells in a combination of epifluorescence and phase microscopy (i). The same image is shown without phase contrast (ii), and imaged in 3D culture at 48 hours (iii), and 96 hours (iv). All images are to the same scale and the representative scale bar is 100 μm.

In observing the effects of a tissue on one of its cells, the assay was changed to a readout of proliferation rather than tissue size. To maintain consistency in assay readout, we decided to revisit the analysis of homogenous Ras and normal tissue signaling effects on each other. Perhaps the cross-sectional growth assay was not of sufficient resolution to observe subtle changes within a tissue. The general concept was to grow homogeneous Ras and normal tissues at fixed distances from each other, and within each homogeneous Ras or normal tissue, track a single cell's level of proliferation by giving it a fluorescent protein-tagged nucleus (Figure 4-6A). The center-to-center tissue pitch was set at 120 um to maintain consistency with the experimental conditions in figure 4-3. Each experiment was also designed to contain controls within each biological replicate (Figure 4-6B). Three biological replicates of grids of 1000 tissue events were observed over two days, after which tissues were fixed, and nuclei counted.

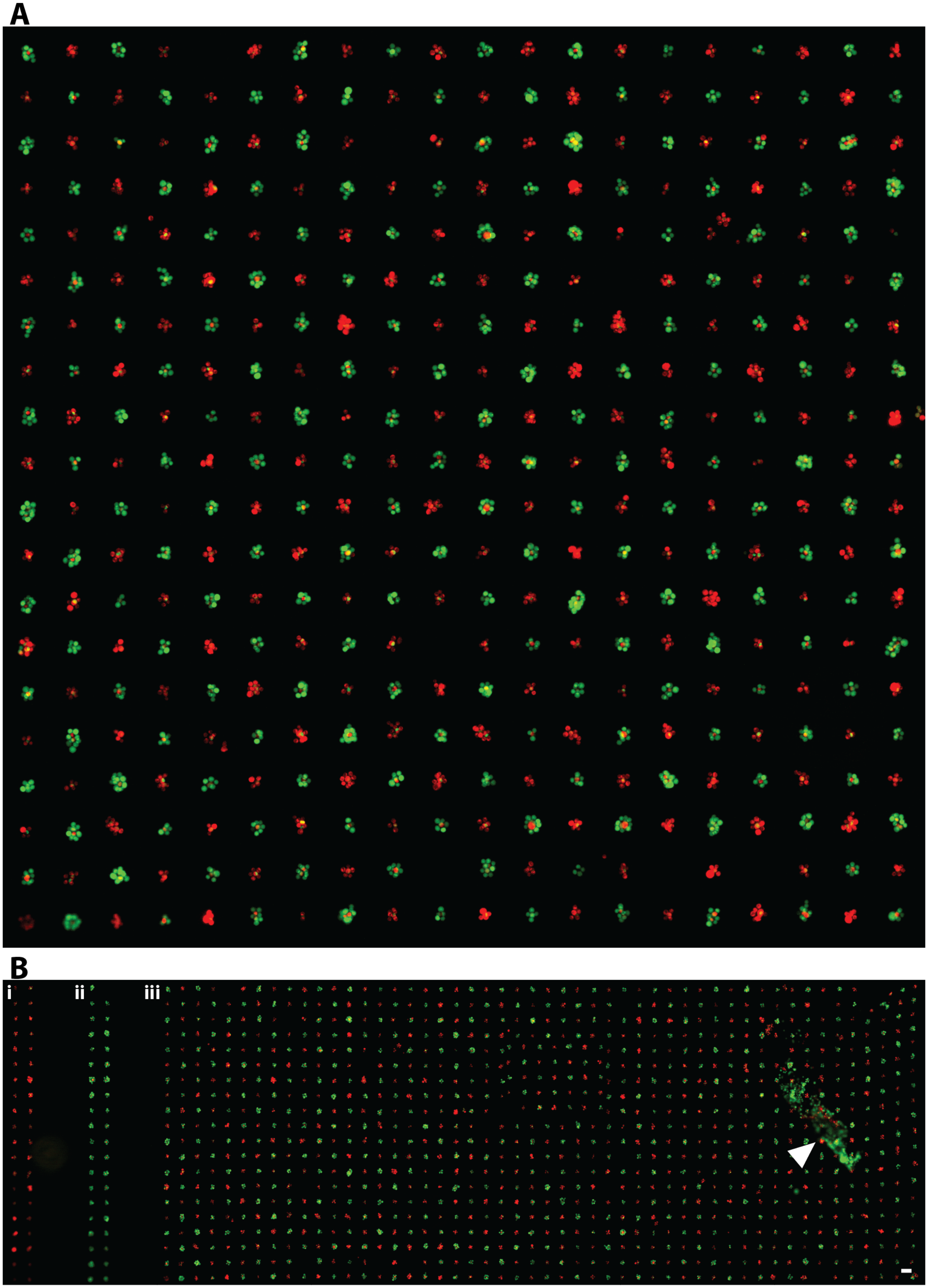
A
B
i
ii
iii

Figure 4-6. Normal tissues growing next to Ras tissues with tissue-specific single-cell proliferation resolution. (A) The top left corner of the heterogeneous pattern is magnified to show the single cell-resolution of creating homogeneous, multi-component tissues. Red ovals are mCherry-tagged nuclei of Ras cells. Green ovals are GFP-tagged nuclei of normal cells. Red circles are CellTracker Green-dyed normal cells. Green circles are CellTracker Red-dyed Ras cells. (B) Ras-only tissues are grown next to each other (i), normal tissues are grown next to each other (ii), and Ras-only and normal-only tissues are grown next to each other (iii) at a pitch of 120 μm. A distortion in the gel is shown by the white arrowhead. Scale bars are all 100 μm.

To simplify the data set and remove the potential skew of normalizing data sets, only tissues that contained a single fluorescent cell were analyzed. The data, while compiled from thousands of events, confirmed our earlier, unremarkable findings that Ras tissues most likely did not affect surrounding tissues within traditional 3D culture (Figure 4-7). Indeed, proliferation measurements of normal tissues growing next to normal tissues did not change significantly when the normal tissues were grown next to Ras tissues. Similarly, the proliferation measurements of Ras tissues did not change regardless of their surrounding tissue types.

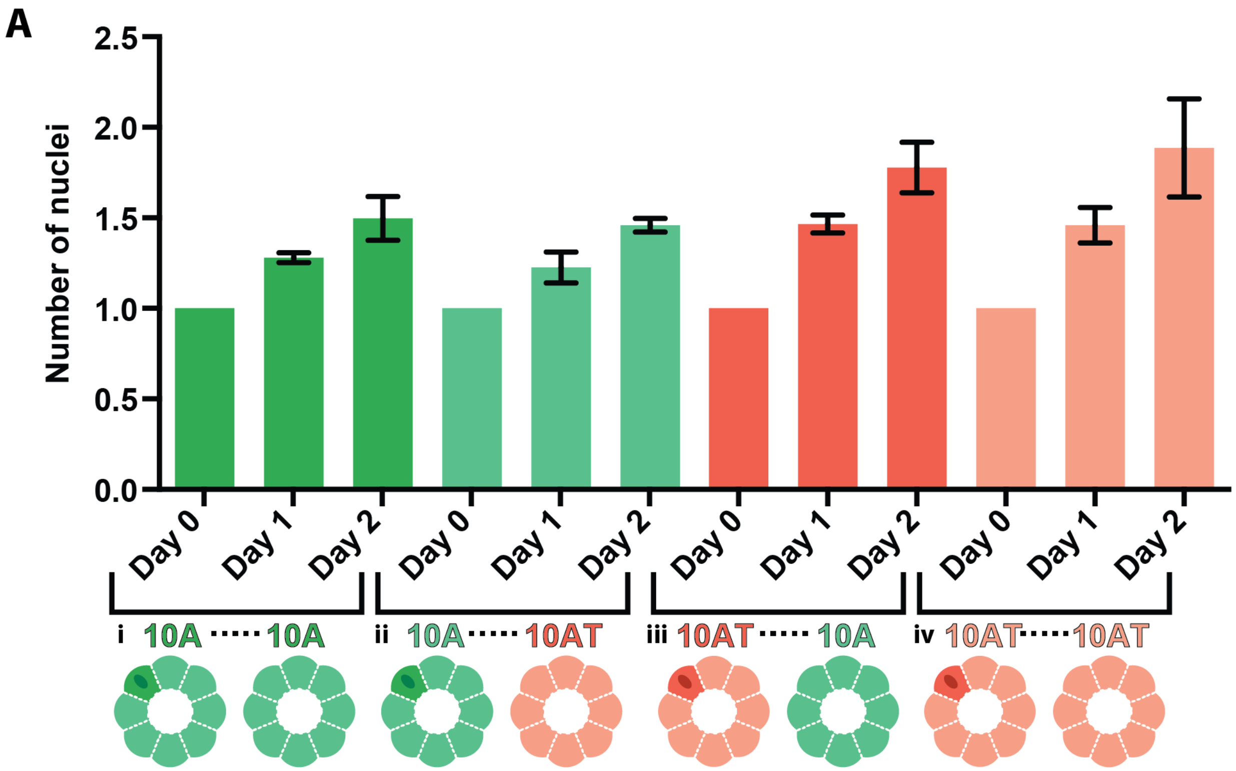

Figure 4-7. The effect of normal tissues growing next to Ras tissues on single-cell proliferation. (A) The nuclei counts for single normal cells within a normal tissue and growing next to normal tissues (i) or Ras tissues (ii) and single Ras cells within a Ras tissue and growing next to normal tissues (iii) or Ras tissues (iv) are shown over 0, 24, and 48 hours. Error bars are standard deviation and all tissues that initially had more than a single fluorescent nucleus were discarded from the data set.

These experiments collectively suggested that, when only considering epithelial tissues, the typical behaviors of normal epithelial tissues are most likely disrupted by aberrant cells within the epithelial tissues themselves rather than other surrounding epithelial tissues. The true biological counterparts of mammary epithelial tissues are never individual spheroids, but ductal in nature (Bissel, Polyak, & Rosen. 2011). On a whim, we constructed epithelial tubes of normal cells that also contained a randomly distributed, ten-percent minority population of Ras cells (Figure 4-8A). Over six days in Matrigel/collagen 3D culture, the Ras cells demonstrated a higher rate of proliferation compared to the normal cells and completely disrupted the tube-like tissue structure with random outgrowth throughout the tissues (Figure 4-8B). This result, while surprising, was consistent with our previous data in MCF-10A acini, in which single Ras cells in normal tissue exhibited no change in its faster relative proliferation rate.

As a follow-up, colleague Michael Todhunter repeated this experiment with the addition of two additional conditions, in which the ten-percent minority population of Ras cells was placed either in the middle or the ends of the MCF-10A tube (Figure 4-8C). Collective Ras cell growth was observed to localize in their original patterned positions within the MCF-10A tube over 72 hours in Matrigel/collagen 3D culture. The data suggested that collective Ras cell growth was better characterized as outgrowth - the collective Ras cell growth seemed to separate externally to the overall tissue for all experimental conditions (Figure 4-8D). But because the Ras cells did not detach from the main tissue, the overall tube-like tissue structure was observed to change depending on the location of the minority population of Ras cells (Figure 4-8E-F). Overall, these experimental results confirmed that internal Ras cells have the ability to disrupt normal epithelial tissue architecture and behavior. However, for normal epithelial tissue structures larger than symmetrical acini, the overall disruption is dependent on the location of the Ras cells within the tissue.

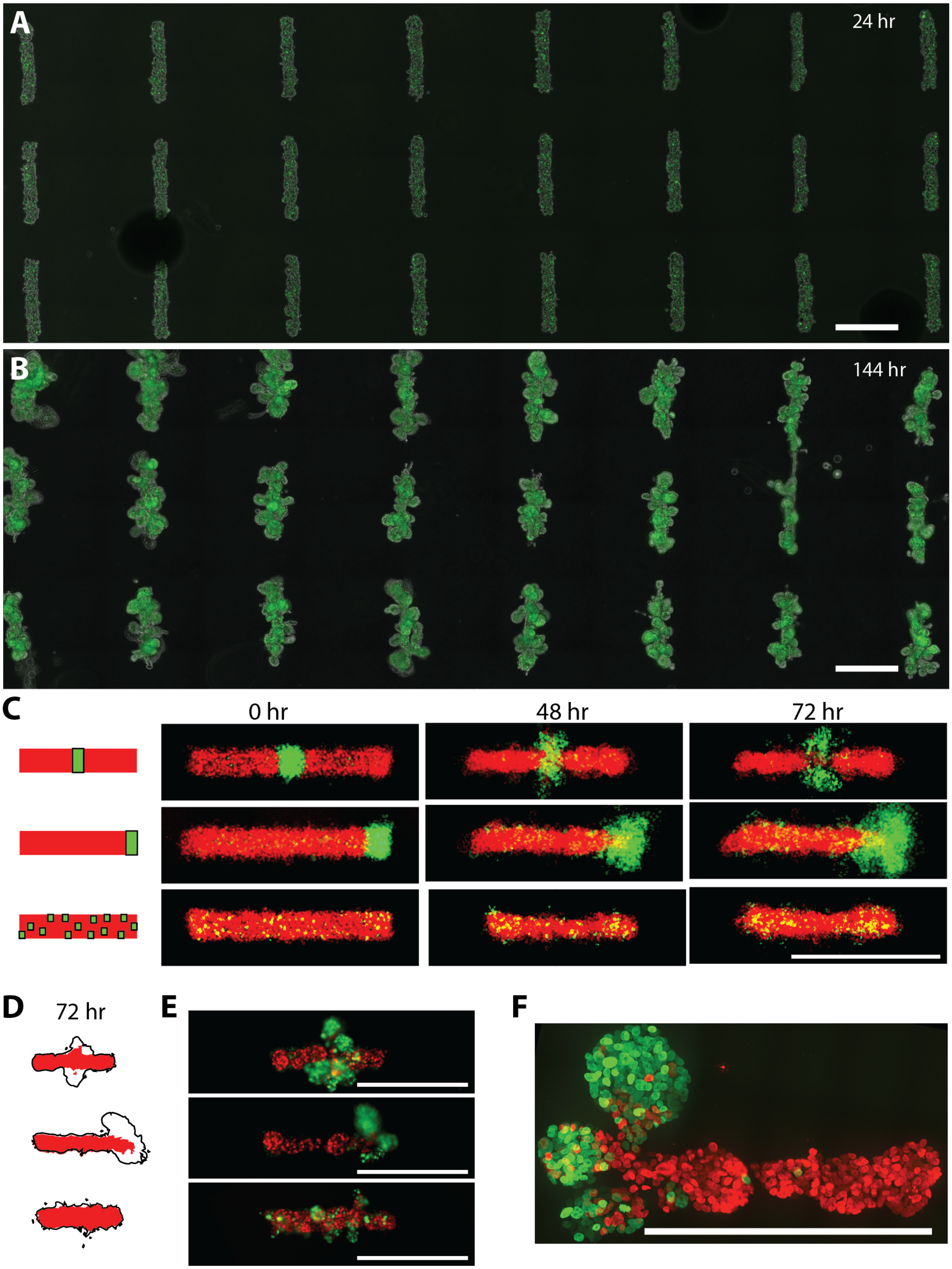
A
24 hr
B
144 hr
C
0 hr
48 hr
72 hr
D
72 hr
E
F

Figure 4-8. Investigating the effects of Ras and normal cell signaling within large tissues on collective cell behavior. (A) Tube-like tissues are built with normal cells and 10% Ras cells, randomly distributed by creating the tissue layer by layer with mixtures of normal and 10% Ras cells. (B) The 10% Ras tissues are cultured for 144 hours in 3D culture. (C) Normal tissues are synthesized via STDPAC with 10% Ras cells placed in the middle or end of the tube-like structure and imaged in 3D culture over 0, 48, and 72 hours. Images are superimposed average intensity projections of 12-14 single confocal sections of 10A MCF10A (red = H2B-mCherry) and Ras MCF10A (green = H2B-eGFP) in Matrigel/collagen mixtures. (D) A collection of same-pattern tissues are averaged and outlined at 72 hours in 3D culture to show the location and shape of the Ras and normal cells. (E) Representative wide field microscopy images of tissue after 72 hr culture. (F) A maximum intensity projection generated from 3D reconstructions of a center-patterned tissue after processing using CLARITY. Scale bars are all 100 µm.

All of the experiments only focused on the epithelium suggested that epithelial cell-derived disruptions to tissue architecture and behavior are mostly due to internal signaling within a tissue. As noted in the introduction, the mammary gland's epithelium must signal with other cell types in the stroma for proper form and function. In order to model mammary epithelium-stroma interactions *in vitro*, we focused on a single stromal component - fibroblasts.

Simple models of the Mammary Stroma: Fibroblasts

Fibroblasts are a common stromal cell type found within the human mammary gland (Wiseman & Werb. 2002). It is unsurprising, considering the fact that fibroblasts are known to constantly remodel matrix proteins (Tamariz & Grinnell. 2002), which are very important in determining mammary gland architecture and function. They are also known to disrupt epithelial tissue architecture (Dang et al. 2011). Unlike epithelial cells, which seem to mostly effect epithelial tissues via intra-tissue signaling, fibroblasts are able to affect and disrupt epithelial tissue architecture through the matrix.

Previous work by Michael Todhunter suggested that lines of fibroblasts acted in unison to create a mechanical pull in a collagen-rich matrix along the major axis of the fibroblast line. This initial experiment was conducted with immortalized skin fibroblasts called 82-6 cells. While it is known that fibroblasts generally can propagate mechanical forces through a matrix, we sought to confirm that such normal behavior was compatible with Matrigel/collagen 3D culture. As such, we created lines of fibroblasts in Matrigel/collagen and assayed for global behaviors consistent with mechanical force propagation. Dr. Michael Todhunter found that a line of fibroblasts was sufficient to pull perpendicular lines of epithelial tissues across a distance of several hundred microns in a manner consistent with mechanical pull originating at the end of the fibroblast line (Figure S4).

While this experiment suggested that global fibroblast alignment is sufficient to propagate mechanical forces across a matrix, the microtissues were too small to see the effects of the mechanical pull across an epithelial tissue surface. The thought was that differential mechanical pull must be felt across a singular surface of a tissue in order to change the intra-tissue architecture (Figure 4-9A - B). An easy change to the experiment was to create larger epithelial tissues. Thus the following experiment was conducted - large Ras tissues were built via multiple steps of programmed assembly. Ras cells were used rather than normal cells in order to bias the epithelial tissue towards changes in phenotype. We patterned a line of 82-6 fibroblasts and placed a single large epithelial tissue aligned with the major axis of the fibroblasts (Figure 4-9C). The fibroblast line was also mirrored along the other side of the epithelial tissue in order to enhance any effects of mechanical pull. The pattern was cultured in Matrigel/collagen 3D culture and the epithelial tissues were assayed for changes in morphology over time via phase contrast microscopy.

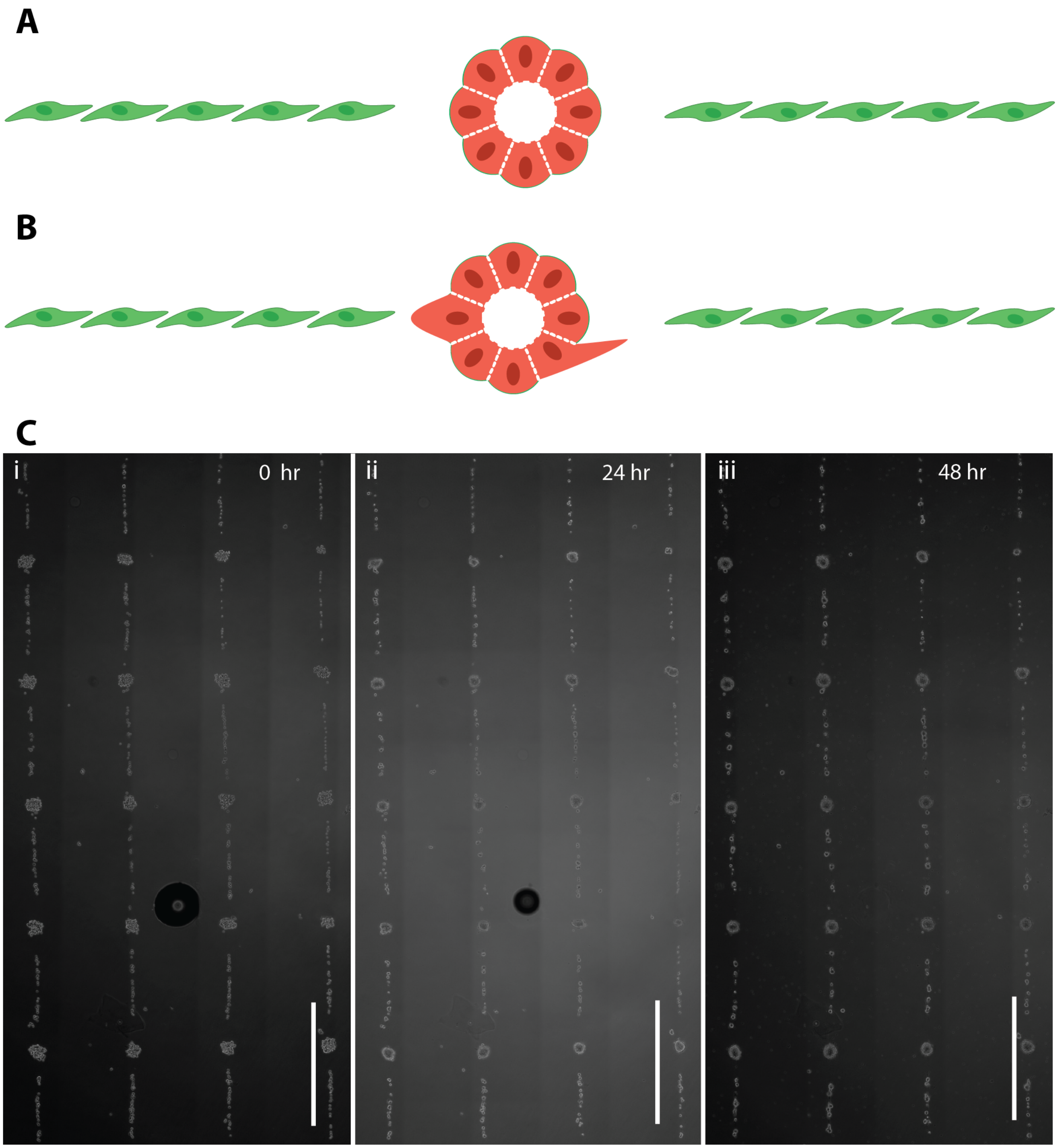

Figure 4-9. Patterns to investigate the mechanical signaling of fibroblasts on epithelium. (A) A designed pattern is meant to augment the effects of fibroblast mechanical pull across an epithelial tissue membrane. (B) Assuming compounded mechanical pull across the axis of a line of fibroblasts, the hypothesized effect of a line of fibroblasts on an epithelial tissue is shown. (C) A line of fibroblasts with large epithelial Ras tissues in between the fibroblast lines are shown in 3D culture at 0 hours (i), 24 hours (ii), and 48 hours (iii). All scale bars are 1 mm.

Three major morphological changes were observed at the surface of the Ras tissues - cell extrusions, finger formations, and tissue elongations (Figure 4-10A). These morphological changes were not surprising and hypothesized to be inter-related - cells must extrude from the tissue before they can become fingers, and finger formations in other tissues are known precede tissue elongation. The patterns were imaged every 24 hours for 72 hours (Figure 4-10B). However, it was not possible to deconvolute fibroblast behavior at the 72 hour time point, and thus the Ras tissues were quantitatively assayed for the three qualitative morphological changes only at the 24 and 48 hour time points (Figure 4-10C). The results confirmed that fibroblasts were able to propagate mechanical force across large distances in collagen-supplemented matrix and affect morphological change across the surface of an epithelial tissue. At 24 hours, ~ 43 percent of the Ras tissues exhibited finger formation, ~ 71 percent exhibited cell extrusions, and ~ 14 percent of the tissues exhibited elongation. It is important to note that these morphological changes are not mutually exclusive - indeed a single Ras tissue was able to exhibit one, two, or all three of the changes to morphology. At the 48 hour time point, the frequency of elongations stayed the same and the number of extrusions decreased to ~ 36 percent. However, finger formation increased to ~ 59 percent. These morphological changes were not too surprising - elongations were qualitatively more frequent at the 72 hour time point and a large fraction of extrusions at the 24 hour time point turned into finger at the 48 hour time point.

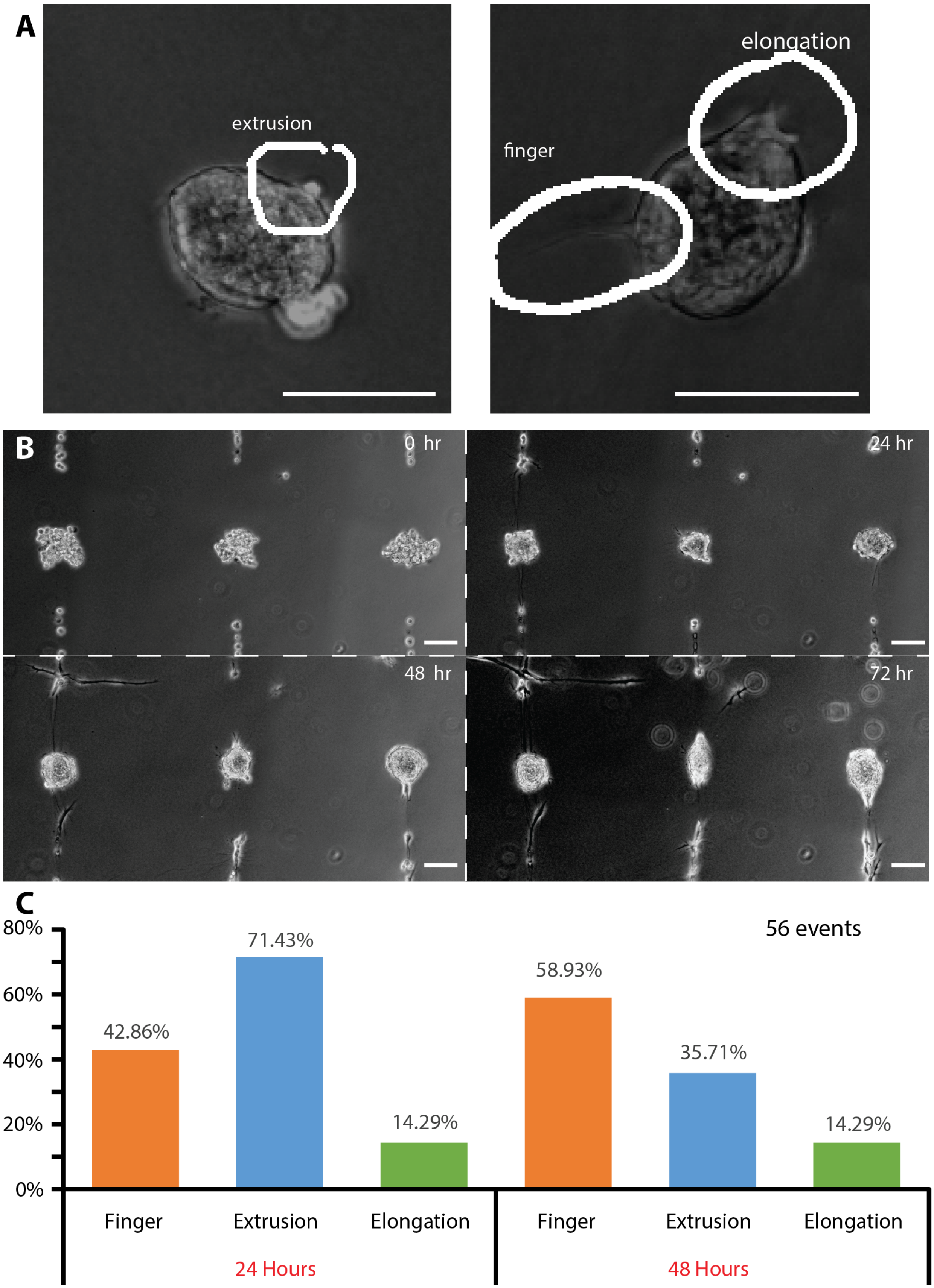
A
extrusion
finger
elongation
B
0 hr
24 hr
48 hr
72 hr
C
80%
60%
40%
20%
0%
56 events
42.86%
71.43%
14.29%
58.93%
35.71%
14.29%
Finger
Extrusion
Elongation
Finger
Extrusion
Elongation
24 Hours
48 Hours

Figure 4-10. Epithelial tissue boundary disruption by fibroblast mechanical signaling. (A) Ras tissues between lines of fibroblasts can exhibit extrusions, fingers, and elongations. (B) Magnified images of three Ras tissues are shown after 0, 24, 48, and 72 hours in 3D culture. Demonstrations of each behavior are visible in the selected tissues. (C) Frequencies of fingers, extrusions, and elongations observed in Ras tissues over 24 and 38 hours in 3D culture. All scale bars are 100 μm.

These experiments were conducted with many technical and biological replicates and imaged at further time points in case other behaviors emerged at later time points (Figure 4-11). Experimental details and replicates can be found in the chapter supplemental information. However, the general conclusion of these data remained that fibroblasts were able to propagate signals through the Matrigel/collagen matrix and affect morphological change on the Ras tissues. This was further supported by the fact that Ras tissues growing without 82-6 fibroblasts did not show any of these morphological changes over time (Figure S4). However, further controls were needed to confirm that the fibroblasts were most likely signaling via mechanical means rather than by a secreted molecule.

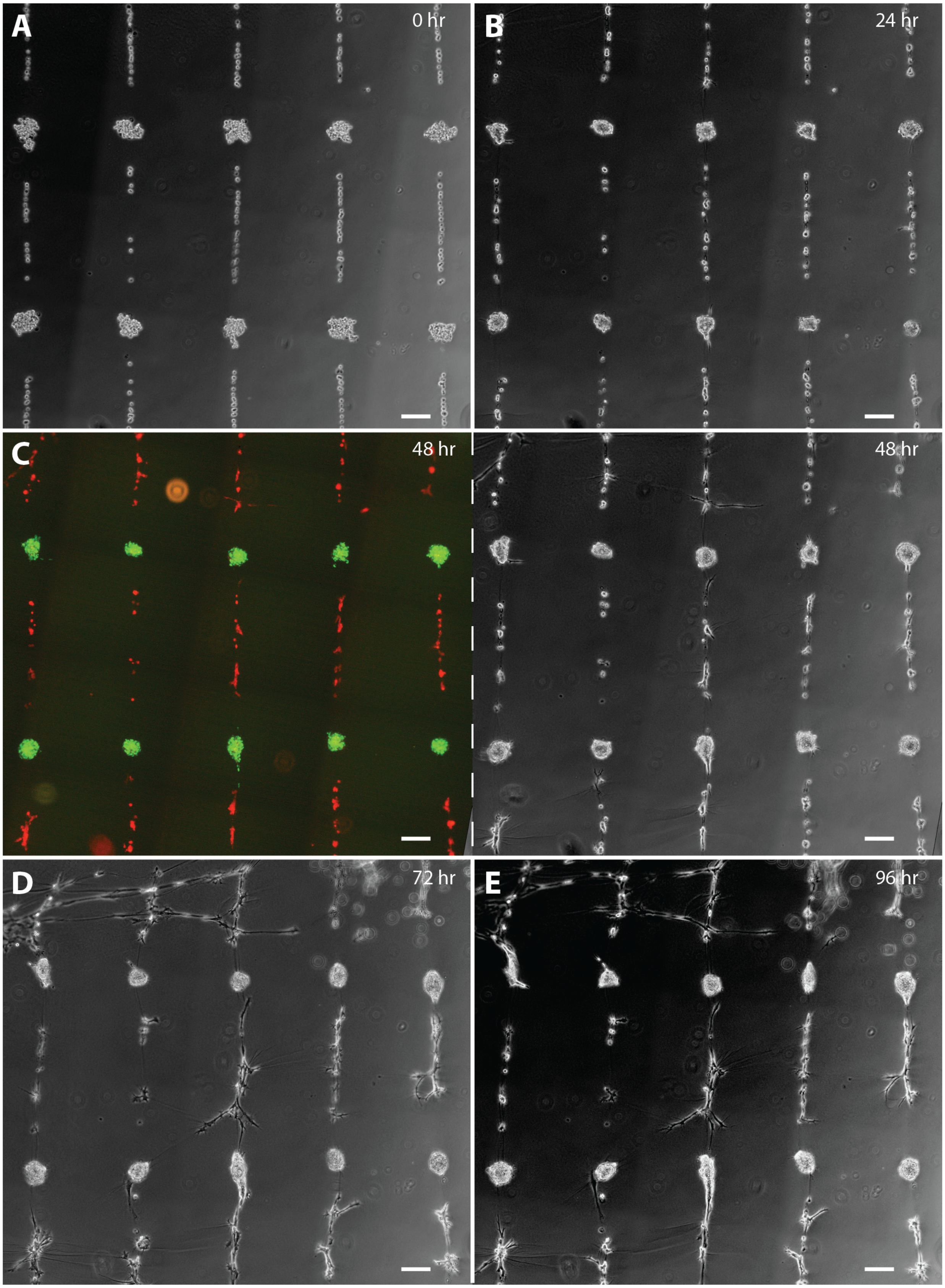
A
0 hr
B
24 hr
C
48 hr
48 hr
D
72 hr
E
96 hr

Figure 4-11. Representative images of fibroblast-epithelium interactions over time. (A) Ras tissues are patterned in between lines of fibroblasts via STDPAC. (B) Ras tissues condense and stress lines form between fibroblasts over 24 hours. (C) Ras cells maintain the CellTracker Green dye and fibroblasts maintain CellTracker Red dye over 48 hours and ensure cell identity over time. (D) The same pattern is shown after 72 hours and (E) 96 hours in 3D culture. All scale bars are 100 μm.

Accordingly, we created patterns of fibroblast and Ras tissue “capacitors” as spatial controls (Figure 4-12). We called these patterns “capacitors” because the overall pattern was similar in look to capacitors, in which two plates (82-6 fibroblast lines) are separated by some medium (Ras tissue) in between them. Parallel lines of fibroblasts were patterned with Ras tissues in between the lines, 3D cultured in Matrigel/collagen, and imaged with phase microscopy at 0, 24, and 48 hour time points (Figure 4-12A - C). Because fibroblasts tend to stretch towards other fibroblasts (Figure 4-11), we hypothesized that the major mechanical pull across the matrix would again be aligned with the line of fibroblasts and according leave the Ras tissue unaffected. The data were mostly consistent with this hypothesis. Very little finger formation and extrusions were observed compared to the experimental condition in figure 4-10, and no Ras tissue elongations were observed (Figure 4-12D). These results were consistent across multiple biological and technical replicates (Figure 4-13). The results were also highly suggestive that mechanical signaling is the major method of fibroblast communication with the epithelial tissues - the spatial control experiment surrounded the Ras tissues with increased density of fibroblasts, which would increase the concentration of secreted signaling molecules and theoretically increase the frequency of observed changes to Ras tissue morphology. Surprisingly, the morphological changes were not completely obliterated from the Ras tissues in the spatial control experiments, suggesting that fibroblasts have the ability to propagate mechanical forces across matrix without the additive effect of linking and pulling across a long line of fibroblasts.

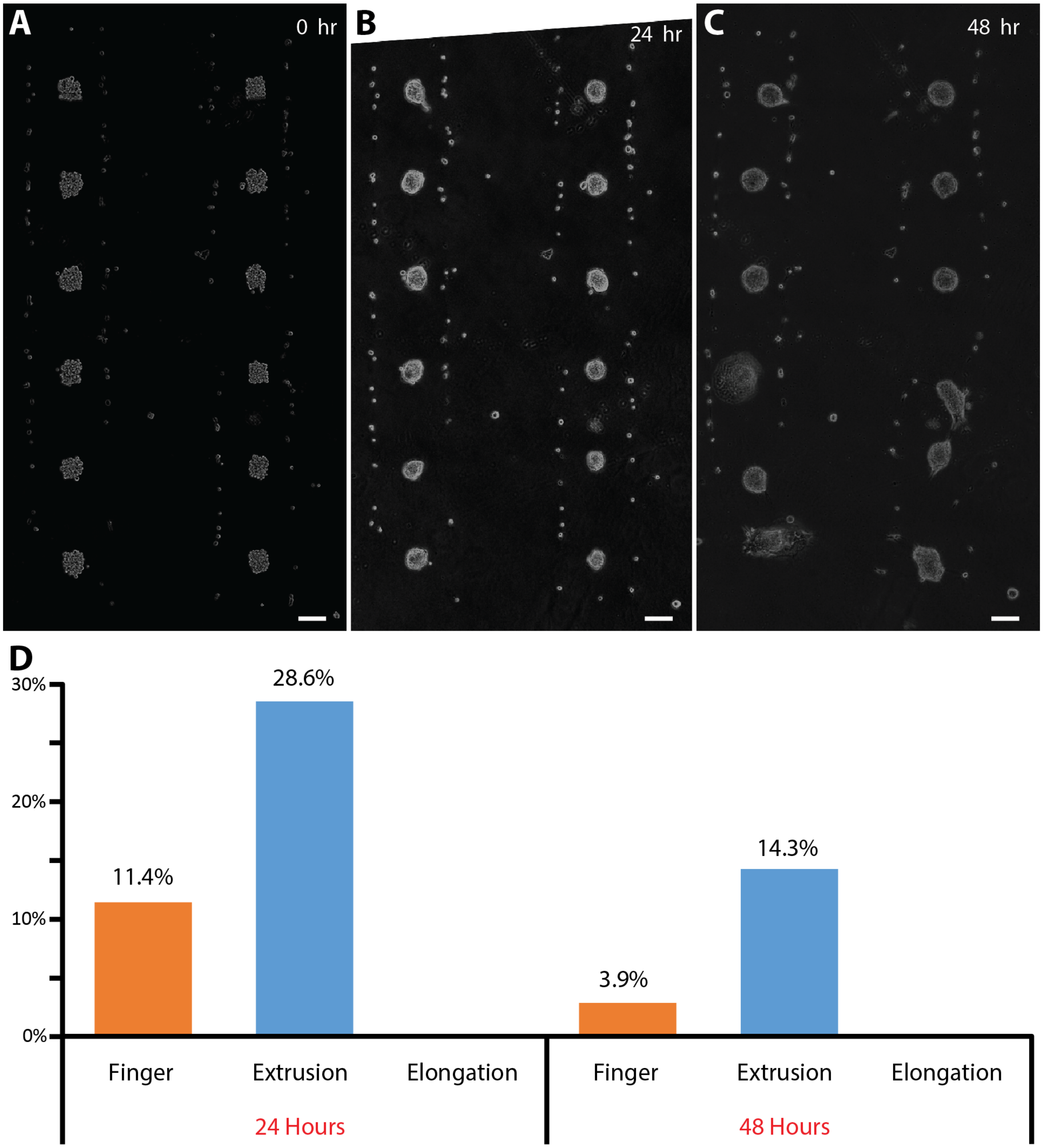

Figure 4-12. Spatial controls for fibroblast-mediated epithelial tissue boundary disruption. (A) Ras tissues are patterned in between lines of tissues such that the tissues are perpendicular to line of fibroblasts and imaged in 3D culture at 0 hours, (B) 24 hours, and (C) 48 hours. (D) The frequencies of finger, extrusion, and elongation of Ras tissues are graphed at 24 and 48 hour time points. Scale bar is 100 μm.

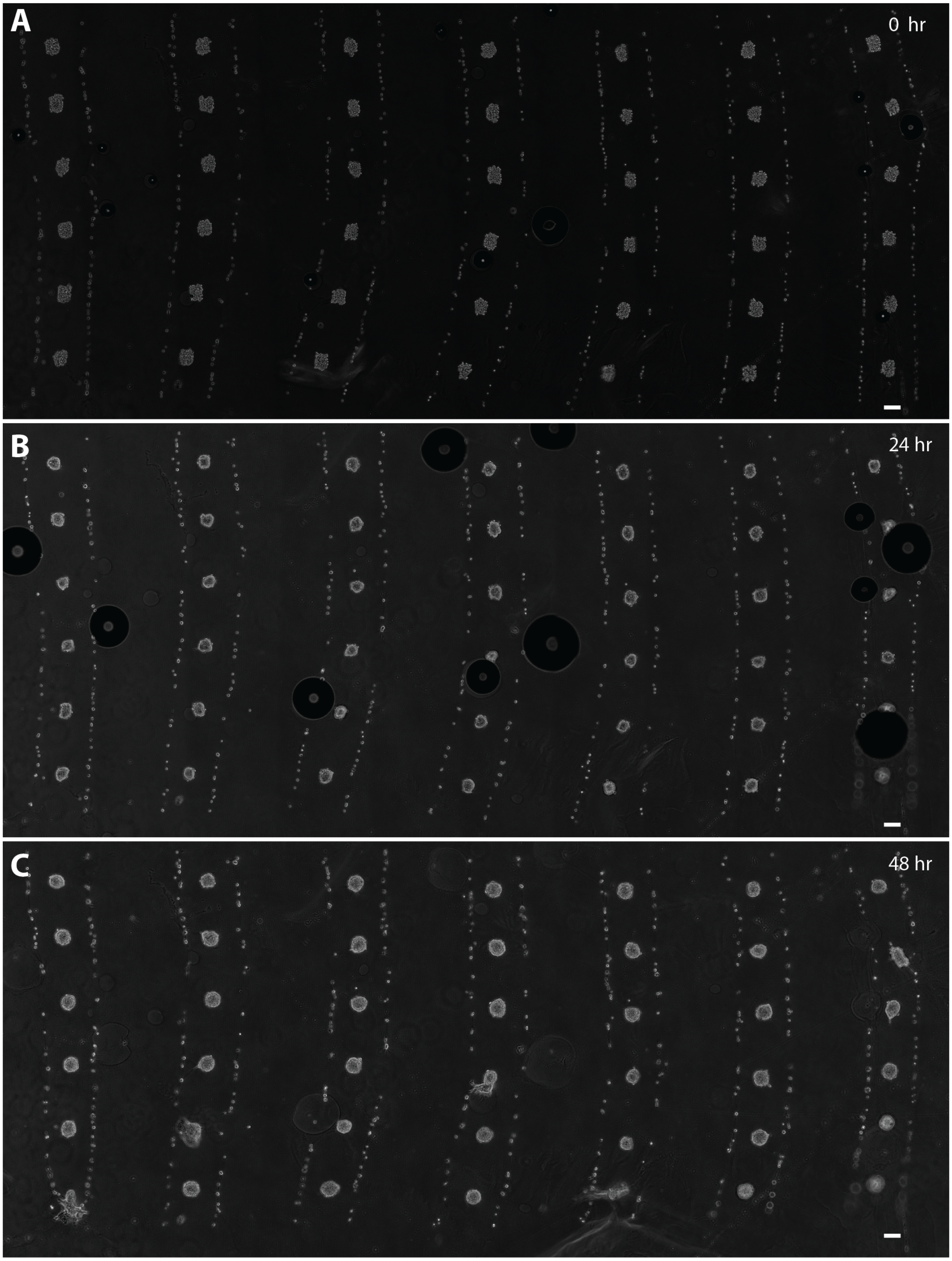

Figure 4-13. Representative images of fibroblast-epithelium "capacitor" patterns. (A) Patterns of Ras tissues in sandwiched between lines of fibroblasts (e.g. capacitors)

are imaged in 3D culture at 0 hours, (B) 24 hours, and (C) 48 hours. All scale bars are 100 µm.

In order to further examine the capability of few fibroblasts in the propagation of mechanical signaling across a matrix, a new pattern was devised in which the number of fibroblasts in the line was reduced by an order of magnitude. Two fibroblasts were aligned on either side of a Ras tissue (Figure 4-14A). While the culture conditions were kept consistent with the experiment described in figure 4-10, these patterns also included rotational controls (discussed in chapter 5), negative controls, and positive controls (4-14A). The hypothesis was that two fibroblasts could effect the same or similar morphological change on the epithelial tissues as when there was a line. After the patterns were imaged at 24, and 48 hour time points, it was quickly determined that the Ras tissues only exhibited finger formation (Figure 4-14B-C). However, a more sophisticated analysis of the finger morphology was conducted to determine whether or not the finger formation in the Ras tissues were aligned towards the fibroblasts, or if they were randomly aligned (Figure 4-14D). An analysis of 143 events determined that close to 60 percent of tissues exhibited finger formation. Forty percent of tissues exhibited aligned fingers and 19 percent exhibited random fingers as determined by quartile analysis (Figure S4). Contrary to our previous beliefs, these results suggested that a small number of fibroblasts could disrupt epithelial tissue morphology by propagating signals across a matrix.

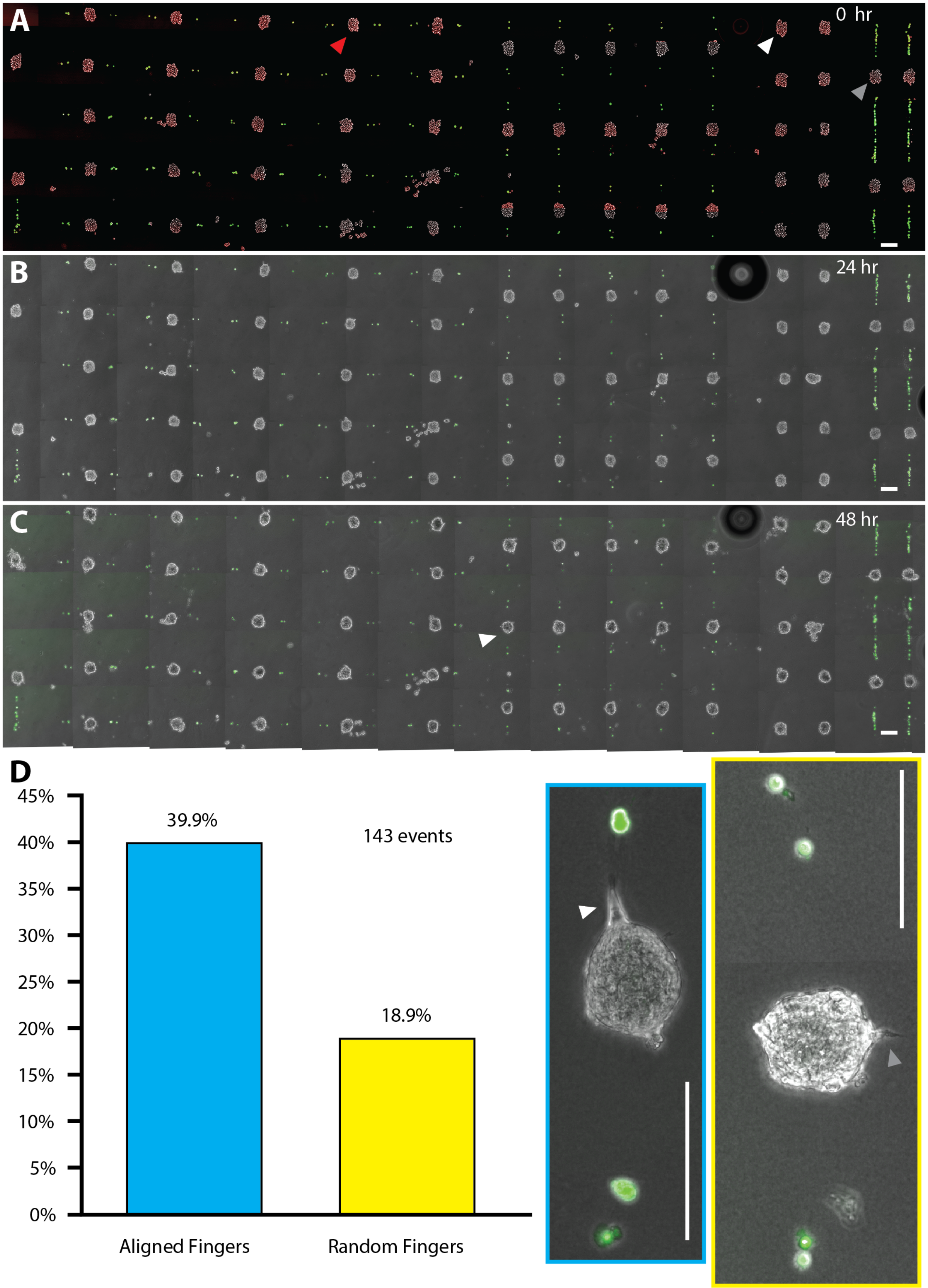
A
0 hr
B
24 hr
C
48 hr
D
45%
40%
35%
30%
25%
20%
15%
10%
5%
0%
39.9%
18.9%
143 events
Aligned Fingers
Random Fingers

Figure 4-14. Minimal fibroblast-induced mechanical signaling on Ras epithelial tissues. (A) Ras epithelial tissues are 3D cultured in between sets of 2 fibroblasts. Experimental events (red arrow) are compared to negative controls (white arrow) and positive controls (gray arrow) within the same gel. Fibroblasts are dyed with CellTracker Green. Live tissue images are obtained at 0 hours, (B) 24 hours, and (C) 48 hours in 3D culture. Rotational controls are also involved to reduce bias from flow direction. (D) Finger formation in the Ras epithelial tissues are evaluated as aligned towards the fibroblasts (white arrow), or non-aligned and pointing elsewhere (gray arrow). Scale bars are 100 μm.

Interestingly, these effected behaviors by fibroblasts were consistent across other patterns and tissues (Figure 3-15, Figure 4-15A). Three HMF cells were observed to cause morphological changes consistent with angiogenesis in neighboring HUVEC tubes (Figure 4-15B). In order to further investigate the effect of fibroblast mechanical pull on HUVEC tissues, we created large patterns of parallel HUVEC tubes and placed three aligned HMF cells in the middle of the HUVEC tubes (Figure 4-16A). These patterns were 3D cultured in Matrigel/collagen and imaged after 48 hours (Figure 4-16B). Individual events were split along their line of symmetry and the HUVEC tubes subsequently analyzed for branching (Figure 4-15B). An analysis of HUVEC tube branching showed that there was a significant increase in branching in the middle of the tissue (aligned with the fibroblasts) compared to the ends of the tissues (not aligned with the fibroblasts) (Figure 4-15C).

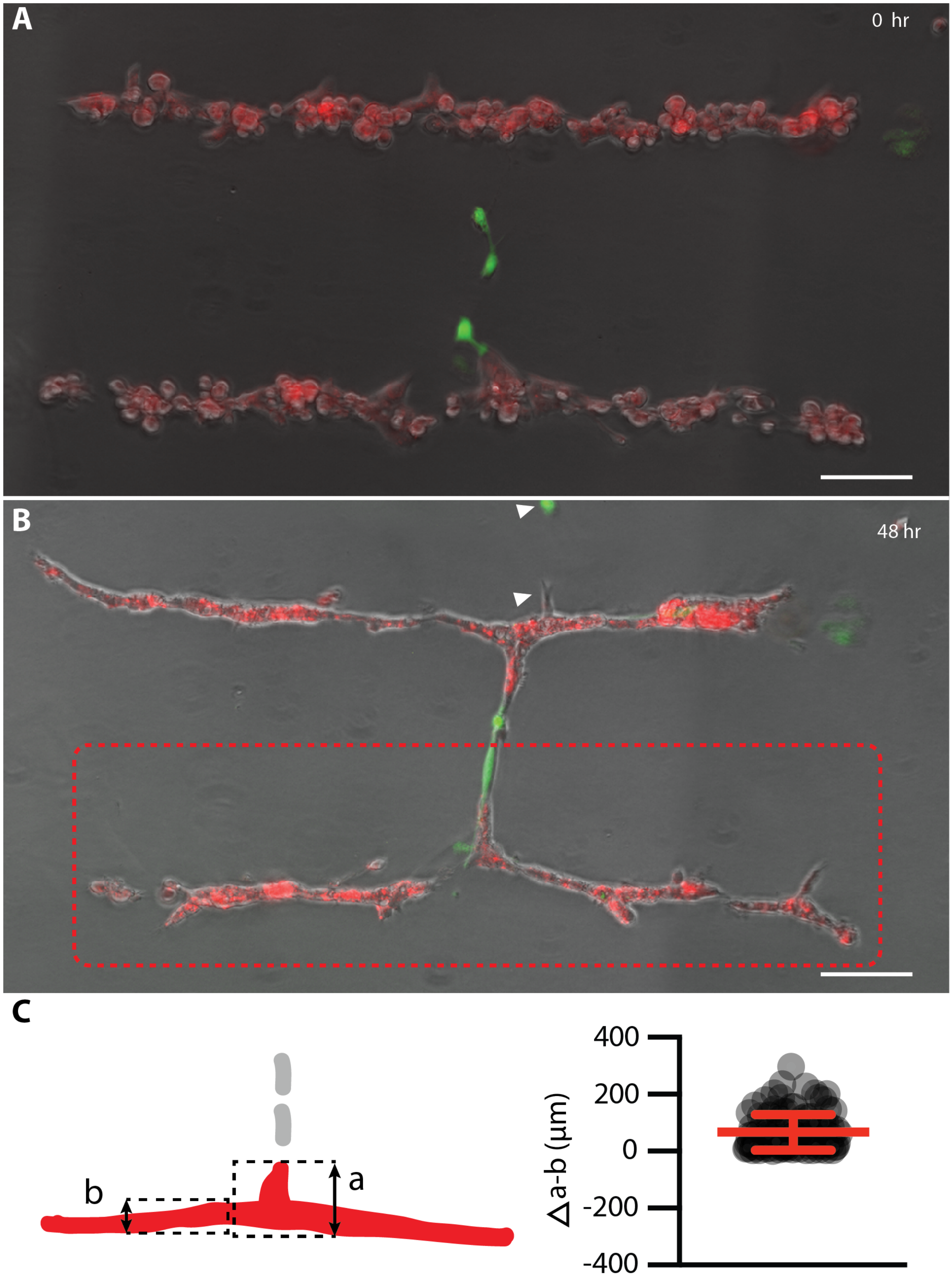
A
0 hr
B
48 hr
C
b
a
400
200
0
-200
-400
Δa-b (μm)

Figure 4-15. Fibroblast-induced mechanical signaling on HUVEC tubes. (A) HUVEC tube-like tissues are patterned as two parallel lines with 3 fibroblasts patterned in a line centered between the HUVEC tissues and imaged in 3D culture at time 0. (B) The same pattern is imaged after 48 hours and assayed for HUVEC tissue distortion towards the fibroblasts. Branching initiation of the HUVEC tissue towards fibroblasts are highlighted with white arrowheads. Each individual HUVEC tissue was analyzed for structural changes (red-dashed box). (C) HUVEC distortion and branching (red drawing) towards fibroblasts (grey drawings) are analyzed as the difference between the total tissue diameter at the distortion point a and the total tissue diameter at the left end of the tissue b. The differences between a-b are depicted as distance measurement in microns in a scatter plot. All scale bars are 100 μm.

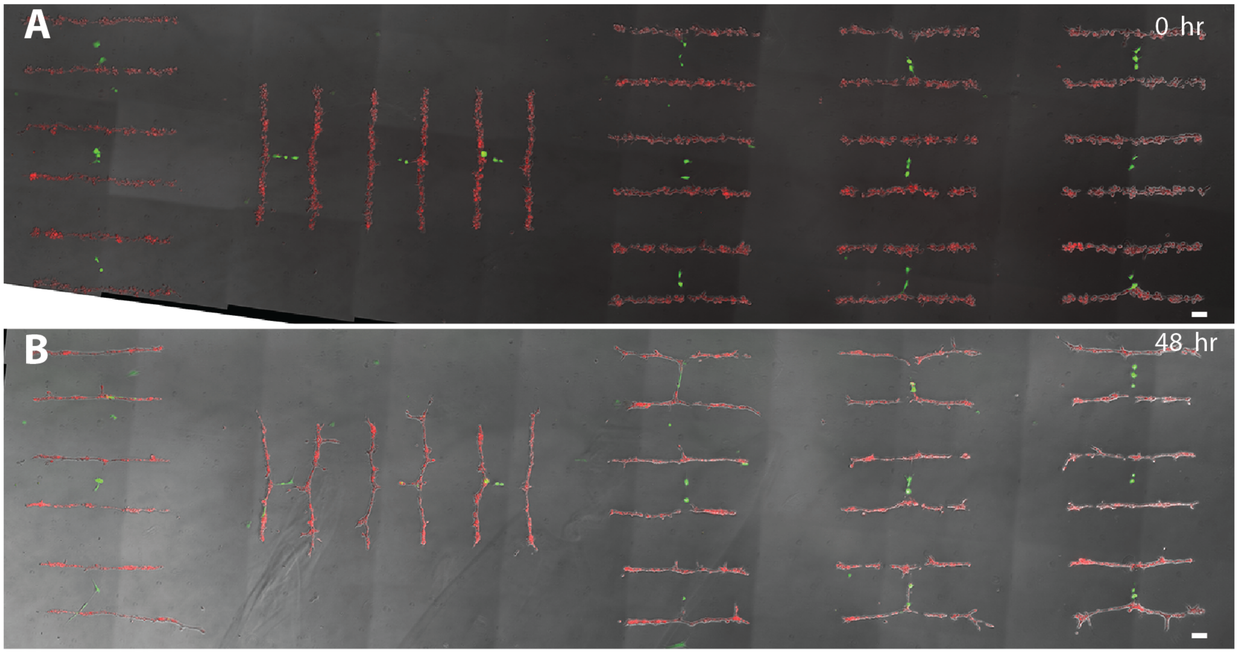

Figure 4-16. Representative images of fibroblast-HUVEC interaction patterns. (A) A large array of HUVEC and fibroblast patterns assembled via STDPAC is shown at 0 hours and (B) 48 hours. All scale bars are 100 μm.

The fibroblast experiments, while incomplete, strongly suggest that fibroblasts are a stromal cell component of the human mammary gland that can affect the structure of surrounding tissues by propagating mechanical signals across a matrix. This is contrary to epithelial cells and tissues, which do not seem to have any effect on other epithelial tissues across a matrix.

Commentary

Building complex tissue models is not trivial. As demonstrated, small steps must first be taken to model each component of a tissue separately, so that these components are individually understood. Even our demonstration of modeled behaviors within the epithelium was simplified for clarity in data interpretation. Based on the capabilities of STDPAC, we have the ability to probe bilayered, two-component epithelial tissues instead of using the MCF-10A model system. It would be very difficult, however, to decouple the behaviors and signaling that occurs simultaneously within and between the two cell-types.

Similarly, we have demonstrated the capability of looking at stromal cell components other than fibroblasts. Why then, did we not add in other stromal cell components to our fibroblast experiments to create a more accurate tissue model? The reason, again, lies in control. While we have control over what cell types we put into a tissue model, we do not have control over the cell behaviors. We also have no way to observe all behaviors within the system we create. Therein lies the conundrum.

Even if the model and its components are correct, the interpretation of the model system and its subsequent behaviors may be impossible. Specifically, if each behavior within a completely correct model system cannot be understood individually, the model system can only be evaluated as a collective unit. This may be sufficient to study collective tissue behavior, but it is impossible to delve deeper and understanding the components. It is much like watching a clock move its hands without being able to take it apart to see how it works. The overall function of a system can be understood, and the effects of individual changes on the whole system can also be understood, but understanding how the collection of cellular components communicates individually is beyond the reach of the system. Thus, because we are not yet sophisticated enough in techniques for observing complex tissue models, the model system itself must be simplified so that individual behaviors can be assayed, and assayed without somehow affecting the system itself.

The challenge is that assay readouts are specific to the system that's being used. In other words, if we synthesize a mammary gland with our lab conditions, the same synthetic mammary may behave differently under different lab conditions. What we are able to observe in our complex models are observations specific to our complex models. There are some that argue that the reproducibility of complex model systems is not as important as what might be learned by them from a single lab (Bissel. 2013). This is a wrong philosophy. Complex tissue model generation only creates relevant model systems if they can be replicated across many scientific hands. The lack of reproducibility would suggest that the specific behaviors observed from the synthetic system are not applicable to other systems, including *in vivo* biology.

The hope is that STDPAC allows others to create the same systems that we can. Even if the experimental goals are different, shared complex model systems enhance our collective ability to trust in the knowledge gained through them.

References

Bissell, M.J., Polyak, K., Rosen, J.M. (2011). The Mammary Gland as an Experimental Model. Cold Spring Harbor Publishing.

Macias, H. and Hinck, L. (2012). Mammary gland development. WIREs Dev Biol *1*, 533–557.

Wiseman, B.S., Werb, Z. (2002). Stromal Effects on Mammary Gland Development and Breast Cancer. Science *296*, 1046–1049.

Debnath, J., Muthuswarmy, S.K., Brugge, J.S. (2003). Morphogenesis and oncogenesis of MCF-10A mammary epithelial acini grown in three-dimensional basement membrane cultures. Methods *30*, 256–268.

Tamariz, E., Grinnell, F. 2002. Modulation of fibroblast morphology and adhesion during collagen matrix remodeling. Mol Biol Cell *13*, 3915–3929.

Dang, T.T., Prechtl, A.M., Pearson, G.W. (2011). Breast cancer subtype-specific interactions with the microenvironment dictate mechanisms of invasion. Cancer Res *71*, 6857–6866.

Bissel, M. (2013). The risks of the replication drive. Nature *503*, 333–334.

Chapter 5: Considerations in Method Development and Experimental Design

Practical Considerations in Experimental Design with STDPAC

Once the capabilities of a technology are understood, it is possible to rush headfirst into an experiment without proper and careful consideration of the intricacies of design. Designing experiments that employ STDPAC first demand consideration of a particular set of constraints specific to this method - the simplest, but most constraining of which are physical constraints, specifically space and time.

The STDPAC method, as described in detail in Chapter 2, employ flow cells materials and reactive glass surfaces that are available off-the-shelf from scientific vendors. Flow cells and reactive glass surfaces are the most important components of spatial considerations in designing experiments with STDPAC. The flow cells operate as crude microfluidic chambers through which cells, matrix, and media are delivered (Figure 5-1A). Most of the experiments described within this thesis employ various flow cells up to a width of 9 mm. Flow cell size is initially limited by laminar flow - the method may simply not work if turbulent flow is introduced into the flow cells. Looking past laminar flow, the flow cell size is also limited based on the type of experiment and the human component involved in the method, not to mention possible technical failures, such as roof collapse.

For example, in the experiment detailing a reconstituted pattern of a mouse mammary fat pad, the largest errors in transfer fidelity were found at the ends of the pattern (Figure 5-1B). This was most likely due to two culprits. First, distortions due to anisotropic gel contraction are enhanced in larger slabs of gels. Second, the pattern lifting process of STDPAC is the most delicate portion of the method, and distortions are most likely at the ends of the flow cells. Smaller flow cells mitigate much of the risk of a bad lift because a larger percentage of the gel surface area is attached to the hydrophilic flow cell during lifting (Figure 5-1C). It is important to consider the experiment itself when choosing the size of a flow cell. An experiment in which very large (> 1 cm) patterns need to retain specific spatial positioning would seek to minimize any distortion of the patterns, and thus a smaller flow cell would need to be used. This is counter-intuitive, considering that creating a large pattern would most likely point to a larger flow cell. It is the combination of experimental requirements, however, that points to a smaller flow cell. First, the experiment requires a large pattern. Second, the experiment requires that the whole pattern be undistorted in 3D culture. Therefore, the large pattern must be made to fit within the smallest flow cell possible.

Different goals, even with a similarly large pattern, are better served with larger flow cells. As a thought experiment, we can imagine an experiment that requires a large array of individual microtissues, none of which are meant to interact with each other and are to be studied as single tissues in isolation. In this case, the goals of the experiment are to observe individual tissue behavior and to evaluate as many events as possible with a single experiment. This pattern could take up even more x-y space than a pattern like the reconstituted mouse mammary fat pad - an array of tens of thousands of individual microtissues can fill up an entire glass slide. Even so, the requirements of the experiment are different. First, the experiment requires a large pattern. There is no second. The experiment does not require that the whole array be undistorted in 3D culture - each tissue is assayed individually, not as a part of the whole array. Distortions do not affect the outcome of the experiment, and the use of a larger flow cell is more practical.

The size of the reactive surface, however, is limited by practical reasons; most vendors only sell reactive glass up to the size of a standard glass slide. Unsurprisingly, the working area of the Nano eNabler is also around 25 square centimeters, about the size of a slide. Reactive glass slides (e.g. Aldehyde silanized glass slides) available for purchase through many scientific vendors are typically sized at 75 x 25 mm. Practically, this means that large pattern creation, if using the Nano eNabler, is limited to a size slightly smaller than the size of a standard glass slide (Figure 5-1D). While large, custom reactive glass slides can be used in conjunction with other patterning techniques to create patterns unlimited in size, such endeavors are impractical. A patterning experiment employing STDPAC is practically limited by flow cell size and the size of a standard glass slide.

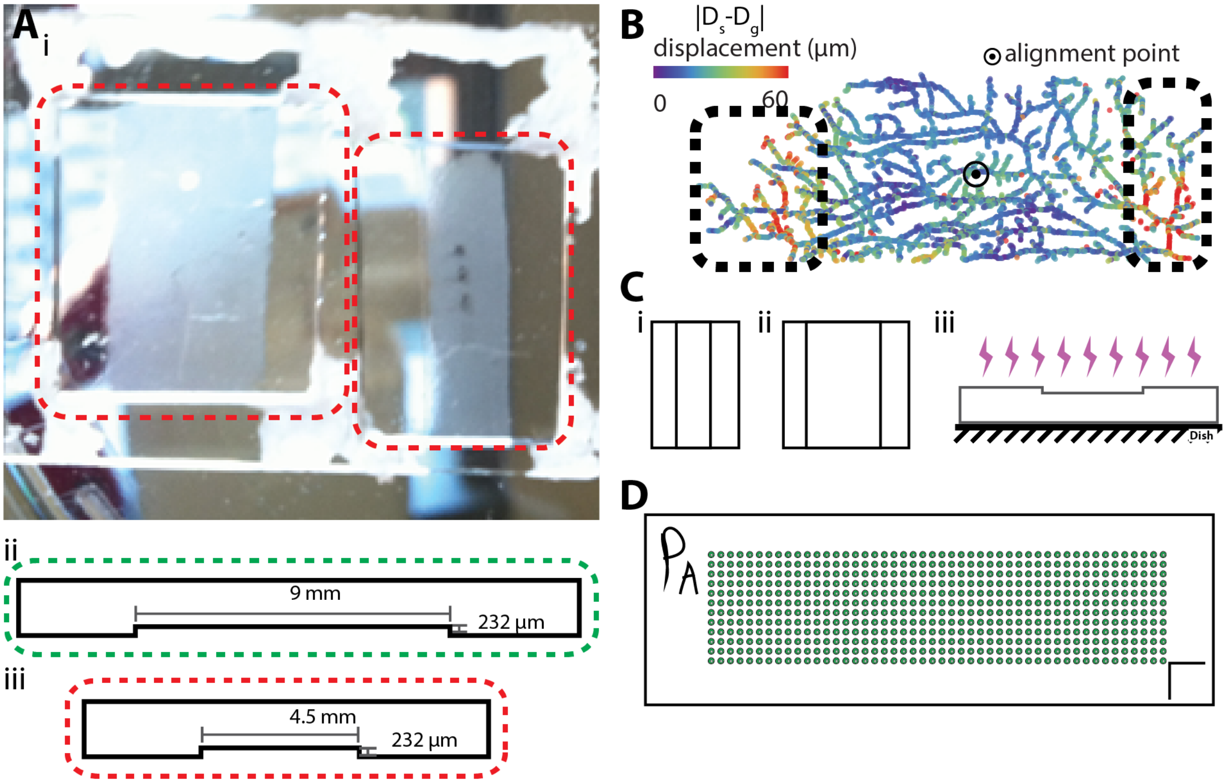

Figure 5-1. Spatial considerations for patterns assembled via STDPAC. (A) Patterns created by surface-templated DPAC are physically limited by the size of the flow cell used for the method (i) and are generally within the constraints of a flow cell with an area of 162 mm2 (ii) or 81 mm2 (iii). (B) Larger patterns transferred to gel have increased susceptibility to distortion of the overall pattern architecture (outlined in dashed boxes). (C) Flow cells can be cast in a multitude of sizes including 81 mm2 (i) and 162 mm2 (ii) but require hydrophilic modifications like plasma treatment in order to ensure proper lifting as the flow cell areas become larger (iii). (D) Patterns the size of an off-the-shelf aldehyde slide are theoretically possible but limited during the lifting step.

The requirement of patterning in the use of STDPAC necessarily links time consideration with pattern size. Patterns of near-limitless complexity can be created with the Nano eNabler. This instrument, however, is limited in multiplexing capabilities because it can only serially deposit single droplets of DNA printing solution. This means that the speed of the instrument is linear and can be described as cycles per second - or more practically, cycles per hour. At a top speed of 2400 spots per hour, large or complicated patterns take hours to print via the Nano eNabler (Figure 5-2A). Previously described experiments of increasing complexity or spot number are color coded to demonstrate how the printing time-length of a single pattern (Figure 5-2B). The number of DNA spots required for patterns like the vascular bed scale exponentially with the size of the pattern itself because total pattern area increases exponentially as the pattern length increases (Figure 5-2C). Considering that a typical experiment includes four repetitions of the same pattern, the time to prepare the DNA patterns must be considered when planning an experiment. DNA patterned slides, however, can be prepared weeks in advance of the actual experiment, and so the actual effect on experiment time is minimal as long as the experiment is planned in advance.

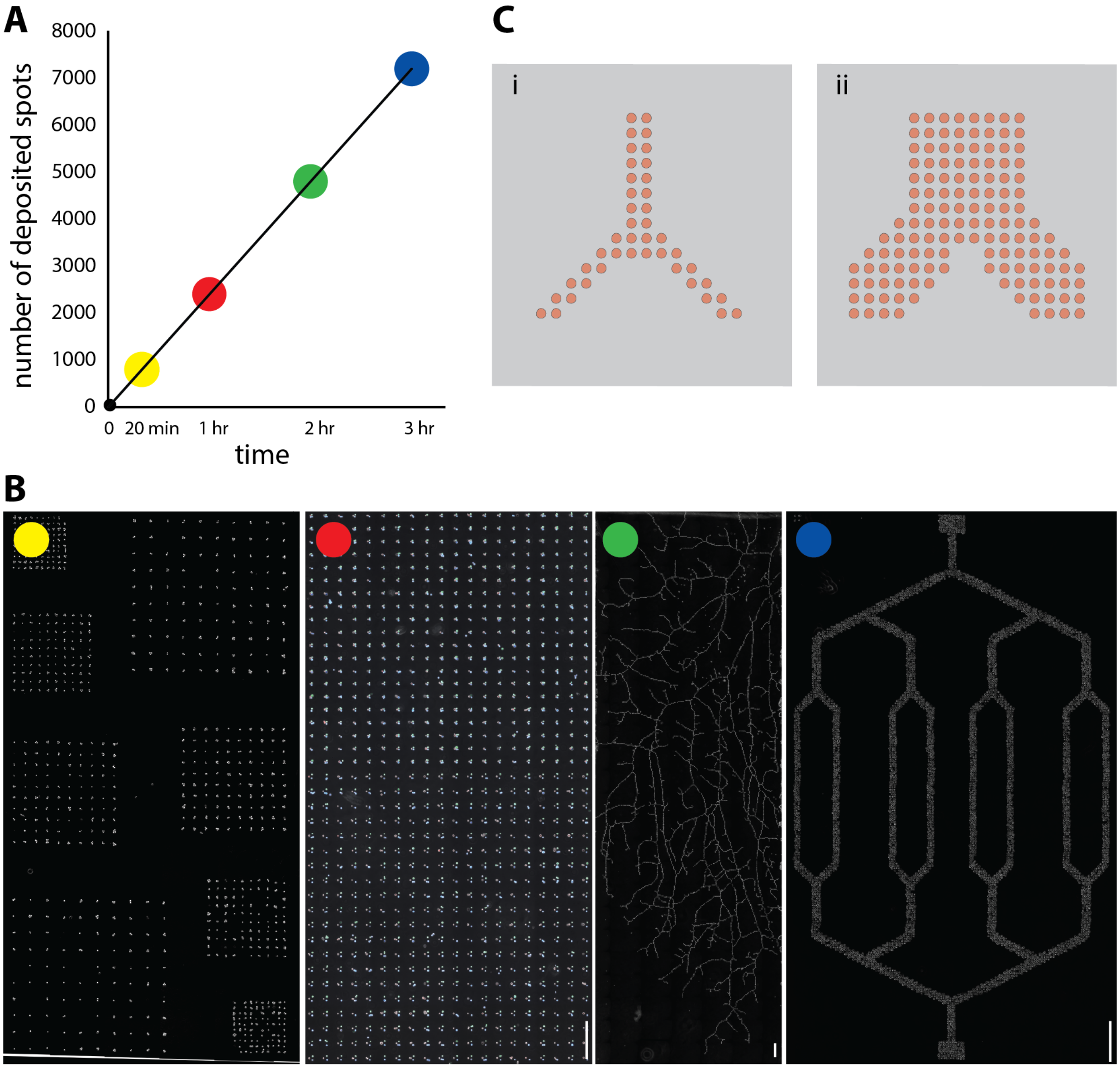

Figure 5-2. Time considerations for DNA patterning with the Nano eNabler. (A) The Nano eNabler operates at a linear rate of 2400 spots per hour assuming a single sequence of DNA. (B) Representative patterns created in the time frame depicted in the graph above are color coded by circles in the top left corner. (C) Patterns scaled larger take exponentially longer to print because a multiple of the number of droplets is required to obtain the larger scaled pattern. Droplets deposited by the Nano eNabler create patterns at a rate under one hertz. All scale bars are 500 µm.

The time duration of an experiment is another matter entirely, and must be heavily considered for the successful completion of a STDPAC experiment. A simple experiment, as the one previously outlined, can be completed within 8 hours (Figure 2-

4B). That is, a pattern can be printed, reconstituted with cells, and transferred to 3D culture within 8 hours. However, the most important time considerations are the durations in which the cells are without media. As described in Chapter 2, cells are necessarily without media throughout the STDPAC experiment until they are place in 3D culture. Specifically, in the 8-hour experiment previously described, the cells are without media for nearly 5 hours (Figure 5-3A). This length of time can increase significantly depending on the complexity of the experiment. For example, in the "twinkie" experiment, 7 steps of assembly were required to assemble the tissue (Figure 3-14B). Each assembly adds roughly 20 minutes to the duration of the experiment – the more complex the experiment (e.g. the more assembly steps required), the longer the experiment takes. The types of cells that are being used are also important - the duration of the experiment is significantly more detrimental to adherent cells, which are usually prone to programmed cell death when in suspension (Gilmore. 2005).

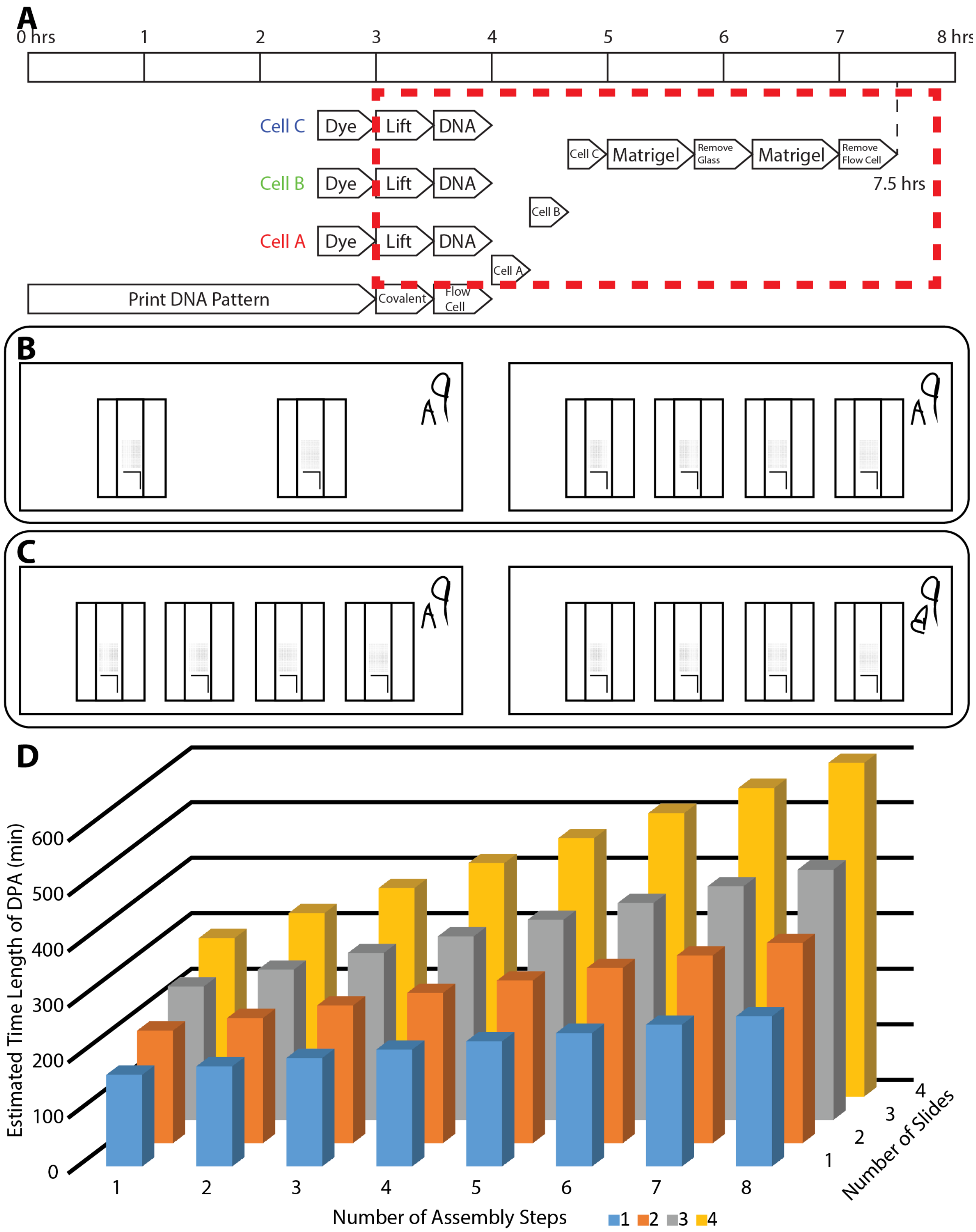

Figure 5-3. Time considerations for STDPAC. (A) Cells involved in a three-step SMDPA are without media and in suspension for 4.5 hours assuming a single slide of flow cells (maximum 4). (B) The timeline for SMDPA is mostly unchanged despite the

number of flow cells if only one slide is used. (C) The timeline of SMDPA dramatically increases as the number of slides increase. (D) The total timeline of SMDPA increases linearly with increasing assembly steps, and exponentially with increasing number of slides.

Careful planning of experimental goals and requirements can help to minimize the time duration of the experiment. With STDPAC, any given experiment is usually completed with 3 technical replicates in tandem. But whether 2, 3, or 4 technical replicates are completed in tandem, there is not much overall increase in the time duration of the experiment. An experiment can be easily completed with up to 4 technical replicates in parallel - this is the limit of how many flow cells can fit on a single slide (Figure 5-3B). However, the addition of each additional slide of flow cells begins to increase the time duration of the experiment because each separate slide must be individually managed in serial (Figure 5-3C). STDPAC experiments with up to four slides have been tested, and while increased experimental complexity increases the duration of the experiment, the time duration is more significantly impacted with the addition of slides (Figure 5-3D). In general, experiments in which the cells are not back in 3D culture within 6 hours of removal from media show decreased viability after the STDPAC process is complete.

Space and time constraints of STDPAC are real, but can be mitigated with careful planning and adaptation of the method to the experimental goals. Similarly, intelligent considerations of DNA sequence, assembly logic, and synthetic reality are important to successful completion of an experiment, especially with the synthesis of multi-component tissue patterns.

The unlimited nature of orthogonal oligonucleotide pairs is previously described in Chapter 2. While true in theory, the practical implications of STDPAC require more complicated approach to oligonucleotide sequence design. STDPAC requirements of DNA sequences are different and more stringent than requirements for DNA barcoding, for which thousands of orthogonal sequences can easily be computationally designed (Xu et al. 2009). Unlike DNA barcodes, in which processes like PCR amplify single sequences, cells assembled via STDPAC are held together by the collective adhesive effect of many DNA duplexes. The avidity effect that enables STDPAC also limits the design of DNA strands that are orthogonal by barcoding standards, but too similar by STDPAC standards. The DNA sequences for our A-sequence DNA and B-sequence DNA seem orthogonal at first glance, and they are indeed by most metrics (Figure 5-4A). However, alignment of the 5-prime and 3-prime ends of the sequences shows that six positions of Watson-Crick base pairing are possible (Figure 5-4B). Intuition suggests that the dissociation constant of these two strands is probably large enough to render the strands orthogonal as barcodes. With STDPAC, however, the avidity effect derives a sufficient collective adhesive property of the weak interactions to drive the assembly of two cells.

Frame-shifting the sequences by one base pair increases the number of Watson-Crick base pairs to 8, which would further increase the probability for cells labeled with the A-sequence DNA to cells labeled with the B-sequence DNA, even though the DNA strands are, by themselves, orthogonal (Figure 5-4C). When the experimental goal is to create two separate assemblies within one pattern, this weak binding effect may be outcompeted by cells labeled with true complementary DNA sequences, or cause what is described as cross-contamination in proportion to the weak binding affinity of the orthogonal strand (Figure 5-4D). Additionally, without proper attention to the logical order of assembly, cells labeled with orthogonal strands of DNA may bind to the wrong surface DNA spots, obstructing the ability for the correct cell to bind. The avidity effect complicates the design of DNA sequences for use in STDPAC, but orthogonal strands can and have been designed by considering these specific requirements (Figure S2).

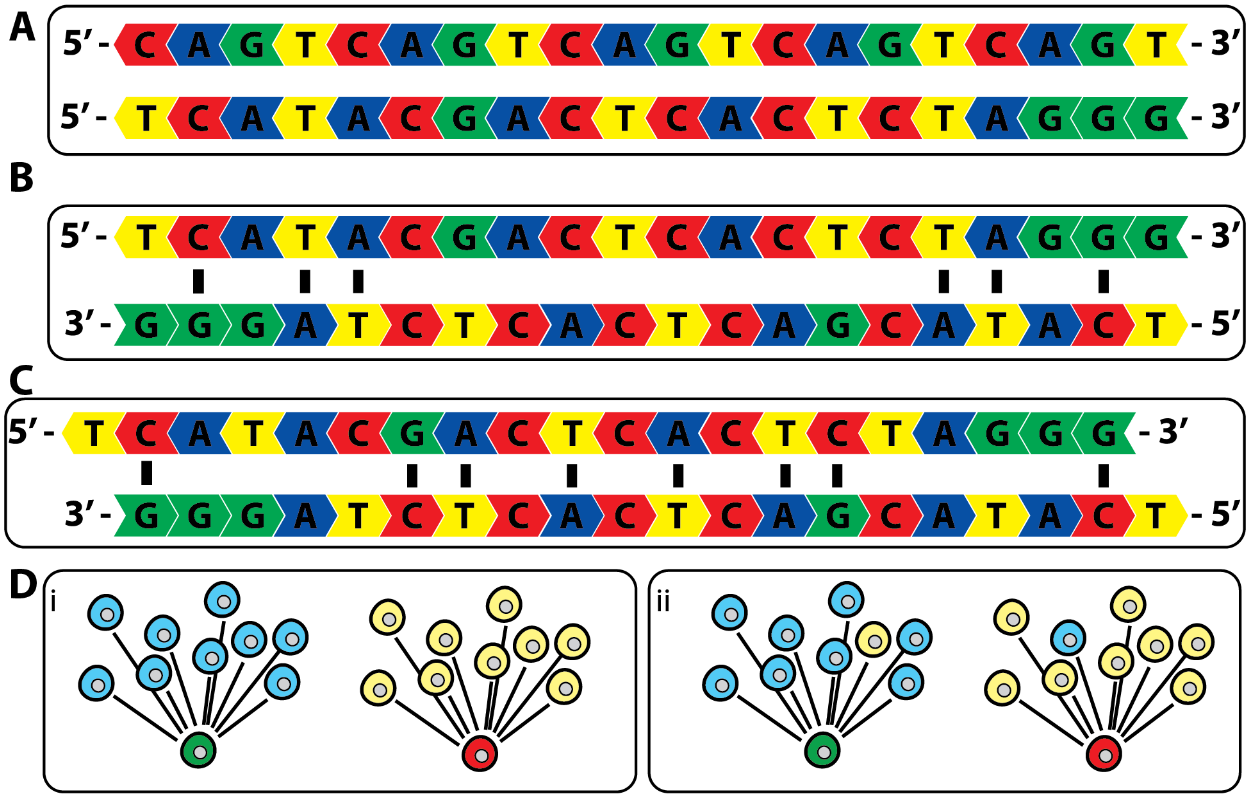
A
5′- C A G T C A G T C A G T C A G T C A G T -3′
5′- T C A T A C G A C T C A C T C T A G G G -3′
B
5′- T C A T A C G A C T C A C T C T A G G G -3′
3′- G G G A T C T C A C T C A G C A T A C T -5′
C
5′- T C A T A C G A C T C A C T C T A G G G -3′
3′- G G G A T C T C A C T C A G C A T A C T -5′
D
i
ii

Figure 5-4. DNA cross reactivity and implications for STDPAC. (A) Two orthogonal DNA sequences denoted A and B are represented by standard color-code. (B) Aligning the A and B sequences shows 6 locations that align for Watson-Crick base-pairing. (C) A frame shift of one nucleotide increases the number of Watson-Crick base-pairs to 8. (D) STDPAC of 4 cell-types labeled with two orthogonal DNA pairs are shown in an

ideal situation (i), as well as likely cross-contamination that occurs because the two sequences are not completely orthogonal (ii).

The logical order of assembly is also an important consideration in the absence of concerns about DNA orthogonality. Again, it is easily demonstration in the synthesis of the “twinkie” (Figure 5-5A). Each step of assembly was carefully considered and designed prior to the experiment to ensure that the layer-by-layer construction of the “twinkie” would not be obstructed in any way (Figure 5-5B). If, for example, the order of assembly was changed such that step 2 was moved to step 5, a proper “twinkie” could not by synthesized (Figure 5-5C). The addition of the green cells would occlude the red cells from later attaching to their respective DNA spots on the glass surface. Cells are not perfect building blocks. Neither is the layer-by-layer construction of tissues by STDPAC a perfect stacking of layers. Assembled cells may attach properly to seed cells bearing complementary DNA, but they will attach with equal probability across all available surface areas of the seed-cell membrane. They will also slide across the membrane and settle, consistent with the effects of gravity. Thus, the 3 assembly steps of green cells in the middle of the mis-designed “twinkie” would create a large occlusion of the red DNA spots because red cells are not already present to prevent the green cells from settling down onto the surface (Figure 5-5C).

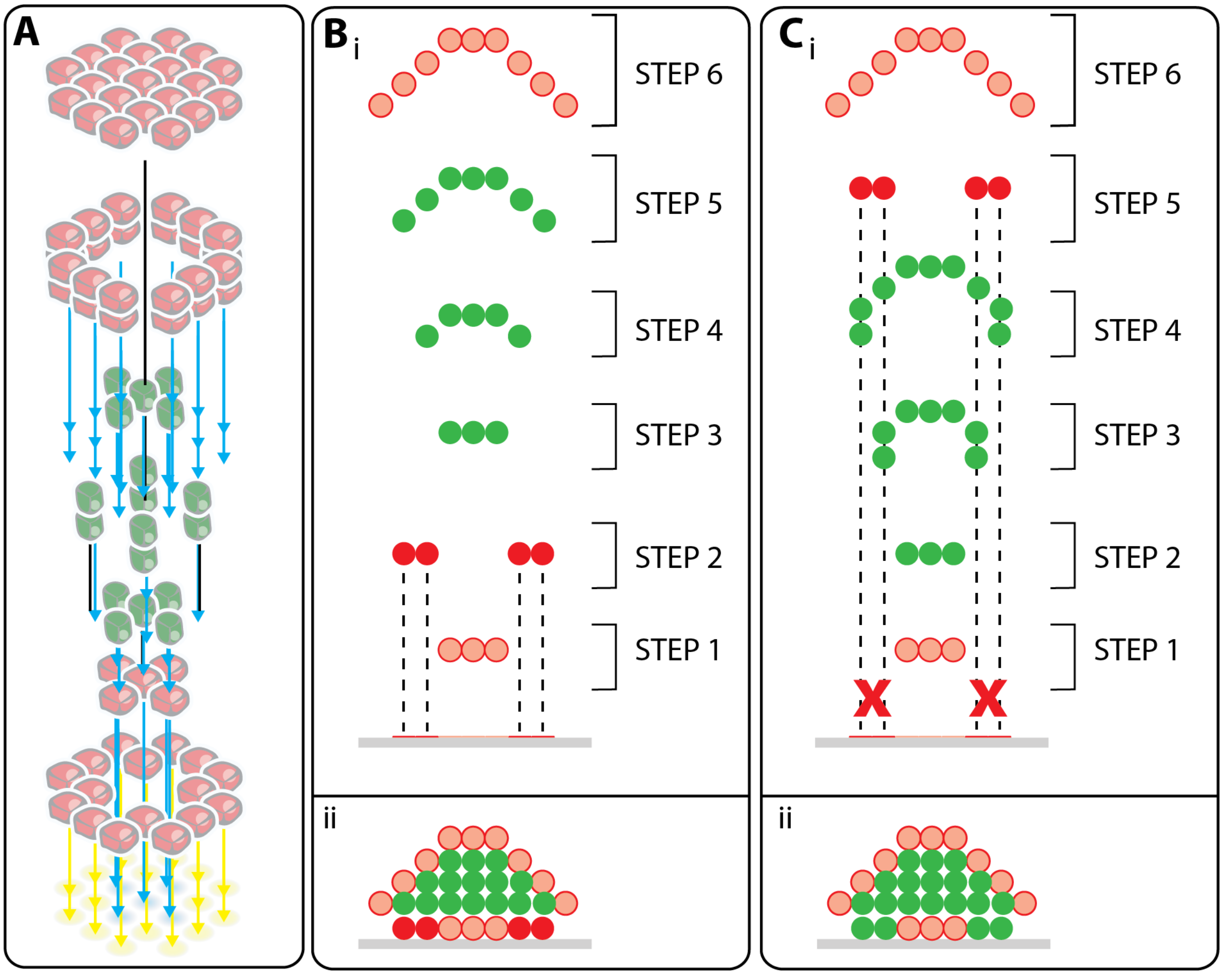

Figure 5-5. SMDPA and order of addition logic. (A) The "twinkie" experiment is conducted via 7 steps of STDPAC in a precise order. (B) The "twinkie" experiment is shown as an ideal set of STDPAC in 2D side-view. The red cells in step 2 can bind unobstructed to the surface DNA (i) to form a proper "twinkie" (ii). (C) The "twinkie" experiment is shown without regard to a logical order of addition. The red cells in step 5 cannot bind to the surface because the DNA spots are obstructed by green cells from previous assembly steps (i) and a proper "twinkie" is not formed (ii).

All tissues synthesized by STDPAC, not only "twinkie" tissues, are built layer-by-layer from the bottom up on a predetermined pattern. This synthetic reality is not unlike the construction of a city, in which buildings are built from the bottom up to create a beautiful skyline (Figure 5-6A). A necessary requirement of bottom up design is that all buildings are aligned at their bottoms (Figure 5-6B). While this reality is intuitive and unimportant in a city, it is easily overlooked during experimental design. For example, let's imagine a person standing between two tall buildings and pointing a flashlight. Even if all structures were lifted 100 feet above the ground, the bottom-justified alignment would still remain. A person holding a flashlight would only be able to illuminate the bottom of the building, and not towards the center-of-mass of the building (Figure 5-6C). In fact, unless the beam width was sufficiently large to cover the entire side of a building, the person would not be able to illuminate the entire building (Figure 5-6D).

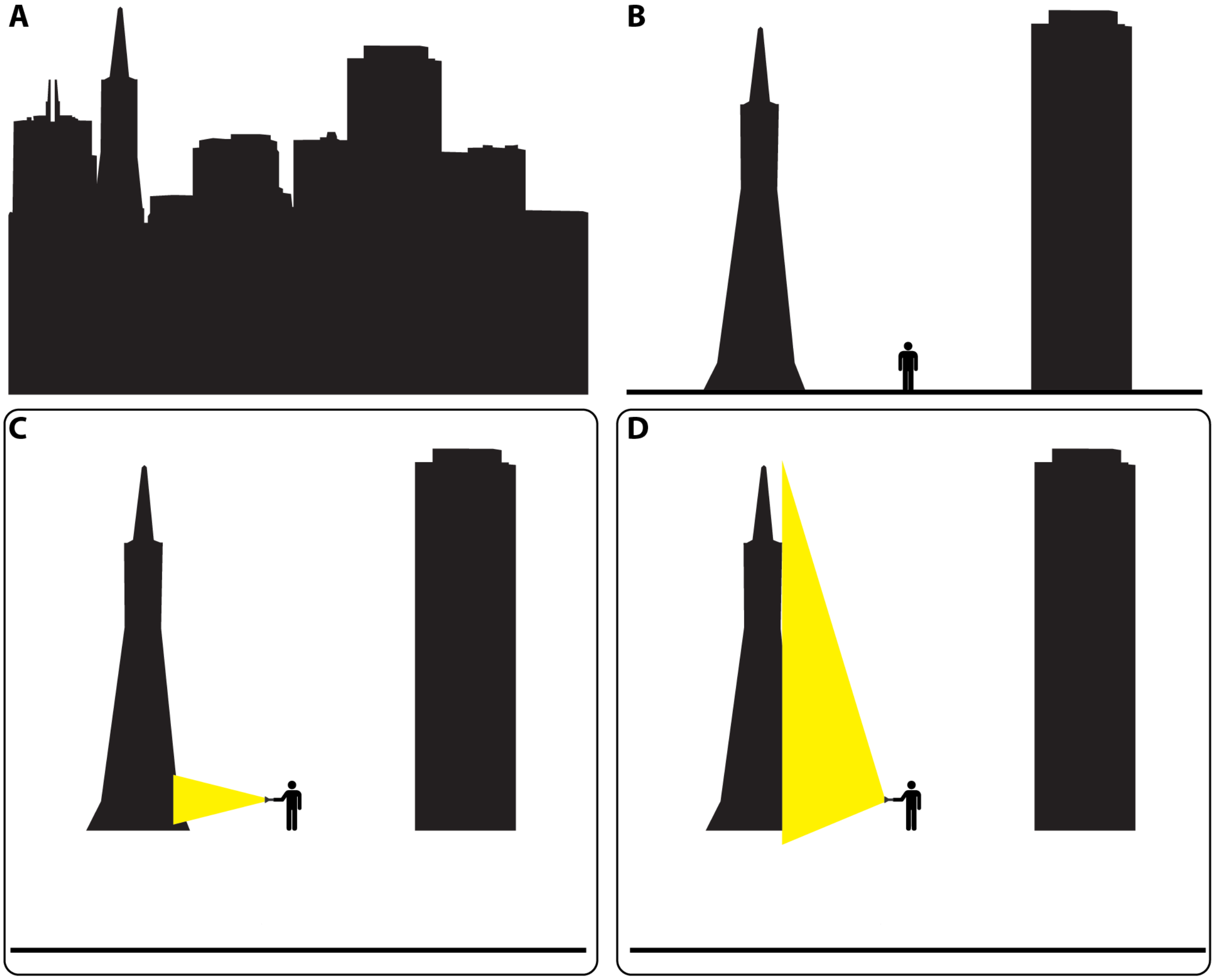

Figure 5-6. Building from the bottom up. (A) A city skyline is only consistent where the buildings meet the ground. (B) Buildings are built from the bottom up. (C) A person shining a flashlight at a building can only reach the bottom of the building even if everything is lifted off of the ground. (D) Light can only cover the entire building if the beam width of the flashlight is sufficiently large.

This scenario holds true when building complex tissue models with STDPAC. All tissues are built from the bottom up, even when there are multiple components involved. As an example, the fibroblast/vasculature pattern is revisited (Figure 4-15). The pattern was synthesized by assembling fibroblasts onto spots of B-sequence DNA while HUVECs were assembled onto spots of A-sequence DNA. The HUVEC tissues, however, comprised 4 total steps of assembly (Figure 5-7A). After the assembly was finished, the HUVEC tissues were 4 times taller than the fibroblast cells (Figure 5-7B). When the entire pattern was embedded in Matrigel/collagen and completely surrounded by matrix, the bottom-justified alignment of tissues remained (Figure 5-7C - D). The experiment was designed to measure the effects of fibroblast signaling on the HUVEC tubes, but the fact that the fibroblasts were aligned to the bottom of the HUVEC tubes was not considered. In fact, the method of data analysis was consistent with the assumption that fibroblasts were aligned across the center of mass of the HUVEC tissue (Figure 5-7E). This was an easy, albeit faulty, assumption to make considering that traditional light microscopy is conducted by imaging from the top or bottom of a pattern (Figure 5-7F). Traditional microscopy therefore produced images that hid the nature of cell and tissue alignment as produced by STDPAC (Figure 5-8G).

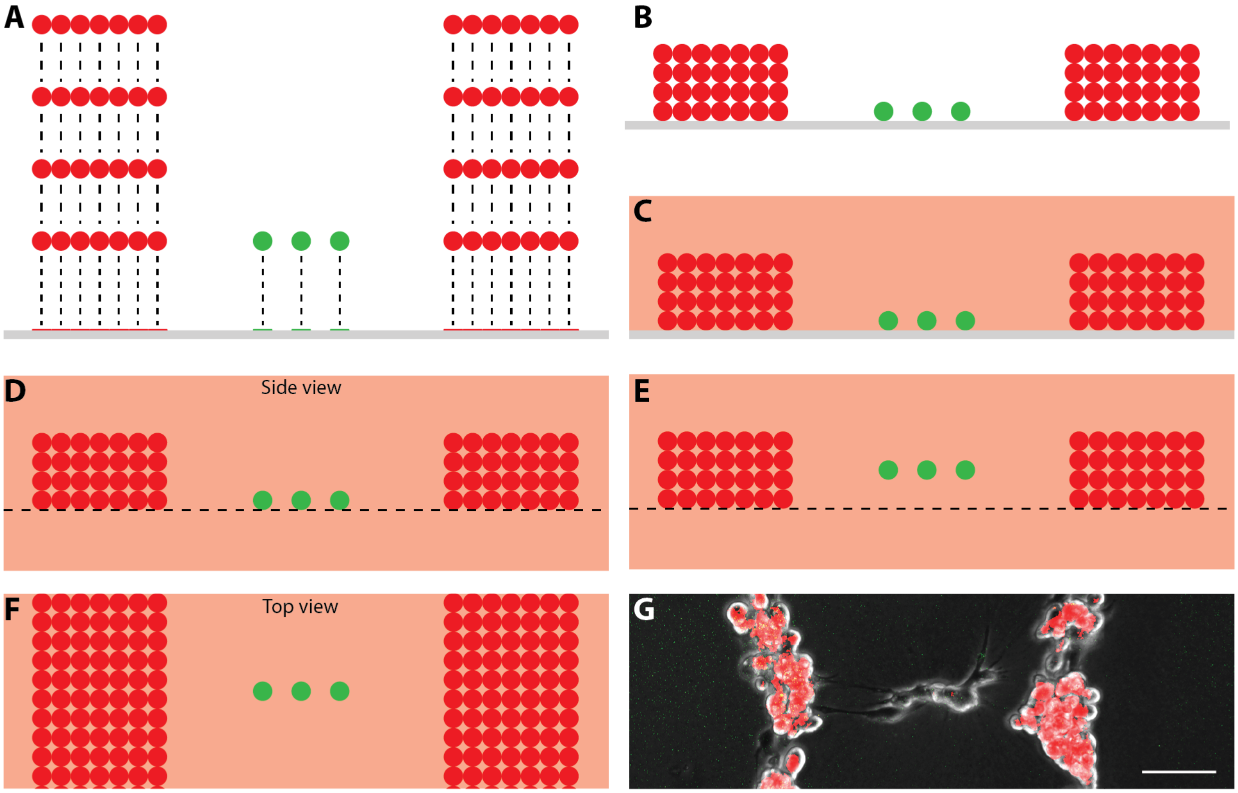

Figure 5-7. The bottom-up nature of surface-templated assembly. (A) Tissues are built layer-by-layer from the bottom up because assemblies begin from a surface. (B) Single cells are necessarily aligned with the bottom of surrounding tissues (C) even when in Matrigel. (D) Tissue patterns fully embedded in Matrigel are aligned to the initial surface. (E) Tissues and cells are not evenly aligned in a single plane across the center-of-mass as imagined or assumed. (F) Tissues and cells seem as if they're aligned across a single plane across the center-of-mass when imaging from the top or (G) bottom with a microscope. Scale bar is 100 µm.

Although these alignment issues most likely produced negligible effects on the experimental output, especially considering the length-scale of the tissues that were produced, they are still important to consider in interpreting data. And specifically, if the physical constraints of STDPAC are considered during the design phase of an experiment, the data collected should be just as trustworthy as any other experimental technique.

Matrix Considerations

3D culture models are completely reliant on the types of gels that they use. For example, large-scale epithelial structures (Nelson et al. 2006) or large-scale vascular tissues (L'Heureux et al. 1998) rely on high-concentration collagen I gels. Even though these matrix formulations are not what the tissues experience *in vivo*, they are necessary to assay for tissue behavior in 3D culture.

The hidden truth of 3D tissue culture systems is that system components are chosen based on whether or not the cells behave in a manner consistent with what the experimenter expects, not necessarily because they are most biomimetic. Cells will behave differently in different matrix formulations. For example, dense MCF-10A grids were grown in 3D culture with the Matrigel supplemented with 0.1 mg/ml Collagen (rat tail collagen I) (Figure 5-8A). Because these cells were patterned with a pitch greater than 18 microns, they would grow into individual tissues in Matrigel. However, many of the tissues combined over time and grew into large tissues after 96 hours in culture. For an experiment that would require side-by-side MCF-10A tissues growing next to each other, this matrix formulation would be discarded after this initial experiment. In fact, for any changes in matrix formulation, conditions were necessarily screened to ensure that MCF-10A acinus morphology was consistent to what was seen in Matrigel (Figure 4-8B - D). Any changes to MCF-10A acinus development would tarnish the believability of experimental results.

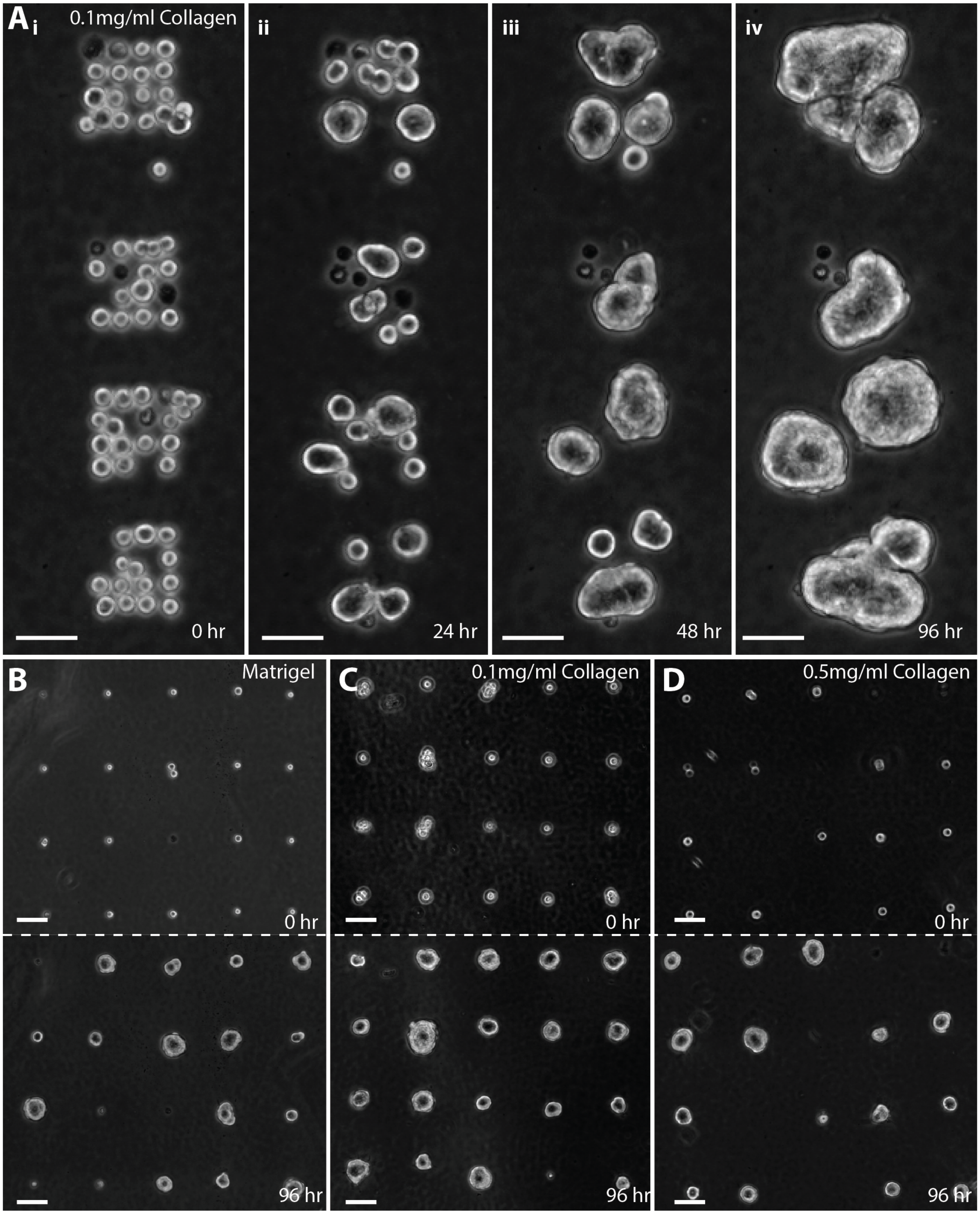
A
i
0.1mg/ml Collagen
ii
iii
iv
0 hr
24 hr
48 hr
96 hr
B
Matrigel
C
0.1mg/ml Collagen
D
0.5mg/ml Collagen
0 hr
0 hr
0 hr
96 hr
96 hr
96 hr

Figure 5-8. Different matrix formulations for 3D culture. (A) 3D culture of single-layer dense patterns of MCF-10A cells in Matrigel supplemented with 0.1 mg/ml collagen enhances tissue fusion as cells grow into tissues from 0 hr (i), 24 hr (ii), 48 hr (iii), and 96 hr (iv). (B) Single cells are shown growing into tissues over 96 hours in

Matrigel. (C) Single cells are shown growing into tissues over 96 hours in Matrigel supplemented with 0.1 mg/ml collagen. (D) Single cells are shown growing into tissues over 96 hours in Matrigel supplemented with 0.5 mg/ml collagen. All scale bars are 100 μm.

The nature of STDPAC places tissue patterns at a potential interface of matrix (Figure 5-9A). This technical detail may confer advantages over other techniques by adding the ability to create more complex model systems (Figure 5-9B). But the system may also skew results if there exists a true interface experienced by cells, but is ignored for the purposes of data analysis. Conjugating dyes to either layer of Matrigel during STDPAC showed that there is a distinct division between the matrix layers at time zero (Figure 5-9C). Over multiple days in culture, the interface resembles a gradient (Figure 5-9D). While dye-conjugated Matrigel showed confocal microscopy-observable matrix bilayers formed by STDPAC - long-term culture of MCF-10A cells showed proper acini development as marked by polarization markers, confirming that the matrix bilayer did not affect the behavior of tissues in 3D culture (Figure 2-7D). Even with the placement of MCF-10A cells at an interface in which one layer of matrix was pure Matrigel and the other layer was Matrigel supplemented with 0.5 mg/ml Collagen, there was no different in tissue morphology as compared to other MCF-10A acini growing in pure Matrigel, or pure collagen-supplemented Matrigel (Figure 5-9E - F, Figure S5).

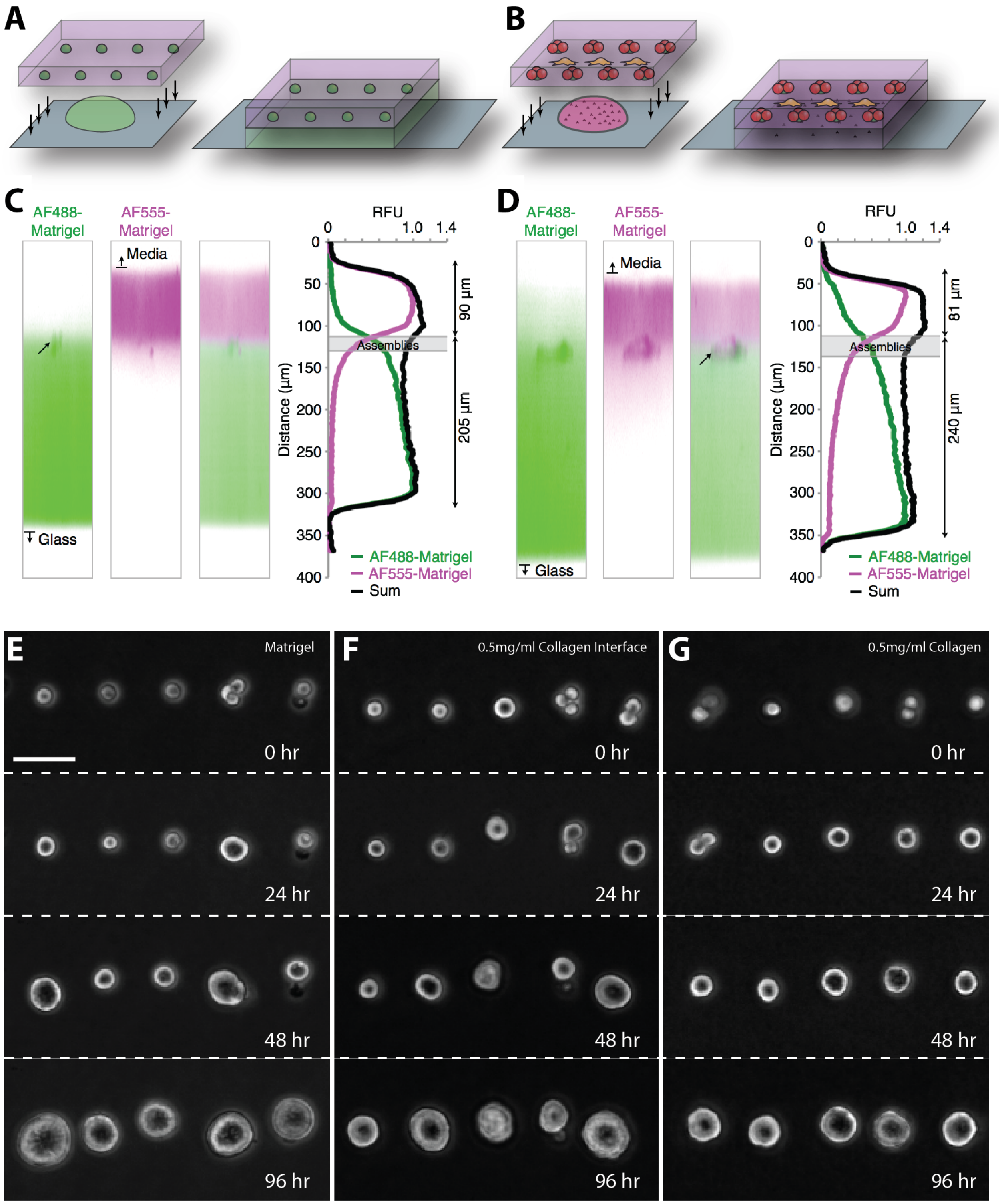

Figure 5-9. Creation of an interface during SMDPA. (A) Patterns created by SMDPA can be embedded and sandwiched in two separate matrix formulations, thus containing the pattern at the interface of the two gels. (B) Differences in matrix formulations between the bottom layer of matrix and the top layer of matrix used during SMDPA may allow diffusion of molecules to occur between the layers. (C) The bottom layer of

Matrigel is covalently labeled with AlexaFluor 488 and the top layer of Matrigel is covalently labeled with AlexaFluor 555 and the entire SMDPA embedded pattern is imaged via confocal microscopy, showing a fine boundary between the two Matrigel layers with cells or tissues embedded in between (arrows). Fluorescence intensity measurements show that a boundary is sharply defined between the two Matrigel layers. (D) The two layers of Matrigel after 24 hours show that diffusion slowly occurs over time. The boundary does not exist as sharply as at time 0. (E) MCF-10A cells are shown growing in Matrigel over 4 days. (F) The same pattern is shown growing at an interface of Matrigel and Matrigel supplemented with 0.5 mg/ml collagen. (G) The same pattern is shown growing in Matrigel supplemented with 0.5 mg/ml collagen. All images are to the same scale. Scale bar is 50 μm.

It is important to consider that not all tissues are equal, even if they are composed of the same cells. The previous experiments consisted of small tissues, but large tissue patterns of MCF-10A cells behave differently than small MCF-10A tissues - the larger the tissue, the more important the matrix formulation. It is seemingly trivial to utilize STDPAC to create large epithelial tissues. Reality differs in that the intrinsic properties of MCF-10A cells bias them to grow into spherical tissues in Matrigel, rather than the large tissues that are assembled via STDPAC. Several optimizations and intuitive leaps were required to discover matrix formulations that created contiguous, cylindrical MCF-10A tissues in 3D culture. While the secret formulation was found to be Matrigel/collagen (6 mg/ml Matrigel and 2 mg/ml rat tail collagen I), it was surprising that there was a stark contrast between the use of non-growth factor reduced Matrigel and growth factor reduced Matrigel. Large MCF-10A tissues assembled via STDPAC and 3D cultured in Matrigel/Collagen became a collection of small tissues when cultured with GFR Matrigel and contiguous large tissues when cultured with nGFR Matrigel (Figure 5-10). There is no real precedence for this dichotomy in behavior based on the two types of Matrigel - typical 3D culture of MCF-10A acini only utilize GFR Matrigel (Debnath et al. 2003).

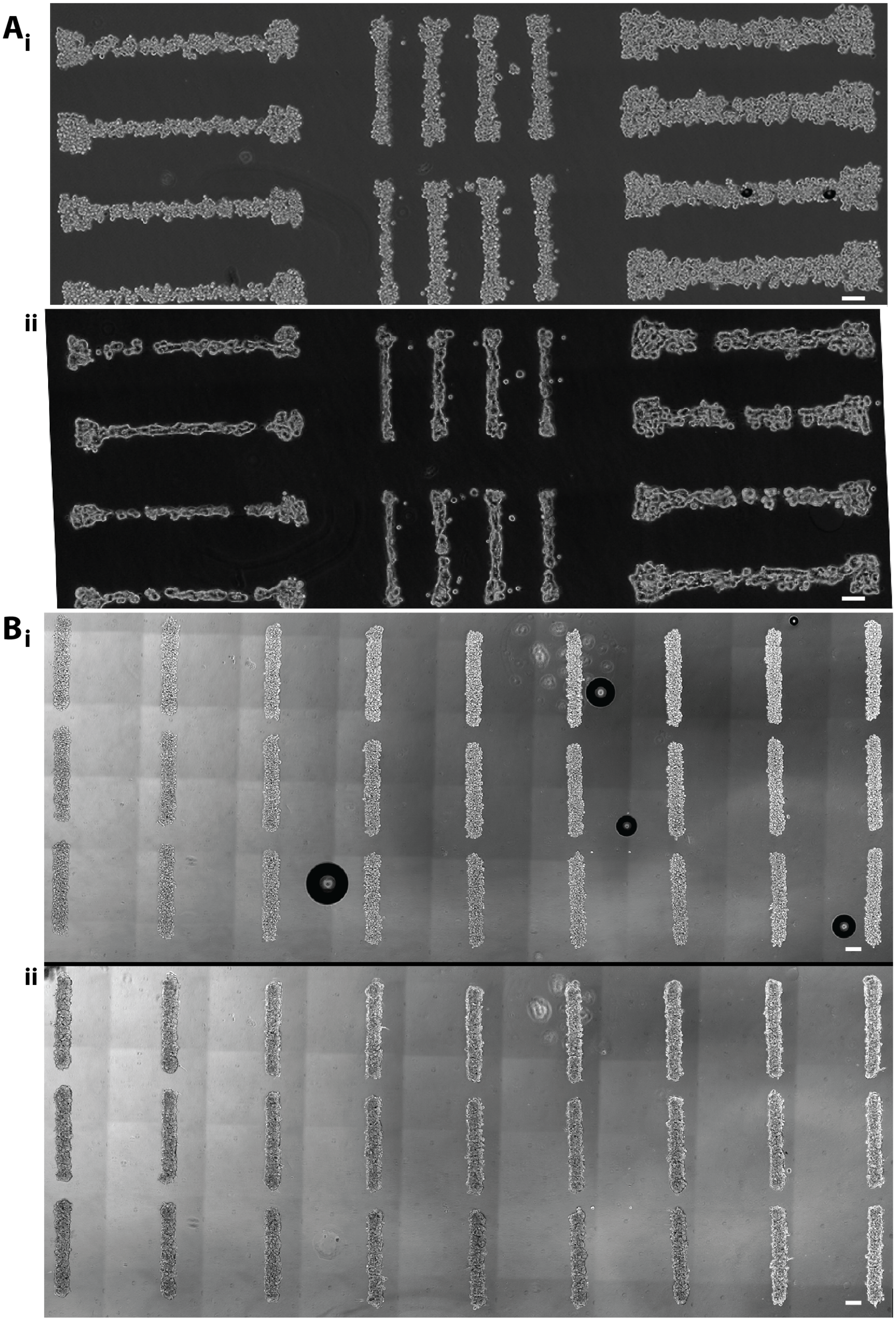
A i
ii
B i
ii

Figure 5-10. Large MCF-10A tube-like tissues growing under different matrix formulations. (A) MCF-10A tube-like tissue patterns are embedded in growth factor reduced Matrigel supplemented with 2 mg/ml collagen (i) and cultured for 24 hours (ii). (B) MCF-10AT tube-like tissue patterns are embedded in non-growth factor reduced Matrigel supplemented with 2 mg/ml collagen (i) and cultured for 24 hours (ii). Scale bars are all 100 μm.

There is a divide between engineering goals and the goals of generating true biological models. Engineering a tissue system requires the complete obedience of cells to collectively form the tissue structure that is designed. In this scenario, any given matrix formulation that accomplishes the engineering goal is sufficient for tissue synthesis. However, generating true biological models is far more difficult. Not only must the matrix formulation give rise to proper tissue structure, subsequent proper function is also required. A secondary goal of maintaining the most biomimetic system possible must also be considered at every step, for there if no true biological model if the system itself is completely foreign to human biology.

Media Considerations

Unlike matrix, media is much more important for proper tissue function than for molding tissue structure in 3D culture. It is a component of 3D culture (and 2D culture as well) that is largely ignored when assaying for tissue or cell behavior. In a sense, this is logical, considering that all experiments for most individual studies are mostly conducted with a constant media formulation. However, the media formulation also feeds into general fact that experiments are designed to show a biological phenotype that is wanted. Therefore, as long as the ingredients are scientifically justified, the “correct” media formulation is usually one that promotes interesting tissue behaviors in culture.

Determining the correct media formulation is especially difficult when co-culturing multiple types of cells. Most media conditions found in literature are formulated for a single cell-type. Investigation of heterotypic cell-cell interactions, therefore, requires new media formulations. At the least, all cell-types must be tested with non-traditional, existing formulations to confirm consistent behavior. Because one of the main goals in the development of STDPAC was to make its application universally available, we mostly tested well-established media formulations from literature, or media kits obtained from scientific vendors.

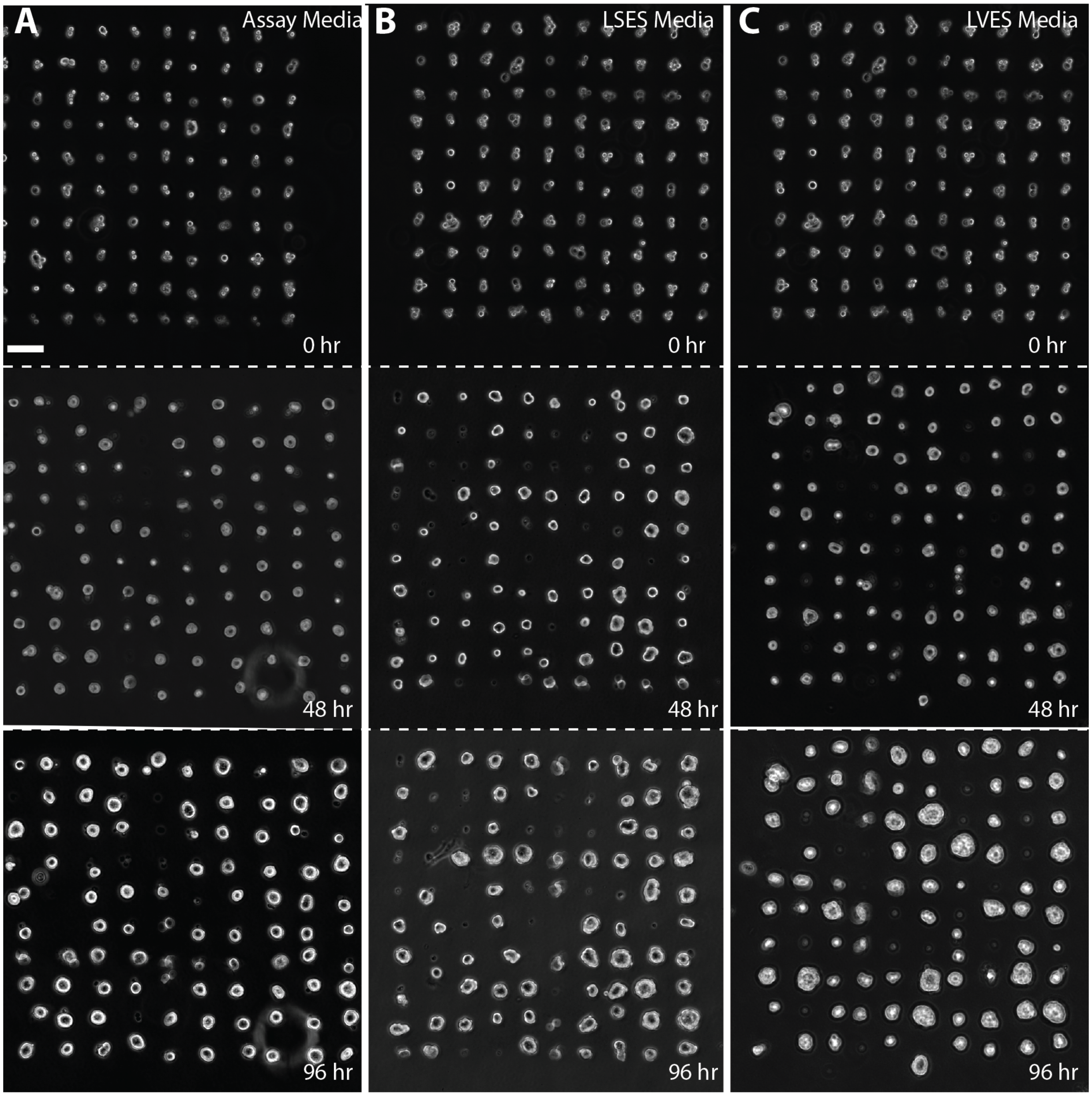
A
Assay Media
B
LSES Media
C
LVES Media
0 hr
0 hr
0 hr
48 hr
48 hr
48 hr
96 hr
96 hr
96 hr

Figure 5-11. MCF-10A tissues growing under different media conditions. (A) MCF-10A tissues are shown growing over 4 days in standard 3D embedded culture in Matrigel with standard assay media. (B) MCF-10A tissues are shown growing over 4 days in standard 3D embedded culture in Matrigel with LSGS HUVEC media. MCF-10A tissues are shown growing over 4 days in standard 3D embedded culture in Matrigel with LVES HUVEC media. All images are to the same scale and the scale bar is 100 µm.

Since MCF-10A tissues were consistently assayed for behavioral changes, they were tested with different media formulations when co-cultured with other cell-types. For example, in preparation for a co-culture experiment of MCF-10A tissues and HUVEC tissues, MCF-10A cells were cultured in traditional Matrigel 3D culture, but with various media formulations (Figure 5-11, Figure S5). Unsurprisingly, MCF-10A tissues growing in various HUVEC media formulations exhibited different morphologies compared the MCF-10A tissues growing in their traditional assay media. In fact, tissue morphology was for co-cultures showed stark differences when grown in different media formulations. In the 3-component pattern of epithelial tissues, endothelial tissues, and fibroblasts, the endothelial tissues exhibited an extraordinary amount of branching when grown in Matrigel/collagen and low serum endothelial supplement (LSES) HUVEC media (Figure 5-12). In stark contrast, the same pattern cultured in the same gel formulation, but with M87a media showed no branching in addition to the fibroblast-mediated branching (Figure 5-13).

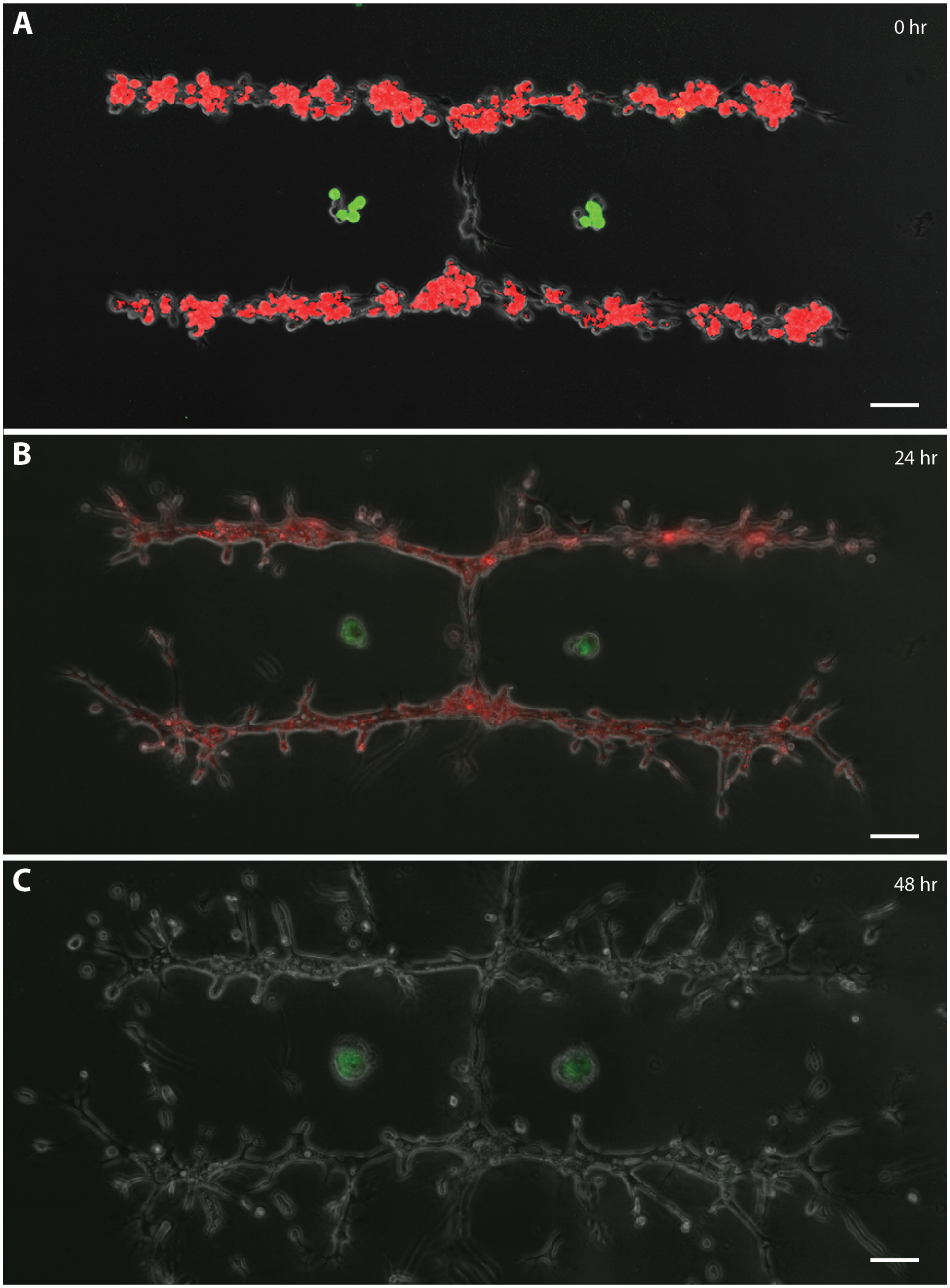
A
0 hr
B
24 hr
C
48 hr

Figure 5-12. Multi-component pattern growing in LSGS HUVEC media. (A) A pattern of HUVEC tubes, fibroblasts, and endothelial cells grown in 3D culture with LSGS HUVEC media at time 0, (B) 24 hours, and (C) 48 hours. All scale bars are 100 µm.

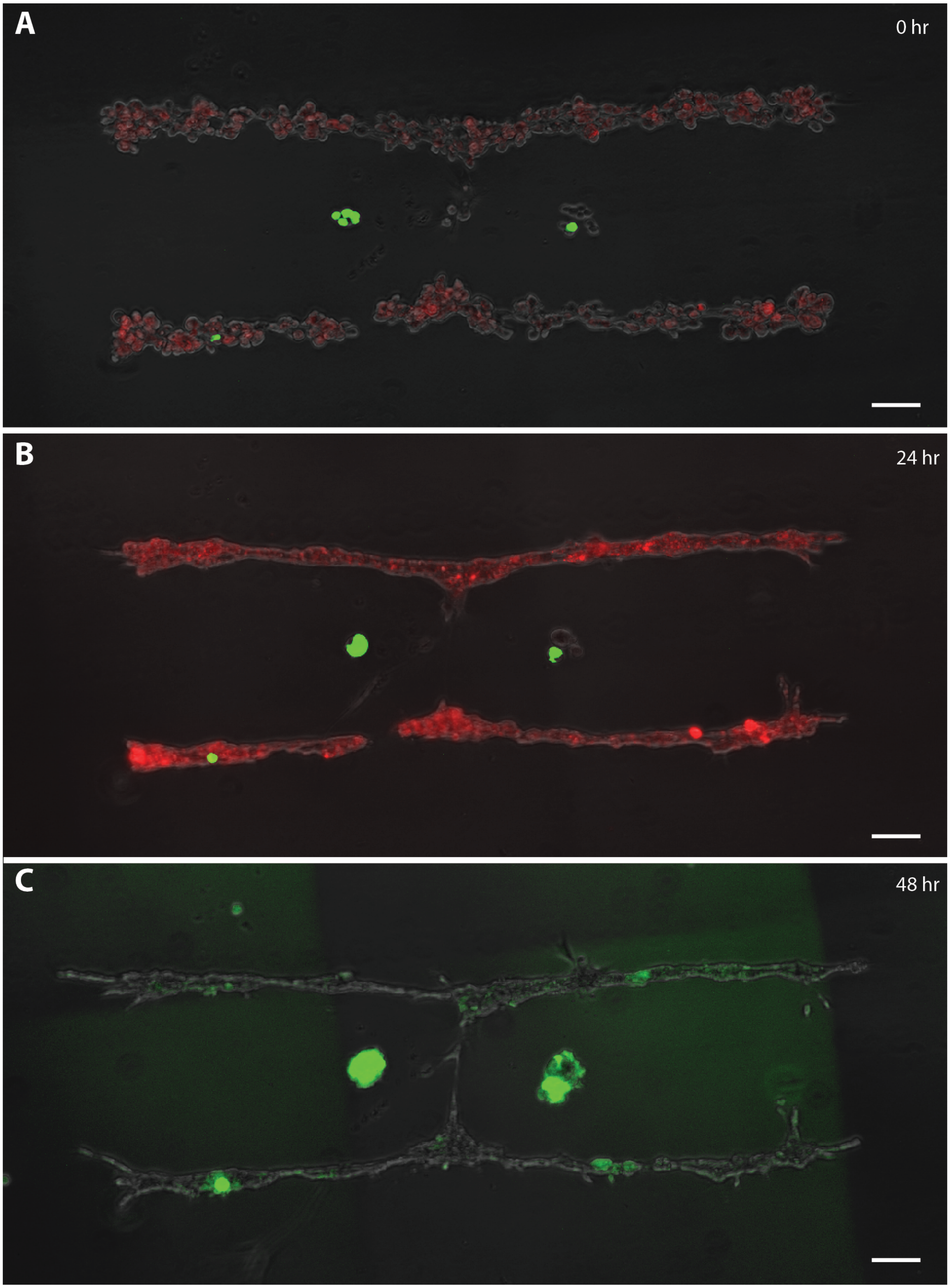
A
0 hr
B
24 hr
C
48 hr

Figure 5-13. Multi-component pattern growing in M87a media. (A) A pattern of HUVEC tubes, fibroblasts, and endothelial cells grown in 3D culture with M87a media at time 0, (B) 24 hours, and (C) 48 hours. All scale bars are 100 μm.

These results strongly suggest that all components of a system must be taken into consideration during experimental analysis. Whether matrix or media formulations, the input of a model system will definitely affect the output.

Commentary

While STDPAC is a powerful technique, there are still aspects of it that should be optimized. However, every technology is a work in progress. Just as crust-less sliced bread improved sliced bread, there are many ways in which STDPAC can be improved.

One concern is the exponential drop off in resolution the taller one builds a tissue. Thus the technique, while able to create large patterns for 3D organotypic culture, is limited to interactions in a single 2 dimensional plane. This feeds back to the importance of design. When designing an experiment, one needs to consider the limitations of the technique and design the experiment around them as to ensure that the results do not presuppose a particular condition that is false. It is very easy to overlook certain falsities assumed true because they are lost in the minutia of the technical details. For example - back to the fibroblast and the epithelial tissue - if one is looking at the mechanical forces that are propagated through a matrix by a fibroblast onto an epithelial tissue, it is important to know how much of the force is spread out over distance. Just like a flashlight (Figure 5-6), if the fibroblast is too close to the epithelial tissue, the mechanical force exerted in the xy direction will be focused on a small point, which may only be the bottom of the tissue. However, if the fibroblast is placed far from the tissue, the mechanical pull propagated through the gel would disperse sufficiently to cover the entire height of the epithelial tissue.

Of course, this is also assuming a perfect system in which cells exert behaviors and interact only in a single XY plane instead of adding a Z component and a 360 degree sphere of influence. It’s also assuming that stochastic cell behaviors are still biased towards the pattern created – that spatial positioning of cells in context to one another has a measurable effect on their behavior. This has not yet been verifiable by any experimental means.

Another concern is that cells are inherently sticky, and there is no passivation of the cell surface. Thus, the DNA is not the sole adhesive molecule that causes cells to stick together when building tissues. They clump or stick to other portions of the pattern where there is no complementary DNA, especially when other cells are present. The limitation to the z-resolution of STDPAC is accentuated by this sticky wicket.

A way to fix this would be to add a passivation step to the treatment of the cells. This would not be unlike the passivation of the glass slide to render it not sticky to cells. For example, if there was a coating on the outside of the cell surface to hide the proteins and sugars of the glycocalyx and only present DNA, it would be a simple matter for the DNA to be the only means by which cells can bind to one another. For example, there could be a poly-ethylene glycol (PEG) layer that insulates the outside surface of the cell. As long as the DNA is unobstructed by the PEG layer, it would be easy to imagine that the cells would not stick to one another except via DNA mediated interactions. On the other hand, PEG, which biologically inert, has a very long half-life, even in bloodstreams. This is because cells do not have mechanisms that are optimized for PEG breakdown. This technique calls for a temporary modification of the cell surface with DNA. In the same way, a temporary passivation, for example, a sugar based brush layer, might be an interesting technique for the passivation of a cell surface because the proteins should be able to break down the sugars much faster than PEG.

The final concern is hubris. There's an aspect of hubris involved when one is developing a technology that is, in one's own point of view, far superior to the existing techniques. Because one is working with a technology that is more enabling than what is currently available, it is easy to forget what the limitations are and how they might obscure the interpretations of results obtained by this method. It is important to remember the plank in one's own eye.

References

Nelson, C., Vanduijn, M., Inman, J., Fletcher, D. & Bissell, M. (2006). Tissue geometry determines sites of mammary branching morphogenesis in organotypic cultures. Science *314*, 298–300.

Gilmore, A.P. (2005). Anoikis. Cell Death and Differentiation *12*, 1473–1477.

Xu, Q., Schlabach, M.R., Hannon, G.J., Elledge, S.J. (2009). Design of 240,000 orthogonal 25mer DNA barcode probes. P.N.A.S. *106*, 2289–2294.

L'Heureux, N., Pâquet, S., Labbé, R., Germain, L. & Auger, F. A. (1998). A completely biological tissue-engineered human blood vessel. FASEB J *12*, 47–56.

Debnath, J., Muthuswarmy, S.K., Brugge, J.S. (2003). Morphogenesis and oncogenesis of MCF-10A mammary epithelial acini grown in three-dimensional basement membrane cultures. Methods *30*, 256–268.

Chapter 6: Conclusion and Perspective

Complex tissue model generation with STDPAC provides an important toolset to the basic and biomedical sciences. The level of control STDPAC provides over reconstituting tissue architecture and components is unprecedented. STDPAC functions as a rapid prototyping tool to explore hypotheses (Figure 2-4), synthesizes 3D tissue models with single cell resolution (Figure 3-5), provides a rapid and orthogonal system to maintain normal cell behavior and viability with any assortment of cell-types (Figure 3-15), and creates 3D tissue models in high throughput while allowing high throughput analysis of tissue behavior (Figure 4-4). These aspects of STDPAC confer significant advancements in the ability for scientists to reconstitute *in vivo* tissue behaviors *in vitro*.

As with most cutting-edge scientific tools and techniques, STDPAC is a very complicated technique to learn. The one, unmet goal of this project has been the ability to make it easily adoptable. The STDPAC method is complicated, and has not been optimized for easy adoption by other scientists. The majority of time and effort have been dedicated solely on reliability of the technique itself, and not on the ease of execution. There are times when the pursuit of a new technology for the sake of intellectual stimulation is acceptable. STDPAC, however, was built with an application in mind – complex tissue model generation. And as discussed in Chapter 4, creating models is inadequate without broad reproducibility. A new technique that is not adoptable is necessarily not reproducible.

Fixing the adoption issue is not trivial, but there are steps being taken towards this goal, as described in the Supplemental Text 2. There are trade-offs in removing complexity from STDPAC. Removing complexity from the method means that, in this case, the tissue models generated are less complex. However, drastically reducing the barrier to adoption may arguably make STDPAC a more powerful scientific tool than before. The final goal and dream, while unachievable by this author, is to simplify STDPAC without removing complexity in the tissue models generated. Until then, STDPAC remains a powerful, but exclusive scientific tool.

Appendix 1: Supplemental Figures and Tables

Supplemental Figures

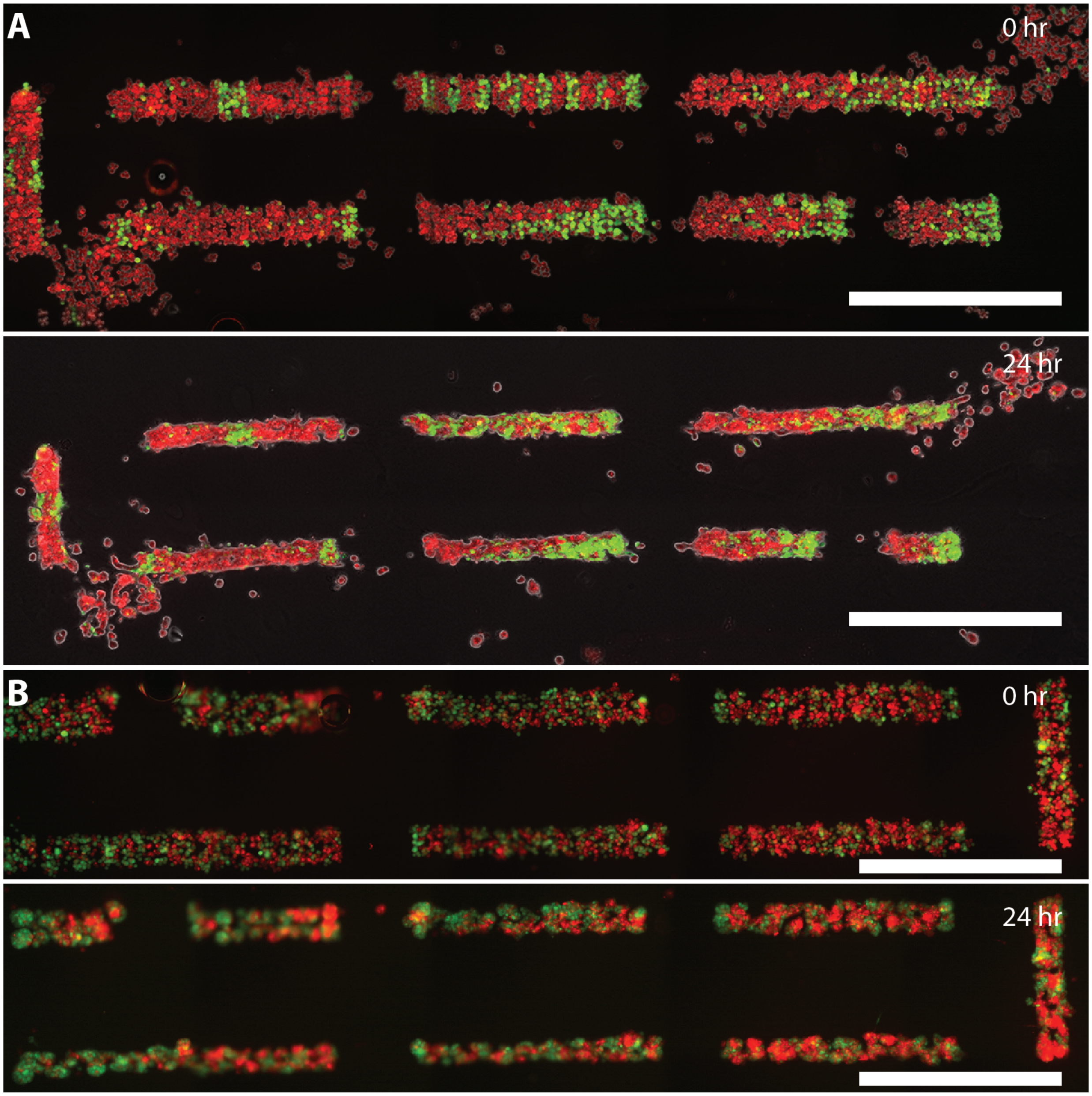

Supplemental Figure S3-1. Nearly patterned multi-component MCF-10A tubes. (A) Multi-component MCF-10A tubes maintain intra-tissue patterns over 24 hours in 3D culture. These patterns exhibit too much background. (B) Multi-component MCF-10A tubes show too much cross contamination and pattern holes to grow into contiguous tubes. The intra-tissue patterns are retained over 24 hours in 3D culture. All scale bars are 1 mm.

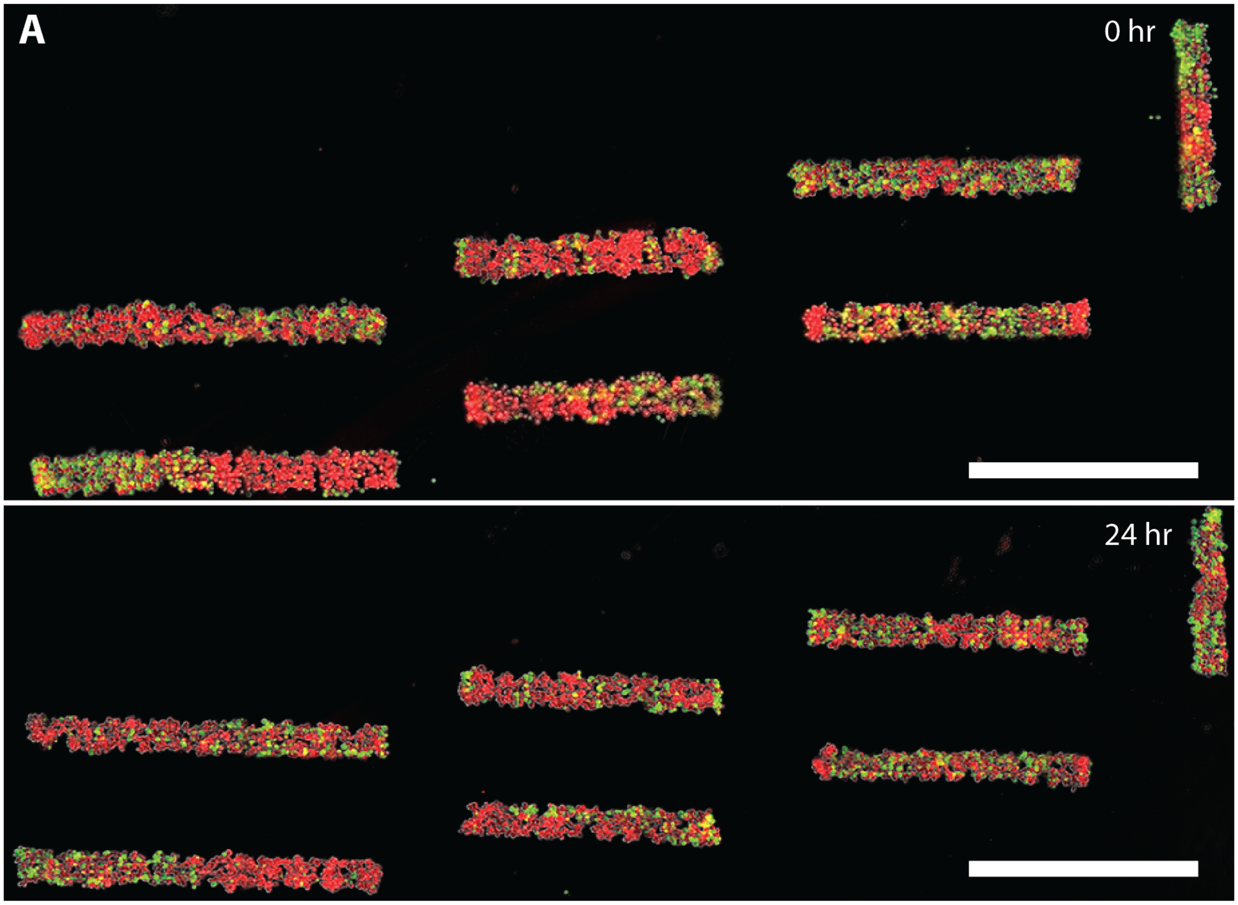

Supplemental Figure S3-2. Repositioned pattern of multi-component MCF-10A tubes. (A) MCF-10A tubes are staggered so that tissues do not obstruct the flow of cells to neighboring tissues. Intra-tissue patterns are retained over 24 hours in 3D culture. All scale bars are 1 mm.

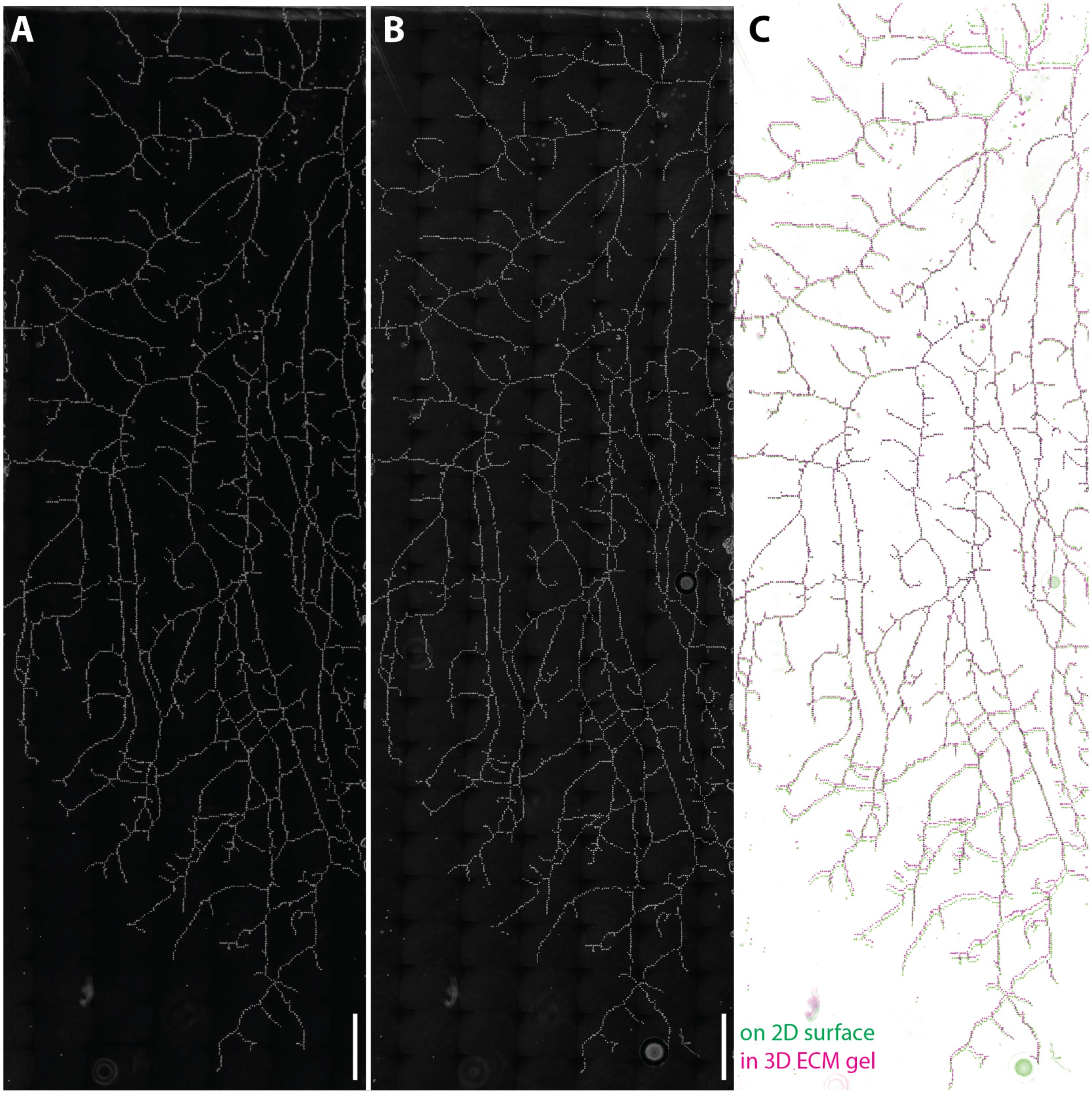

Supplemental Figure S3-3. Large pattern transfer fidelity in Matrigel. (A) An MCF-10A reconstituted pattern of a mouse mammary fat pad is imaged on glass. (B) The same pattern is transferred to Matrigel and lifted. (C) An overlay of the pattern before and after lifting show high transfer fidelity of STDPAC patterns over large distances. All scale bars are 1 mm.

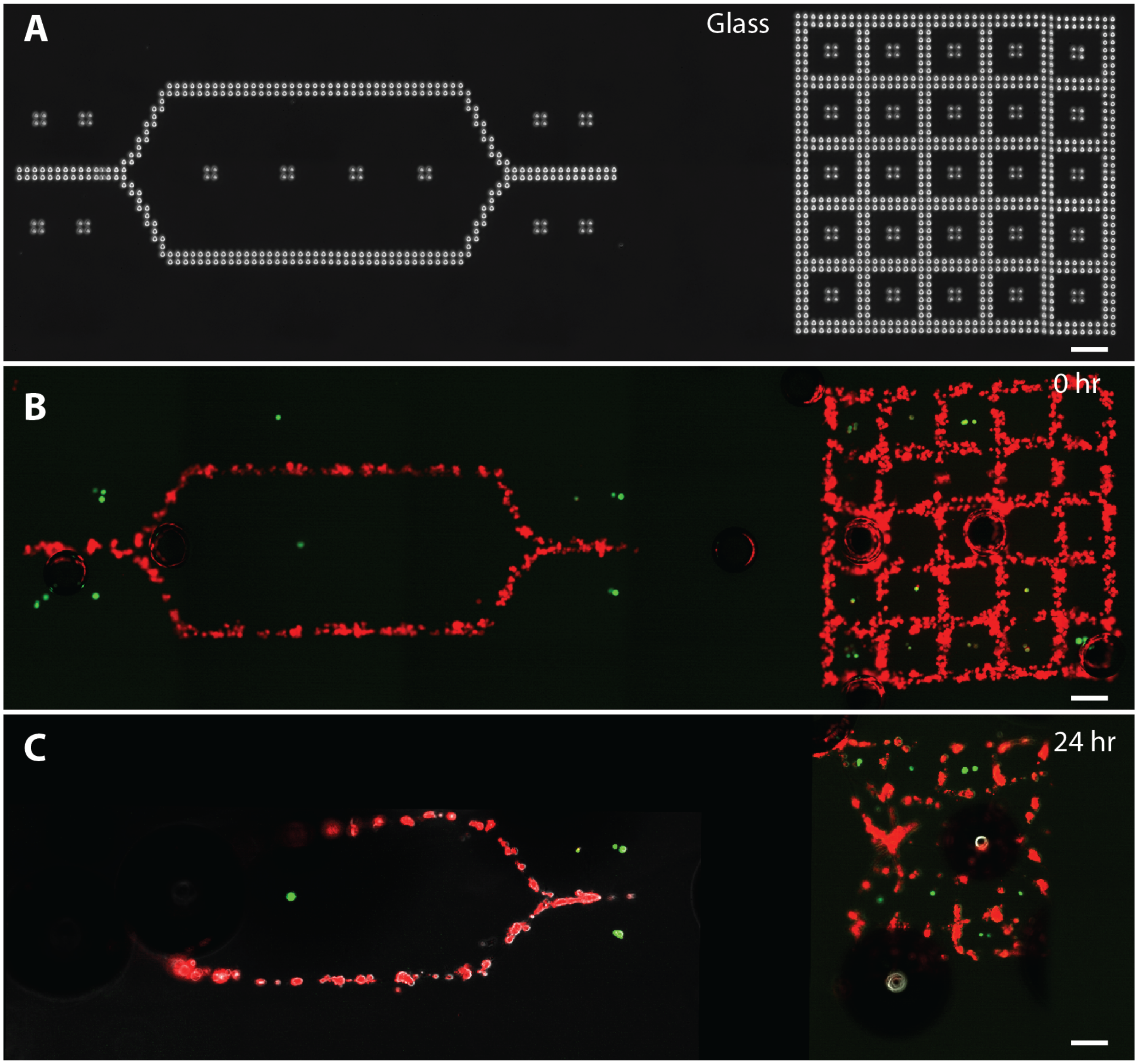

Supplemental Figure S3-4. Highly synthetic multi-component patterns of HUVECs and MCF-10A cells. (A) Highly synthetic vascular beds are designed with A-sequence DNA with B-sequence DNA interspersed between the vascular bed patterns. (B) Cells attach well to the A-sequence DNA but not to the B-sequence DNA. (C) No contiguous tissues grow after 24 hours, but HUVEC contraction distorts the gel after 24 hours. All scale bars are 100 µm.

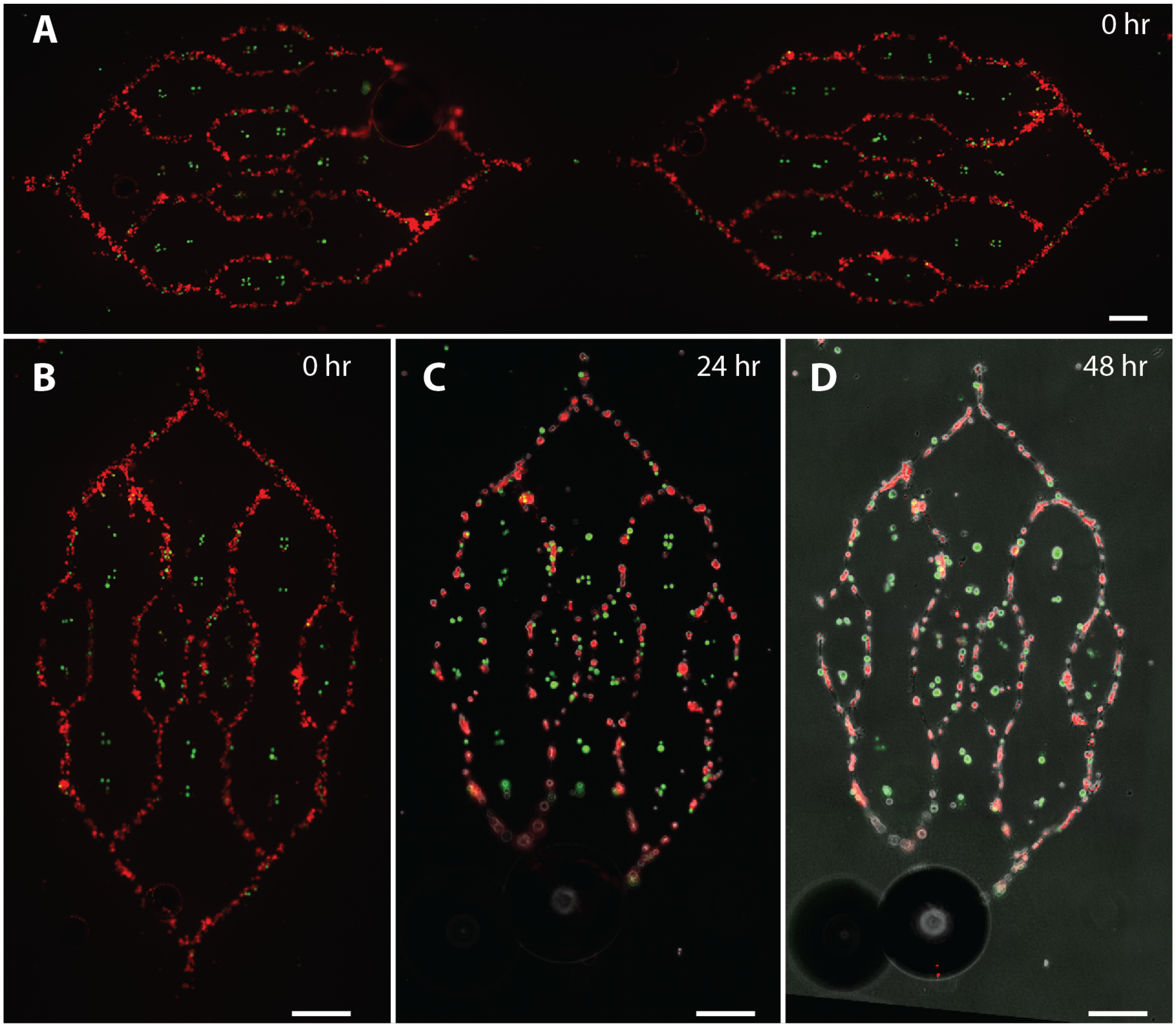

Supplemental Figure S3-5. First pass vascular bed multi-component patterns of HUVECs and MCF-10A cells. (A) Synthetic vascular beds are designed with A-sequence DNA with B-sequence DNA interspersed between the vascular bed patterns. Cells are attached with no assembly steps. (B) Major cross-contamination is observed at 0 hours. (C) Cells do not grow into contiguous tissues after 24 hours. (D) Cross-contamination is enhanced over 48 hours. All scale bars are 100 μm.

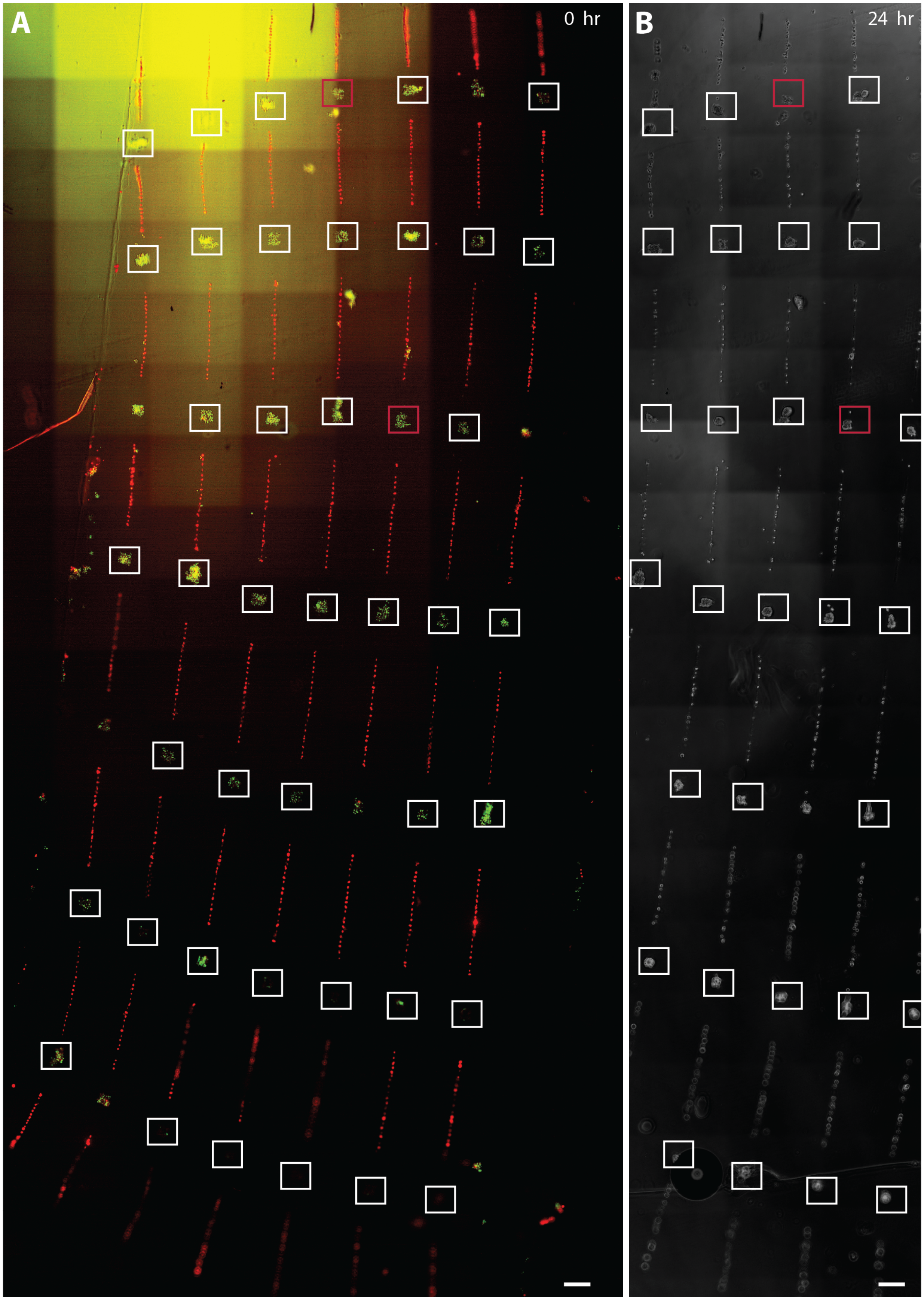
A
0 hr
B
24 hr

Supplemental Figure S4-1. Scoring fibroblast line experiments. (A) Ras tissues are only assayed for behavioral change if they do not exhibit cross-contamination of fibroblasts within the tissue at 0 hours. White boxes mean assay, red boxes mean don't assay. (B) The same scoring is carried through for tissues across all time points. Scale bars are all 100 μm.

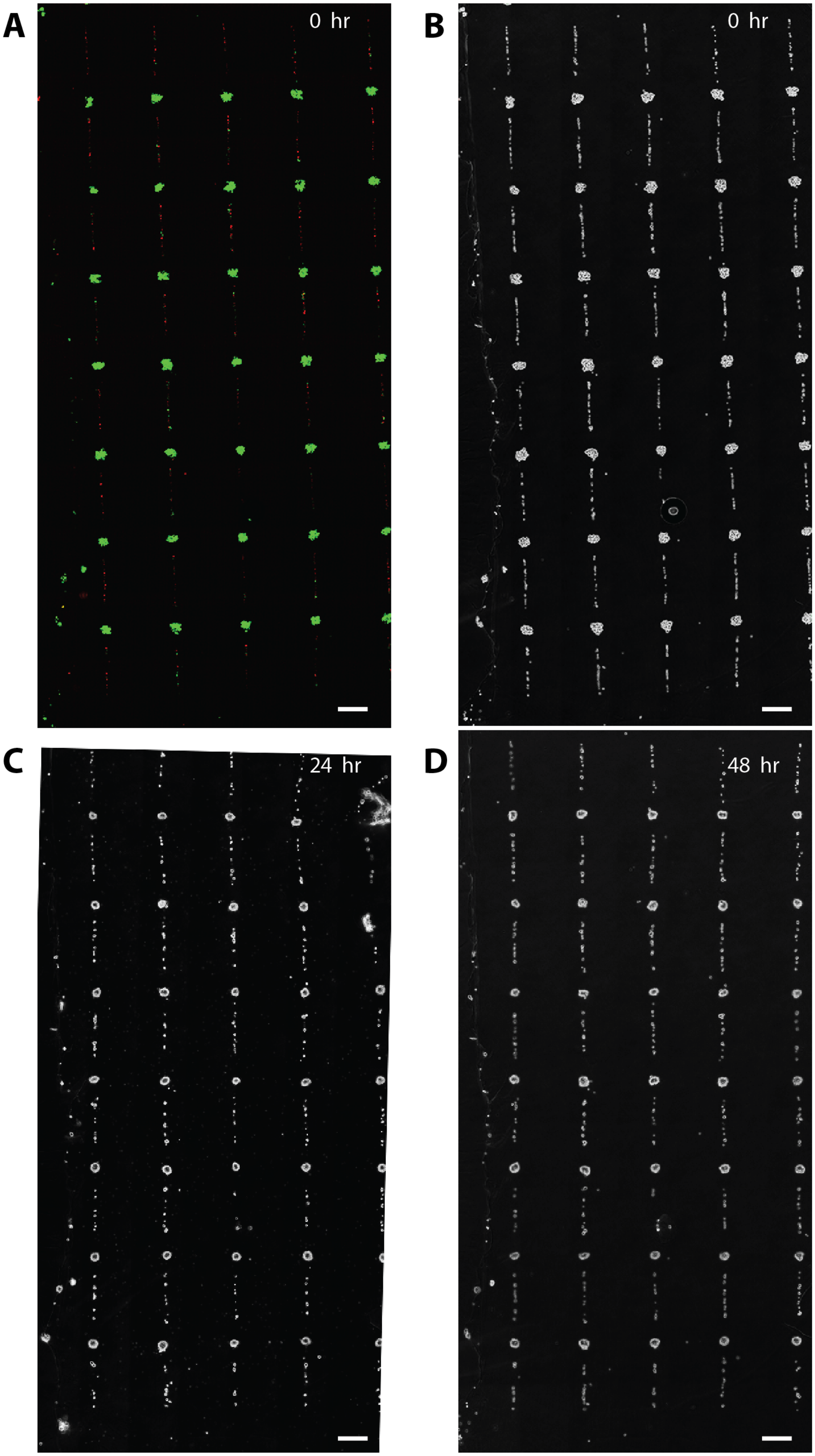
A
0 hr
B
0 hr
C
24 hr
D
48 hr

Supplemental Figure S4-2. Examples of fibroblast line experiments. (A) Fibroblasts are labeled red and Ras cells are labeled green to ensure proper scoring from 0 hours. (B) Tissues are scored in phase contrast. (C) The pattern at 24 hours. (C) The pattern at 48 hours. Scale bars are all 100 μm.

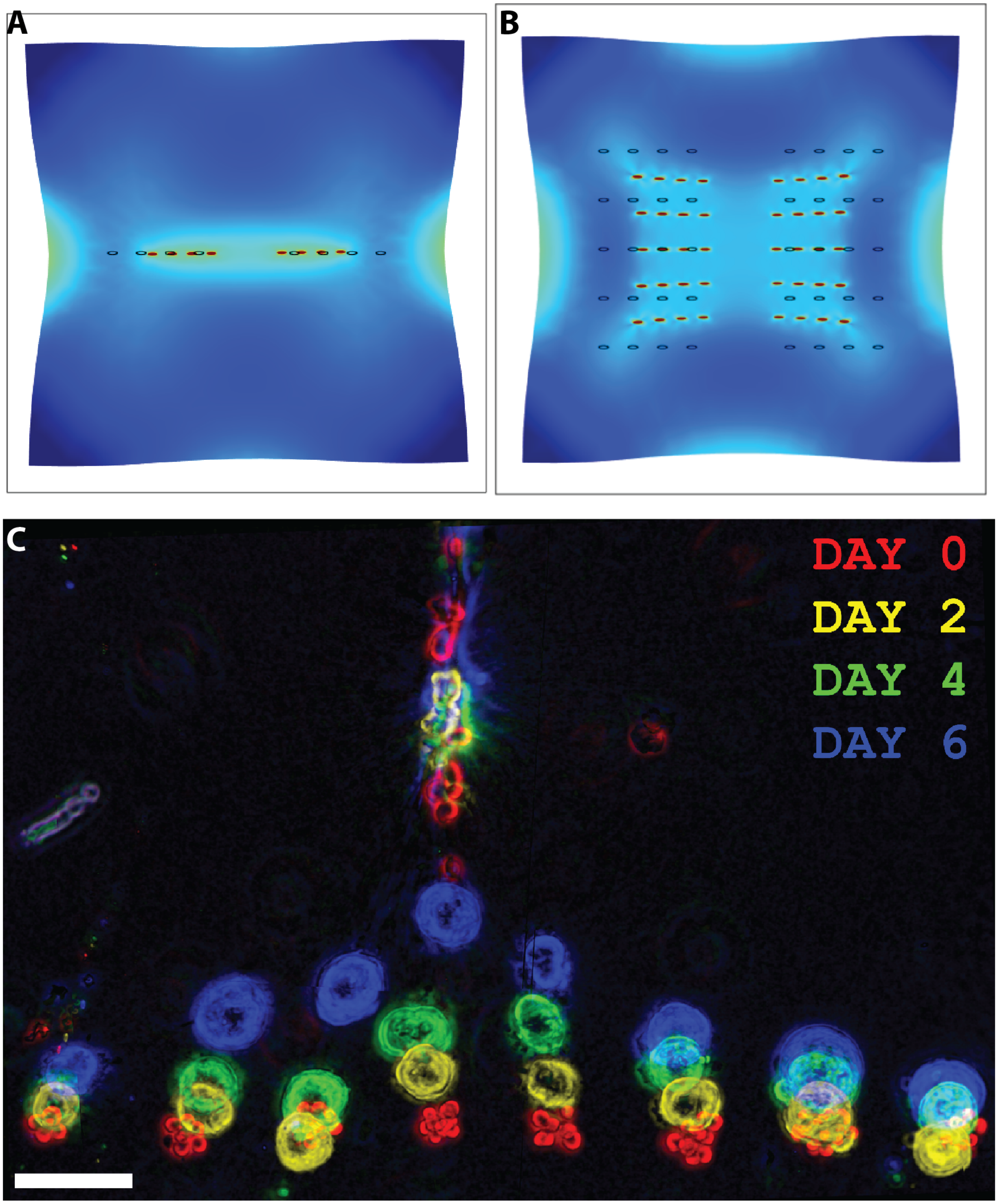

Supplemental Figure S4-3. Modeled fibroblast mechanical pull. (A) Computational models of two lines of fibroblasts show that the most force is exerted between the two lines (light blue is more force). (B) Computational models of many parallel lines of fibroblasts show that the most force is exerted in between parallel lines (light blue is more force). (C) Single fibroblast lines condense in culture and pull lines of small normal tissues along the axis of the fibroblast lines. Scale bar is 200 μm.

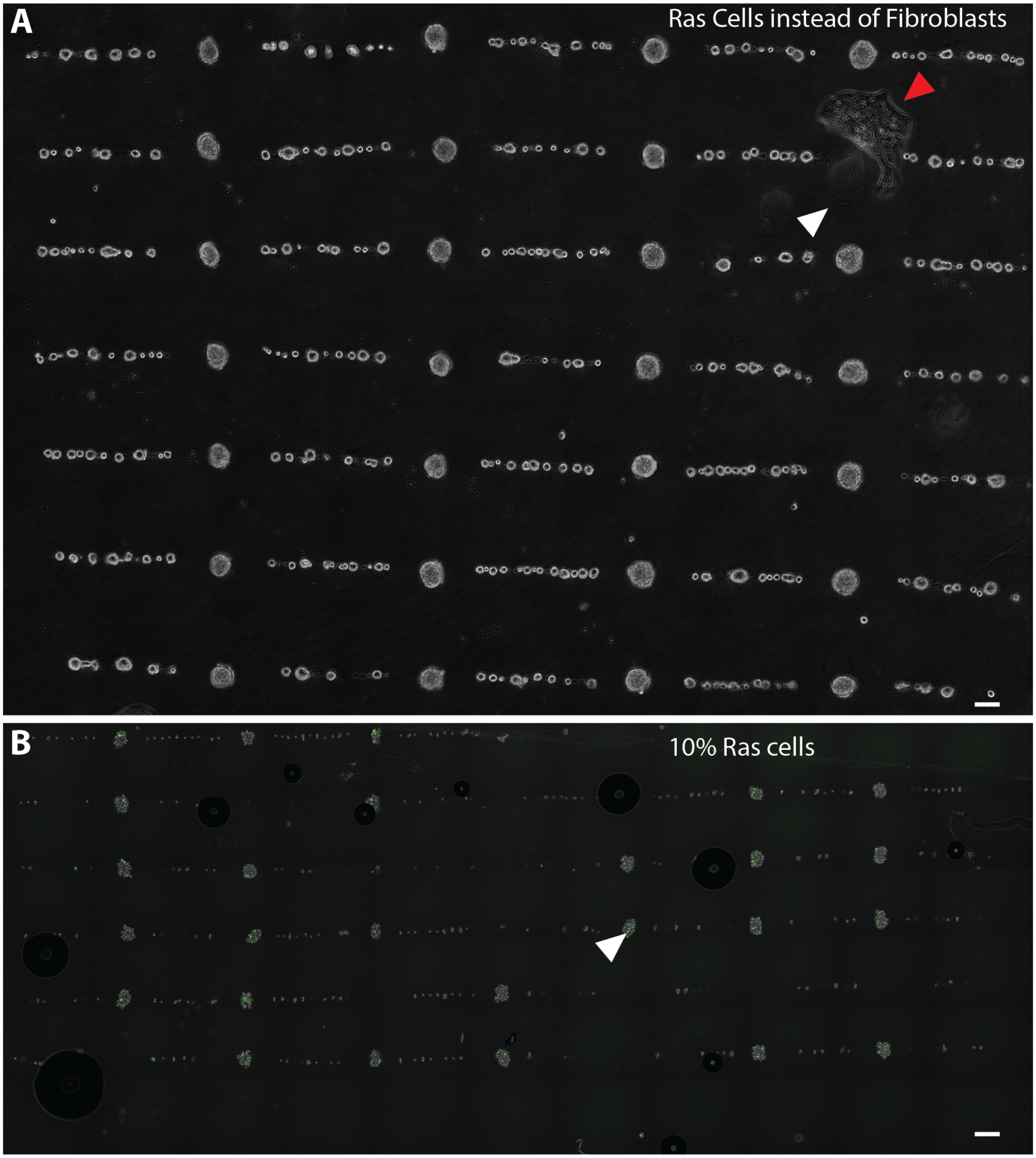

Supplemental Figure S4-4. Pattern perturbation by changing Ras cell locations. (A) Lines of fibroblasts are replaced with lines of Ras cells to test if the pattern itself causes mechanical pull rather than the cell type within the particular pattern. Some Ras tissues spread across the bottom of the gel (red arrow) and left a blank space within the gel (white arrow). (B) Tissues are changed to include 10% Ras cells with 90% normal cells. Scale bars are all 100 µm.

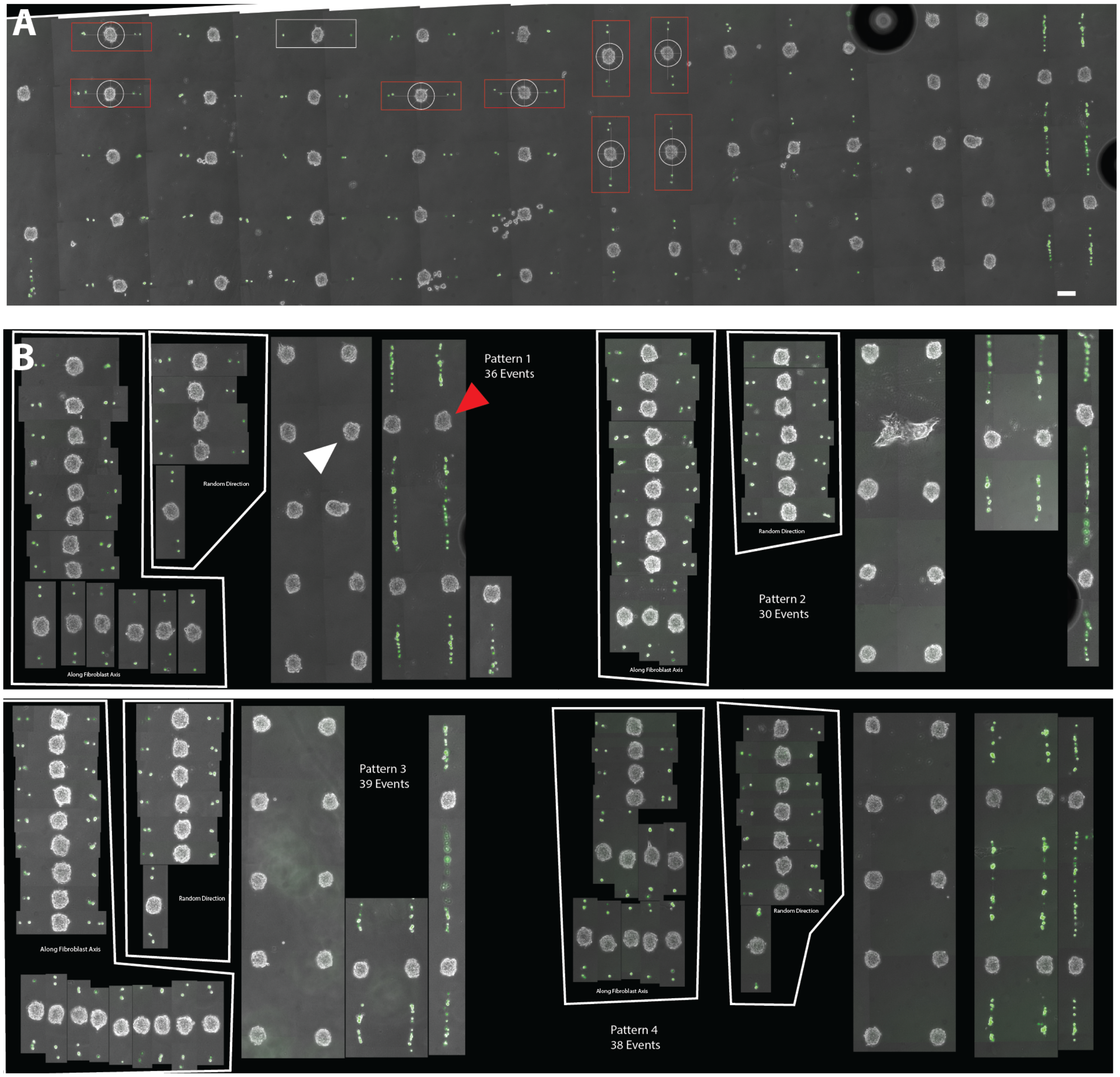
A
B
Pattern 1
36 Events
Random Direction
Along Fibroblast Axis
Random Direction
Along Fibroblast Axis
Pattern 2
30 Events
Pattern 3
39 Events
Random Direction
Along Fibroblast Axis
Along Fibroblast Axis
Random Direction
Pattern 4
38 Events

Supplemental Figure S4-5. Scoring the 2-fibroblast mechanical pull experiment. (A) Tissues are only scored if no cross-contamination is detected. White boxes means assay, red boxes means don't assay. Tissues are assayed by placing circles above Ras tissues and determining in which quartile fingers form. (B) Scored and assayed tissues are selected and placed in single images for comparison to negative (white arrow) and positive controls (red arrow). Scale bars are all 100 μm.

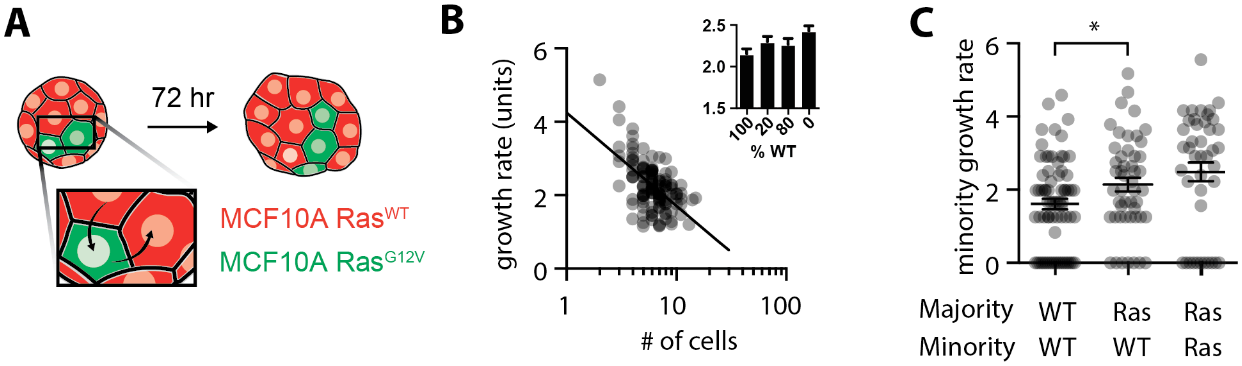

Supplemental Figure S4-6. Measuring the impact of composition on single and collective cell behaviors in 3D epithelial microtissues (A) Scheme for assessing the impact of tissue compositional heterogeneity on the growth rate of 10A and RasG12V-expressing MCF10A cells. (B) The effect of initial tissue size on cell growth rate for 10A MCF10A. Inset shows average growth rate for tissues of different compositions. (C) Growth rates of single cells (minority) cultured in microtissues having the indicated majority cell-type.

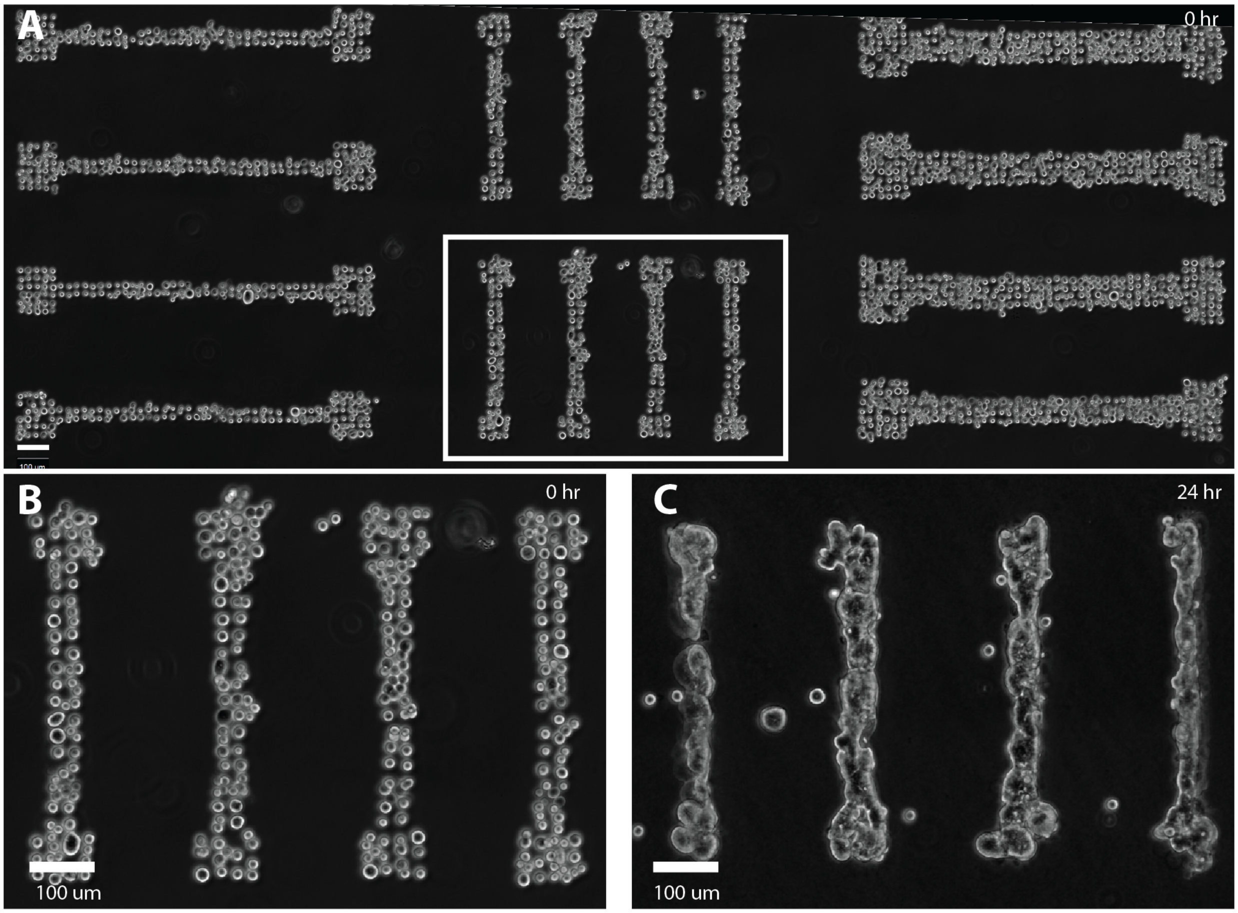
A
0 hr
100 µm
B
0 hr
100 um
C
24 hr
100 um

Supplementary Figure S5-1. MFC-10A tubes in Matrigel/collagen. (A) An array of multi-scale MCF-10A tubes at 0 hours. (B) A portion of the pattern is magnified. (C) The same pattern after 2 rounds of assembly and 24 hours in culture. All scale bars are 100 µm.

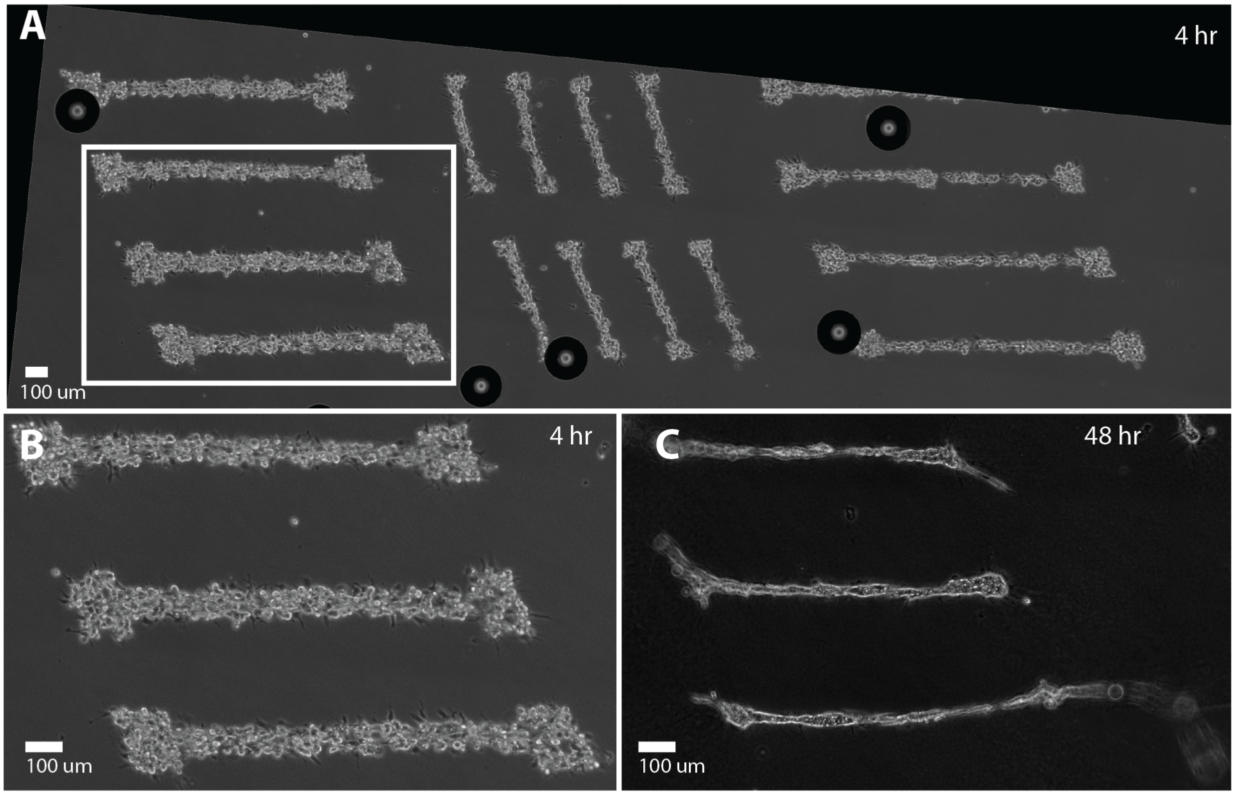
A
4 hr
100 um
B
4 hr
100 um
C
48 hr
100 um

Supplementary Figure S5-2. HUVEC tubes in Matrigel/collagen. (A) An array of multi-scale HUVEC tubes at 0 hours. (B) A portion of the pattern is magnified. (C) The same pattern after 2 rounds of assembly and 24 hours in culture. All scale bars are 100 μm.

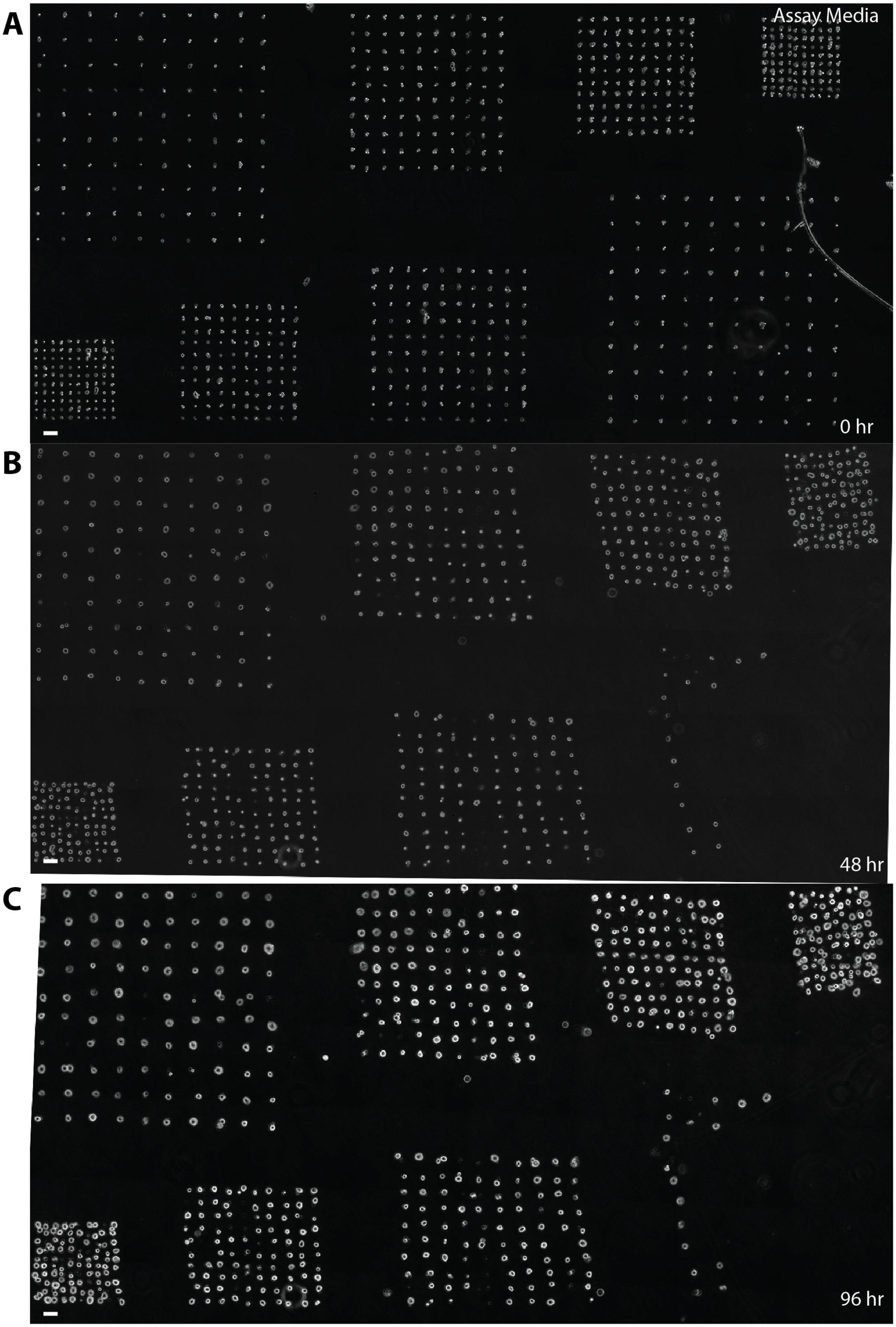
A
Assay Media
0 hr
B
48 hr
C
96 hr

Supplementary Figure S5-3. MCF-10A grids growing in Assay Media. (A) MCF-10A grids of increasing pitch are grown in assay media and shown at 0 hours, (B) 48 hours, and (C) 96 hours. All scale bars are 100 µm.

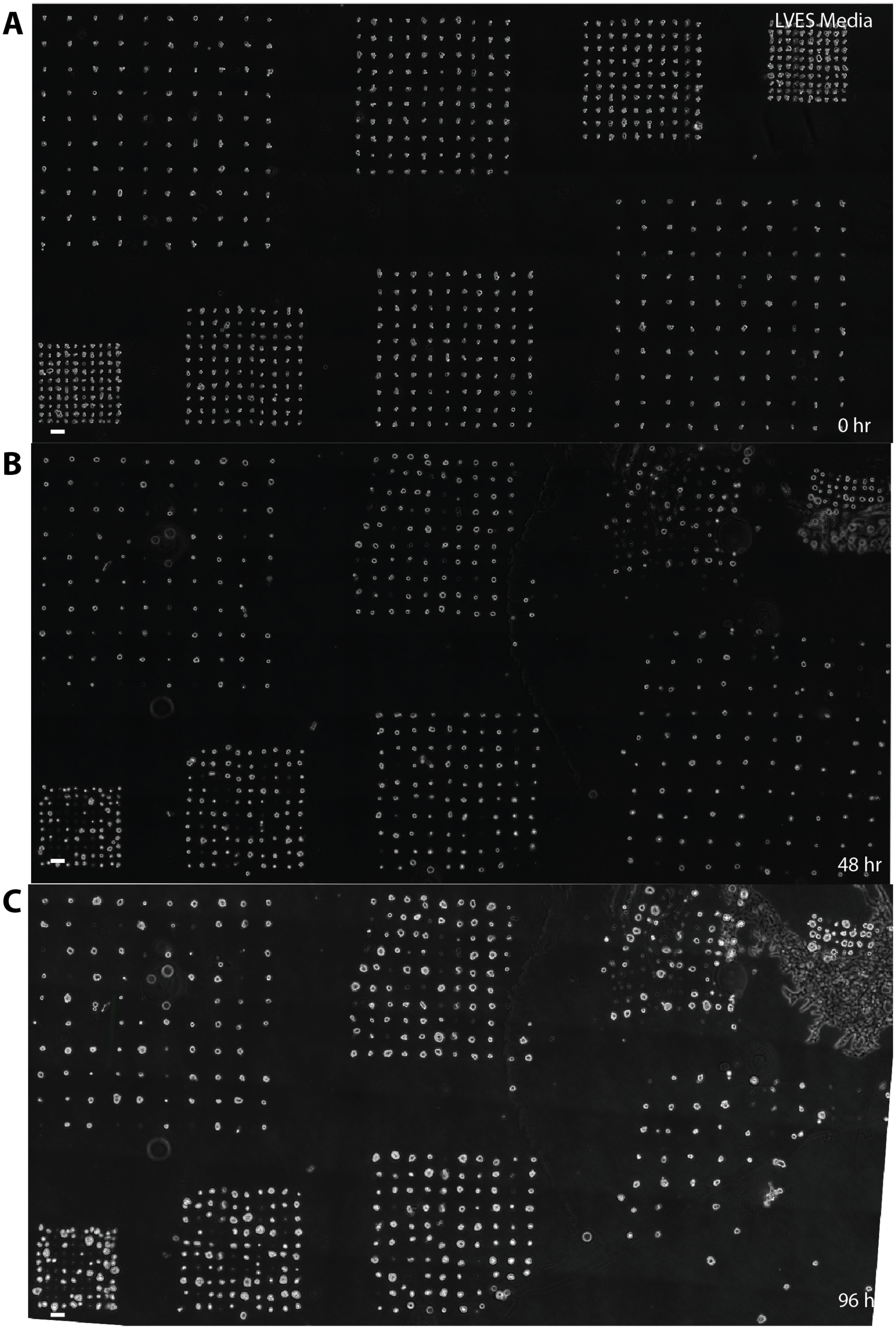
A
LVES Media
0 hr
B
48 hr
C
96 hr

Supplementary Figure S5-4. MCF-10A grids growing in LVES HUVEC media. (A) MCF-10A grids of increasing pitch are grown in LVES HUVEC media and shown at 0 hours, (B) 48 hours, and (C) 96 hours. All scale bars are 100 µm.

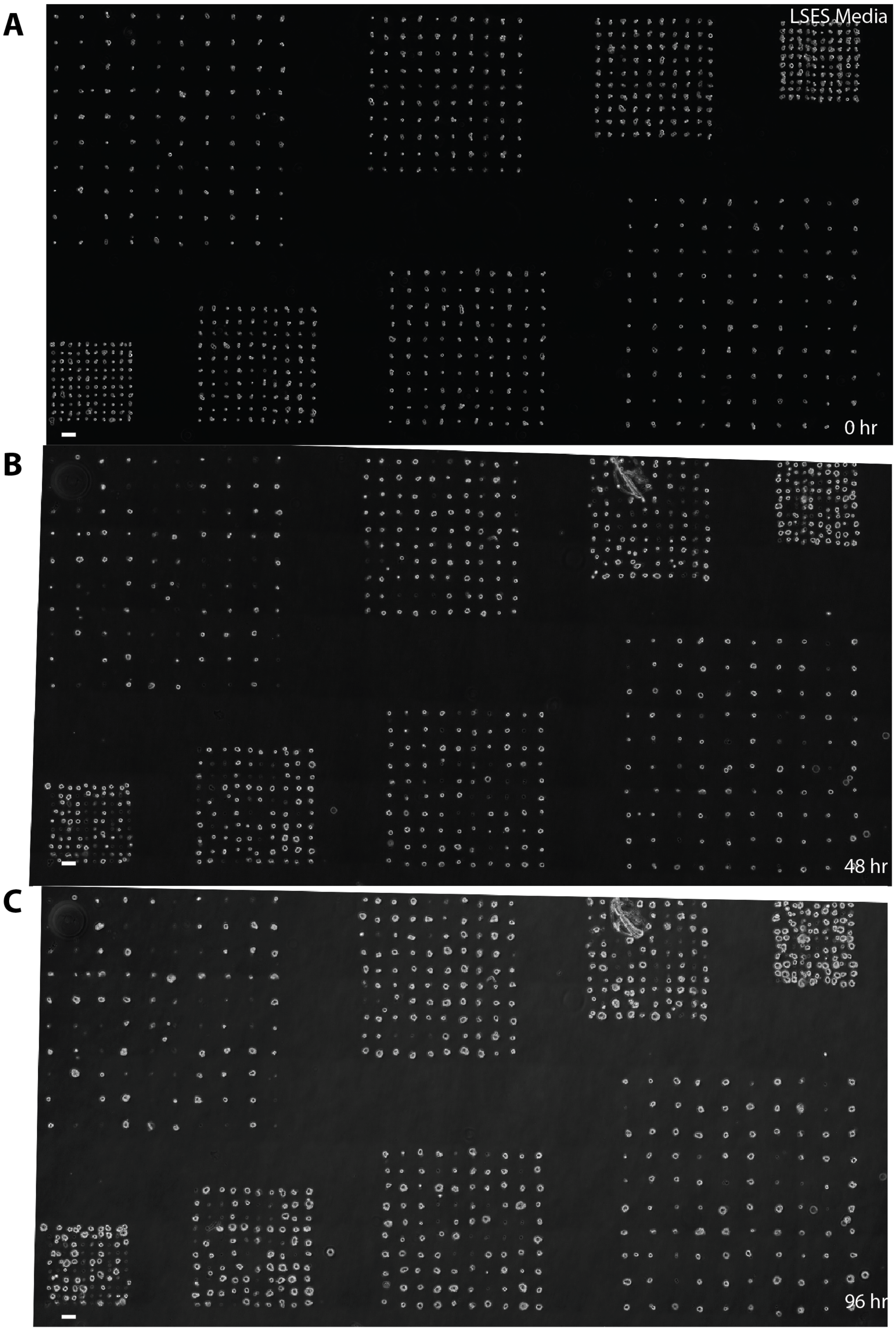
A
LSES Media
0 hr
B
48 hr
C
96 hr

Supplementary Figure S5-5. MCF-10A grids growing in LSES HUVEC media. (A) MCF-10A grids of increasing pitch are grown in LSES HUVEC media and shown at 0 hours, (B) 48 hours, and (C) 96 hours. All scale bars are 100 μm.

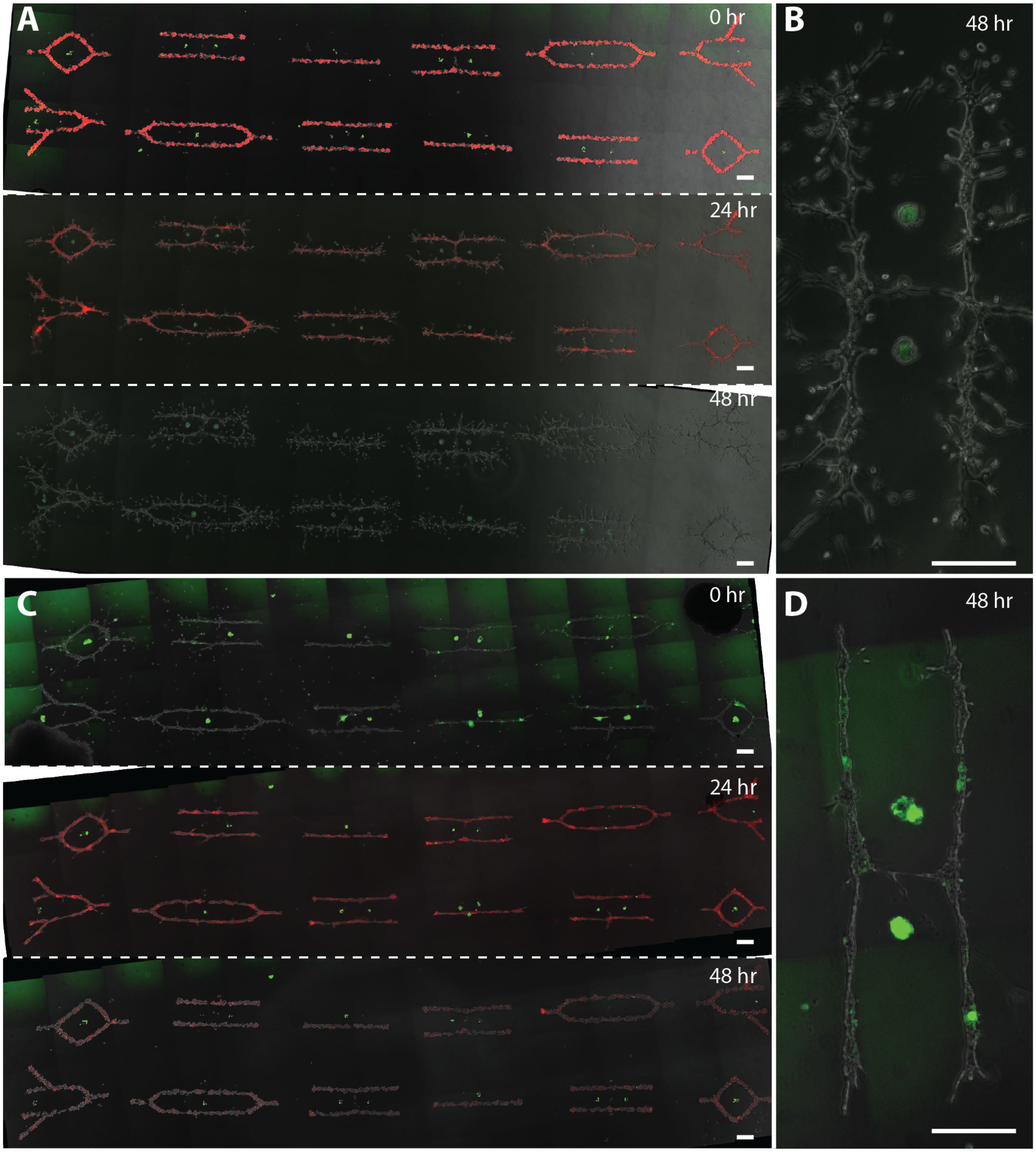

Supplementary Figure S5-6. Multi-scale multi-component patterns growing in different media. (A) A multi-scale multi-component pattern is grown in LSES HUVEC media and cultured over 48 hours. (B) A portion of the pattern is magnified to show massive branching along the HUVEC tubes. (C) A multi-scale multi-component pattern is grown in M87a media and cultured over 48 hours. (C) A portion of the pattern is magnified to show no branching along the HUVEC tubes. All scale bars are 100 µm.

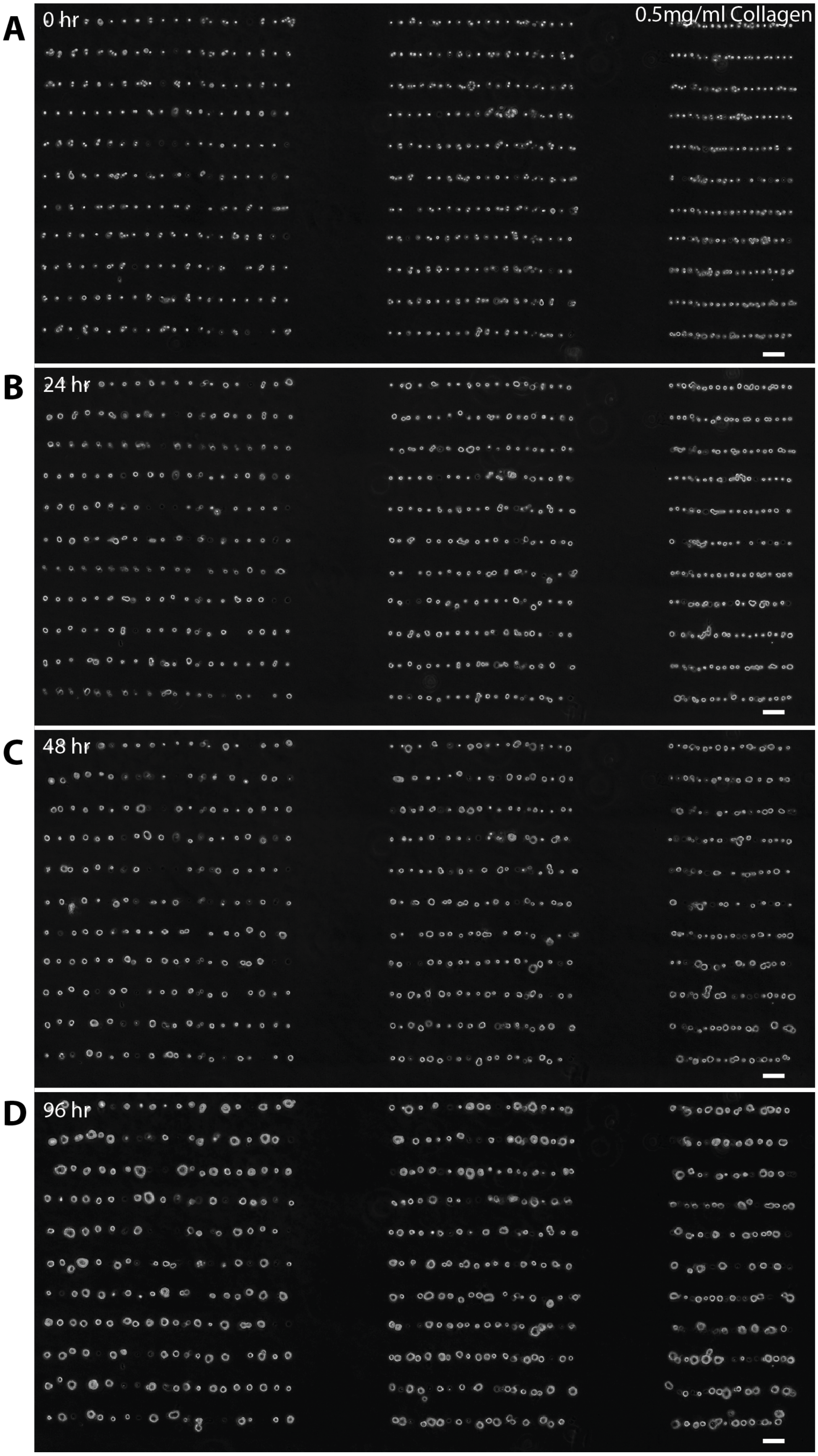
A
0 hr
0.5mg/ml Collagen
B
24 hr
C
48 hr
D
96 hr

Supplementary Figure S5-7. MCF-10A lines of various spacing growing Matrigel with a 0.5 mg/ml collagen supplement. (A) Lines of MCF-10A cells of decreasing pitch are grown in Matrigel supplemented with 0.5 mg/ml collagen and imaged at 0 hours, (B) 24 hours, (C) 48 hours, and (D) 96 hours. All scale bars are 100 µm.

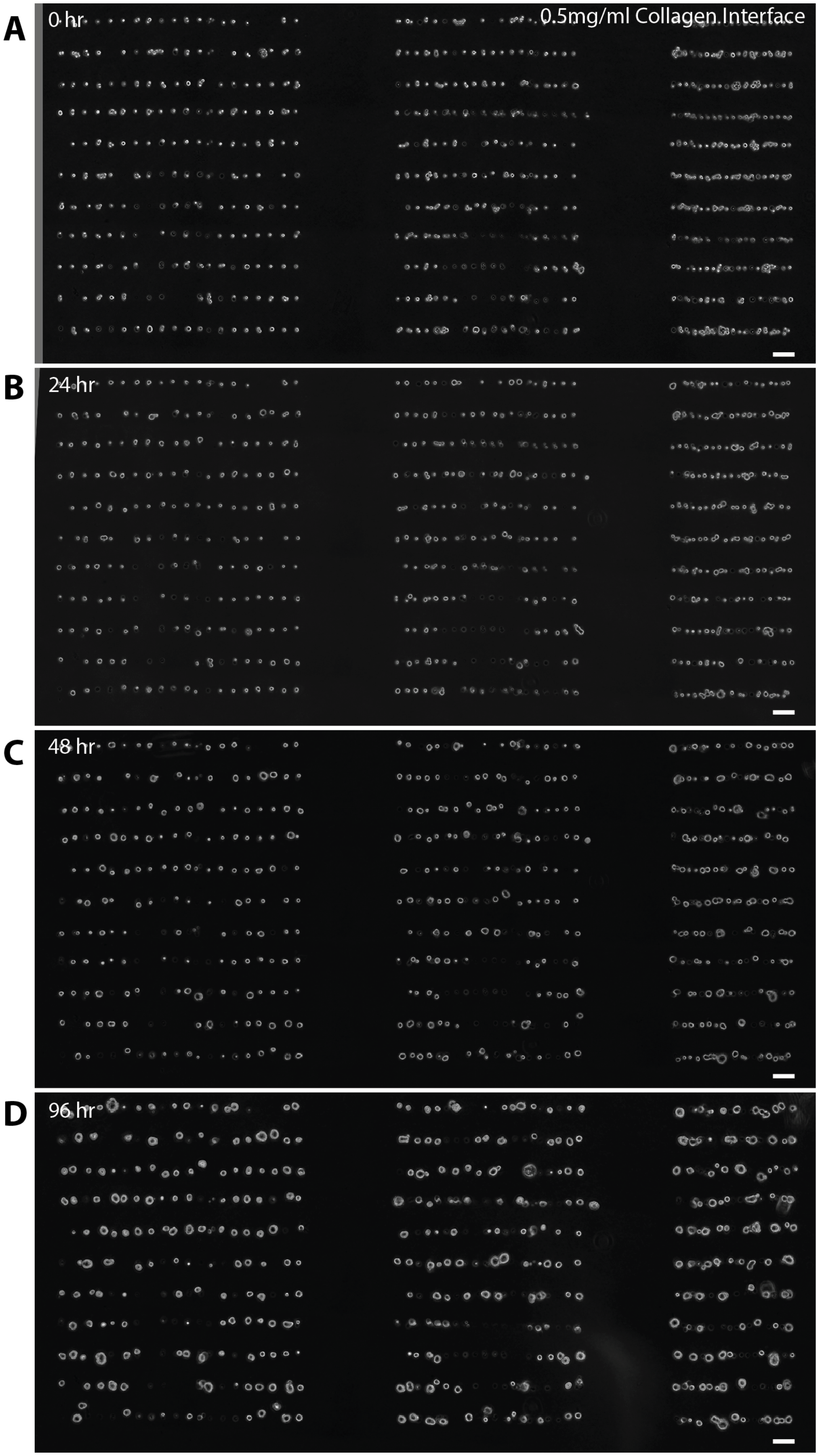
A
0 hr
0.5mg/ml Collagen Interface
B
24 hr
C
48 hr
D
96 hr

Supplementary Figure S5-8. MCF-10A lines of various spacing growing at an interface of Matrigel and Matrigel with a 0.5 mg/ml collagen supplement. (A) Lines of MCF-10A cells of decreasing pitch are grown at an interface of Matrigel and Matrigel supplemented with 0.5 mg/ml collagen and imaged at 0 hours, (B) 24 hours, (C) 48 hours, and (D) 96 hours. All scale bars are 100 μm.

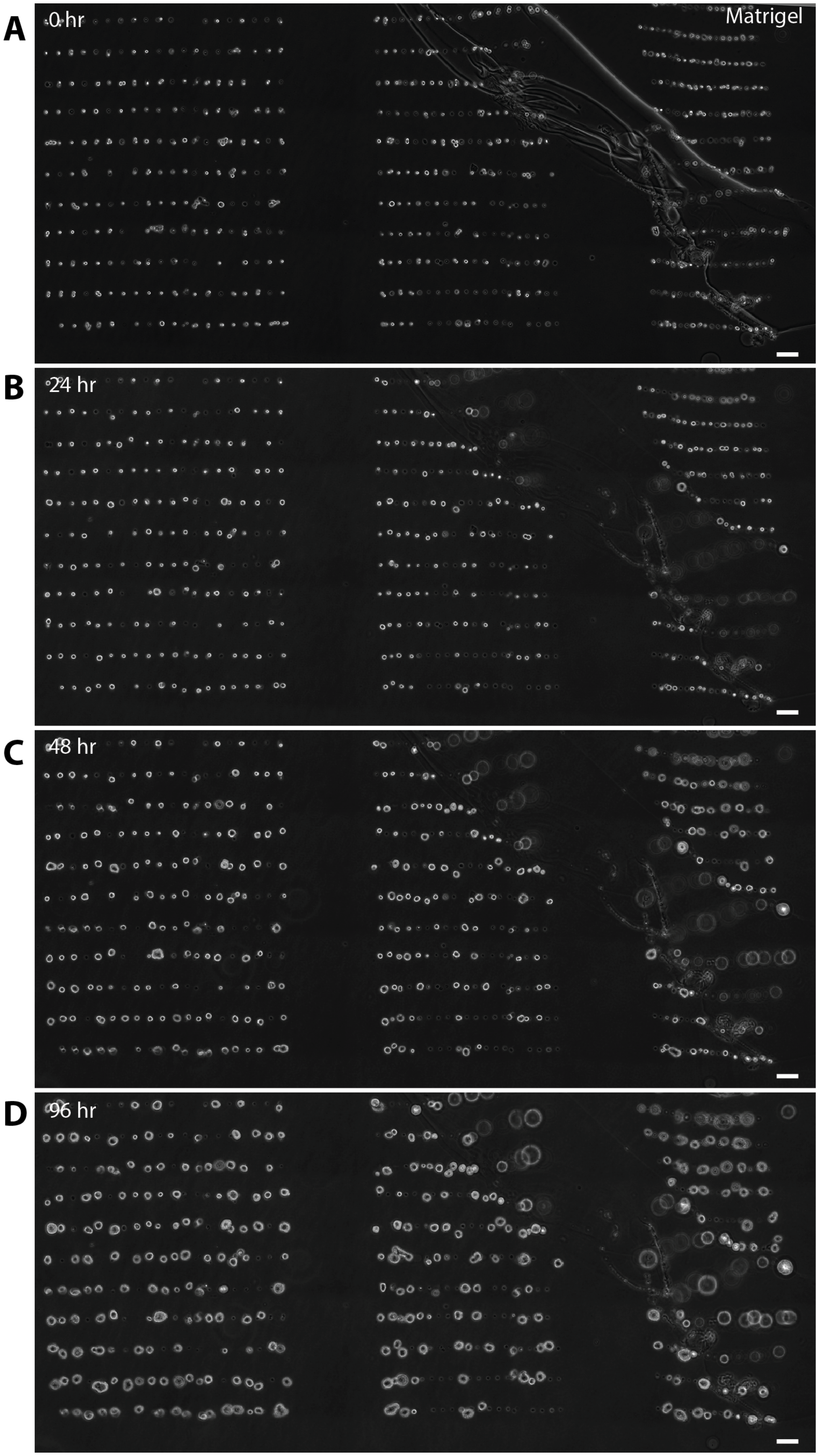
A
0 hr
Matrigel
B
24 hr
C
48 hr
D
96 hr

Supplementary Figure S5-9. MCF-10A lines of various spacing growing at in Matrigel. (A) Lines of MCF-10A cells of decreasing pitch are grown in pure Matrigel and imaged at 0 hours, (B) 24 hours, (C) 48 hours, and (D) 96 hours. All scale bars are 100 μm.

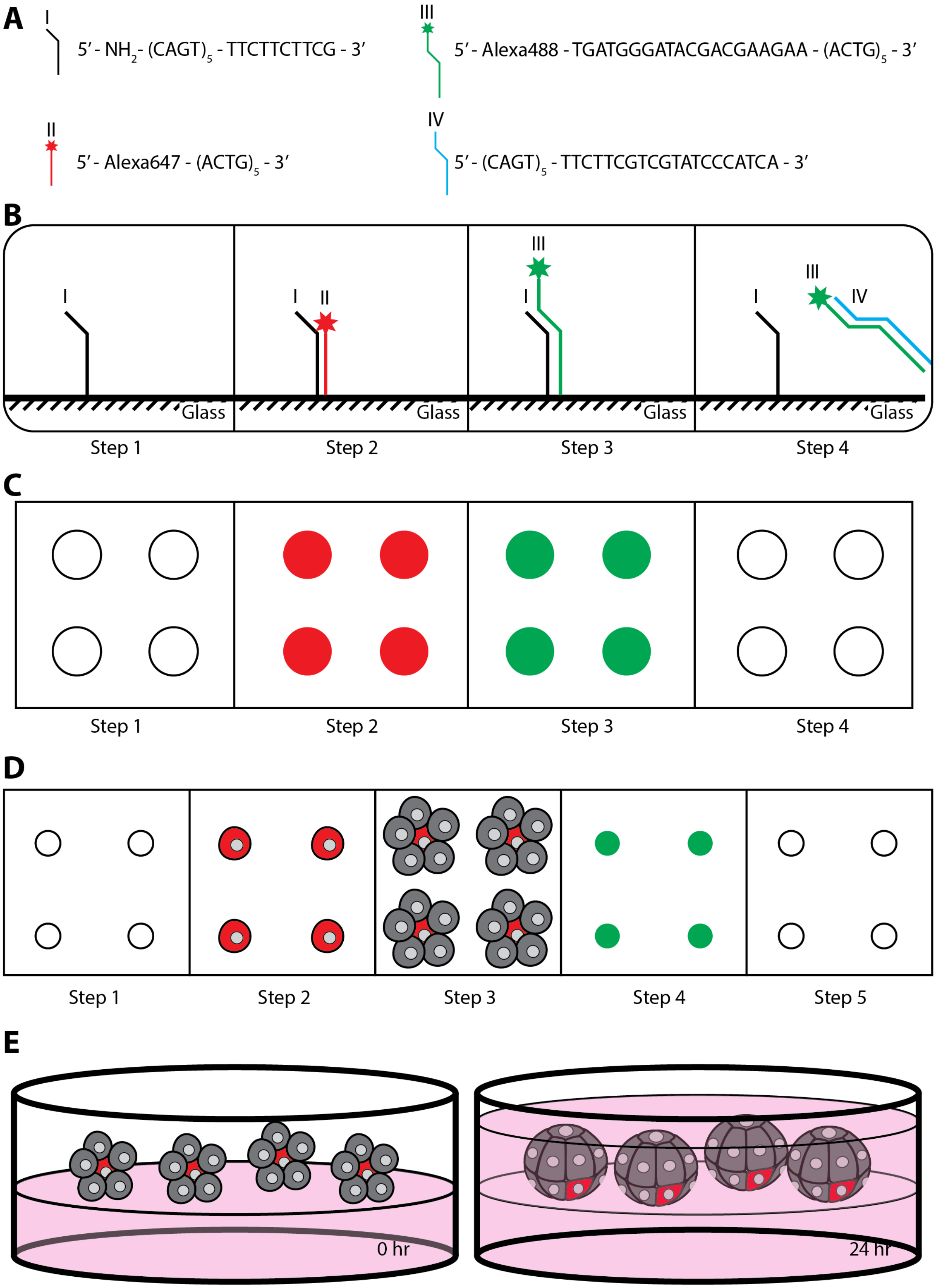
A
I
5′- NH$_2$- (CAGT)$_5$ - TTCTTCTTCG - 3′
III
5′- Alexa488 - TGATGGGATACGACGAAGAA - (ACTG)$_5$ - 3′
II
5′- Alexa647 - (ACTG)$_5$ - 3′
IV
5′- (CAGT)$_5$ - TTCTTCGTCGTATCCCATCA - 3′
B
I
I II
III I
III IV I
Glass
Glass
Glass
Glass
Step 1
Step 2
Step 3
Step 4
C
Step 1
Step 2
Step 3
Step 4
D
Step 1
Step 2
Step 3
Step 4
Step 5
E
0 hr
24 hr

Supplemental Figure S6. Theoretical STDPAC Printer. (A) DNA strands and sequences used for a proof-of-concept strand displacement experiment mimicking a STDPAC tissue printer. (B) The theoretical order of DNA strand addition for a proof-of-concept strand displacement experiment mimicking a STDPAC tissue printer. Strand I is printed on a surface. Strand II mimics a cell binding to the strand I spot. Strand III displaces the cell-mimic strand II. Strand IV regenerates the pattern of strand I DNA. (C) The same sequence of events, except imagining spots of DNA instead of strands of DNA. (D) A theoretical sequence for printing tissues with a strand displacement STDPAC tissue printer. (E) Culturing the theoretical printed tissues in 3D culture over 24 hours.

Supplemental Table

	Code Name	Modification		DNA Sequence	
STDPAC	A	DAG/NH2	5'	CAG TCA GTC AGT CAG TCA GT	3'
	A prime	DAG/NH2	5'	ACT GAC TGA CTG ACT GAC TG	3'
	D	DAG/NH2	5'	ACT GAT GGT AAT CTG CAC CT	3'
	D prime	DAG/NH2	5'	AGG TGC AGA TTA CCA TCA GT	3'
	B	DAG/NH2	5'	TCA TAC GAC TCA CTC TAG GG	3'
	B prime	DAG/NH2	5'	CCC TAG AGT GAG TCG TAT GA	3'
STDPAC Printer	Printed Strand	NH2	5'	CAG TCA GTC AGT CAG TCA GTT TCT TCT TCG	3'
	Lipid Strand	Alexa647	5'	ACT GAC TGA CTG ACT GAC TG	3'
	Displacement Strand	Alexa488	5'	TGA TGG GAT ACG ACG AAG AAA CTG ACT GAC TGA CTG ACT G	3'
	Regeneration Strand		5'	CAG TCA GTC AGT CAG TCA GTT TCT TCG TCG TAT CCC ATC A	3'

Supplemental Table 1. List of Modified DNA Sequences

Appendix 2: Supplemental Text

Supplemental Text 1: Alternative Surface Passivation

This entire supplemental text is reproduced from works of Michael Todhunter as communicated to Noel Jee. It is reproduced with permission.

PREPARATION

In advance, prepare Priming Buffer: 0.1% Tween-20, 5mM NaCl, 0.1mg/mL $MgCl_2$+$CaCL_2$, 25mM acetic acid, pH=2.5. 60 Celsius. Use same day because Tween-20 degrades within a day under warm acidic conditions.

In advance, prepare Flow Buffer: 2% BSA in PBS, calcium/magnesium-free. Sterile-filtered, ice-cold.

In advance, cast PDMS flow cells from glass and tape mold.

TREATMENT OF PATTERNED SLIDE AND FLOW CELL ASSEMBLY

Prepare a soln of 0.25% $NaBH_4$ in 25% ethanol, 75% PBS. 25mL is more than enough for one slide. Place the slide, in its dish, on a shaker at 120rpm. Add enough $NaBH_4$

solution to cover, and let it react for 15 minutes. Suck up the NaBH4 soln and replace it in its vessel. WARNING: NaBH4 evolves H2 gas. Do not tightly cap any containers of this soln, and do not store near an open flame. Do not dump fresh NaBH4 solutions down the drain. Either inactivate with dilute acid or wait at least 24 hours for the solution to spontaneously decompose.

Make a solution of 0.1% SDS (diluted 1/20 in dH2O from 2% SDS) and pour enough into the slide's dish to cover the slide. Swish 10 times, dump soln into sink (make sure you're holding the slide!). Repeat SDS wash. Then, repeat three more times, substituting pure dH2O for the SDS solution. That makes five washes total.

Fill a Coplin jar with 60mL dichloromethane. Add 600uL perfluoro-dimethylchlorosilane (specifically, (tridecafluoro-1,1,2,2-tetrahydrooctyl)dimethylchlorosilane). Add 600uL triethylamine. Mix. Fill five 50mL polypropylene conical tubes with: dichloromethane, dichloromethane again, ethanol, water, ph=4.5 25mM acetic acid in water.

Immerse the slide in 10% acetic acid. Dry slide under stream of air. Immerse slide in Coplin jar of DCM+silane+TEA. Let shake at 120rpm for 15 minutes. Then, using paddle tweezers, transfer slide into conical tubes of successive washing solutions: 1st DCM-> 2nd DCM-> ethanol -> dH2O. For each wash, securely cap the conical tube and invert ten times before transferring slide to next tube in the series. Upon transfer to tube of pH=4.5 acetic acid, shake at 120rpm for 30 minutes. Remove slide from tube and dry under stream of air. WARNING: dichloromethane is not compatible with all plastics. It is advisable to verify, before use, that your conical tubes do not dissolve or soften upon solvent exposure. It is advisable to discard tubes after use.

Using a razor blade, cut out PDMS flow cells. Cut an inlet and outlet from either end. Clean the PDMS by applying Scotch tape to the surface, pressing firmly, and peeling it away. Repeat this twice for both surfaces of the PDMS. Using a wax stick, apply a thin layer of microcrystalline wax to the ceiling of the flow cell.. Apply the PDMS, channel-side down (you should be able to feel the channel with your finger as well as see it), to the slide, centering the flow cell over the patterned region. Using the blunt edge of a razor blade, press the PDMS into the slide to establish a light seal. WARNING: if the slide is on a hard surface (like a benchtop), pressing into the PDMS can fracture the slide. Use a soft surface, such as a self-healing mat (or possibly a mousepad) for this step.

Use a grease pencil to draw barriers between the inlets and outlets of adjacent flow cells. This prevents cross-contamination between adjacent flow cells and prevents any liquid that accumulates at the inlet or outlet from creeping along the sides of the flow cells.

Place the slide on the base of the mounted toggle clamp. Place a styrofoam spacer atop the flow cells. Place an acrylic spacer atop the polystyrene. Clamp down on the acrylic with gentle pressure. The slide should be sufficiently clamped to immobilize it but not so strongly clamped that the flow cells are compressed.

Prime the flow cell with Priming Buffer. Pipet 100-200uL and slowly inject it into the flow cell, tilting the flow cell vertically such that the flow is against gravity. Try not to introduce air bubbles into the flow cell. Let the flow cell incubate 1-2 minutes before flushing it with another 100-200uL of warm Priming Buffer. Repeat for three total exchanges of Priming Buffer. Then, equilibrate each flow cell with 300uL Flow Buffer. Add a small volume (10-30uL) of Flow Buffer to the inlet and outlet to prevent evaporation from the inside of the flow cell and store, covered, at 4C, until ready to attach cells. Flow cells can be stored in this manner for up to one day as long as evaporation is prevented.

Supplemental Text 2: An Outline of Paper Figures Detailing a Theoretical STDPAC Tissue Printer

DPA is a powerful and versatile tool for building compositionally controlled tissues within the context of a larger pattern. In many circumstances, the context of a larger pattern is unnecessary for the purposes of the experiment. Many experiments require the simplification of a system such that complexity does not obscure the observed results. In the study of tissues in vitro, the vast body of literature describes mostly observations of individual cells within single tissues or single tissue units, without giving much thought to the specific interactions between different tissues. This is partly due to the fact that, until recently, methods did not exist to create tissues in the context of a larger pattern. It is more likely, however, that scientists focus on the level of single cells or tissues in order to understand basic behavior as a precursor to understanding complex, collective behaviors of systems.

In order to facilitate the creation of compositionally controlled tissues to study single cell and tissue behavior, we imagined the creation of a tissue printer using STDPAC as its core technology (Supplemental Figure S6). The outline of theoretical paper figures that describe this theoretical tissue printer is envisioned as follows.

LS = lipid strand
CS = cell strand
DS = Displacement Strand

RS = Regenerating Strand

Figure 1: Proof of Concept with DNA

A. Scheme
B. Dry spots of DNA printed - the only phase images
C. Blank screen with no color but taking pictures with all fluorescent channels
D. First DNA strand added (Red spots)
E. Strands displaced with Green DNA strands (Green spots) -- There should be no yellow visible.
F. Blank screen with the addition of the RS or DI water

Figure 2: Proof of Concept with Cells

A. Green Jurkat cells attached to a grid
B. Red Jurkat cells assembled onto the grid
C. Displacement strand with no Jurkat cells left and the addition of just a green DNA spot
D. Efficiency of the Displacement strand in washing away cells
E. Blank space with DS1 washed away

Figure 3: Demonstration with Useful Cells and Fidelity of Pattern Regeneration

A. Attachment and assembly of MCF-10A cells of different color
B. Comparison of 1st, 2nd, 5th, 10th occupancy of the pattern
C. Graph of attachment efficiency over number of repeats
D. Graph of attachment efficiency of 2’OMe vs Phosphorothioate vs Normal over time

E. Changing the pattern to more than just a single one dot matrix

Figure 4: Demonstration of Method to Create Compositionally Controlled MCF-10A Tissues (over time)

A. MCF-10A assemblies seeded on top of Matrigel
B. Graph of MCF-10A assembly composition and distribution
C. MCF-10A assemblies seeded on top of Matrigel after 4 days
D. Graph of MCF-10A assemblies composition and distribution after 4 days + added aphidicolin — is it possible to compositionally control the MCF-10A assemblies for a prolonged period of time
E. MCF-10A tubes printed and seeded. Do they stay as tubes over time? No quantification needed.

Supplemental Text 3: General Materials and Methods

General Materials and Reagents

Aldehyde-silanized glass slides (Nexterion® Aldehyde AL, Schott), Sigmacote® (Sigma-Aldrich), Slygard® 184 (Fisher Scientific), sodium borohydride ($NaBH_4$, ACROS, 98%), Pluronic® F108 NF (BASF), ethanol (Fisher Scientific), trypsin inhibitor from *Glycine max* (Sigma-Aldrich), Matrigel® (BD Biosciences), rat-tail collagen 1 (BD Biosciences), Turbo DNase (Life Technologies), amine-modified ssDNA (5′-amine-X_{20}, Operon), PBS (UCSF Cell-Culture Facility), PBS-CMF (UCSF Cell-Culture Facility), trypsin (UCSF Cell-Culture Facility), 100x penicillin/streptomycin, heat-inactivated fetal bovine serum (UCSF Cell-Culture Facility), RPMI media (UCSF Cell-Culture Facility) were used as received without further purification. Lipid-modified ssDNA (5'-lipid-T_{80}-X_{20}) was synthesized as previously described (Selden et al. 2012).

Cell Culture

MCF-10A cells were kindly provided by Professor Jay Debnath (UCSF), and MCF-10AT cells were obtained from the Karmanos Cancer Institute (Detroit). Both cell lines were cultured as previously described (Dawson et al. 1996; Debnath et al. 2003). Primary human mammary epithelial cells at passage 4 were established and maintained in M87A medium according as previously described (Stampfer et al. 2013). All other cells were cultured according to standard practices listed on American Type Culture Collection or Lonza.

DNA sequences

A-amine: 5'-amine-ACTGACTGACTGACTGACTG-3'

A-lipid: 5'-lipid-
TTTTTTTTTTTTTTTTTTTTTTTTTTTTTTTTTTTTTTTTTTTTTTTTTTTTTTTTTTTTTTT
TTTTTTTTTTTTTTTTTACTGACTGACTGACTGACTG-3'

Aprime-lipid: 5'-lipid-
TTTTTTTTTTTTTTTTTTTTTTTTTTTTTTTTTTTTTTTTTTTTTTTTTTTTTTTTTTTTTTT
TTTTTTTTTTTTTTTTTCAGTCAGTCAGTCAGTCAGT-3'

B-amine: 5'-amine-TCATACGACTCACTCTAGGG-3'

B-lipid: 5'-lipid-
TTTTTTTTTTTTTTTTTTTTTTTTTTTTTTTTTTTTTTTTTTTTTTTTTTTTTTTTTTTTTTT
TTTTTTTTTTTTTTTTTTCATACGACTCACTCTAGGG-3'

Bprime-lipid: 5'-lipid-
TTTTTTTTTTTTTTTTTTTTTTTTTTTTTTTTTTTTTTTTTTTTTTTTTTTTTTTTTTTTTTT
TTTTTTTTTTTTTTTTTCCCTAGAGTGAGTCGTATGA-3'

D-amine: 5'-amine-GTAACGATCCAGCTGTCACT-3'

Dprime-lipid: 5'-lipid-
TTTTTTTTTTTTTTTTTTTTTTTTTTTTTTTTTTTTTTTTTTTTTTTTTTTTTTTTTTTTTTT
TTTTTTTTTTTTTTTTTGTAACGATCCAGCTGTCACT-3'

Dprime-lipid: 5'-
lipidTTTTTTTTTTTTTTTTTTTTTTTTTTTTTTTTTTTTTTTTTTTTTTTTTTTTTTTTTTTT
TTTTTTTTTTTTTTTTTTTTAGTGACAGCTGGATCGTTAC-3'

F-amine: 5'-amine- AGAAGAAGAACGAAGAAGAA-3'

F-lipid: 5'-lipid-
TTTTTTTTTTTTTTTTTTTTTTTTTTTTTTTTTTTTTTTTTTTTTTTTTTTTTTTTTTTTTTT
TTTTTTTTTTTTTTTTTAGAAGAAGAACGAAGAAGAA-3'

Fprime-lipid: 5'-lipid-
TTTTTTTTTTTTTTTTTTTTTTTTTTTTTTTTTTTTTTTTTTTTTTTTTTTTTTTTTTTTTTT
TTTTTTTTTTTTTTTTTTTCTTCTTCGTTCTTCTTCT -3'

Antibodies

For immunofluorescence, the following antibodies were used at the specified dilutions:

Anti-human Keratin 19 Sigma C6930 (clone A53-B/A2) (1:50)

Anti-human Keratin 14 Thermo RB-9020-P (poly) (1:50)

Anti-human CD49f Millipore MAB1378 (clone GoH3) (1:50)

Preparation of PDMS Flow Cells

Flow cells were cast with Sylgard 184 according to the specifications provided by Dow Corning. Briefly, the polymer and curing agent were mixed at a 10:1 ratio, degassed under vacuum, and cured over the flow cell master at 70 ˚C. The master was prepared with No. 1 thickness coverslips (Fisher Scientific) cut to the dimensions of 4.5mm x 18mm and attached to double-sided tape (3M, cat. 665) of .0762 µm thickness. The final dimensions of the flow cell master was 4.5 mm x 18 mm x 0.22 mm attached to a Nunclon® (Fisher Scientific) petri dish. Each PDMS flow cell was individually cut to have 1mm-thick side walls and to have a 4.5mm-wide inlet and outlet. Flow cells were treated with atmospheric plasma prior to use, as described below.

Preparation of DNA-patterned Surfaces

Cell and tissue patterns were designed as bitmap images in Microsoft Paint and translated into 6-8 µm-diameter droplets of 1.5 mM 5’-amine-modified ssDNA (5′-amine-X_{20}, Operon) in a spotting solution of 225 mM NaCl, 22.5 mM sodium citrate, 5% w/v trehalose, 0.1 mg/mL N-octylglucoside, pH=9.5 onto aldehyde-silanized glass slides

(Nexterion® Aldehyde AL, Schott) via the BioForce Nano eNabler. Upon completion of printing, ssDNA patterns were baked at 120 ˚C for 15 minutes and then stored in a vacuum desiccator until use.

Patterned slides were reduced in a solution of 0.25% $NaBH_4$ in 25% ethanol, 75% PBS for 15 minutes. Slides were washed twice with 0.1% SDS, three times with dH_2O, and then air-dried. For silanization, 150 µL of Sigmacote (Sigma-Aldrich) was pipetted onto the slide and a coverslip placed on top. After five seconds, the coverslip was removed and the slide submerged into a tube of 50 mL absolute ethanol. The slide was inverted ten times then transferred into a fresh tube of 50 mL absolute ethanol. The inverting was repeated, and the slide was transferred into a tube of ddH_2O for a final set of inversions. The slide was removed from the tube and dried under a stream of air. A flow cell was cut for each pattern on the slide, cleaned of dust with tape, and subjected to atmospheric plasma in a Plasma Etch PE-50 for 35 seconds under 200 mTorr pressure with 15 cc/min gas flow and at intermediate power. Flow cells were immediately positioned over the patterned slide and secured with gentle finger pressure. The flow cells were primed with a solution of RPMI-1640, 10% FBS, 63.7 mg/L penicillin G, 100 mg/L streptomycin sulfate, and 1% Pluronic F108. The solution was left in the flow cell for 5 minutes at room temperature to block the surface, and then the flow cell was equilibrated with four flow-cell volumes of calcium/magnesium-free PBS (PBS CMF) and left undisturbed until ready for programmed assembly.

Preparation of DNA-labeled Cells

All cell-lines were labeled with lipid-ssDNA prepared according to a published procedure[1]. Briefly, cells were incubated for 5 min at room temperature with 5 μM of lipid–DNA. Sequences were chosen according to the requirements of each specific experiment. DNA-labeled cells were washed three times with PBS CMF and temporarily stored at 4 ˚C until required for programmed assembly.

Programmed Assembly and Tissue Embedding of Cell Patterns

DNA-labeled cells were resuspended to a concentration of 10^7 cells/mL, and 20 μL of these cells were introduced to one end of the flow cell. The cells were either allowed to settle to the surface by gravity for 5-10 minutes, or the slide was centrifuged for 3 min at 8 g in a Sorvall Legend RT+ centrifuge with acceleration and deceleration set to minimum. Ten flow cell volumes of PBS CMF were flowed into the flow cell to wash out unhybridized cells. The procedures in this paragraph were repeated for each assembly step desired, taking 5-15 minutes for each successive assembly step.

Once the desired cell populations were assembled in the flow cell, a mixture of liquid hydrogel (e.g. Matrigel) and DNase was flowed across the surface. One typical formulation was 6.1 mg/mL Matrigel, 2.1 mg/mL collagen I, 40 U/mL Turbo DNase, ice-cold. Another typical formulation was 9.0 mg/mL Matrigel, 40 U/mL Turbo DNase, ice-cold. The flow cell was put in an incubator at 37 ˚C for 30 minutes to allow for DNA cleavage and for the liquid gel to set as a solid hydrogel. Next, a border of 20 μL PBS CMF was applied all around the flow cell to reduce stiction, and then a sterile razor blade was used to slide the flow cell off the surface and onto a 20uL droplet of molten hydrogel waiting in a 3.5 cm culture dish. The dish was transferred to an incubator at 37 ˚C for 30 minutes to allow the underlying gel to set. 3 mL prewarmed culture media was added to the dish so as to completely submerge the flow cell. Sharp tweezers were used to carefully slide the flow cell off the set hydrogel. The released flow cell was then removed from the dish. The dish was returned to the incubator to begin tissue culture.

Immunofluorescence

All samples were fixed with 4% formaldehyde for 20 minutes and then incubated in blocking buffer (10% heat-inactivated goat serum in PBS+0.5% Triton X-100) at 4 ˚C for at least one day. Primary antibodies were then diluted in blocking buffer and added to the sample. After at least one day incubating at 4 ˚C with the primary antibodies, samples were washed several times with PBS+Triton X-100 for at least one day and incubated with fluorophore-conjugated secondary antibodies diluted at a concentration of 1:200 in blocking buffer for approximately one day. All sample were washed with PBS+1 µg/mL DAPI for at least one hour before imaging.

Image Acquisition

All confocal microscopy images were acquired using a temperature, atmosphere, and humidity controlled spinning disk confocal microscope (Zeiss Cell Observer Z1 equipped with a Yokagawa spinning disk and running Zeiss Zen Software). All other images were acquired using an inverted epifluoresence microscope (Zeiss Axiovert 200M running SlideBook software).

Cell Growth Measurements

Cell assemblies in 20x20 square arrays with pitch xy of 300 µm were imaged approximately every 24 hours by driving the Zeiss Cell Observer spinning disc confocal microscope to a pre-set list of nominal xy positions at 20x magnification with a z-slice spacing of 3 µm. Cell nuclei in red and green emission channels were counted manually from raw tiff z-stacks and maximum intensity projection images. Growth rates for each assembly were calculated as the slope of plots of $\log_2 (N/N_o)$ vs. t where N is cell number at time t and N_o is initial cell number, assuming logarithmic growth of cells.

HUVEC Extension Measurements

For each microtissue, a local horizontal axis was determined by inspecting the image of the microtissue at day 0. The image of the microtissue at day 2 was rotated according to this local axis. The image was binarized on the red fluorescence channel. Two portions of the microtissue were analyzed: the leftmost third and the center third. For each portion, the height of the bounding box was measured. A one-tailed Welch's p-test was performed to test for significant differences between bounding box heights across the population of microtissues.

Tissue Clearing

A simplified version of the CLARITY protocol was performed to make dense microtissues suitable for 3D imaging (Church & Deisseroth. 2013). Tissues were incubated in hydrogel solution (4% acrylamide, 0.2% bis-acrylamide, 0.25% VA-044, 4% paraformaldehyde in PBS) for a day at 4 C. The hydrogel was then polymerized by heating to 60 C for an hour. The sample was cleared by incubation in clearing solution (4% sodium dodecyl sulfate, 200 mM boric acid, pH = 8.5 with sodium hydroxide) for five days at room temperature with gentle shaking. The sample was exchanged into PBS + 0.1% Trition-X100 for two days, then mounted with FocusClear before confocal imaging.

References

Selden, N. S. *et al.* (2012). Chemically Programmed Cell Adhesion with Membrane-Anchored Oligonucleotides. J Am Chem Soc *134,* 765–768.

Dawson, P. J., Wolman, S. R., Tait, L., Heppner, G. H. & Miller, F. R. (1996). MCF10AT: a model for the evolution of cancer from proliferative breast disease. Am J Pathol *148,* 313–319.

Debnath, J., Muthuswamy, S. K. & Brugge, J. S. (2003). Morphogenesis and oncogenesis of MCF-10A mammary epithelial acini grown in three-dimensional basement membrane cultures. Methods *30,* 256–268.

Stampfer, M. R., LaBarge, M. A. & Garbe, J. C. (2013). *Cell and Molecular Biology of Breast Cancer* (ed. Schatten, H.) Humana Press, 323–361.

Chung, K. & Deisseroth, K. (2013). CLARITY for mapping the nervous system. Nat Methods *10*, 508–513.

Supplemental Text 4: Glossary of Terms, Acronyms, and Phrases

Assembly: A collection of cells held together by synthetic DNA adhesion molecules.

Attachment Efficiency: The extent to which all spots of DNA on a surface are occupied by at least 1 cell.

Collagen: Refers to rat tail collagen I unless otherwise stated

DNA-Programmed Assembly: The self-assembly of cells based on their synthetic adhesive identities conferred by labeling the surface with ssDNA

Gel lifting: Removal of a matrix-embedded pattern along with its flow cell from a glass surface.

HUVEC: Human Umbilical Vascular Endothelial Cell

Matrigel/collagen 3D culture: cells embedded in a mixture of 6 mg/ml Matrigel and 2 mg/ml rat tail collagen I.

MCF-10A: An immortalized, normal human mammary epithelial cell line; also called normal cells

MCF-10AT: An MCF-10A cell stably transduced to express an oncogenic form of Ras

Priming buffer: 1% w/v pluronic F108, 10% v/v FBS, RPMI 1640 media

Ras cell: MCF-10AT cell

Rotational control: A control experiment that considers space and relative positioning of patterns; a 2D pattern can be rotated 90° within a flow cell is an example of a rotational control.

Single-Cell Occupancy: The extent to which single cells attach to single spots of DNA on a surface

STDPAC: Surface Templated DNA Programmed Assembly of Cells (pronounced seInt DEE-pahk).

Technology: A tool that is useful for the study of science; synonymously used with method or technique.

Tissues: Cells or assemblies of cells that grow into a unit with a singular identity.

Transfer Fidelity: The extent to which a pattern transferred to 3D culture retains the same shape when cells are first patterned onto glass.

Zip code: Spots of sequence-specific DNA on surfaces that only attaches complementary-DNA labeled cells

Appendix 3: List of Publications and Patents

Todhunter M*, **Jee NY*** (**Co-First Authorship)**, Cerchiari AE, Garbe J, Farlow JT, Gartner ZJ. (2015). Rapid 3D tissue prototyping by DNA-programmed assembly. *In Review*.

Cerchiari AE, Garbe J, **Jee NY**, Todhunter ME, Broaders K, Peehl DM, Desai TA, LaBarge MA, Thomson M, Gartner ZJ. (2014). A strategy for tissue self-organization that is robust to cellular heterogeneity and plasticity. P.N.A.S. *112*, 2287–2292.

Cerchiari, AE, Garbe J, Todhunter, ME, **Jee NY**, LaBarge, MA, Desai TA, Gartner ZJ. (2014) Formation of spatially and geometrically controlled 3D tissues in soft gels via Sacrificial Micromolding. Tissue Engineering Part C *21*, 541–547.

Provisional Patent: Publication Number WO2014071388 A1; ***Title***: Methods of patterning cells on a surface of a substrate and programmed assembly of three-dimensional living tissues, **2013.**

Full Patent Application: Publication Number WO2013067203 A1; ***Title***: Invention of membrane-anchored polynucleotides and their use in research and therapeutic applications, **2012.**

Selden NS, Todhunter ME, **Jee NY**, Liu JS, Broaders KE, Gartner ZJ. (2012). Chemically Programmed Cell Adhesion with Membrane-Anchored Oligonucleotides. J Am Chem Soc. *134*, 765-8.

Appendix 4: Contributor Validations for Thesis Work Attributions

Parts of this dissertation are a reproduction of materials previously published or submitted for publication and contains contributions from collaborators listed therein. Chapter 1 and Supplemental Text 3 are reproduced in part with permission from Todhunter ME*, Jee NY* (Co-First Authorship), Cerchiari AE, Garbe J, Farlow JT, Gartner ZJ. 2015. Rapid 3D tissue prototyping by DNA-programmed assembly. *In Review.* The artwork in Figure 2-2 is reproduced in part with permission from Selden NS, Todhunter ME, Jee NY, Liu JS, Broaders KE, Gartner ZJ. (2012). Chemically Programmed Cell Adhesion with Membrane-Anchored Oligonucleotides. J Am Chem Soc. *134*, 765-8.

This thesis work was a joint project between myself - Noel Jee - and Michael Todhunter. The entire work was overseen by Professor Zev Gartner. **All work presented in this dissertation were completed by Noel Jee with the following exceptions:**

The procedural details relating to flow cells and surface passivation described in Figures 2-1, 2-3, and 2-5 are attributed to Michael Todhunter.

Alec Cerchiari fixed and stained the tissues and collected the images in Figure 2-7C-D. Noel Jee conducted the experiment.

Samantha Liang conceived of the artwork and Michael Todhunter completed the

STDPAC experiment in Figure 3-2. MT

Michael Todhunter conceived of the patterns used in Figure 3-5 and Figure 3-6. Noel Jee conducted all experiments. MT

Michael Todhunter created the digital pattern in Figure 3-6A-E. Justin Farlow performed the analyses in Figure 3-6G-H. Noel Jee conducted all experiments. MT

James Garbe passaged and prepared the cells used in Figure 3-14C-D. Alec Cerchiari fixed, stained, and imaged the tissues in Figure 3-14C-D.

Michael Todhunter conducted the data analysis and created all graphs in Figure 4-2. MT

Michael Todhunter conducted the data analysis and created all graphs in Figure 4-4C. MT

Michael Todhunter conducted the experiments, data analyses, and graphical depictions in Figure 4-8C-D. MT

Michael Todhunter conducted the data analyses and created all graphs in Figure 4-15C.

MT

Alex Hughes conducted the experiments, data analyses, and graphical depictions in Figure 5-9C-D. AJH

Michael Todhunter created the digital pattern used in Supplemental Figure S3-3.

MT

Kyle Broaders created the mathematical models in Supplemental Figure S4-3A-B. Michael Todhunter conducted the experiments, data analyses, and images for Supplemental Figure S4-3C. MT

Alex Hughes conducted the experiments, data analyses, and graphical depictions Supplemental Figure S4-6. AJH

Michael Todhunter and Robert Weber intellectually contributed to the theoretical STDPAC printer project depicted in Supplemental Figure S6.

RW MT

Michael Todhunter contributed the entirety of Supplemental Text 1. MT

Many of the basic images that form the figure artwork panels were collaborations with Michael Todhunter and Zev Gartner. MT

Publishing Agreement

It is the policy of the University to encourage the distribution of all theses, dissertations, and manuscripts. Copies of all UCSF theses, dissertations, and manuscripts will be routed to the library via the Graduate Division. The library will make all theses, dissertations, and manuscripts accessible to the public and will preserve these to the best of their abilities, in perpetuity.

Please sign the following statement:

I hereby grant permission to the Graduate Division of the University of California, San Francisco to release copies of my thesis, dissertation, or manuscript to the Campus Library to provide access and preservation, in whole or in part, in perpetuity.

Author Signature

6/1/2015

Date